# Fundamentals of Efficient Spectrum Access and Co-Existence with Receiver Nonlinearity

Aditya V. Padaki

Dissertation submitted to the Faculty of the
Virginia Polytechnic Institute and State University
in partial fulfillment of the requirements for the degree of

Doctor of Philosophy
in
Electrical Engineering

Jeffrey H. Reed, Chair
Ravi Tandon
A. A. (Louis) Beex
Michael J. Marcus
Kwang J. Koh
Anil Kumar S. Vullikanti

December 01, 2017
Blacksburg, Virginia

Keywords: Co-Existence, Receiver Nonlinearity, Adjacent Channel Interference
Copyright 2017, Aditya V. Padaki

# Fundamentals of Efficient Spectrum Access and Co-Existence with Receiver Nonlinearity

Aditya V. Padaki

(ABSTRACT)

RF front-ends are nonlinear systems that have nonlinear frequency response and, hence, can impair receiver performance by harmful adjacent channel interference in non-intuitive ways. Next generation wireless networks will see unprecedented diversity across receiver and radio technologies accessing the same band of spectrum in spatio-temporal proximity. Ensuring adjacent channel co-existence is of prime importance for successful deployment and operations of next generation wireless networks. Vulnerabilities of receiver front-end can have a severe detrimental effect on network performance and spectrum co-existence. This dissertation addresses the technological challenges in understanding and accounting for receiver sensitivities in the design of next generation wireless networks. The dissertation has four major contributions.

In the first contribution, we seek to understand *how receiver nonlinearity impacts performance*. We propose a computationally efficient framework to evaluate the adjacent channel interference in a given radio/spectrum environment. We develop novel tractable representation of receiver front-end nonlinearity to specify the adjacent channel signals that contribute to the interference at the desired channel and the total adjacent channel interference power at a given desired channel.

In the second contribution, we seek to understand *how the impact of receiver nonlinearity performance can be quantified*. We quantify receiver performance in the presence of adjacent channel interference using information theoretic metrics. We evaluate the limits on achievable rate accounting for RF front-end nonlinearity and provide a framework to compare disparate receivers by forming generalized metrics.

In the third contribution, we seek to understand *how the impact of receiver nonlinearity can be managed at the network level*. We develop novel and comprehensive wireless network management frameworks that account for the RF nonlinearity, impairments, and diversity of heterogeneous wireless devices. We further develop computationally efficient algorithms to optimize the proposed framework and examine network level performance. We demonstrate through extensive network simulations that the proposed receiver-centric frameworks provide substantially high spectrum efficiency gains over receiver-agnostic spectrum access in dense and diverse next generation wireless networks.

In the fourth contribution, we seek to understand *how scalable interference networks are with receiver nonlinearity*. We propose practical achievable schemes for interference avoidance and assess the scalability of the next generation wireless networks with interference due to receiver nonlinearity. Further, we develop an algorithmic scheme to evaluate the upper bound on scalability of nonlinear interference networks. This provides valuable insights on scalability and schemes for nonlinear adjacent channel interference avoidance in next generation shared spectrum networks.

# Fundamentals of Efficient Spectrum Access and Co-Existence with Receiver Nonlinearity

Aditya V. Padaki

(General Audience Abstract)

There has been a dramatic increase in the demand for mobile data, since the introduction of smartphones. Over the air transmission of data utilizes a natural resource called radio frequency spectrum. The efficient utilization of the radio frequency spectrum and clever wireless network management is key for satisfying this demand. Besides improving the quality of wireless services, efficient spectrum utilization will also have profound economic benefits and spur growth. It has been shown that spectrum is most efficiently used when shared among various services rather than licensed to specific users and communication systems. This implies that next generation wireless networks will comprise of diverse types of wireless devices. Thus, network design and regulation should ensure their harmonious co-existence. However, the practicality of spectrum sharing technology and regulation is still in its infancy. In particular, the effect of radio receiver performance and vulnerabilities from signals in the spectral neighborhood on spectrum regulation and management is not well understood. A detailed study and analysis of this is of paramount importance spectrum sharing and regulation in next generation wireless networks. In this dissertation we develop the fundamentals, limitations, and management strategies on the impact of receiver performance on efficient spectrum access and co-existence. In addition, this key insights to maximize network efficiency in next generation wireless systems are presented. The outcome of this dissertation will aid in developing frameworks to increase social awareness about low-quality wireless devices and their implications on capacity. In summary, this dissertation provides a the necessary foundations to understand, design, and optimize the next generation wireless networks, which will have far reaching economic and social benefits.

# Dedication

*To my parents...*

# Acknowledgments

Through the years of my graduate school at Virginia Tech, I have been fortunate to be blessed with a nourishing and enriching ecosystem consisting of faculty, staff, colleagues, and friends. This section could easily span the length of the entire dissertation itself, such has been the impact of people through these years. Nevertheless, I will try and maintain brevity.

At the outset, I would like to thank the US National Science Foundation for enabling my graduate work through grants ECCS EARS 1247928 and CNS NeTS 1564148.

Foremost, I express my deepest gratitude to Dr. Jeffrey Reed for his able tutelage, encouragement, and support. The academic and non-academic training that I have received under his guidance has enabled me to remarkably grow as an engineer, a researcher, and a professional. It will remain as the greatest asset throughout my life. Thank you for instilling the necessary confidence in me and for believing in me even during those times when I doubted myself. His brilliant knack of identifying new impactful engineering problems and shaping it as viable research problems by carefully deconstructing them, has taught me a lot on how to conceptualize and formulate research problems. He has been a constant source of inspiration and his passion serves as a great motivator to all. It has truly been a privilege to pursue my graduate studies under his supervision.

I am extremely grateful for having found a great mentor and guru in Dr. Ravi Tandon through my years at Virginia Tech. Working with him has extensively taught me on the ways of approaching a problem and carrying out research, and has tremendously improved my problem solving skills. I have learned a lot through hours of brainstorming, coffee breaks, and friendly discussions. Thank you for patiently explaining the minute details on a host of topics that we discussed and worked on. I am also thankful for the enormous amount of time and attention he gave me despite his busy schedule. Collaborating with him and learning from him has been one of the best things that has happened to me.

Dr. Louis Beex was one of the first professors I met at Virginia Tech at the graduate recruiting

weekend, even before I was enrolled as a student. That discussion which was scheduled for half an hour, went on for over an hour and left a lasting impression on me. I earnestly thank him not only for serving on my committee, but also for all the support, encouragement, and feedback given to me over the years, be it the FCC presentation, or the NSF meeting, just to name a couple. I would like to convey my special thanks to Dr. Michael Marcus for consistently taking the time to talk to me, provide me with valuable feedback on my work, and also for giving new research directions over the years. I have learned a lot from our monthly meetings throughout my graduate school, and discussions from his technical and life experiences have truly enriched my learning experience. Thank you for your constant support, encouragement, and advice. I would like to thank Dr. Anil Vullikanti and Dr. Kwang J. Koh for serving on my dissertation committee, reviewing my work and providing valuable feedback.

I am specially grateful to Dr. Vuk Marojevic for his tremendous support, encouragement, and guidance. He was always there whenever I wanted to brainstorm an idea, and his valuable feedback has helped me gain unique perspectives on the ways of research. His insights on transitioning tough research problems from paper to the lab bench have given me the much needed exposure to the practical world. Thank you for always being there! My learning experience would not have been complete if it were not for those countless intense discussions we had.

Randall Nealy has been a brilliant guide for anything and everything related to practical implementation. I have learned more about RF systems through valuable discussions and interactions with him than what any text book could perhaps ever teach me. Thank you for the innumerable sessions of tech talk and for patiently explaining even the silliest of my doubts. I would also like to thank Dr. Michael Buehrer for the various courses and discussions, which have greatly improved my understanding of wireless communications. I would like to thank Dr. Andrew Clegg for his able mentorship and the enriching experience during my internship at Google.

A big shout out to Hilda and Nancy for making our work place colorful and all the more enjoyable. The seamless manner in which they take care of the many many things to make our lives easy is truly commendable. I am incredibly grateful to Hilda for having stood by me like a strong pillar, and extending all the help when I was stuck abroad. Even in the most literal sense, you have truly enabled me to finish this dissertation and I am forever indebted to you for that!

For those who were a part of my home away from home – who made life at Blacksburg so memorable! Vishwas and Varuni – just, thank you for everything! Special thanks to Dhiraj, for

all the incredible discussions, support, and for listening to my whines and rants. Another special thanks to Avik who took multiple avatars over the years − starting off as PhD-mate to labmate to roommate. Special thanks to Deven for all the laughs and arguments. For the incredible and awesome Atul − thank you for all the laughs, fights, and support. A special vote of thanks for Abhijin and Anu for being the glue to the Kannada folks in Blacksburg. Atashi, Mahesh, Vireshwar, Sriram, Sruthi, and all others, thank you for the awesome times shared.

In the lab family, most special thanks to Mahi for all the support, laughs, discussions, and rants! Special thanks to Raghu and Priyabrata for the awesome laughs over coffee. Special thanks due to Munawwar for the awesome times. Thank you Tad for the long chats and tech talks. Thanks to Eyosias for all the guidance. Thanks Amr and Mohammad for the cordial research collaborations. Matt, Mehrnaz, Mohammad Mozaffari, Nistha, Jennifer, Komal, Ahmad, Tarun, Shem, Daniel, Chris Headley, Chris O'Lone, and several others, thank you for the great times we shared!

I am beholden to my entire extended family for providing a loving environment and kind support all along. I am grateful to the spiritual and divine wisdom of the philosophical traditions of India, which has been a source of colossal strength and has paved the way for my holistic well-being. Lastly and most importantly, words cannot express how indebted I am to my parents for their unconditional love, eternal support, and steadfast encouragement, which has been the most significant factor all my life and also through my graduate work.

# Contents


**1 Introduction** **1**

1.1 Contributions . . . . . 8

1.1.1 Simplified Tractable Representations of Receiver Nonlinearity . . . . . 8

1.1.2 Quantifying Impact of Receiver Nonlinearity on Performance . . . . . 9

1.1.3 Frameworks for Efficient Spectrum Access with Receiver Nonlinearity . . 9

1.1.4 Scalability of Interference Networks with Receiver Nonlinearity . . . . . 10

1.1.5 List of Relevant Publications . . . . . 11

1.2 Organization of the Dissertation . . . . . 13

**2 Preliminaries and Background** **14**

2.1 Receiver Model and Nonlinearity . . . . . 14

2.2 Why is Nonlinear Distortion a Problem? . . . . . 15

2.3 Elevated Noise Floor . . . . . 17

**3 Simplified Tractable Representations of Receiver Nonlinearity** **22**

3.1 Introduction . . . . . 22

3.1.1 Main Contributions . . . . . 23

3.2 Preliminaries: Taxonomy and Background . . . . . 24

3.3 Representation Using Toeplitz Matrices . . . . . 25

3.4 Representation Using Unit Basis Vectors . . . . . 26

3.4.1 Two-Tone Intermodulation Products . . . . . 27

3.4.2 Three-Tone Intermodulation Products . . . . . 29

3.4.3 Cross-Modulation . . . 30
3.4.4 Compressive Distortion . . . 32
3.4.5 Formulation of Type II Representation . . . 33
3.4.6 Example of the proposed representation using unit basis vectors . . . 34
3.4.7 Expediency of the Proposed Representation . . . 37
3.4.8 Computational Efficiency . . . 37
3.5 Validations through Simulations and Experiments . . . 38
3.5.1 Validation of the Representation with Numerical Simulations . . . 38
3.5.2 Validation of the Representation with Experimental Measurements . . . 39
3.6 Conclusions . . . 40

**4 Quantifying the Impact of Receiver Nonlinearity on Performance 41**
4.1 Introduction . . . 41
4.1.1 Main Contributions . . . 42
4.2 Achievable Rates for non-ideal receivers . . . 42
4.2.1 Evaluating Third Order Distortion Power for Reference Test Input . . . 44
4.2.2 No Knowledge at Transmitter . . . 46
4.2.3 With Knowledge at Transmitter . . . 47
4.3 Receiver Performance Metrics . . . 50
4.4 Numerical Simulations and Experimental Results . . . 51
4.4.1 Adjacent Channel Interference for Example Practical Measurement . . . 51
4.4.2 Adjacent Channel Interference . . . 53
4.4.3 Achievable Rates . . . 53
4.4.4 Receiver Performance Metrics . . . 53
4.4.5 Bit Error Rate . . . 56
4.4.6 Theoretical Receiver Performance Metric and Practical Throughput . . . 56
4.4.7 Random RF Environment and Worst Case Performance . . . 58
4.5 Conclusions . . . 60

**5 Receiver Nonlinearity Aware Dynamic Resource Allocation: Two User Case 62**

5.1 Introduction . . . 62

5.1.1 Main Contributions . . . 62

5.2 System Model . . . 63

5.3 Problem Formulation . . . 64

5.3.1 Lower Bound . . . 65

5.3.2 Upper Bound . . . 66

5.4 Simulation Results . . . 66

5.4.1 Sum Data Rate with Varying IIP3 . . . 67

5.4.2 Variation of Minimum Rate Constraint . . . 68

5.4.3 Rate, Power and Bandwidth per User . . . 68

5.4.4 Different Receiver Nonlinearity . . . 69

5.5 Conclusions . . . 71

**6 Receiver-Centric Efficient Spectrum Access: Multi-RAT Network Co-existence with Receiver Nonlinearity 72**

6.1 Introduction . . . 72

6.1.1 Main Contributions . . . 73

6.2 Framework for Single Transmitter, Multiple Receivers . . . 73

6.2.1 Adjacent Channel Interference Formulation . . . 75

6.2.2 Channel Assignment Framework . . . 76

6.2.3 Problem Formulation . . . 77

6.2.4 Greedy Algorithm for Channel Assignment . . . 78

6.2.5 Pre-selector Spans a Factor of the Entire Band . . . 79

6.3 Generic Framework for Multiple Transmitter-Receiver Pairs . . . 81

6.3.1 Adjacent Channel Interference Formulation . . . 81

6.3.2 Framework for Channel Assignment . . . 84

6.3.3 Heuristic Algorithm: Simulated Annealing . . . 85

6.3.4 Pre-selector Spans a Factor of the Entire Band . . . 87

6.4 Modeling Transmitter Masks and OOBE . . . 88
6.5 Simulation Results . . . 91
6.5.1 Case 1: Single Transmitter, Multiple Receivers . . . 91
6.5.2 Multiple Transmitter-Receiver Pairs . . . 94
6.6 Conclusions . . . 98

**7 Receiver Impairment Aware Efficient Spectrum Access 99**
7.1 Introduction . . . 99
7.1.1 Main Contributions: . . . 101
7.2 Impact of Receiver Impairments . . . 103
7.2.1 Mixer – Image Frequency Rejection . . . 103
7.2.2 Phase Noise . . . 103
7.2.3 ADC Aliasing . . . 104
7.2.4 Entire Receiver Chain . . . 105
7.3 Case 1: Co-Located Transmitters with Multiple Receivers . . . 106
7.3.1 Adjacent Channel Interference Formulation . . . 107
7.3.2 Objective Function . . . 108
7.3.3 Problem Formulation . . . 109
7.3.4 Algorithms for Channel Assignment . . . 111
7.4 Generalization for Multiple Transmitter-Receiver Pairs . . . 112
7.4.1 Adjacent Channel Interference Formulation . . . 112
7.4.2 Framework for Channel Assignment . . . 114
7.4.3 Heuristic Algorithm: Simulated Annealing . . . 115
7.5 Simulation Results . . . 117
7.5.1 Single Transmitter, Multiple Receivers . . . 117
7.5.2 Multiple Transmit-Receive Pairs . . . 119
7.6 Conclusions . . . 123

**8 Scalability of Interference Networks with Receiver Nonlinearity 124**

8.1 Introduction . . . 124
8.1.1 Main Contributions . . . 125
8.2 Nonlinear Adjacent Channel Interference Network (NACIN) . . . 126
8.3 Adjacent Symbol Interference . . . 127
8.3.1 Intermodulation Interference . . . 128
8.3.2 Cross Modulation Interference . . . 129
8.4 Interference Avoidance in a $3 \times 3$ NACIN . . . 130
8.5 Practical Achievable Scheme for Interference Avoidance in a $N \times N$ NACIN . . . 132
8.5.1 Definitions and Notations . . . 132
8.5.2 Problem Formulation . . . 133
8.5.3 Practical Achievable Scheme . . . 134
8.6 Protection of Incumbent with Sensitive Receivers . . . 134
8.6.1 Problem Formulation . . . 135
8.6.2 Practical Achievable Schemes for Incumbent Protection . . . 136
8.7 Upper Bound Scalability for $3 \times 3$ NACIN . . . 138
8.8 Upper Bound for $N \times N$ NACIN . . . 141
8.9 Conclusions . . . 143

**9 Conclusions** **147**

**Bibliography** **151**

# List of Figures


1.1 Illustration of receiver diversity to adjacent channel interference: LTE receiver shows better tolerance than WiFi. . . . . 5

1.2 Impact of receiver characteristics on spectrum allocation. Figure reproduced from PCAST report [3] . . . . . 7

2.1 An illustrative schematic of the receiver front-end nonlinear system. . . . . 14

2.2 A measured example of third order intermodulation intercept point $\mathsf{IIP}_3$ . . . . . 16

2.3 Adjacent channel interference due to nonlinear distortion . . . . . 16

2.4 Detrimental effects of non-linear distortion in the presence of a strong adjacent channel interfering signal . . . . . 17

2.5 (a) Low power networks operating in the same band, under the umbrella of a high power base station (b) Illustration of co-channel Interference faced by low power cell networks operating under the umbrella of a high power LTE base station. . . . 19

2.6 Example of unutilized frequency resource blocks in LTE. . . . . 19

3.1 Taxonomy of Third Order Distortion Terms. . . . . 24

3.2 Example of matrix representation using unit basis vectors for two-tone intermodulation distortion . . . . . 35

3.3 Example of matrix representation using unit basis vectors for three-tone intermodulation distortion . . . . . 36

3.4 Example of expediency of representation using unit basis vectors for two-tone intermodulation distortion . . . . . 37

3.5 Comparison of the computational complexity as a function of number of bins, $N$ . 38

3.6 Simulation for validation of the proposed representations with the third order nonlinear model . . . . . 39

3.7 Schematic Diagram for Experimental Setup for Validation of Proposed Representation . . . . . 39

4.1 (a) Practical measured spectrum and computation of third order distortion levels (b) Variation of Mean Interference Power between 660 MHz-670 MHz due to Adjacent Channel Interference for different $\mathsf{IIP}_3$ and front-end filter Bandwidths for the measured spectrum. . . . . 52

4.2 Variation of Adjacent Channel Interference, $P_{\mathsf{ACI}}$ with $\beta$, $\mathsf{IIP}_3 = -15$ dBm. . . . . 54

4.3 Variation of Achievable Rate with $\beta$, $P = -60$dBm. . . . . 54

4.4 Variation of Achievable Rate with $\beta$, $P = -60$dBm, No Compressive Distortion. . 55

4.5 Variation of Fractional Rate Loss, $\varepsilon$ with $\beta$, $P = -60$dBm, No Compressive Distortion. . . . . 55

4.6 Bit Error Rate for RSC Coded 16-QAM system for different receiver nonlinearities 57

4.7 Bit Error Rate for RSC Coded 64-QAM system for different receiver nonlinearities 57

4.8 Schematic Diagram of Experimental Setup for Throughput Measurement. . . . . 59

4.9 Average variation of Fractional Rate Loss in a random radio environment and empirical upper bound . . . . . 61

5.1 System Model . . . . . 64

5.2 Variation of Sum Data Rate with IIP3 for $R_{min} = 0$ bps/Hz . . . . . 68

5.3 Sum Data Rates for different Minimum Rate Constraints . . . . . 69

5.4 Individual data rates achieved for each user for $R_{min} = 3$ bps/Hz . . . . . 70

5.5 Optimal Power and Bandwidth allocations for $R_{min} = 3$ bps/Hz . . . . . 70

5.6 Data Rates for Different Receiver Nonlinearity, $R_{min} = 3$ bps/Hz . . . . . 71

6.1 Illustration of heterogeneous nodes on different channels with diverse RF front-ends with a single transmitter . . . . . 74

6.2 Illustration of a receiver with $M$ pre-selector filters spanning the band of operation of $N$ channels, where $\frac{N}{M}$ is a positive integer. . . . . 80

6.3 Illustration of heterogeneous nodes with diverse RF front-ends sharing spectrum in the wireless network. . . . . 80

6.4 Example of transmit mask with Out Of Band Emissions (OOBE) where desired channel is $\ell = 3$. It ideally should restrict all transmit power to that channel. . . . . 90

6.5 Variation of Network Sum Rate with $\mathsf{IIP}_3$ diversity. Proposed Greedy Algorithm is close to true optimal solution. . . . . 90

6.6 Network Sum Rate with Increasing Node Density, pre-selector spans entire bandwidth: Receiver-Centric assignment is spectrally efficient with high gains for network scalability . . . . . 93

6.7 Network Sum Rate with Increasing Node Density, pre-selector spans a factor of bandwidth: High spectrum efficiency for Receiver-Centric assignment aids in network scalability . . . . . 93

6.8 Network Sum Rate with increasing $\mathsf{IIP}_3$ diversity: High spectrum efficiency gains for more diverse-RAT networks . . . . . 95

6.9 Sample convergence of proposed Simulated Annealing (SA) algorithm for $N = 8$: Order Optimal solution obtained . . . . . 95

6.10 Sample convergence of proposed Simulated Annealing (SA) algorithm for $N = 100$: $\sim 17,000$ iterations to converge . . . . . 97

6.11 Network Sum Rate with Increasing Node Density: Receiver-Centric assignment gives high spectrum efficiency gains, enabling scalability and node densification . . 97

7.1 An example direct conversion receiver architecture . . . . . 100

7.2 Transfer characteristics of a typical receiver . . . . . 100

7.3 Illustration of spectral redistribution in a receiver due to front-end impairments . . 101

7.4 Illustratiion on the importance of receiver-characteristics-aware resource allocation 102

7.5 Illustration of heterogeneous nodes with diverse RF front-ends with a single/co-located transmitter. . . . . 107

7.6 Illustration of heterogeneous nodes with diverse RF front-ends sharing spectrum in the wireless network . . . . . 113

7.7 Comparison of network throughput with varying diversity of receiver impairments: Significant spectrum efficiency gains with receiver impairment aware spectrum access. . . . . 119

7.8 Comparison of network throughput with increasing node density of receiver impairments: Significant spectrum efficiency gains with receiver impairment aware spectrum access. . . . . 120

7.9 Convergence of the SA Algorithm for a network with $N = 10$ nodes for a random network realization. . . . . 121

7.10 Comparison of network throughput with varying diversity of receiver impairments: Significant spectrum efficiency gains with receiver impairment aware spectrum access. . . . . 122

7.11 Comparison of network throughput with increasing node density of receiver impairments: Significant spectrum efficiency gains with receiver impairment aware spectrum access. . . . . 122

8.1 Nonlinear Adjacent Channel Interference Network (NACIN). Dashed lines represent interference . . . . . 126

8.2 $3 \times 3$ NACIN and Interference Avoidance through Transmitter Nulling . . . . . 130

8.3 practical achievable scheme with Interference Avoidance for NACIN . . . . . 133

8.4 Practical achievable schemes with Incumbent Protection for NACIN . . . . . 136

8.5 $3 \times 3$ NACIN . . . . . 138

8.6 Upper Bound for $N \times N$ NACIN . . . . . 143

# List of Tables

1.1 Experiment Specifications for comparison of LTE vs WiFi adjacent channel interference tolerance. . . . . 6

3.1 Experimental validation of proposed representation to evaluate nonlinear distortions in receivers . . . . . 40

5.1 Simulation Parameters . . . . . 67

7.1 Example Matrix Representation [102] of Receiver Impairments for $N = 4,\ Q = 2$ 106

8.1 Information received by different users per time slot . . . . . 139

# Chapter 1

# Introduction

The demand for quality wireless services and the number of connected devices has been increasing exponentially, and is expected to increase further in the future [1]. This places an enormous demand on the Radio Frequency (RF) spectrum. RF spectrum is well recognized as a finite natural resource, which can spur tremendous economic development [2, 3]. It is hence, expensive and tightly regulated. Traditionally, spectrum regulations were driven by dividing the entire RF spectrum into bands and licensing them to various services. With the exception of a few MHz of unlicensed bands, most spectrum at microwave frequencies until recently[1] was licensed to services for exclusive use based on long-term leases. Users not licensed to a particular band were legally prohibited to transmit in those bands, irrespective of its actual spatio-temporal occupancy by the original lease holders.

Consequently, this led to an extremely poor utilization of the scarce spectral resource, with large amounts of spectrum underutilized despite the mounting congestion on a small fraction of the overall RF spectrum. Large guard bands, lack of flexibility in spectrum reuse, and co-existence issues of different devices are among the many other factors leading to under-utilization of the available resource. In addition, several analytical and empirical spectrum occupancy models were also created to examine occupancy, and also revealed the under-utilization of spectrum [4–10]. Several researchers have pointed out that this model of exclusive spectrum allocation is inefficient and have emphasized that paving the way for co-existence through sharing and dynamic need-based allocations, could lead to a better utilization [3, 11–20].

Several technological advancements in recent years, such as LTE's carrier aggregation,

[1]The United States Federal Communications Commission (FCC) opened up the 3550-3700 MHz Citizen's Broadband Radio Service (CBRS) band for opportunistic access in 2015, but it is not yet operational.

multi-band radios, spectrum sensing, database driven spectrum management (e.g. IEEE 802.22 TV Whitespace) etc., enable radios to use the otherwise unused spectrum, dynamically as a function of time and geographical location. In order to ease spectral congestion and improve overall spectrum utilization, the FCC recently announced the adoption of a spectrum sharing model in the 3550GHz-3700GHz band [21, 22]. In addition, the recently auctioned AWS-3 band is also based on co-existence with military systems [23]. Worldwide, many such efforts are underway or have already been taken by several regulatory bodies in an effort to cope with the enormous demand for wireless spectrum. In order to ensure co-existence, and protect the systems operating in the same spectrum band from interference, several frameworks based on sensing, beacons, and driven by databases have been proposed [11]. Such frameworks will allow multitudes of radio access technologies to co-exist in the same band without causing harmful interference to each other. Next generation wireless networks will see an unprecedented diversity in radio access and RF front-end technologies operating in spatio-temporal-spectral proximity. Frameworks with co-existence and sharing have an onerous task of managing wireless networks with diverse technologies, optimizing over several parameters to maximize spectral efficiency.

One of the most important factors in wireless network design is the bandwidth requirement per node. While the communication link parameters specify the amount of spectrum required to achieve a given Quality of Service, in practice, individual receiver RF front-ends dictate the overall amount of spectrum *consumed* by a node in the network. Receiver front-ends contain nonlinear analog components that adversely affect performance. Nonlinearity makes the receivers susceptible to interference from adjacent channel signals, which can degrade the desired signal quality. Meticulous spectrum planning is imperative to avoid the detrimental effects of nonlinear adjacent channel interference.

Conventionally, receivers were protected from adjacent channel interference by carefully allocating static bands for transmitters with strict overlay mask regulations along with guard bands. Existing spectrum regulations impose stringent restrictions on transmitters and give a free hand to receiver designs, which purely concentrate on cost optimization with certain standardized performance constraints. This was largely based on an assumption that poor receivers with weak selectivity would be downplayed by the market. However this assumption was misplaced, since receivers were almost never vulnerable to adjacent channel interference [20, 24]. Next generation radio environments will present increased RF pollution, making receivers vulnerable to adjacent channel interference. The current framework of not accounting for receiver front-end nonlinearity, is insufficient when diverse Radio Access Technologies (RAT) with different overlay

mask regulations operate in the same band.

## Vulnerabilities of Open Ended Receiver Designs

Historically, the issue of interference due to intermodulation distortion surfaced way back in 1952 during the initial days of UHF television. Nicknamed as "UHF Taboos" [25, 26], the spectrum regulations and assignment were framed to avoid intermodulation distortion on operating channels. This was done by sufficiently spacing out transmitters in frequency, to ensure that the operating channels did not suffer any distortion due to receiver nonlinearity and imperfections. The rules however, were based on a projection of anticipated receiver performance. As a result, only one out of every six channels was usable for practical purposes in a given geographical location. This example reveals how the complex set of blanket rules agnostic to the specific characteristics and vulnerabilities receivers can lead to exceedingly low spectrum utilization and efficiency. Only with the advancement of digital technology were these rules relaxed to increase spectrum occupancy.

Another example of intermodulation distortion adversely affecting receiver operations is the impact of the commercial FM band below $107.6$ MHz on the the aviation safety Instrument Landing Systems (ILS) band between $108.10$-$111.95$ MHz [26]. The International Telecommunications Union-Radio communication sector (ITU-R) had to address this issue from a frequency assignment perspective to avoid harmful interference. The International Civil Aviation Organization has also prescribed stringent receiver performance norms for ILS systems to maintain operationability by alleviating intermodulation distortions even while facing strong adjacent channel signals. While imposing stringent receiver regulations work for specific systems, they will be counterproductive for diverse multi-RAT wireless networks, that strive to reduce the cost of consumer radios.

The controversy over Personal Communication Service (PCS) and auctioning the H block spectrum is another example of the complexities involved in spectrum regulations accounting for receiver vulnerabilities. The H block is a 10 MHz block of paired spectrum between $1915$-$1920$ MHz for the uplink and $1995$-$2000$ MHz for the downlink. The PCS band sits next to this spectrum, and concerns over interference from H block services to PCS mounted when the FCC wanted to auction the H block spectrum. This resulted in a gridlock perplexing auctions, innovations, and deployment for along time, and the FCC finally had to put various blanket rules on H block spectrum to ensure the protection of PCS band, making the H block less lucrative for prospective bidders. Dynamic management taking into account the specific vulnerabilities of actual receivers operating could

potentially have alleviated this issue instilling the necessary confidence for both PCS and H block users alike.

The LightSquared controversy of 2011 is also a classic testimony to the ill effects of open-ended receiver designs, devoid of ways to quantify their performance on spectrum efficiency. In early 2011 the FCC granted permission to a company named LightSquared to deploy terrestrial LTE repeaters in the L-band between 1525 MHz and 1559 MHz. It was anticipated that these repeaters would substantially improve the coverage, capacity and reliability of cellular systems. This band however, which is adjacent to the civilian GPS channels, also lies in the L-band from about 1560 MHz to 1610 MHz. Further to the clearance from FCC, LightSquared made elaborate plans and investment of close to $3B to roll out their technologies and solutions in the cellular market [27].

However, later that year, commercial GPS operators raised an objection to the deployment of the LTE repeaters stating that these would cause severe interference to the GPS systems operating in the adjacent band. The US National Telecommunication and Information Administration (NTIA) and the FCC then carried out detailed analysis and testing to see the impact of these repeaters on GPS receivers. The results threw a grim fact on the poor tolerance of commercial GPS receivers to adjacent channel signals, that the interference would practically make the GPS systems dysfunctional. Despite the fact that GPS receivers need very high sensitivity, the selectivity of those receivers was found to be so weak that their performance was being drastically affected by signals at sufficiently distant adjacent bands even with power levels of $-70$ dBm. As a result, the FCC was forced to suspend the access of those bands to LightSquared in February 2012. This took a heavy toll, on both wireless service and economic benefits brought with it. This problem could have been potentially avoided had the manufacturers of commercial GPS systems been encouraged to provide receivers with higher selectivity and better interference rejection.

Incorporation of quantifiable metrics on receiver performance and making them available to the consumer market would automatically build a healthy competition to provide good quality receivers. For example, policy driven notifications to consumers that poor receivers are liable to be denied service at certain times, will change the wireless market dynamics with the least possible impact to current beneficiaries. This will also help in significantly improving spectrum utilization and efficiency.

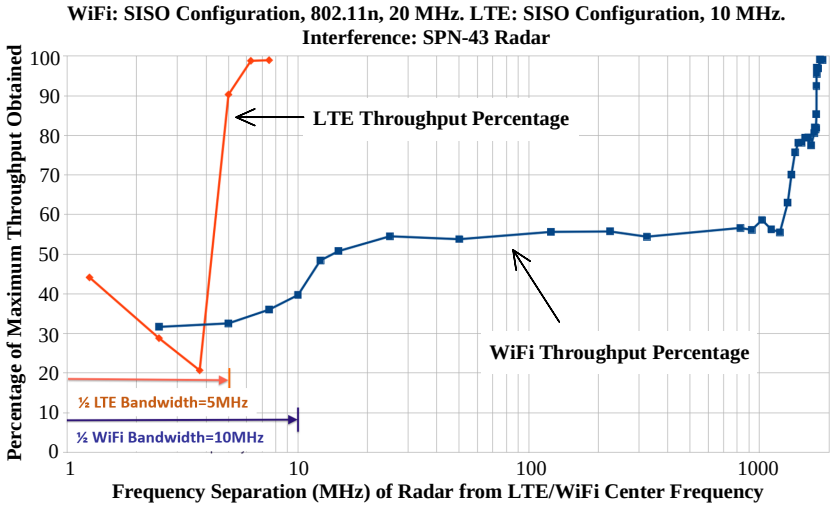


Figure 1.1: Illustration of receiver diversity to adjacent channel interference: LTE receiver shows better tolerance than WiFi.

# Illustration of Receiver Diversity: LTE vs WiFi

We provide an example on receiver diversity and how different receiver technologies have varied tolerance to adjacent channel blockers. Fig. 1.1 illustrates the results of a case study we carried out to examine the impact of receiver diversity on performance. It shows an experimental study on two widely used technologies: LTE and WiFi with setup in Table 1.1. It demonstrates the difference in susceptibility of LTE and WiFi receivers to adjacent channel interference. A SPN-43 radar signal was swept across frequency, in the channels overlapping and adjacent to LTE and WiFi. The degradation in throughput in each case was measured. The LTE receiver achieved almost $100\%$ of the maximum throughput as soon as the radar signal moved out of the channel, indicating a good out-of-band interference rejection capability. The WiFi receiver, on the other hand, has poor adjacent channel interference tolerance, even when the adjacent channel signal is $100$ MHz apart. This is in part due to the typical inexpensive WiFi receivers, having poor selectivity and wider nonlinear operating regions.

Table 1.1: Experiment Specifications for comparison of LTE vs WiFi adjacent channel interference tolerance.

| | |
|---|---|
| LTE Bandwidth | 10 MHz |
| LTE Configuration | TDD-SISO |
| LTE Power | $-33$ dBm in 10 MHz |
| WiFi Bandwidth | 20 MHz |
| WiFi Configuration | 802.11n, SISO |
| WiFi Power | $-30$ dBm in 20 MHz |
| Radar Pulse Interval | 889 ($\pm 20$) $\mu$s |
| Radar Pulse Width | 0.9 ($\pm 0.15$) $\mu$s |
| Radar Power | $-46.9$ dBm |
| Radar Bandwidth | 1.3 MHz |

# Benefits of Receiver Performance Characterization

A possible approach to increase spectrum efficiency and network performance is to impose stringent regulations on receiver performance. Receiver regulation is a very complex topic entangled in socio-economic, technological, and political aspects. In order to provide strong support of technological innovations, the 2012 PCAST report [3] recommended that regulation and guidelines must be carefully defined to facilitate the adoption of new technology while protecting legacy systems. However, consumer electronics generally disapprove the imposition of minimum performance regulations because of economic reasons. This could potentially end up in a gridlock, slowing down research, development, innovation, and economic growth.

The benefits of utilizing receiver characteristics for spectrum allocations are exemplified in Fig. 1.2 [3]. The three receivers A, B, and C along with their filter profiles are shown. The upper panel shows frequency allocation without the knowledge of receiver characteristics. An overlap indicated that signal from the other band would interfere causing degradation in performance, which happens in the upper panel of the figure. However, with knowledge of the receiver characteristics, a more informed allocation can take place so that all the receivers are protected without compromising spectrum efficiency. This is shown in the lower panel of the figure. Much better frequency allocation can be achieved with the knowledge of receiver characteristics, transmit power, receive power at the nodes by avoiding interference using a different signal band allocation scheme. It illustrates how knowledge of the receiver characteristics can be used to optimize the frequency allocation that minimizes guard bands while minimizing interference from adjacent channels to improve spectral and power efficiency over the entire network.

In this dissertation, we propose receiver-centric wireless design that obviates the need for receiver

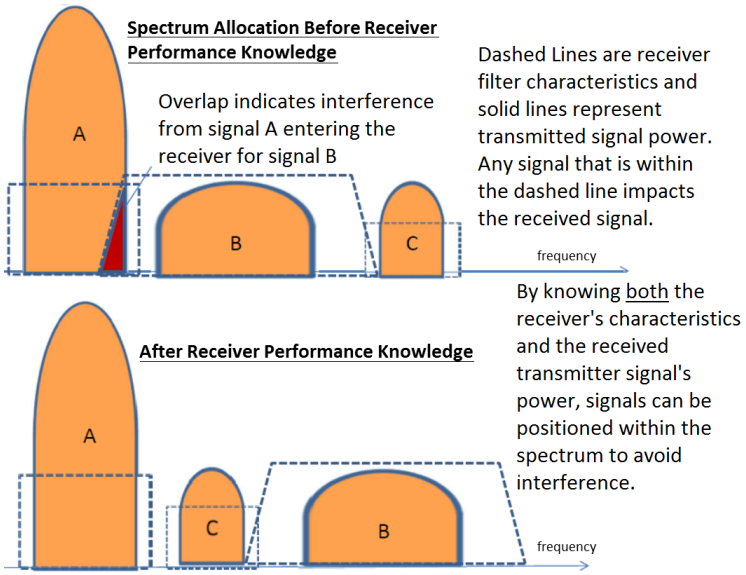


Figure 1.2: Impact of receiver characteristics on spectrum allocation. Figure reproduced from PCAST report [3]

regulation. The proposed analysis and framework incorporates the specific receiver performance and tolerance limits to optimize network objectives (e.g. network throughput). The need for this has been repeatedly emphasized in the reports of several regulating agencies [30–35] and requires a thorough characterization of receiver(s) in terms of spectrum occupancy and interference tolerance.

The model based spectrum management [36, 37] approach of the upcoming IEEE 1900.5.2 standard has asserted that the receiver models are indispensable for next generation dynamic spectrum access networks. By participating in the discussions in the standards committee meetings, we learned that the standard would prescribe simplistic receiver models as a necessary component for optimization, but would not describe means to specify or arrive at the receiver model and performance metrics. The proposed receiver characterization aims to provide a systematic approach to quantifying receiver performance for more efficient spectrum access and wireless network performance.

The Receiver Harm Claims Threshold as described by the FCC Technological Advisory Council in [30] will prescribe in-band and out-of-band interference tolerance limits for receivers, above which receivers can claim protection. In other words, receivers cannot claim any 'harmful' interference till the power levels reach the threshold limits. We are aware of the ongoing efforts by the Wireless Innovation Forum to describe the Harm Claims Threshold for receivers. Such a description, though useful for initial analysis, is insufficient to optimize and completely exploit the available spectrum. This is because, it is possible to optimize for a better network performance for the same interference

(or radio) environment, for example, through a simple re-arrangement of the channels allotted as illustrated in Fig. 1.2. Moreover, the definition of harmful interference itself depends on the technology and application, as elaborated in [38].

The harmful impact of two-tone intermodulation was previously reported in [39], with formulations to compute the in-band interference due to adjacent channel signals. However, the analysis was carried out for the specific case of only two adjacent channel carriers interfering with the desired signal. This perhaps was sufficient for traditional wireless systems, but is insufficient for next generation wireless systems which are foreseen to have unprecedented diversity of dense node distribution, accessing the same band of spectrum. An approximate analysis of two-tone interference intermodulation interference, in the presence of multiple adjacent channel signals and its harmful effects were discussed in [40]. While [40] provides the much needed basis for an initial study, the analysis is an approximation and lacks the holistic analysis of all the underlying phenomena observed in third order distortions. Also, none of the works thus far present a clear quantification of the receiver front-end performance. A comprehensive understanding of the impact of RF front-end nonlinearity on efficient spectrum access and co-existence is absent in the state-of-the-art.

## 1.1 Contributions

The dissertation deals with the fundamentals, limitations, and management strategies of efficient multi-RAT spectrum access and co-existence with receiver nonlinearity by broadly addressing the following questions:

*(a) How does receiver nonlinearity impact performance?*
*(b) How much does the nonlinearity affect performance?*
*(c) How can it be managed from a network level perspective?*
*(d) How scalable are these networks for dense deployment?*

### 1.1.1 Simplified Tractable Representations of Receiver Nonlinearity

Nonlinear response of the receiver front-end results in adjacent channel interference. In order to completely understand the impact of receiver nonlinearity on performance, it is imperative to get

a clear understanding of the spectral characteristics (equivalent to frequency response) of nonlinearity. In particular, formulations to track the changes in the output spectrum for a third order polynomial model of receiver is challenging, since such changes are functions of the input spectrum to the nonlinear system. Front-end nonlinear distortions result in the spectral redistribution of the input signal. In Chapter 3, we study how the receiver nonlinearity impacts performance. We propose a fundamental framework to analyze adjacent channel co-existence by quantifying the impact on performance of receiver RF front-end nonlinearity. We develop novel tractable discrete representations of third order intermodulation, cross-modulation, and compressive distortion of the receiver front-end to describe adjacent channel interference using unit basis vectors. We further validate the proposed representations through simulations and experimental measurements using Universal Software Radio Peripheral (USRP) X310 and B210 devices, for various front-end configurations.

### 1.1.2 Quantifying Impact of Receiver Nonlinearity on Performance

Metrics, that can be used to generate boundary values of performance, and comparing disparate receivers are important for future receiver development and standardization. In Chapter 4, we seek to address how much receiver nonlinearity affects performance. We analyze the impact of nonlinearity on receiver performance by evaluating the limits on achievable rate accounting for RF front-end nonlinearity. Based on this analysis we provide a framework to compare disparate receivers by forming generalized metrics. We then use these metrics to quantify the performance detriment for a reference input spectrum. We illustrate the importance of the proposed frameworks and the ensuing rate analysis for reference inputs for adjacent channel co-existence analysis and quantifying receiver performance, through theory and simulations. Further, we provide experimental throughput measurements using USRP X310 for different front-end configurations, and use these results to benchmark the proposed information theoretic receiver performance metrics.

### 1.1.3 Frameworks for Efficient Spectrum Access with Receiver Nonlinearity

Dynamic network optimization with the knowledge of receiver characteristics and vulnerabilities leads to a significant improvement in spectrum efficiency and utilization. This involves the development of network level frameworks and algorithms for spectral resource allocation

accounting for receiver nonlinearity and impairments. Adjacent channel interference due to nonlinearity imposes challenging constraints on the formulation of the joint optimization framework owing to the interplay between variables. In this contribution, we propose receiver-centric frameworks that account for receiver front-end nonlinearity and impairments for networks with diverse RF layer characteristics. Further, we propose computationally efficient algorithms to optimize the receiver-centric frameworks and examine network level performance gains, describing how to manage receiver nonlinearity from a network level perspective.

In Chapter 5, we develop a dynamic resource allocation (bandwidth and power control) framework which accounts for nonlinear distortions due to adjacent channel interference in receivers, for a two user case. We use this framework for maximizing sum data rate with minimum rate constraints. We optimize over transmit powers and bandwidth allocations for the users based on their nonlinearity and minimum rate requirements. We demonstrate though simulations that receiver nonlinearity-aware resource allocation will yield a considerably higher network data rate and spectrum efficiency while ensuring the minimum required Quality of Service for all users.

Channel assignments (spectral arrangement of nodes) agnostic to receiver characteristics can have a severe detrimental effect on network level performance of a wireless network. In Chapter 6, we develop a novel dynamic channel assignment framework which accounts for the vulnerabilities imposed by the RF front-end, in particular, receiver front-end nonlinearity, pre-selector filter bandwidth, and transmitter out-of-band emission characteristics. In Chapter 7, we extend this framework to include other receiver front-end impairments, namely, poor image frequency rejection, phase noise, and ADC aliasing. We propose computationally efficient algorithms to optimize the receiver-centric framework and examine network level performance. We demonstrate through extensive network simulations that the proposed receiver-centric framework provides substantially high spectrum efficiency gains over receiver-agnostic spectrum access and ensures co-existence in dense and diverse next generation wireless networks. We further demonstrate through simulations that the proposed algorithms achieve order-optimal solutions for complex receiver-centric network optimization.

### 1.1.4 Scalability of Interference Networks with Receiver Nonlinearity

The contributions discussed hitherto, concentrated on maximizing the network sum rate through efficient channel allocation so as to minimize the impact of nonlinear adjacent channel

interference. The fundamental questions regarding the scalability of such networks through network level interference avoidance are addressed in this contribution. The next generation wireless networks in heterogeneous and dynamic spectrum environments, whose operations are constrained by the nonlinear interference emanating from signals on adjacent channels, are termed Nonlinear Adjacent Channel Interference Networks (NACIN) in this dissertation. In Chapter 8, we propose practical achievable schemes for interference avoidance and assess the scalability of the next generation NACIN. We further propose schemes for complete interference protection from secondary operations in adjacent channels in the spatio-temporal vicinity of incumbents with sensitive receiver requirements. Next, we propose algorithmic schemes to evaluate the upper bounds on the performance of such networks. Through numerical evaluations, we analyze the performance of proposed practical achievable schemes relative to the upper bounds. Valuable insights on scalability and schemes for nonlinear adjacent channel interference avoidance in next generation shared spectrum networks with co-existence are the outcomes.

### 1.1.5 List of Relevant Publications

The work presented in this dissertation is primarily based on the following publications:

1. Aditya V. Padaki, Ravi Tandon and Jeffrey Reed, "On Adjacent Channel Co-existence with Receiver Nonlinearity" *Under Review, IEEE Transactions on Wireless Communications*

2. Aditya V. Padaki, Ravi Tandon and Jeffrey Reed, "Receiver-Centric Efficient Spectrum Access: Adapting to RF Front-End Nonlinearity," *Under Review, IEEE Transactions on Wireless Communications.*

3. Aditya V. Padaki, Eyosias Y. Imana, Vuk Marojevic, Taeyoung Yang, Ravi Tandon and Jeffrey Reed, "Receiver Impairments Aware Efficient Spectrum Access and Co-Existence for Multi-RAT Wireless Networks," *Under Review, IEEE Transactions on Vehicular Technology.*

4. Aditya V. Padaki, Ravi Tandon and Jeffrey Reed, "Scalability of Interference Networks with Receiver Nonlinearity," *Under Preparation, to be submitted to IEEE Transactions on Communications.*

5. Aditya V. Padaki, Ravi Tandon and Jeffrey Reed, "On Scalability and Interference Avoidance in Nonlinear Adjacent Channel Interference Networks," *IEEE ICC 2017*, May 2017, Paris,

France.

6. Aditya V. Padaki, Vuk Marojevic, and Jeffrey Reed, "Impact of RF front-end Nonlinearity on Dynamic Spectrum Access Networks," *Half Day Tutorial, IEEE DySPAN 2017*, March 2017, Baltimore, USA.

7. Aditya V. Padaki, Ravi Tandon and Jeffrey Reed, "Efficient Spectrum Sharing with RF Diversity: Adapting to Nonlinearity of front-ends," *IEEE GLOBECOM 2015*, December 2015, San Diego, CA, USA.

8. Aditya V. Padaki, Ravi Tandon and Jeffrey Reed, "Receiver Non-Linearity Aware Resource Allocation for Dynamic Spectrum Access Systems," *IEEE MILCOM 2014*, October 2014, Baltimore, Maryland, USA.

9. Aditya V. Padaki, Vuk Marojevic and Jeffrey Reed, "Role of Receiver Performance Data in Efficient Spectrum Utilization," *IEEE DySPAN 2014*, April 2014, Washington DC, USA.

10. Aditya V. Padaki and Jeffrey Reed, "Impact of Intermodulation Distortion on Spectrum Preclusion for DSA: A New Figure of Merit," *IEEE DySPAN 2014*, April 2014, Washington DC, USA.

Other related publications include:

1. Amr Nabil, Aditya V. Padaki, Mohammad J. Abdel Rahman, Allen MacKenzie, and Jeffrey Reed, "On the Optimal Resource Allocation in Multi-RAT Wireless Networks with Receiver Characteristic Awareness," *Under Preparation, to be submitted to IEEE Transactions on Cognitive Communications and Networking.*

2. Jennifer DSouza, Aditya V. Padaki, Vuk Marojevic, and Jeffrey Reed, "Analysis of Symbol Error Rate with Receiver Non-linearity for M-PSK Modulation," *Under Review, IEEE ICC 2018*.

3. Amr Nabil, Aditya V. Padaki, Mohammad J. Abdel Rahman, Allen MacKenzie, and Jeffrey Reed, "Receiver Characteristic Aware Optimal Resource Allocation in Multi-RAT Wireless Networks," *IEEE PIMRC 2017*, Montreal, Canada.

4. Jeffrey Reed, Andrew Clegg, Aditya V. Padaki, Taeyoung Yang, Carl Dietrich, Christopher Anderson, Mike Mearns, "On the co-existence of TD-LTE and radar over 3.5 GHz band: An experimental study," *IEEE Wireless Communications Letters,* August 2016.

5. Aditya V. Padaki, Ravi Tandon, and Jeffrey Reed, "Network Aware Spectrum Efficiency Metric for Heterogeneous and Dynamic Radio Environments," *2014 Asilomar Conference on Signals, Systems and Communications*, November 2014, Pacific Grove, California, USA.

6. Aditya V. Padaki, Avik Sengupta, Mahi Abdelbar, Jeffrey Reed, and William Tranter, "An Orthogonal Spectrum Sharing Scheme for Cognitive LTE Networks," *SDR-WinnComm 2014*, March 2014, Chicago, IL, USA.

7. Stephen M. Dudley, William C. Headley, Marc Lichtman, Eyosias Y. Imana, Xiaofu Ma, Mahi Abdelbar, Aditya V. Padaki, Abid Ullah, Munawwar M. Sohul, Taeyoung Yang, and Jeffrey Reed, "Practical Issues for Spectrum Management with Cognitive Radios," *Proceedings of the IEEE*, vol. 102, no. 3, pp.242-264, March 2014.

## 1.2 Organization of the Dissertation

This dissertation is organized as follows: In Chapter 2, we give the necessary background and context for the dissertation. In Chapter 3, we develop novel tractable representations to understand how receiver nonlinearity impacts performance. In Chapter 4, we develop the quantification of receiver performance using information theoretic metrics. In Chapter 5, we develop a receiver nonlinearity aware network resource allocation framework for a two-user case, and demonstrates the potential benefits of accounting receiver characteristics for spectrum access. In Chapter 6, we give a comprehensive receiver-centric spectrum access frameworks and algorithms accounting for pre-selector filter bandwidth, front-end nonlinearity, and leakage due to transmission masks. In Chapter 7, we develop receiver impairment aware spectrum access frameworks and algorithms accounting for imperfect image frequency rejection, phase noise, and ADC aliasing. In Chapter 8, we introduce adjacent channel interference networks with receiver nonlinearity, with practical achievable schemes and upper bounds on scalability. Finally, in Chapter 9, we conclude the dissertation.

# Chapter 2

# Preliminaries and Background

## 2.1 Receiver Model and Nonlinearity

We consider a memoryless polynomial receiver model with input-output relation described by [41–44],

$$V_{\mathsf{out}} = \alpha_0 + \alpha_1 V_{\mathsf{in}} + \alpha_2 V_{\mathsf{in}}^2 + \alpha_3 V_{\mathsf{in}}^3 + \alpha_4 V_{\mathsf{in}}^4 + \dots \tag{2.1}$$

where $V_{\mathsf{in}}$ is the input, $V_{\mathsf{out}}$ is the output, $\alpha_i$'s are the coefficients for $i^{th}$ order terms, and $\alpha_1$ is the linear gain of the RF chain. An illustrative schematic of the receiver front-end is shown in Fig. 2.1. The pre-selector filter is the foremost filter of the front-end. Note that each component exhibits a nonlinearity and the entire receiver can be approximated by the equation (2.1) analyzing the nonlinearity in cascade [41].

When subjected to a two tone input of the form, $V_{in}(t) = A_1 \cos(\omega_1 t) + A_2 \cos(\omega_2 t)$, the several terms that feature in the output, $V_{out}(t)$ are: (1) The DC term is given by the $\alpha_0$, although not the only DC term. (2) The first order term produces outputs at $\omega_1$ and $\omega_2$. (3) The second order term

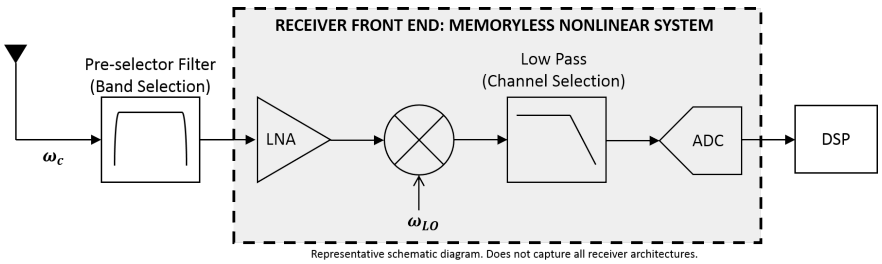


Figure 2.1: An illustrative schematic of the receiver front-end nonlinear system.

produces outputs at DC, $\omega_1 - \omega_2$ and $\omega_1 + \omega_2$. (4) The third order term produces outputs at DC, the fundamental frequencies ($\omega_1$ and $\omega_2$), third order harmonics ($3\omega_1$ and $3\omega_2$), and certain new frequencies at $2\omega_1 + \omega_2$, $\omega_1 + 2\omega_2$, $2\omega_1 - \omega_2$ and $2\omega_2 - \omega_1$. In this, we observe that $2\omega_1 - \omega_2$ and $2\omega_2 - \omega_1$ fall in the region of operation of the device, while others can be filtered out. (5) The fourth order term generates outputs at DC, $2\omega_1$, $2\omega_2$, $4\omega_1$, $4\omega_2$, $\omega_1 \pm \omega_2$, $2\omega_1 \pm 2\omega_2$, $3\omega_1 \pm \omega_2$ and $3\omega_2 \pm \omega_1$ and so on.

In general, we can easily deduce that the two tone input generates distortions at various frequencies surrounding the harmonics of both the input signals. At a given harmonic, the frequencies produced are spaced at $\Delta\omega = \mid \omega_1 - \omega_2 \mid$. We can thus generalize the spurious frequencies to be present at $\omega_{out} = \mid \pm p\omega_1 \pm q\omega_2 \mid$ where $p$ and $q$ assume positive integer values. Upon expanding the terms, we also find that the power of the intermodulation signals decreases as the polynomial order increases. The three-tone intermodulation products are generated at $\omega_i + \omega_j - \omega_k; \forall i, j, k \in [1, N], i \neq j \neq k$. In addition, there are crossmodulation products and compressive distortion terms [41, 42].

The even order terms produce harmonics outside the desired band, which can easily be filtered out, while the odd order terms on the contrary produce intermodulation terms within the desired band [41,42]. The third order term contributes significantly more to the in-band distortion products than the other odd order harmonics. Thus, a third order approximation gives a good estimate of the non-linearity for receivers. To quantify the extent of non-linearity, a standard procedure is to extend the third order and the fundamental curves on the transfer characteristics plot of powers on the decibel scale, so that they intersect. The point of intersection is known as third order intercept point or $\mathsf{IIP_3}$ [41, 42, 46] (or Intermodulation Intercept Point). It can be shown that, $\mathsf{IIP_3} = \sqrt{\frac{4}{3}\left|\frac{\alpha_1}{\alpha_3}\right|}$ [41, 42]. Throughout the discussion, we assume a linear gain, $\alpha_1 = 1$. Thus, we have $\alpha_3 = \left(\frac{4}{3}\frac{1}{\mathsf{IIP_3}^2}\right)$ in terms of $\mathsf{IIP_3}$. Note that this $\mathsf{IIP_3}$ denotes the nonlinearity for the entire receiver front-end chain. This can be computed easily by cascade modeling of the nonlinearity of each receiver component or stage [41, 42]. Example values of $\mathsf{IIP_3}$ are $-16$ dBm for 802.11n dual band WiFi receivers, $-5$ dBm for 3G/WCDMA receivers, and $0$ dBm for LTE receivers [47, 48].

## 2.2 Why is Nonlinear Distortion a Problem?

Nonlinear distortion adversely affects the receiver performance, especially when the interacting signals operate in the nonlinear region of the receiver. Fig. 2.3a shows the resulting adjacent channel interference for a receiver approximated by the third order model, with an $\mathsf{IIP_3}$ of

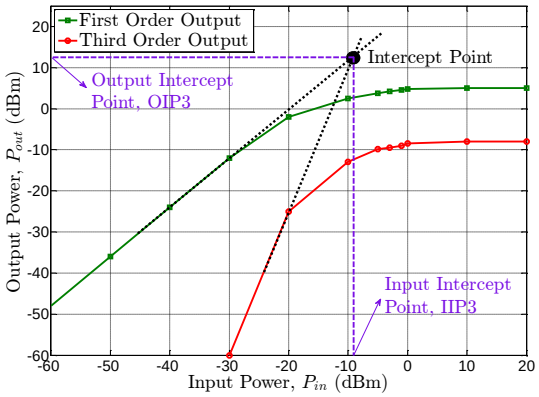


Figure 2.2: A measured example of third order intermodulation intercept point $\mathsf{IIP}_3$

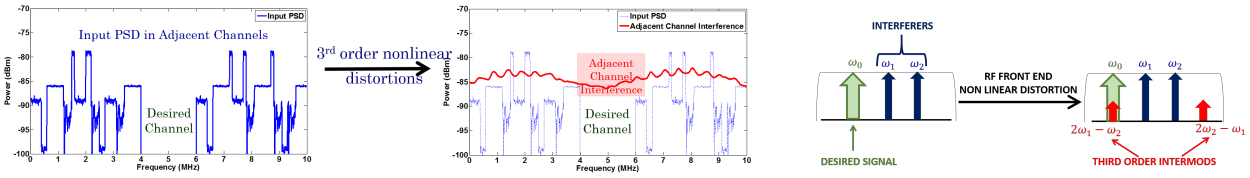


(a) (b)

Figure 2.3: Adjacent channel interference due to nonlinear distortion

$-10$ dBm. Consider three band limited signals in adjacent channels, centered around frequencies $\omega_0$, $\omega_1$, and $\omega_2$ such that $\mid \omega_0 - \omega_1 \mid = \mid \omega_1 - \omega_2 \mid$. Suppose that they enter the pre-selector filter of a receiver whose desired signal is centered around $\omega_0$, as shown in Fig. 2.3b. The third order distortion results in a double convolution of the signals in the frequency domain and produces an intermodulation interference product centered directly around the desired signal, $\omega_0 = 2\omega_1 - \omega_2$. Fig. 2.3b illustrates detrimental effect that adjacent channel signals can cause for a desired signal. The possible ways in which nonlinear distortion can be avoided are reducing the signal power and having multiple overlapping narrow band pre-selector filters, such that adjacent channel signals do not enter the front-end. The former is an infeasible option and the latter has cost and design constraints.

To illustrate the extent of detriment of non-linear distortion, we present the results of a simulation experiment in Fig. 2.4. We wish to draw the attention of the reader to the fact that nonlinear distortion due to adjacent channel interference can cripple the receiver performance as compared to co-channel interference, which can be overcome by increasing the in-band desired signal power. We vary the desired received signal power. Note the changes to $\mathsf{SINR}$ in the presence of only co-channel interference and compare it with the case where only adjacent channel

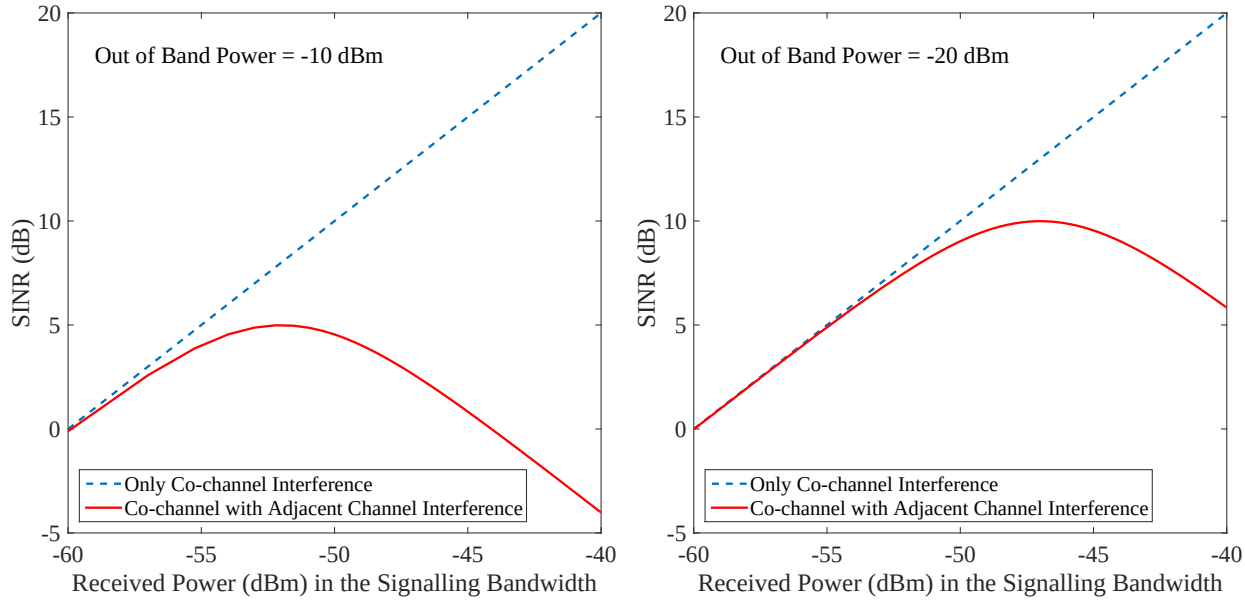


Figure 2.4: Detrimental effects of non-linear distortion in the presence of a strong adjacent channel interfering signal

interference is present. In both cases, powers of interfering signals were equal. As seen from the figure, if the interfering signal is strong enough, co-channel interference can be overcome by increasing the transmit power (and thereby increasing the received power). However, adjacent channel interference due to nonlinear distortion can potentially jeopardize the entire receiver operation, since increasing the transmit power of the desired signal also will adversely affect the performance. Thus, adjacent channel interference can be extremely detrimental if not carefully managed [49].

## 2.3 Elevated Noise Floor

In this section, we briefly mention why receivers will likely operate in the nonlinear region of the RF front-end in next generation networks. Ideally, the noise floor for a receiver is given by $N_0 = kTB$, where $k$ is Boltzmann's constant, $T$ is the temperature, and $B$ is the bandwidth. At room temperature, this assumes a value of $-175$ dBm/Hz. However, wireless technologies of the future will face a substantially higher ambient noise due to RF pollution, which will increase the overall noise floor. In this section, we discuss the various reasons for the elevation of the noise floor in futuristic wireless systems.

**Large Pre-selector Bandwidths**

The receivers of next generation networks need to operate in a wide range of channels covering multiple bands. In order to reduce the cost of consumer electronics, the pre-selector filter will likely span a wide bandwidth. For example, in the newly opened 3.5 GHz CBRS, while the operating channel bandwidth is only 10 MHz, the receivers need to offer agile access covering 150 MHz of bandwidth. Large front-end filters will significantly increase the noise floor of the receivers, pushing their operations to nonlinear regions.

**Co-existence of a Low Power Small Cell under the 'Umbrella' of a High Power Macro Cell**

Next generation networks will consist of small cell and device-to-device operations under an umbrella of a macro cell as shown in Fig. 2.5a. Many such networks will be deployed in the same band by service providers, so that they operate without causing interference to the macro cell base station and devices. However, these low power small networks will face interference from the macro cell base station. This will severely increase the co-channel interference and hence the noise floor for receivers in low power networks. As an example, in Fig. 2.5b, we present the received power (which is co-channel interference) from a macro cell LTE base station transmitting at the maximum EIRP of 62 dBm, prescribed in 3GPP standards, using the Cost-231 Hata propagation model for various frequencies. For $1$ MHz bandwidth, the noise floor can potentially increase from $-105$ dBm to about $-60$ dBm or more due to co-channel interference, as seen from the figure.

**Operation in 'Spectrum Holes' Around Multi-Carrier Modulation Signals**

Multi-carrier modulations are widely used in state-of-the-art wireless systems (e.g. LTE, WiFi). However, at a given spatio-temporal location, the entire frequency resource may not be occupied. These frequencies may be dynamically accessed by other technologies or by other users of the same service (e.g. small cells, device-to-device, etc.). However, the spectral tail of multi-carrier modulation systems presents a substantially increased ambient noise level in the unused frequencies.

To illustrate this, we used the Rhode & Schwarz CMW 500 Wide Range Communication Tester as an LTE base station transmitting a downlink OFDM signal with QPSK modulation at $751$ MHz

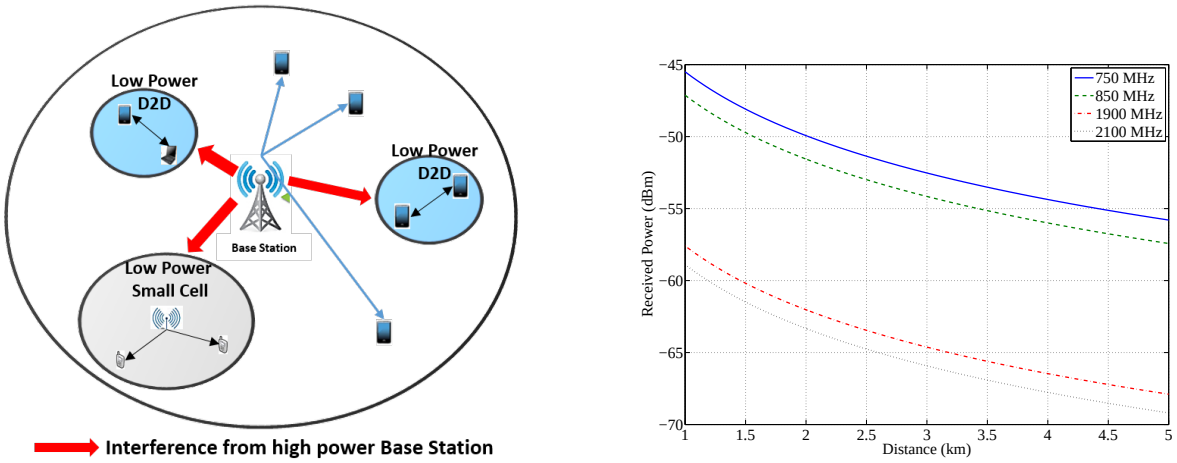


(a) (b)

Figure 2.5: (a) Low power networks operating in the same band, under the umbrella of a high power base station (b) Illustration of co-channel Interference faced by low power cell networks operating under the umbrella of a high power LTE base station.

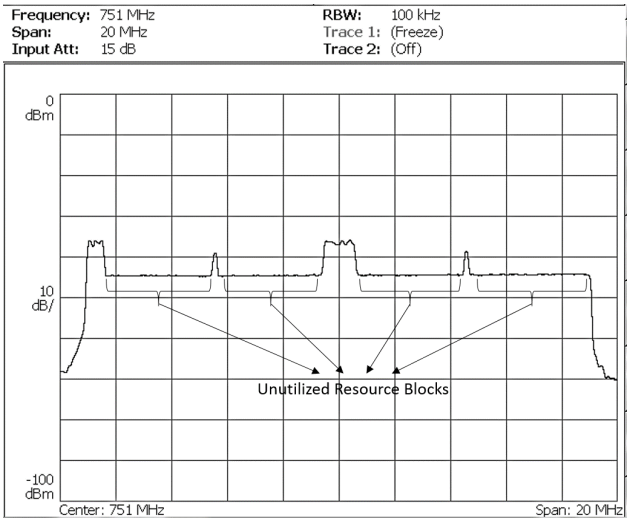


Figure 2.6: Example of unutilized frequency resource blocks in LTE.

for a $20$ MHz bandwidth with maximum configurable transmit power of the tester ($-38.7$ dBm). The output of the spectrum analyzer for this signal is shown in Fig. 2.6. The noise floor in the frequency resources adjacent to the occupied blocks are just $5$-$7$ dB lower than the maximum power. Irrespective of the maximum transmit power, the spectral splatter characteristics remain the same for this signal. Thus, services and users operating in the 'Spectrum Holes' around such multi-carrier modulation schemes suffer from a substantially high ambient noise power.

**Operation in Bands Adjacent to High Power Transmitters**

With new spectrum opening up for sharing with high power incumbents (e.g. Radars in 3.5 GHz, TV stations), the bands adjacent to these very high power transmitters can potentially get polluted with high noise power. The transmit power of the radars can be sufficiently high to substantially increase the ambient noise (or interference) power at channels adjacent to its operating frequency. The services and users operating in this region, thus will have to overcome this noise power to achieve the desired QoS.

**Dense Networks with Uncoordinated Power Control**

As described earlier, future wireless networks will comprise of diverse technologies with several heterogeneous networks operating in close geographic proximity. It is possible to reduce the average noise power due to interference if the power control across all devices of all technologies is centrally optimized. However, practical realization of such power control is not feasible, and at best networks can individually optimize for power levels. Due to the inherent heterogeneity and diversity of technologies, the inter-network interference will increase, thereby substantially increasing the overall noise floor.

**Rapidly Changing Radio Environment**

Dynamic Spectrum Access opens up a plethora of opportunities to intelligently exploit spectrum usage by various services. This changes the dynamics of radio environment from existing patterns to a more rapidly changing environment. This will make the devices vulnerable to changes in the radio environment. These changes can manifest in many ways, for example, as a sudden increase in the noise floor or presence of a high power adjacent channel signal. This will change the expected

noise floors in radios, which have to be prepared to accept interference, especially if the devices are secondary users in a shared spectrum framework.

**Noise Floor Elevation and Receiver Non-Linearity**

The noise floor elevation for radio systems pushes the networks to operate at powers closer to the saturation region of receivers to achieve the desired QoS. As the received signal power increases beyond the linear region of the receivers, the receiver non-linearity adversely affects receiver performance, causing distortions to desired signals. However, accounting for receiver nonlinearity during wireless network design and spectrum management can significantly increase spectrum efficiency [50, 51].

# Chapter 3

# Simplified Tractable Representations of Receiver Nonlinearity

## 3.1 Introduction

In order to efficiently manage spectrum dynamically, tractable models which describe the impact of adjacent channel signals are essential. A precise understanding of the nonlinear phenomena in receivers from a spectrum-centric point of view was neither required nor relevant to address the practical engineering problems of static spectrum planning. Consequently, the exact impact of one or more adjacent channel signals at given spectral locations relative to the desired signal in a channelized radio receiver has not been studied. A clear representation of the spectral redistribution and the signals affecting a given desired channel is required in the next generation dynamic and heterogeneous radio environments for various purposes such as evaluation of interference, interference management, possible interference mitigation, efficient spectral planning, efficient RF systems design, among many other things. We develop a precise, computationally efficient framework to evaluate the adjacent channel interference in a given radio/spectrum environment based on the third order nonlinear model. We seek not only to specify a means to evaluate the adjacent channel interference power (at a given desired channel), but also the exact adjacent channels that contribute to the interference at the desired channel.

While receiver nonlinearity has been studied in great detail by several researchers [40–42, 52–55, 57–59], an exact spectral characterization of the kind required for *adjacent channel co-existence analysis*, is missing in the literature. In [60] the spectral location based effect of interferers on cognitive radio receiver operations was presented for specific and

limited cases of 3 and 4 interfering signals. The impact of two adjacent channel blockers on sensing with nonlinear receivers has been studied in [61]. The impact of other receiver impairments like IQ imbalance and mirror images and its mitigation, has been previously studied in [52, 62] Digital compensation through suppression of nonlinear distortions in wideband receivers was discussed in [53, 54]. Past works specify the number of distortion products at a given frequency bin [57, 59] but do not specify which frequencies impact a given frequency bin, how to calculate the exact distortion power, nor is there any such representative model. This chapter develops a systematic framework which re-imagines the third order nonlinearity to create a compact and convenient model, which acts as a technology enabler for multi-RAT co-existence, efficient spectrum access, and nonlinear adjacent channel interference cancellation, among other things.

### 3.1.1 Main Contributions

We present a new mathematical workbench with compact and computationally simpler methodology for frequency specific third order distortion calculations, based on the well established third-order nonlinear model. This is important for co-existence analysis in adaptive radio technologies (cognitive radios, opportunistic access, etc.). In the process, we have explored some important nuances required for this, that have been left out in the literature. The main contributions of this chapter are:

1. We develop tractable discrete representation of spectrum redistribution for third order polynomial approximation of the RF front-end, to describe the phenomena of third order intermodulation, cross-modulation and compressive distortion of the receiver front-end nonlinear distortions (also in Section 3.4). This representation aids in the adjacent channel co-existence analysis of multi-RAT systems, can be utilized for system level design and network optimization, and can be used for quantifying receiver performance;

2. We analyze two-tone (pairwise) and three-tone (triplet) intermodulation, unitary and pairwise cross-modulation, and compressive distortion, and propose formulations for exact identification of all the adjacent tones of these terms for a given channel in Section 3.4. This enables a clear understanding of the nonlinear adjacent channel interference;

3. We carry out simulation and experimental validations of the proposed framework to evaluate adjacent channel interference using USRP platforms in Section 3.5.

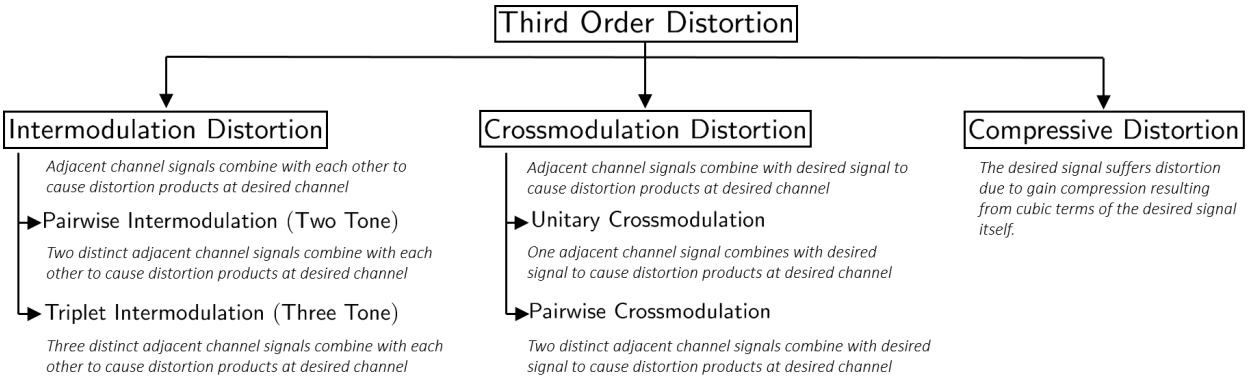


Figure 3.1: Taxonomy of Third Order Distortion Terms.

In Section 3.2, we describe the taxonomy and background, and in Section 3.3, we describe a representation using Toeplitz matrices.

## 3.2 Preliminaries: Taxonomy and Background

In Fig. 3.1 we formally describe the taxonomy of the various effects due to third order distortions. We refer to this taxonomy throughout this chapter.

Let an arbitrary input signal with the spectrum $A(f)$ enter the receiver chain with pre-selector filter bandwidth $B << f_n \in [f_1, f_N]$, where $[f_1, f_N]$ denotes the set of carrier frequencies that the pre-selector spans (or the receiver operates). The spectral mix up (redistribution) from intermods and crossmods, due to receiver RF front-end nonlinearity results in Adjacent Channel Interference (ACI). This interference falls in the desired channel and elevates the noise floor. However, unlike the typical white noise, the adjacent channel interference is frequency selective. We denote the amplitude spectrum of this frequency selective noise, which essentially is the additive adjacent channel interference, by $P_{\mathsf{ACI}}(f)$. This can potentially cause a significant drop in the achievable rate for a given receiver. A clear understanding of the spectral redistribution is imperative for efficient spectral planning, allocation, and evaluation of achievable rates of non-ideal receivers.

In practice, it is easy to deal with discrete models. Thus, consider that the input power spectral density is discretized in the frequency domain. Further, let $\boldsymbol{A} = [A_1 \; A_2 \ldots A_B]^T$ represent a $B \times 1$ vector of the discretized input spectrum $A(f)$ for a receiver pre-selector with bandwidth $B$. In general, the entire pre-selector filter can be equally divided into $N$ frequency bins, with each bin centered around a frequency $f_n$, $n \in [1, N]$, having a frequency width of $\mathcal{W} = \frac{B}{N}$. We then

represent $\boldsymbol{A}$ by a $(N \times 1)$ vector, whose $n^{\text{th}}$ entry is, $A_n = \int_{f_n - \frac{\mathcal{W}}{2}}^{f_n + \frac{\mathcal{W}}{2}} A(f)\, df = \sqrt{\int_{f_n - \frac{\mathcal{W}}{2}}^{f_n + \frac{\mathcal{W}}{2}} 2P(f)\, df}$ where $P(f)$ is the RMS received power spectral density. We choose to use the amplitude spectrum instead of the power spectrum for ease of representation and tractability of nonlinearity. The discrete amplitude spectrum of adjacent channel interference due to third order nonlinearity is represented by the vector $\boldsymbol{\rho}$.

## 3.3 Representation Using Toeplitz Matrices

We need the frequency domain representation of the spectral redistribution resulting from third order nonlinearity. The third order term $\{V_{\text{in}}^3\}$ in the time domain will result in a double convolution in the frequency domain. If $A(f)$ is the spectrum at the input of the receiver, the frequency domain model for ACI, $\rho(f)$ can be written as,

$$\rho(f) = A(f) * A(f) * A(f) = \alpha_3 \int_{-\infty}^{\infty} s(\nu) A(f - \nu) d\nu \tag{3.1}$$

where $s(f) = \int_{-\infty}^{\infty} A(-\nu) A(f - \nu) d\nu$ is the first convolution, $\nu$ is the dummy convolution variable, the integration limits denote the length of convolutions, and $(*)$ represents convolution. $\rho(f)$ in the range $f_1 \leq f \leq f_2$ gives the in-band ACI.

For band limited spectrum, whose $f_c >> B$, where $f_c$ is the center frequency of spectrum, and $B$ is the total bandwidth in consideration, it suffices to consider only the positive part of the spectrum for evaluating the spectral redistribution. Consider now, the discrete model, with the positive part of the input spectrum represented by $\boldsymbol{A} = [A_1 A_2 \dots A_N]^T$. The spectrum of adjacent channel interference can be deduced as $\boldsymbol{\rho} = [\rho_1\ \rho_2\ \cdots\ \rho_{(3N-2)}]^T = \alpha_3(\boldsymbol{A} * \boldsymbol{A} * \boldsymbol{A})$, where $(*)$ represents convolution operation. A matrix whose entries are constant on each diagonal is called a Toeplitz matrix. Toeplitz matrices are often used to represent discrete convolution [63–65]. Details of its application to convolution are provided in [64]. Consider the Toeplitz matrices formed with the PSD vector $\boldsymbol{A}$: $\mathbf{Q}$ is a Toeplitz matrix of $\boldsymbol{A}$ with dimensions $(3N - 2) \times (2N - 1)$, and $\mathbf{R}$ is a Toeplitz matrix of $\boldsymbol{A}$ with dimensions $(2N - 1) \times N$.

$$\mathbf{Q} = \underbrace{\begin{bmatrix} A_1 & 0 & 0 & \cdots & 0 \\ A_2 & A_1 & 0 & \cdots & 0 \\ A_3 & A_2 & A_1 & \cdots & 0 \\ \vdots & \ddots & \ddots & \ddots & \vdots \\ A_N & A_{N-1} & A_{N-2} & \ddots & 0 \\ 0 & A_N & A_{N-1} & \ddots & 0 \\ \vdots & \ddots & \ddots & \ddots & \vdots \\ \vdots & \ddots & \ddots & \ddots & \vdots \\ 0 & 0 & \ddots & \ddots & A_N \end{bmatrix}}_{(3N-2)\times(2N-1)}; \quad \mathbf{R} = \underbrace{\begin{bmatrix} A_N & 0 & 0 & \cdots & 0 \\ A_{N-1} & A_N & 0 & \cdots & 0 \\ A_{N-2} & A_{N-1} & A_N & \cdots & 0 \\ \vdots & \ddots & \ddots & \cdots & \vdots \\ A_1 & A_2 & A_2 & \cdots & A_N \\ 0 & A_1 & A_1 & \cdots & A_{N-1} \\ \vdots & \ddots & \ddots & \ddots & \vdots \\ \vdots & \ddots & \ddots & \ddots & \vdots \\ 0 & 0 & \ddots & \ddots & A_1 \end{bmatrix}}_{(2N-1)\times(N)} \tag{3.2}$$

The adjacent channel interference can be represented as, $\boldsymbol{\rho} = \frac{3}{4}\alpha_3 \mathbf{Q}\mathbf{R}\boldsymbol{A}$. The output power vector of the RF chain, $\boldsymbol{A}_{\mathsf{out}}$, can be written as $\boldsymbol{A}_{\mathsf{out}} = \boldsymbol{A} + [\boldsymbol{\rho}]_{N:2N-1}$. Note that $\boldsymbol{\rho}$ vector has a length of $(3N-2)$, and the desired range is obtained by omitting $(N-1)$ values on either side of the vector. $\boldsymbol{\rho}$ gives the sum total of intermodulation, cross modulation, and compressive distorion products at each frequency, which represents the third order distortion.

## 3.4 Representation Using Unit Basis Vectors

Representation using Toeplitz matrices only gives the overall distortion power at a given frequency bin. This representation, though useful in tracking the signal distortion given the input spectrum, becomes cumbersome if there is a change in the received power, or re-arrangement of input spectrum, as almost all the entries need to be re-written and matrices need to be re-formulated. However, we seek to explicitly identify the exact adjacent channel frequencies causing distortions at a given frequency. This is not readily available through this representation. One has to physically expand the terms of double convolution to obtain the partial distortion products at any frequency bin $n$. This is not only cumbersome and inconvenient, but also is ill-suited for various applications mentioned before like, nonlinear interference cancellation, real-time channel allocation, etc.

Representation using Toeplitz matrices will not be convenient for many real-time scenarios, such as optimizing for spectrum access dynamically or evaluating the interference if the radio

environment changes swiftly as expected in next generation shared spectrum and heterogeneous networks. Thus, it is of interest to develop representations of third order nonlinearity which involve minimal changes in the matrix entries with a changing environment. We now develop a representation using the standard basis vectors and sparse matrices to enable efficient real time computation of third order distortions.

### 3.4.1 Two-Tone Intermodulation Products

In this section, we discuss a representation of two-tone intermodulation products exploiting the inherent properties.

**Lemma 1.** *Two signals at frequency bins $j$ and $k$ respectively, $j, k \in [1, N]$ produce third order intermodulation products at a frequency bin $n \in \{1, N\}; n \neq j, n \neq k$, if the condition, $\mid j - k \mid = \min\{\mid n - j \mid, \mid n - k \mid\}$ is satisfied.*

*Proof.* Consider two signals $A_j \cos(\omega_j t)$ and $A_k \cos(\omega_k t)$ where $\omega_i = 2\pi f_i;\ f_i > 0$ entering the RF chain, where $j \neq k; j, k \in \{1, N\}$ are the indices of frequency bins. The in-band terms of third order distortion of the sum of these two signals is given by $\frac{3}{2}A_j^2 A_k \cos(2\omega_j - \omega_k) + \frac{3}{2}A_j^2 A_k \cos(2\omega_k - \omega_j)$.

*Case 1. $j < k$:* Let $\omega_n = 2\omega_j - \omega_k \Rightarrow \omega_j - \omega_n < \omega_k - \omega_n$. Hence, $k - j = j - n = \min\{\mid n - j \mid, \mid n - k \mid\}$.

*Case 2. $j > k$:* Let $\omega_n = 2\omega_j - \omega_k \Rightarrow \omega_n - \omega_j < \omega_n - \omega_k$. Hence, $j - k = n - j = \min\{\mid n - j \mid, \mid n - k \mid\}$. □

**Lemma 2.** *The second order multiplicative term of the intermodulation product of two signals at bins $j$ and $k$ respectively produced at bin $n$ is produced by the signal in the bin $n \pm \min\{\mid n - j \mid, \mid n - k \mid\} \in \{j, k\}; \forall j, k, n \in [1, N]$.*

*Proof.* Consider two signals $A_j \cos(\omega_j t)$ and $A_k \cos(\omega_k t)$ where $\omega_i = 2\pi f_i;\ f_i > 0$ entering the RF chain. Without loss of any generality, assume $j < k; j, k \in \{1, N\}$ are the indices of frequency bins. From the Lemma 1 we have,

*Case 1. $\omega_n = 2\omega_j - \omega_k$:* $\min\{\mid n - j \mid, \mid n - k \mid\} = \mid n - j \mid$. $n \pm \mid n - j \mid = j \Rightarrow \omega_j$ produces a second order term at $\omega_n$.

*Case 2.* $\omega_n = 2\omega_k - \omega_j$*:* $\min\{\mid n-j \mid, \mid n-k \mid\} = \mid n-k \mid$. $n \pm \mid n-k \mid = k \Rightarrow \omega_k$ produces a second order term at $\omega_n$. This can be verified by the terms of third order intermodulation distortion of the sum of these two signals, which is given by $\frac{3}{2}A_j^2 A_k \cos(2\omega_j - \omega_k) + \frac{3}{2}A_j^2 A_k \cos(2\omega_k - \omega_j)$. □

Based on these properties, it is possible to characterize the adjacent channel frequency bins producing two-tone intermodulation products at a desired frequency bin $n$.

**Theorem 1.** *$\Psi_n$ is the set of all ordered pairs $(j,k); \forall j,k \in [1,N]; \forall j,k \neq n$ of adjacent channel frequency bins that produce intermodulation products at a given frequency bin $n \in [1,N]$, where,*

$$\Psi_n = \left\{ \left( n - 2\left\lfloor \frac{n-1}{2} \right\rfloor, n - \left\lfloor \frac{n-1}{2} \right\rfloor \right), \cdots, (n-2, n-1), \right.$$
$$\left. (n+1, n+2), \cdots, \left( n + \left\lfloor \frac{N-n}{2} \right\rfloor, n + 2\left\lfloor \frac{N-n}{2} \right\rfloor \right) \right\}$$

*Proof.* Consider a frequency bin $n$. From Lemma 1, the ordered pair of frequency bins causing intermodulation products at $n$ are $(j,k) = (n+i, n+2i); i = 1,2,3,\ldots$ for $j > n, k > n$ and $(j,k) = (n-2i, n-i); i = 1,2,3,\ldots$ for $j < n, k < n$.

Since we have, $n + 2i \leq N \Rightarrow i = \left\lfloor \frac{N-n}{2} \right\rfloor$, the maximum values for
$(j,k) = \left(n + 2\left\lfloor \frac{N-n}{2} \right\rfloor, n + \left\lfloor \frac{N-n}{2} \right\rfloor\right)$.

Similarly, $n - 2i \geq 1 \Rightarrow i = \left\lfloor \frac{n-1}{2} \right\rfloor$, the minimum values for $(j,k) = \left(n - 2\left\lfloor \frac{n-1}{2} \right\rfloor, n - \left\lfloor \frac{n-1}{2} \right\rfloor\right)$.

Thus, $\Psi_n = \left\{ \left(n - 2\left\lfloor \frac{n-1}{2} \right\rfloor, n - \left\lfloor \frac{n-1}{2} \right\rfloor\right), \cdots, (n-2, n-1), (n+1, n+2), \cdots, \right.$
$\left. \left(n + \left\lfloor \frac{N-n}{2} \right\rfloor, n + 2\left\lfloor \frac{N-n}{2} \right\rfloor\right) \right\}$ □

**Example:** Consider a receiver whose pre-selector spans $N = 5$. For the desired channel, $n = 1$, the pair-wise intermods are generated by $\Psi_1 = \{(2,3), (3,5)\}$. However, if the desired channel is $n = 2$, the pairwise intermods are generated by $\Psi_2 = \{(3,4)\}$. This generalized relation of the frequency bins that cause distortions at a given channel is formalized in Theorem 1, using the properties of third order nonlinearity stated in Lemma 1 and Lemma 2, for a channelized receiver.

We propose to use the standard basis for the Euclidean $\Re^N$. Standard basis vectors, $\mathbf{e}$ for a Euclidean space are the set of unit vectors pointing in the direction of the axes of a Cartesian coordinate system. We denote a diagonal matrix $\mathbf{G} = \mathrm{diag}(A_1^2, A_2^2, \cdots, A_N^2)$. This matrix is used to pick the second order multiplicative terms of intermodulation products. We define $\Phi_n$ as the set

of all frequency bins producing second order multiplicative terms of the two-tone intermodulation products at frequency bin $n \in [1, N]$. Using Lemma 2 and Theorem 1,

$$\Phi_n = \left\{ n - \left\lfloor \frac{n-1}{2} \right\rfloor, \cdots, n-2, n-1, n+1, n+2, \cdots, n + \left\lfloor \frac{N-n}{2} \right\rfloor \right\} \tag{3.3}$$

We define the Second Order Multiplicative Matrix $\mathbf{L}_n^{\mathsf{A}}$, whose non-zero column entries of the $n^{\text{th}}$ row represent the frequency bins producing the second order multiplicative terms at the frequency bin $n$, as deduced from $\Phi_n$ in (3.3). Mathematically,

$$\mathbf{L}_n^{\mathsf{A}} = \sum_{\forall j \in \Phi_n} \mathbf{e}_n \mathbf{e}_j^T \tag{3.4}$$

For every second order multiplicative term, $j \in \Phi_n$, we define a set $\Theta_n$ of ordered pairs $(j, k); k \in [1, N]; k \neq n$,

$$\Theta_n = \{(j, k)\}; \;\; \text{where} \;\; k = 2j - n \tag{3.5}$$

$k$ is the frequency bin producing the first order multiplicative term in the intermodulation product. We define the First Order Multiplicative Matrix $\mathbf{L}_n^{\mathsf{B}}$, whose non-zero column entries of the $j^{\text{th}}$ row correspond to the frequency bin producing the first order multiplicative term with the signal at frequency bin $j$. Mathematically,

$$\mathbf{L}_n^{\mathsf{B}} = \sum_{\forall (j,k) \in \Theta_n} \mathbf{e}_j \mathbf{e}_k^T \tag{3.6}$$

**Proposition 1.** *The two tone intermodulation distortion at frequency bin $n$, $\rho_{n_{\mathsf{IM}}}^{\mathsf{2tone}}$, can be formulated as,*

$$\rho_{n_{\mathsf{IM}}}^{\mathsf{2tone}} = \frac{3}{4}\alpha_3 \underbrace{[1 \; 1 \; \cdots \; 1]}_{1 \times N} \underbrace{\mathbf{L}_n^{\mathsf{A}} \, \mathbf{G} \, \mathbf{L}_n^{\mathsf{B}}}_{N \times N} \underbrace{\boldsymbol{A}}_{N \times 1} \tag{3.7}$$

### 3.4.2 Three-Tone Intermodulation Products

In this section, we discuss the representation of three-tone intermodulation products. Three signals at frequency bins $i, j, k \in [1, N]$ combine to produce an intermodulation product at a frequency bin, $n \in [1, N]$, such that $n = i + j - k$, $\forall i, j, k \in [1, N], i \neq j \neq k \neq n$. For any given frequency bin $n \in [1, N]$, $\Upsilon_n$ denotes the set of all triplets $(i, j, k)$; $i, j, k \in [1, N]$ which produce a three-tone intermodulation product at $n$. The amplitude of the intermodulation product is given by $A_i A_j A_k$. Finding the set $\Upsilon_n$ involves testing all the ${}^{N}\mathsf{P}_3$ combinations of $i, j, k \in [1, N]$ that satisfy the equation $n = i + j - k$. However, it is not required to test for all the combinations and

Algorithm 1 proposed here reduces the search space from $\mathcal{O}(N^3)$ to $\mathcal{O}(N^2)$.

**Algorithm 1** Triplets for Three-Tone Intermodulation Product

```
INITIALIZE: Υ_n = ∅ (Set of triplets initialized as null set)
for i = 1, 2, ..., N do
    for j = i + 1, 2, ..., min(N, N + n − i) do
        k = i + j − n
        if k ∈ {1, N}, k ≠ i, j, n then
            Υ_n = Υ_n ∪ {(i, j, k)}
        end if
    end for
end for
```

Using the set of triplets $\Upsilon_n$, we formulate three sets as follows.

$$\Upsilon_n^{\iota} = \bigcup\{i : i = n - j + k\},\ \forall i, j, k, n \in [1, N],\ i \neq j \neq k \neq n \tag{3.8}$$

We further define the following sets of ordered pairs as,

$$\Upsilon_{n,i}^{\mathsf{C}} = \{(i, j)\};\ \ \forall\{(i, j, k)\} \in \Upsilon_n;\ \ \Upsilon_{n,i}^{\mathsf{D}} = \{(j, k)\};\ \ \forall\{(i, j, k)\} \in \Upsilon_n \tag{3.9}$$

We next define a matrix $\mathbf{L}_{n,i}^{\mathsf{C}}$, whose non-zero column entries of the $(i, j)$ select the frequency bin $j \in \{(i, j, k)\}, \forall i \in \Upsilon_n^{\iota}$ of the three tone intermodulation at the frequency bin $n$. Similarly, we define a matrix $\mathbf{L}_{n,i}^{\mathsf{D}}$, whose non-zero column entries of the $(j, k)$ select the frequency bin $k \in \{(i, j, k)\}, \forall i \in \Upsilon_n^{\iota}$ of the three tone intermodulation at the frequency bin $n$. Mathematically,

$$\mathbf{L}_{n,i}^{\mathsf{C}} = \sum_{\forall(i,j)\in\Upsilon_{n,i}^{\mathsf{C}}} \mathbf{e}_i\mathbf{e}_j^T;\ \ \mathbf{L}_{n,i}^{\mathsf{D}} = \sum_{\forall(j,k)\in\Upsilon_{n,i}^{\mathsf{D}}} \mathbf{e}_j\mathbf{e}_k^T \tag{3.10}$$

**Proposition 2.** *The three-tone intermodulation distortion at bin $n$, $\rho_{n_{\mathsf{IM}}}^{\mathsf{3tone}}$ is given by,*

$$\rho_{n_{\mathsf{IM}}}^{\mathsf{3tone}} = \frac{3}{2}\alpha_3 \sum_{\forall i\in\Upsilon_n^{\iota}} \underbrace{\boldsymbol{A}^T}_{1\times N} \underbrace{\mathbf{L}_{n,i}^{\mathsf{C}}\mathbf{G}^{1/2}\mathbf{L}_{n,i}^{\mathsf{D}}}_{N\times N} \underbrace{\boldsymbol{A}}_{N\times 1} \tag{3.11}$$

### 3.4.3 Cross-Modulation

In this section we describe the representation of cross-modulation terms which result from third order distortion.

**Lemma 3.** *A signal at any frequency bin $j \neq n, j, n \in [1, N]$ produces a cross-modulation product upon combining with the desired signal at frequency bin $n$. This is unitary cross-modulation.*

*Proof.* Consider that the input to the RF chain is, $A_n \cos(\omega_n t) + A_j \cos(\omega_j t)$, where $\omega_n$ is the frequency of the desired signal in bin $n$ and $\omega_j$ is an adjacent channel signal in bin $j \neq n$; $n, j \in [1, N]$. Expanding $(A_n \cos(\omega_n t) + A_j \cos(\omega_j t))^3$ and grouping the third order output terms at the desired frequency $\omega_n$ is given by, $\alpha_3(A_n^3 + A_j^2 A_n)$. If $A_n << A_j$, the dominant component is $\alpha_3 A_j^2 A_n$. Thus, the output obtained is the modulated version of the desired signal in accordance with the adjacent channel signal [41]. □

To represent cross-modulation products using basis vectors, we formulate the vector $\mathbf{s}_n$ using Lemma 3 , whose non-zero entries denote bins producing distortions at frequency bin $n$ as,

$$\mathbf{s}_n = \sum_{\forall k \neq n} \mathbf{e}_k \; ; \quad k, n \in [1, N] \tag{3.12}$$

**Lemma 4.** *Two signals at distinct frequency bins $i$ and $j$, $i, j \in [1, N]$ produce a cross-modulation product upon combining with the desired signal at frequency bin $n \in [1, N]$ if the condition $n = \frac{i+j}{2}$ is satisfied.*

*Proof.* We now consider the input to the RF chain to be a three tone signal, $A_n \cos(\omega_n t) + A_i \cos(\omega_i t) + A_j \cos(\omega_j t)$ where $\omega_n$ is the frequency of the desired signal in bin $n$ and are adjacent channel signal $\omega_i, \omega_j$ in bin $i, j \neq n$; $n, i, j \in [1, N]$.

In general for three signals to combine and form a third order product at $n$, the condition $n = i + j - k$ should be satisfied. For generating a cross-modulation product however, any one of $\{i, j, k\}$ should be equal to $n$, and $i \neq j \neq k \; \forall i, j, k, n \in [1, N]$.

The cases for which $i = n$ or $j = n$, the condition $i \neq j \neq k$ is not satisfied. Thus, $k = n$ is the only possibility for a pairwise crossmodulation product. If $k = n$, it follows by the condition, $n = i + j - k \Rightarrow 2n = i + j$. Thus, $n = \frac{i+j}{2}$ has to be satisfied. □

**Theorem 2.** *$\Lambda_n$ is the set of all ordered pairs $(i, j); \forall i, j \in [1, N]$ of adjacent channel frequency bins that produce pairwise crossmodulation products upon combining with the signal at the desired frequency bin $n \in [1, N]$ where,*

$$\Lambda_n = \{(n-1, n+1), (n-2, n+2), \ldots, (n - \min[n-1, N-n], n + \min[n-1, N-n])\} \tag{3.13}$$

*Proof.* From Lemma 4 we see that $n = \frac{i+j}{2}$ is the arithmetic mean of $i$ and $j$. Thus, the only values of $i, j \in \mathbb{Z}, i \neq j$ that satisfy the condition are of the form $\{i, j\} = \{(n-\ell), (n+\ell)\}, \forall \ell \in \mathbb{Z} \setminus \{0\}$ since $i \neq n, j \neq n$. Thus, $\{(n-1, n+1), (n-2, n+2), \ldots\}$ combine with $n$ to form cross-modulation products. However, we also note that $i, j \in [1, N]$ has to be satisfied.

We know that, $n - \ell \geq 1 \Rightarrow \ell \leq n-1$. Also, $n + \ell \leq N \Rightarrow \ell \leq N - n$.

Combining these two inequalities, the least possible value that can be taken by $\ell = \min[n-1, N-n]$. Thus the set $\Lambda_n = \{(n-1, n+1), (n-2, n+2), \ldots, (n - \min[n-1, N-n], n + \min[n-1, N-n])\}$ is obtained. □

**Example:** Consider a receiver whose pre-selector spans $N = 5$. For the desired channel, $n = 3$, the pairwise crossmodulation products are generated by $\Lambda_3 = \{(2, 4), (1, 5)\}$. However, if the desired channel is $n = 2$ the pairwise crossmodulation products are generated by $\Psi_2 = \{(1, 3)\}$. This generalized relation of the frequency bins that cause pairwise crossmodulation distortions at a given channel is formalized in Theorem 2, using properties of third order nonlinearity stated in Lemma 4 for a channelized receiver.

We now define a set $\Lambda_n^{\mathsf{E}}$ from $\Lambda_n$ as, $\Lambda_n^{\mathsf{E}} = \{n-1, n-2, \ldots, n - \min[n-1, N-n]\}$. We further use these sets to formulate two matrices using basis vectors as,

$$\mathbf{L}_n^{\mathsf{E}} = \sum_{\forall i \in \Lambda_n^{\mathsf{E}}} \mathbf{e}_n \mathbf{e}_i^T \;\; ; \;\; \mathbf{L}_n^{\mathsf{F}} = \sum_{\forall (i,j) \in \Lambda_n} \mathbf{e}_i \mathbf{e}_j^T \tag{3.14}$$

**Proposition 3.** *The cross-modulation distortion at bin* $n \in [1, N]$*,* $\rho_{n_{\mathsf{CM}}}$ *is given by*

$$\rho_{n_{\mathsf{CM}}} = \frac{3}{2}\alpha_3 \left( \underbrace{[1\ 1\ \cdots\ 1]}_{1 \times N} \underbrace{\mathbf{G}\mathbf{s}_n \mathbf{e}_n^T}_{\text{Unitary CMD}} + \underbrace{\boldsymbol{A}^T \mathbf{L}_n^{\mathsf{E}} \mathbf{G}^{1/2} \mathbf{L}_n^{\mathsf{F}}}_{\text{Pairwise CMD}} \right) \boldsymbol{A} \tag{3.15}$$

### 3.4.4 Compressive Distortion

When an input spectrum undergoes third order distortion, there are cubic terms of the original input signals produced at the fundamental frequencies, scaled by third order coefficients. At high input powers, this can potentially result in gain compression of the overall front-end [41]. Let $\boldsymbol{\varrho} = [A_1^3\ A_2^3 \cdots A_N^3]^T$. For the bin $n$ this compressive distortion can be described as $\rho_{n_{\mathsf{CD}}} = \frac{3}{4}\alpha_3 \mathbf{e}_n^T \boldsymbol{\varrho}$.

### 3.4.5 Formulation of Type II Representation

**Proposition 4.** *The discrete amplitude spectrum of the third order distortion is* $\boldsymbol{\rho} = [\rho_1\ \rho_2\ \cdots\ \rho_N]^T$*, where,* $\rho_n$ *the amplitude at bin* $n$*, is given by the equation in (3.16).*

$$\rho_n = \alpha_3 \Bigg( \left(\frac{3}{4}[1\ 1\ \cdots\ 1]\left(\mathbf{L}_n^{\mathsf{A}}\,\mathbf{G}\,\mathbf{L}_n^{\mathsf{B}} + \frac{3}{2}\mathbf{G}\mathbf{s}_n\mathbf{e}_n^T\right) + \frac{3}{2}\boldsymbol{A}^T\mathbf{L}_n^{\mathsf{E}}\mathbf{G}^{1/2}\mathbf{L}_n^{\mathsf{F}}\right)\boldsymbol{A} + \frac{3}{2}\sum_{\forall i \in \Upsilon_n^{\iota}} \boldsymbol{A}^T\mathbf{L}_{n,i}^{\mathsf{C}}\mathbf{G}^{1/2}\mathbf{L}_{n,i}^{\mathsf{D}}\boldsymbol{A} + \frac{3}{4}\mathbf{e}_n^T\boldsymbol{\varrho}\Bigg) \quad (3.16)$$

The discretized multi-tone input can be represented in the time domain as $s(t) = \sum_{n=1}^{N} A_n \cos(\omega_n t)$, where $A_n$ is the amplitude of the frequency bin $\omega_n$. The overall third order distortion can then be represented in the time domain as equation (3.17).

$$r(t) = \sum_{n=1}^{N} \Bigg( A_n \Bigg( \alpha_1 + \underbrace{\frac{3}{4}\alpha_3 A_n^2}_{\text{Compressive Distortion}} + \underbrace{\frac{3}{2}\alpha_3 \sum_{\forall i \neq n} A_i^2}_{\text{Unitary CMD}} + \underbrace{\frac{3}{2}\alpha_3 \sum_{(i,j)\in\Lambda_n} A_i A_j}_{\text{Pairwise CMD}} \Bigg) + \underbrace{\frac{3}{4}\alpha_3 \sum_{(i,j)\in\Psi_n} A_i^2 A_j}_{\text{2 Tone IMD}} + \underbrace{\frac{3}{2}\alpha_3 \sum_{(i,j,k)\in\Upsilon_n} A_i A_j A_k}_{\text{3 Tone IMD}} \Bigg) \cos(\omega_n t) \quad (3.17)$$

Note that this representation is also valid to evaluate the baseband interference by symbols of adjacent channels where each entry in $\boldsymbol{A}$ denotes a complex baseband modulated symbol of that particular frequency bin (channel). Also, this formulation assumes that signals combine in phase to produce distortions and represents the worst case scenario. This can be modified to account for random phase combinations and obtain an estimate of expected power [56, 57] by accordingly changing the matrices $\boldsymbol{A}$ and $\mathbf{G}$ to denote power values. From the formulation in equation (3.16), we see that only $\boldsymbol{A}$ and $\mathbf{G}$ matrices need to be populated in real time, each of which have only $N$ entries, as against Type I using Toeplitz matrices. Although there is a summation of products, the number of partial products is $\mid \Upsilon_n^{\iota} \mid \leq N$. We term these two matrices $\boldsymbol{A}$ and $\mathbf{G}$ 'Radio Environment (RE)' matrices. All the other required matrices are sparse and can be formulated

offline as they depend only on the specific frequency bin $n$ and the total number of bins $N$, and are independent of the radio environment. Moreover, in dynamic spectrum environments, only those entries of the RE matrices whose values have altered need to be changed and the entire matrix need not be re-populated. Furthermore, this formulation provides ease in designing real time spectrum access algorithms as they can be easily manipulated with matrix algebra for incorporating channel information, distance between nodes, specific receiver information, and permuted using permutation matrices, by pre and post multiplying with RE matrices, as required.

### 3.4.6 Example of the proposed representation using unit basis vectors

We present examples of the pairwise intermodulation and triple intermodulation matrices developed in the proposed representation for the case of $N = 5$. We further show how the representation yields the intermodulation products that are generated for a given input. This will bring more clarity to the proposed representation. Other distortions follow a similar representation.

**Pairwise Intermodulation Distortion:** The formulation of the various sets and matrices involved in developing proposed representation for pairwise intermodulation in Section III-A, with $N = 5$ and $n = 1$ is shown in Fig. 3.2. We see that $\{A_2, A_3\}$ and $\{A_3, A_5\}$ form intermod products at $n = 1$. The matrices are developed accordingly using unit basis vectors and the formulation gives these intermodulation products.

**Triple Intermodulation Distortion:** Similarly, the formulation of the various sets and matrices involved in developing proposed representation for triple intermodulation in Section III-B, with $N = 5$ and $n = 2$ is shown in Fig. 3.3 of this document. $\{A_1, A_4, A_3\}$, $\{A_1, A_5, A_4\}$, and $\{A_3, A_4, A_5\}$ form intermod products at $n = 2$.

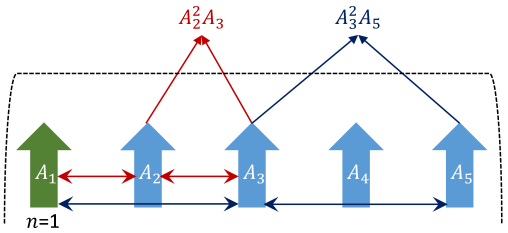


$$\Psi_1 = \{(2,3),(3,5)\}$$

$$\Phi_1 = \{2,3\}$$

For every $j \in \Phi_n$, we define a set $\Theta_n$,

$$\Theta_n = \{(j,k)\}; \quad \text{s.t.} \quad k = 2j - n$$

$$\Theta_1 = \{(2,3),(3,5)\}$$

$$\mathbf{L}_1^{\mathsf{A}} = \begin{bmatrix} 0 & 1 & 1 & 0 & 0 \\ 0 & 0 & 0 & 0 & 0 \\ 0 & 0 & 0 & 0 & 0 \\ 0 & 0 & 0 & 0 & 0 \\ 0 & 0 & 0 & 0 & 0 \end{bmatrix} = \sum_{\forall j \in \Phi_1} \mathbf{e}_1 \mathbf{e}_j^T$$

$\mathbf{e}$ is the standard basis vector in $\Re^5$

$$\mathbf{L}_1^{\mathsf{B}} = \begin{bmatrix} 0 & 0 & 0 & 0 & 0 \\ 0 & 0 & 1 & 0 & 0 \\ 0 & 0 & 0 & 0 & 1 \\ 0 & 0 & 0 & 0 & 0 \\ 0 & 0 & 0 & 0 & 0 \end{bmatrix} = \sum_{\forall (j,k) \in \Theta_1} \mathbf{e}_j \mathbf{e}_k^T$$

We define $\mathbf{G} = \text{diag}(A_1^2, A_2^2, A_3^2, A_4^2, A_5^2)$

$$\rho_{n_{\text{IM}}}^{\text{2tone}} = \alpha_3 \underbrace{[1\ 1\ \cdots\ 1]}_{1\times N} \underbrace{\mathbf{L}_n^{\mathsf{A}}\ \mathbf{G}\ \mathbf{L}_n^{\mathsf{B}}}_{N\times N} \underbrace{\boldsymbol{A}}_{N\times 1}$$

$$\underbrace{\begin{bmatrix} 0 & 1 & 1 & 0 & 0 \\ 0 & 0 & 0 & 0 & 0 \\ 0 & 0 & 0 & 0 & 0 \\ 0 & 0 & 0 & 0 & 0 \\ 0 & 0 & 0 & 0 & 0 \end{bmatrix}}_{\mathbf{L}_n^{\mathsf{A}}} \underbrace{\begin{bmatrix} A_1^2 & 0 & 0 & 0 & 0 \\ 0 & A_2^2 & 0 & 0 & 0 \\ 0 & 0 & A_3^2 & 0 & 0 \\ 0 & 0 & 0 & A_4^2 & 0 \\ 0 & 0 & 0 & 0 & A_5^2 \end{bmatrix}}_{\mathbf{G}} \underbrace{\begin{bmatrix} 0 & 0 & 0 & 0 & 0 \\ 0 & 0 & 1 & 0 & 0 \\ 0 & 0 & 0 & 0 & 1 \\ 0 & 0 & 0 & 0 & 0 \\ 0 & 0 & 0 & 0 & 0 \end{bmatrix}}_{\mathbf{L}_n^{\mathsf{B}}} \underbrace{\begin{bmatrix} A_1 \\ A_2 \\ A_3 \\ A_4 \\ A_5 \end{bmatrix}}_{\boldsymbol{A}}$$

$$\begin{bmatrix} 1 & 1 & 1 & 1 & 1 \end{bmatrix} \begin{bmatrix} 0 & A_2^2 & A_3^2 & 0 & 0 \\ 0 & 0 & 0 & 0 & 0 \\ 0 & 0 & 0 & 0 & 0 \\ 0 & 0 & 0 & 0 & 0 \\ 0 & 0 & 0 & 0 & 0 \end{bmatrix} \begin{bmatrix} 0 & 0 & 0 & 0 & 0 \\ 0 & 0 & 1 & 0 & 0 \\ 0 & 0 & 0 & 0 & 1 \\ 0 & 0 & 0 & 0 & 0 \\ 0 & 0 & 0 & 0 & 0 \end{bmatrix} \begin{bmatrix} A_1 \\ A_2 \\ A_3 \\ A_4 \\ A_5 \end{bmatrix} = \begin{bmatrix} 1 & 1 & 1 & 1 & 1 \end{bmatrix} \begin{bmatrix} 0 & 0 & 0 & 0 & 0 \\ 0 & 0 & A_2^2 & 0 & 0 \\ 0 & 0 & 0 & 0 & A_3^2 \\ 0 & 0 & 0 & 0 & 0 \\ 0 & 0 & 0 & 0 & 0 \end{bmatrix} \begin{bmatrix} A_1 \\ A_2 \\ A_3 \\ A_4 \\ A_5 \end{bmatrix} = \begin{bmatrix} 1 & 1 & 1 & 1 & 1 \end{bmatrix} \begin{bmatrix} 0 \\ A_2^2 A_3 \\ A_3^2 A_5 \\ 0 \\ 0 \end{bmatrix} = A_2^2 A_3 + A_3^2 A_5$$

Figure 3.2: Example of matrix representation using unit basis vectors for two-tone intermodulation distortion

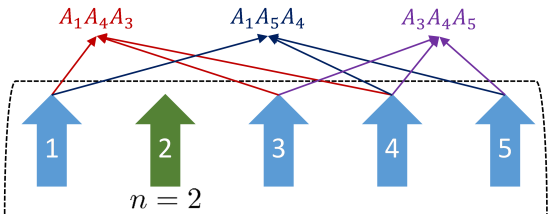


$$\Upsilon_2 = \{(1,4,3),(1,5,4),(3,4,5)\}$$

Using $\Upsilon_2$, we define the following set with $i$'s,

$$\Upsilon_2^{\iota} = \{1,3\}$$

For each $i$ in $\Upsilon_2^{\iota}$, we define the sets $\Upsilon_{2,i}^{\mathsf{C}}$ and $\Upsilon_{2,i}^{\mathsf{D}}$

$$\Upsilon_{2,1}^{\mathsf{C}} = \{(1,4),(1,5)\}$$
$$\Upsilon_{2,1}^{\mathsf{D}} = \{(4,3),(5,4)\}$$
$$\Upsilon_{2,3}^{\mathsf{C}} = \{(3,4)\}$$
$$\Upsilon_{2,3}^{\mathsf{D}} = \{(4,5)\}$$

$$\mathbf{L}_{2,1}^{\mathsf{C}} = \begin{bmatrix} 0&0&0&1&1\\0&0&0&0&0\\0&0&0&0&0\\0&0&0&0&0\\0&0&0&0&0 \end{bmatrix} = \sum_{\forall (i,j)\in\Upsilon_{2,1}^{\mathsf{C}}} \mathbf{e}_i\mathbf{e}_j^T$$

$\mathbf{e}$ is the standard basis vector in $\Re^5$

$$\mathbf{L}_{2,1}^{\mathsf{D}} = \begin{bmatrix} 0&0&0&0&0\\0&0&0&0&0\\0&0&0&0&0\\0&0&1&0&0\\0&0&0&1&0 \end{bmatrix} = \sum_{\forall (j,k)\in\Upsilon_{2,1}^{\mathsf{D}}} \mathbf{e}_j\mathbf{e}_k^T$$

$$\mathbf{L}_{2,3}^{\mathsf{C}} = \begin{bmatrix} 0&0&0&0&0\\0&0&0&0&0\\0&0&0&1&0\\0&0&0&0&0\\0&0&0&0&0 \end{bmatrix} = \sum_{\forall (i,j)\in\Upsilon_{2,3}^{\mathsf{C}}} \mathbf{e}_i\mathbf{e}_j^T$$

$$\mathbf{L}_{2,3}^{\mathsf{D}} = \begin{bmatrix} 0&0&0&0&0\\0&0&0&0&0\\0&0&0&0&0\\0&0&0&0&1\\0&0&0&0&0 \end{bmatrix} = \sum_{\forall (j,k)\in\Upsilon_{2,3}^{\mathsf{D}}} \mathbf{e}_j\mathbf{e}_k^T$$

$$\underbrace{[A_1\ A_2\ A_3\ A_4\ A_5]}_{\boldsymbol{A}^T} \underbrace{\begin{bmatrix} 0&0&0&1&1\\0&0&0&0&0\\0&0&0&0&0\\0&0&0&0&0\\0&0&0&0&0 \end{bmatrix}}_{\mathbf{L}_{2,1}^{\mathsf{C}}} \underbrace{\begin{bmatrix} A_1&0&0&0&0\\0&A_2&0&0&0\\0&0&A_3&0&0\\0&0&0&A_4&0\\0&0&0&0&A_5 \end{bmatrix}}_{\mathbf{G}^{1/2}} \underbrace{\begin{bmatrix} 0&0&0&0&0\\0&0&0&0&0\\0&0&0&0&0\\0&0&1&0&0\\0&0&0&1&0 \end{bmatrix}}_{\mathbf{L}_{2,1}^{\mathsf{D}}} \underbrace{\begin{bmatrix} A_1\\A_2\\A_3\\A_4\\A_5 \end{bmatrix}}_{\boldsymbol{A}} = \boldsymbol{A}^T\mathbf{L}_{2,1}^{\mathsf{C}}\mathbf{G}^{1/2}\mathbf{L}_{2,1}^{\mathsf{D}}\boldsymbol{A}$$

$$[0\ \ 0\ \ 0\ \ A_1\ \ A_1] \begin{bmatrix} 0&0&0&0&0\\0&0&0&0&0\\0&0&0&0&0\\0&0&A_4&0&0\\0&0&0&A_5&0 \end{bmatrix} \begin{bmatrix} A_1\\A_2\\A_3\\A_4\\A_5 \end{bmatrix} = [0\ \ 0\ \ A_1A_4\ \ A_1A_5\ \ 0] \begin{bmatrix} A_1\\A_2\\A_3\\A_4\\A_5 \end{bmatrix} = A_1A_4A_3 + A_1A_5A_4$$

Similarly, $\boldsymbol{A}^T\mathbf{L}_{2,3}^{\mathsf{C}}\mathbf{G}^{1/2}\mathbf{L}_{2,3}^{\mathsf{D}}\boldsymbol{A} = A_3A_4A_5$

Thus, $\rho_{2_{\mathsf{IM}}}^{3\text{tone}} = \boldsymbol{A}^T\mathbf{L}_{2,1}^{\mathsf{C}}\mathbf{G}^{1/2}\mathbf{L}_{2,1}^{\mathsf{D}}\boldsymbol{A} + \boldsymbol{A}^T\mathbf{L}_{2,3}^{\mathsf{C}}\mathbf{G}^{1/2}\mathbf{L}_{2,3}^{\mathsf{D}}\boldsymbol{A}$

$$\rho_{2_{\mathsf{IM}}}^{3\text{tone}} = \sum_{\forall i\in\Upsilon_2^{\iota}} \boldsymbol{A}^T\mathbf{L}_{2,i}^{\mathsf{C}}\mathbf{G}^{1/2}\mathbf{L}_{2,i}^{\mathsf{D}}\boldsymbol{A} \qquad \Upsilon_2^{\iota} = \{1,3\}$$

Figure 3.3: Example of matrix representation using unit basis vectors for three-tone intermodulation distortion

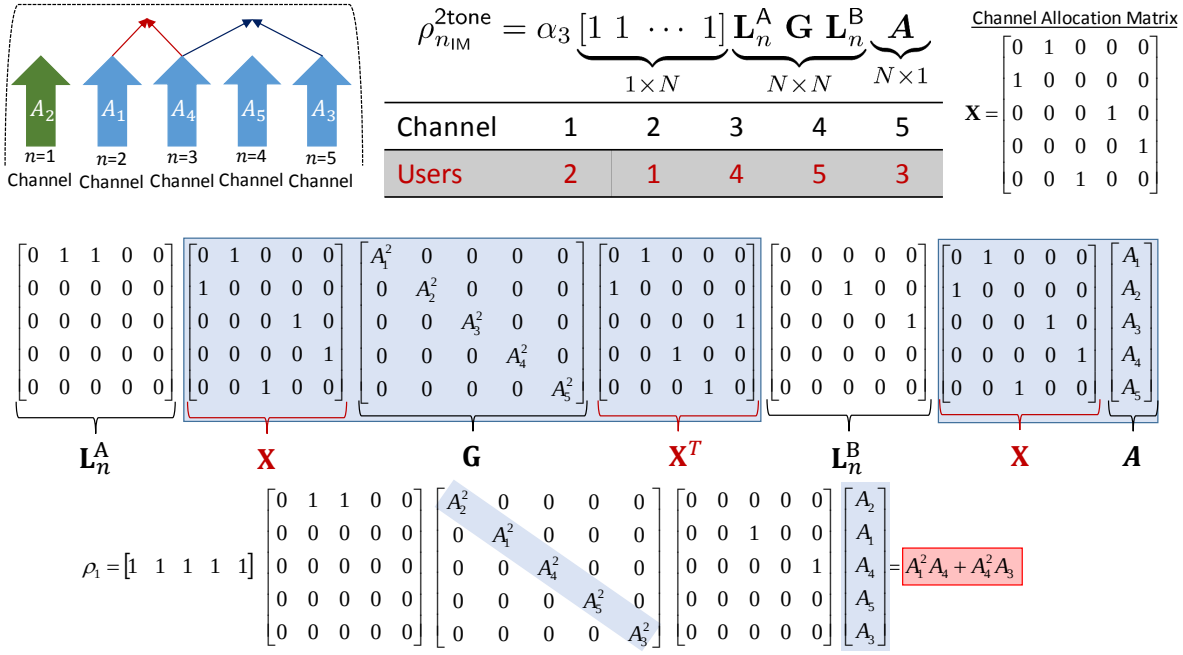


Figure 3.4: Example of expediency of representation using unit basis vectors for two-tone intermodulation distortion

### 3.4.7 Expediency of the Proposed Representation

We now provide an example of the utility of the proposed representation in evaluating co-existence in real time spectrum management for next generation networks. Consider $5$ users, $\{A_1, A_2, A_3, A_4, A_5\}$, and $5$ channels indexed by $n$. Let these users be allocated channels as shown in Fig. 3.4. If we want to calculate the impact of two-tone interference arising from adjacent channels at the desired channel $n = 1$, operated by used $A_2$, we can immediately exploit the properties of the proposed representation to multiply the Radio-Environment matrices with channel allocation permutation matrix to obtain the power of intermodulation distortion. Similar operations can be carried out to calculate three-tone intermods, crossmods and other distortion components. This provides immense utility for real time spectrum management, nonlinear adjacent channel interference cancellation, etc., in next generation wireless systems.

### 3.4.8 Computational Efficiency

In this section, we discuss the computational efficiency of the proposed representation compared to the representation using Toeplitz matrices. Consider the example case of $N = 5$ and the number

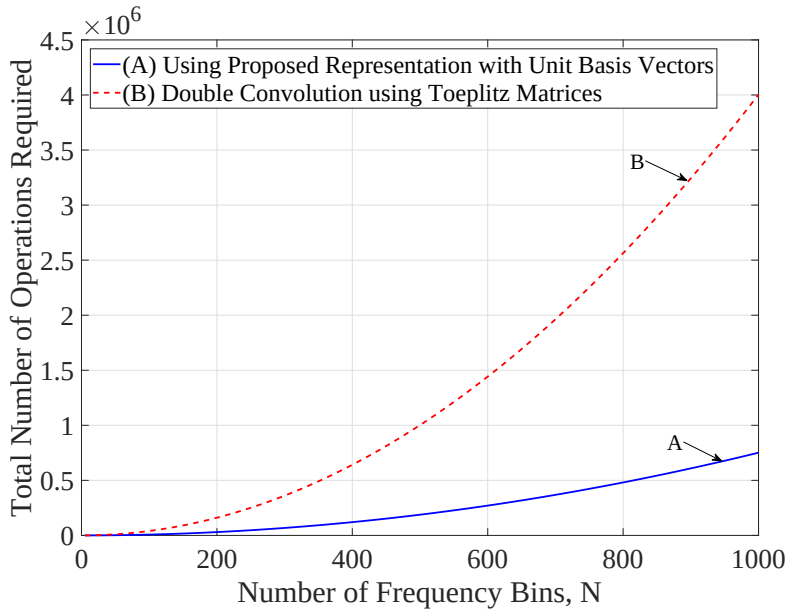


Figure 3.5: Comparison of the computational complexity as a function of number of bins, $N$

of operations required to compute third order distortions the bin $n = 1$. Using Toeplitz matrices, the number of operations required if found to be 120 operations but with the proposed framework using unit basis vectors the number of operations required is only 29. The comparison of the two representations for increasing number of frequency bins, $N$ is presented in Fig. 3.5.

## 3.5 Validations through Simulations and Experiments

In this section, we present the validation of the proposed representation through simulations and measurement.

### 3.5.1 Validation of the Representation with Numerical Simulations

In this section, we carry out a simple numerical experiment to validate the proposed representations. We choose $N = 10$ frequency bins. Each bin receives a sinusoidal signal of power $-30$dBm, and $\mathsf{IIP}_3 = -20$dBm. We perform the experiment by:

1. Obtaining the output of the third order term in the time domain and transforming the output signal to the frequency domain by taking an FFT (baseline for comparison)

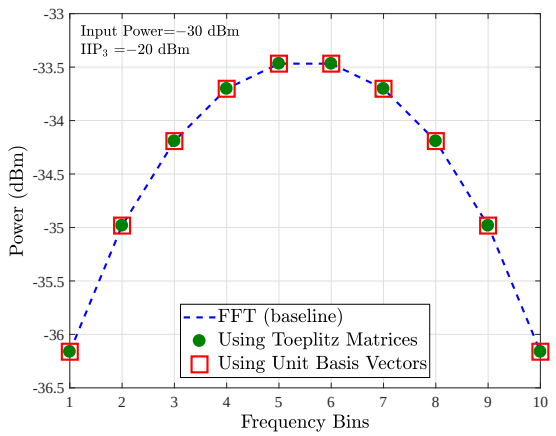


Figure 3.6: Simulation for validation of the proposed representations with the third order nonlinear model

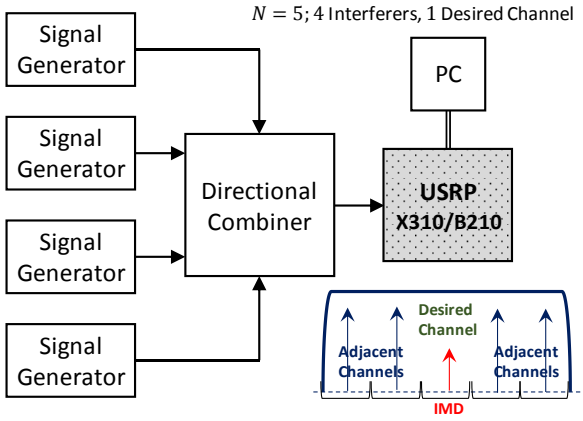


Figure 3.7: Schematic Diagram for Experimental Setup for Validation of Proposed Representation

2. Representation using Toeplitz matrices

3. Representation using unit basis vectors as shown in (3.16)

Figure 3.6 shows the results of the numerical experiment. As evident, the proposed representation of third order nonlinear distortions matches with the frequency response obtained using FFT.

### 3.5.2 Validation of the Representation with Experimental Measurements

In this section, we provide measurement examples to validate the applicability of the developed mathematical workbench to evaluate the adjacent channel interference due to receiver nonlinearity. We consider two USRP radio receivers, X310 and B210, that have a direct conversion architecture. We first measure the $\mathsf{IIP}_3$ of these radios for different front-end RF gains using the two-tone test. We use this to evaluate the expected intermodulation distortion using the proposed representation using unit basis vectors, for an example case with $N = 5$, where distortion is measured for the channel $n = 3$ as shown in Fig. 3.7. This experiment was conducted for various desired channels, and without loss of generality, we are presenting results for the case of $n = 3$ for brevity. Tone signals are used to excite the device under test, at $1542$ MHz, $1543$ MHz, $1545$ MHz, and $1546$ MHz and distortion is measured at $1544$ MHz. The measured distortion is compared with the evaluated value using the proposed representation (signals in random phase combine in power to produce intermods). As shown in Table 3.1, they match within a margin of $2$ dB, which is due to random phase of signals and experimental errors.

Table 3.1: Experimental validation of proposed representation to evaluate nonlinear distortions in receivers

| USRP | Gain (dB) | $\mathsf{IIP}_3$ (dBm) | Input Power per Channel (dBm) | Distortion Evaluated (dBm) (using proposed representation) | Distortion Measured (dBm) |
|---|---|---|---|---|---|
| X310 | 0 | 7.5 | $-25.5$ | $-83.8$ | $-82.8$ |
| | 15 | 6.4 | $-31.2$ | $-81.3$ | $-83.7$ |
| B210 | 25 | 7.3 | $-25.4$ | $-56.1$ | $-58.0$ |
| | 39 | $-7.4$ | $-39.6$ | $-55.3$ | $-57.2$ |

## 3.6 Conclusions

In this chapter we developed a fundamental, novel framework to analyze, quantify, and evaluate the impact of front-end nonlinearity on receiver performance. This serves as a comprehensive generalized framework for adjacent channel co-existence analysis. We consider the third order polynomial approximation model for receivers and formulate the analysis to ascertain the detriments caused by specific adjacent channel signals. The proposed matrix representations provide convenient structures to formulate and analyze a variety of problems, viz., evaluate adjacent channel co-existence between wireless systems, design network level algorithms for efficient spectral access, quantify and compare the performance between disparate receivers, develop comprehensive mechanisms for real time spectrum management, among others. The proposed framework can be extended to include higher order terms in the polynomial approximation following similar methodology and standard basis vectors can be used to represent the spectral re-distribution due to receiver nonlinearity. Convenient forms of nonlinear representation of higher order terms can be especially useful for the analysis and mitigation of self-interference and reverse intermodulation products in full-duplex communication systems.

# Chapter 4

# Quantifying the Impact of Receiver Nonlinearity on Performance

## 4.1 Introduction

Quantifying the extent of performance degradation in receivers is important for network optimization and co-existence analysis in next generation shared spectrum access systems. Performance detriment due to nonlinear distortions is dependent both on front-end nonlinearity and the spectral characteristics of adjacent channel signals. Frameworks for comparative assessment of performance and adjacent channel co-existence capabilities between disparate receivers are crucial for successful deployment and operations of 5G systems. In this chapter, we present information theoretic analysis to derive bounds on performance of nonlinear receivers. Further, using the information theoretic analysis, we present a new framework for developing metrics for receivers taking into account their nonlinearity and therefore sensitivity to adjacent channel interference. Metrics, that can be used to generate boundary values of performance, and comparing disparate receivers are important for future receiver development and standardization.

The input spectrum plays a crucial role in limiting the performance of nonlinear receivers. It is not possible to abstract the input spectrum to analyze bounds on performance. Thus, we use the tractable uniform spectrum as a test input to analyze its impact on nonlinear receivers. To our best knowledge, such a spectrum-centric analysis using information theoretic metrics has not been done before. Thus, it is novel not only from a receiver quantification point of view, but also provides crucial insights to evaluate the feasibility of adjacent channel co-existence for a given receiver.

### 4.1.1 Main Contributions

In this chapter, we analyze bounds on the achievable rate of nonlinear receivers for a tractable test input spectrum and obtain closed form expressions exploiting the properties and characteristics of the nonlinear model. We then use the rate analysis to propose metrics for quantifying receiver performance with nonlinearity, compare disparate receivers' operations for a given radio environment, and evaluate the feasibility (or performance detriment) of a given receiver to operate in a specific radio environment. The main contributions are:

1. We analyze the behavior of adjacent channel interference for a reference input spectrum and study the interplay between front-end filter bandwidth and nonlinearity, in Section 4.2.1;
2. We evaluate the bounds on achievable rate for a tractable reference input spectrum, which is a uniform power spectrum, by obtaining closed form expressions for nonlinear receivers, in Section 4.2;
3. In Section 4.3, we propose receiver performance metrics, to compare disparate receivers using the analysis carried out for the reference input signal. This provides a generalized framework for quantifying receiver performance; and
4. Present extensive numerical evaluations to illustrate the potential impact on achievable rates due to receiver nonlinearity through information theoretic quantification, in Section 4.4.

## 4.2 Achievable Rates for non-ideal receivers

In this section, we evaluate limits on achievable rates for the reference input spectrum. We will use this analysis to quantify receiver performance. Let an arbitrary signal characterized by the Power Spectral Density (PSD), $P(f)$ enter the receiver pre-selector filter. The information theoretic maximum rate of information transfer over the wireless channel for an ideal receiver, $C_{\mathsf{IdealRx}}$ is given by Shannon's limit,

$$C_{\mathsf{IdealRx}} = \int_{f_1}^{f_2} \log_2 \left(1 + \frac{P(f)}{N_0}\right) df, \tag{4.1}$$

where $N_0$ is the AWGN noise power per Hertz. Shannon's limit however is applicable to an ideal receiver and does not account for the limitations imposed by the RF front-end nonlinearity.

Receiver front-end components exhibit nonlinear behavior, which results in Adjacent Channel Interference (ACI) that falls in the desired channel and can essentially be treated as additive noise. However, unlike white noise, the adjacent channel interference is frequency selective. The PSD of this noise, $P_{\mathsf{ACI}}(f)$, is essentially the adjacent channel interference power. This additional interference can cause a significant drop in the achievable rate for a given receiver. In order to characterize the achievable rates of non-ideal receivers, a clear understanding of their behavior is imperative. It is important to note that two main factors lead to adjacent channel interference: (1) Receiver nonlinearity and imperfections, and (2) the RF environment, which dictate the out-of-band power entering the receiver pre-selector. If $P_{\mathsf{max}}$ is the maximum in-band power, the achievable rate of a non-ideal receiver, $C_{\mathsf{NonidealRx}}$, becomes limited by $P_{\mathsf{ACI}}(f)$,

$$C_{\mathsf{NonidealRx}} = \max_{\int_{f_1}^{f_2} P(f) \leq P_{\mathsf{max}}} \int_{f_1}^{f_2} \log_2 \left(1 + \frac{P(f)}{P_{\mathsf{ACI}}(f) + N_0}\right) df \tag{4.2}$$

We have described ways to obtain the $P_{\mathsf{ACI}}(f)$ spanning the desired range of frequencies, $f_1 \leq f \leq f_2$ (desired channel) in the previous chapter. The information theoretic rate of such a channel can be shown to be [66, 67],

$$C_{\mathsf{NonidealRx}} = \frac{1}{2} \int_{f_1}^{f_2} \log_2 \left(1 + \frac{(v - P_{\mathsf{ACI}}(f))^+}{P_{\mathsf{ACI}}(f) + N_0}\right) df \tag{4.3}$$

where $v$ is chosen so that it satisfies $\int (v - P_{\mathsf{ACI}}(f))^+ df = P_{\mathsf{max}}$ [66]. Since each frequency within the bandwidth has a different noise power, the total transmit power has to be accordingly distributed across frequencies to maximize capacity. It can be shown that the optimal distribution is to transmit highest powers on frequencies corresponding to lowest noise power, thus extracting the maximum capacity from the best channels. This optimal distribution can be obtained via the water-filling algorithm [67]. In the ensuing analysis we assume a uniform input power spectrum to evaluate the achievable rate expressions. The procedure to evaluate bounds on achievable rates for any known arbitrary power spectrum remains the same. We use a uniform input spectrum (multi-tone comb input) as a test signal to quantify receivers, and hence the analysis is specific to this input.

### 4.2.1 Evaluating Third Order Distortion Power for Reference Test Input

In this section, we present some results on the total distortion power for the reference test input spectrum. We use the definitions and results developed here to derive bounds on achievable rates.

#### Continuous Domain

Consider a receiver RF chain, with a pre-selector filter bandwidth $B$. The desired channel lies between $f_1$ and $f_2$ with a signaling bandwidth $W = f_2 - f_1, W < B$. Continuous domain analysis is done by letting $\mathcal{W} \to 0$ and integrating over the specific frequencies of interest.

**Definition 1.** *The ratio of the desired signal bandwidth to the pre-selector filter bandwidth is defined using the parameter* $\beta = \frac{W}{B}$.

We carry out the ensuing analysis for a reference input of power spectrum uniform across the pre-selector filter frequencies. (Note that the in-band to out-of-band power ratio are not equal, and they depend on the ratio of signal bandwidth, $W$, to pre-selector bandwidth, $B$). The pre-selector bandwidth spans from $-\frac{B}{2}$ to $\frac{B}{2}$ w.r.t the center of baseband, which is $f = 0$ for this analysis. The amplitude spectrum is,

$$A(f) = A\left(u(f + \frac{B}{2}) - u(f - \frac{B}{2})\right) \tag{4.4}$$

where $A$ is the amplitude units per Hz, and $u(\bullet)$ is the unit step function.

The amplitude and power spectra of the adjacent channel interference for a uniform input spectrum are respectively given by,

$$A_{\mathsf{ACI}}(f) = \alpha_3 A^3 \left(\frac{3}{4}B^2 - f^2\right); \quad -\frac{B}{2} \leq f \leq \frac{B}{2} \tag{4.5}$$

$$P_{\mathsf{ACI}}(f) = \alpha_3^2 P^3 \left(\frac{3}{4}B^2 - f^2\right)^2; \quad -\frac{B}{2} \leq f \leq \frac{B}{2} \tag{4.6}$$

where $P = A^2$ denotes the power of the signal per Hz. If the desired signal lies arbitrarily in $-\frac{W}{2} \leq f \leq \frac{W}{2}$, the total adjacent channel interference power for a uniform input spectrum is given by,

$$P_{\mathsf{ACI}} = \alpha_3^2 B^5 P^3 \left(\frac{1}{5}\beta^5 - \frac{1}{2}\beta^3 + \frac{9}{16}\beta\right) \tag{4.7}$$

**Lemma 5.** *If the input spectrum $A(f)$ is uniform, the adjacent channel interference power $P_{\mathsf{ACI}}(f)$ is maximum at the center of the pre-selector filter $f = 0$, where preselector spans in $\frac{-B}{2} \leq f \leq \frac{B}{2}$.*

*Proof.* Consider the power spectrum of adjacent channel interference, $P_{\mathsf{ACI}}(f) = \alpha_3^2 \left(\frac{3}{4}B^2 - f^2\right)^2$. To find the maxima, we set the first derivative to zero: $\frac{d(P_{\mathsf{ACI}}(f))}{df} = -2f \cdot 2\alpha_3^2 \left(\frac{3}{4}B^2 - f^2\right) = 0$.

This yields $f = 0$ and $f = \pm\frac{\sqrt{3}}{2}B$. Since the pre-selector span is $-\frac{B}{2} \leq f \leq \frac{B}{2}$ and $|\frac{\sqrt{3}}{2}B| > |\frac{B}{2}|$, the solution $f = \pm\frac{\sqrt{3}}{2}B$ is invalid.

Taking the second derivative we have, $\frac{d^2(P_{\mathsf{ACI}}(f))}{df^2} = -2f \cdot 2\alpha_3^2 \left(\frac{3}{4}B^2 - 2f\right) - 2 \cdot 2\alpha_3^2 \left(\frac{3}{4}B^2 - f^2\right)$.

Evaluating at $f = 0$, we obtain $\frac{d^2(P_{\mathsf{ACI}}(f))}{df^2}|_{f=0} = -3\alpha_3^2 B^2 < 0$. Thus, $f = 0$ is a maximum. □

**Discrete Domain**

Consider a receiver RF chain, with a pre-selector filter spanning $N$ discrete channels (frequency bins). Let the desired signal span $K \in [1, N]$ channels, arbitrarily between $n_1 \in [1, N]$ and $n_2 \in [1, N]$; $(n_2 > n_1)$ such that $K = n_2 - n_1 + 1$. As with the continuous domain, we carry out the analysis for a reference input of uniform spectrum amplitude $A$ per bin given by, $A(n) = A\left(u[1] - u[N]\right)$, where $u[\bullet]$ represents the discrete unit step function. This essentially is a multi-tone input as the reference test signal. Using this as the input spectrum and solving the double convolution in the discrete domain, the third order distortion at any frequency channel can be obtained. Post convolution, the indices for the desired range of the pre-selector filter will span the frequency bins $n \in [N, (2N-1)]$ and the desired channel range is derived to be $\kappa_1 = n_1 + N - 1$, $\kappa_2 = n_2 + N - 1$.

$$\rho_n = \alpha_3 A^3 \left(3N(1-N) - 2n(n+1) + 6nN\right); \quad N \leq n \leq 2N-1 \tag{4.8}$$

The total adjacent channel interference power for the $K$ desired channels is given by $P_{\mathsf{ACI}} = \sum_{n=\kappa_1}^{\kappa_2} \rho_n^2$ and is computed to be,

$$\begin{aligned} P_{\mathsf{ACI}} = & \frac{1}{15} K \big(-270\kappa_1 N^3 - 270\kappa_2 N^3 + 240\kappa_1^2 N^2 + 240\kappa_2^2 N^2 + 240\kappa_1 N^2 + 240\kappa_1\kappa_2 N^2 + 480\kappa_2 N^2 \\ & - 90\kappa_1^3 N - 90\kappa_2^3 N - 90\kappa_1^2 N - 90\kappa_1\kappa_2^2 N - 270\kappa_2^2 N - 90\kappa_1^2\kappa_2 N - 180\kappa_1\kappa_2 N - 180\kappa_2 N \\ & + 12\kappa_1^4 + 12\kappa_2^4 + 12\kappa_1^3 + 12\kappa_1\kappa_2^3 + 48\kappa_2^3 - 8\kappa_1^2 + 12\kappa_1^2\kappa_2^2 + 36\kappa_1\kappa_2^2 + 52\kappa_2^2 - 8\kappa_1 + 12\kappa_1^3\kappa_2 \\ & + 24\kappa_1^2\kappa_2 + 16\kappa_1\kappa_2 + 8\kappa_2 + 135N^4 - 270N^3 + 135N^2\big) \end{aligned} \tag{4.9}$$

### 4.2.2 No Knowledge at Transmitter

In this section, we analyze bounds on achievable rates of non-ideal receivers, assuming no knowledge of the receiver characteristics at the transmitter. Thus, the variation of interference power as a function of frequency is unknown at the transmitter and the latter cannot carry out frequency selective power allocation to compensate for the nonlinear adjacent channel interference. The achievable rate treating interference as noise [68–70] in this case is given by,

$$C_{\mathsf{NoTx}} = \int_{-\frac{W}{2}}^{\frac{W}{2}} \log_2\left(1 + \frac{P}{P_{\mathsf{ACI}}(f) + N_0}\right) df = \int_{-\frac{W}{2}}^{\frac{W}{2}} \log_2\left(1 + \frac{P}{\alpha_3^2 P^3 \left(\frac{3}{4}B^2 - f^2\right)^2 + N_0}\right) df \tag{4.10}$$

Evidently the closed form expression for (4.10) is extremely complex and hence we give some simple bounds.

#### Lower Bound

A lower bound on $C_{\mathsf{NoTx}}$ is obtained by setting $f = 0, \forall f \in [-\frac{W}{2}, \frac{W}{2}]$ (also evident from Theorem 5). Thus,

$$C_{\mathsf{NoTx}} \geq W \log_2\left(1 + \frac{P}{\frac{9}{16}\alpha_3^2 P^3 B^4 + N_0}\right) \tag{4.11}$$

#### Upper Bound

A upper bound on $C_{\mathsf{NoTx}}$ is obtained by setting $\mid f \mid = \frac{W}{2}, \forall f \in [-\frac{W}{2}, \frac{W}{2}]$ (also evident from Lemma 5). Thus,

$$C_{\mathsf{NoTx}} \leq W \log_2\left(1 + \frac{P}{\frac{1}{16}\alpha_3^2 P^3 B^4 (3 - \beta^2)^2 + N_0}\right) \tag{4.12}$$

#### Loss in SINR

It is useful to quantify the loss in SINR due to nonlinearity. We give a range for loss with respect to the upper and lower bounds, but note that the gap is not significant for practical purposes. The

loss in SINR, $\Delta\mathsf{SINR}$ (dB)= $\mathsf{SINR}_{\mathsf{Ideal}}$(dB)$-\mathsf{SINR}_{\mathsf{NoTx}}$(dB) for this case is given by,

$$10\log_{10}\left(1+\frac{\frac{1}{16}\alpha_3^2P^3B^4(3-\beta^2)^2}{N_0}\right)\leq\Delta\mathsf{SINR}\leq 10\log_{10}\left(1+\frac{\frac{9}{16}\alpha_3^2P^3B^4}{N_0}\right) \tag{4.13}$$

**Discrete Domain**

For the discrete channelized spectrum, the achievable rate $C_{\mathsf{NoTx|dis}}$ can be computed as,

$$C_{\mathsf{NoTx|dis}}=\sum_{n=\kappa_1}^{\kappa_2}\log_2\left(1+\frac{P}{\alpha_3^2P^3\left(3N(1-N)-2n(n+1)+6nN\right)^2+N_0}\right) \tag{4.14}$$

where $P$ is the power per channel, $n$ is the channel index, $N$ is the total number of channels, and $N_0$ is the noise power per channel.

### 4.2.3 With Knowledge at Transmitter

In this section, we analyze the achievable rates of non-ideal receivers assuming the transmitter can carry out frequency selective power allocation. The problem reduces to a communication link using parallel channels with different interference levels, and water-filling is shown as optimal for such a case [66, 67]. The level $v$ of the water-filling technique is found out as, $\int_{-\frac{W}{2}}^{\frac{W}{2}}\left(v-(P_{\mathsf{ACI}}(f)+N_0)\right)^+df=P_{\mathsf{max}}$ where $P_{\mathsf{max}}=PW$ assuming that the transmit power is $P$ per Hertz. It is not possible to arrive at a closed form expression for $v$ without making some assumptions on $P$, and hence a closed form expression for the achievable rate is also not obtainable. However, we provide some approximations. Changing the power levels in the desired channels effectively results in small changes in the adjacent channel interference, and hence the achievable rate should reflect these changes. In this analysis, we ignore these minor and insignificant changes in lieu of mathematical tractability. Consider the adjacent channel interference $P_{\mathsf{ACI}}(f)=\alpha_3^2P^3\left(\frac{3}{4}B^2-f^2\right)^2$, which is biquadratic in $f$. Thus, the line $y=v$ intersects the $P_{\mathsf{ACI}}(f)$ curve at a maximum of two points. Further, since $P_{\mathsf{ACI}}(f)$ is an even function, the points are equidistant from the y-axis. Let the frequency co-ordinates of these two points be denoted by $\pm f_a,\ f_a\in\left[-\frac{W}{2},\frac{W}{2}\right]$. Since $P_{\mathsf{ACI}}(f)>v,\ \forall f\in[-f_a,+f_a]$, frequencies in the range $[-f_a,+f_a]$ will not be allocated any power by the water-filling technique. Thus, the fraction of channels utilized for communication is given by $\left(\frac{2f_a}{W}\right)$, and for this range of frequencies, $v-(P_{\mathsf{ACI}}(f)+N_0)>0$ is satisfied.

We now obtain the frequency co-ordinate intercepts, $\pm f_a$ of the line $y = v$ and the curve $y = P_{\mathsf{ACI}}(f) + N_0$ by solving the equation $v = \alpha_3^2 P^3 \left(\frac{3}{4}B^2 - f_a^2\right)^2 + N_0$ for $f_a$ as,

$$f_a = \pm\frac{B}{\sqrt{2}}\sqrt{\left(\frac{3}{2} \pm \sqrt{\frac{9}{4} - 4\left(\frac{9}{16} - \frac{v - N_0}{\alpha_3^2 P^3 B^4}\right)}\right)} \tag{4.15}$$

In practice, since $B >> f_a$, we approximate by ignoring the fourth order terms and obtain $f_a$ as

$$f_a = \pm B\sqrt{\frac{2}{3\alpha_3^2 P^3 B^4}\left(\frac{9}{16} - v\right)} \tag{4.16}$$

Using (4.16), we provide an approximation on the value of $v$ for any given set of parameters for which all channels will have a non-zero power allocation, by solving for $v$ in $2f_a \leq 0$ as, $v \geq \frac{9}{16}$W/Hz. Substituting $P_{\mathsf{ACI}}(f) = \alpha_3^2 P^3 \left(\frac{3}{4}B^2 - f^2\right)^2$ in $\int_{-\frac{W}{2}}^{\frac{W}{2}} \left(v - (P_{\mathsf{ACI}}(f) + N_0)\right)^+ df = P_{\mathsf{max}}$,

$$2v\left(\frac{W}{2} - f_a\right) - \alpha_3 P^3\left(\frac{9}{16}B^4\left(\frac{W}{2} - f_a\right) + \frac{W^5}{32} - f_a^5 - \frac{3}{2}B^2\left(\frac{W^3}{8} - f_a^3\right)\right) = P_{\mathsf{max}} \tag{4.17}$$

To obtain a closed form for $v$, we need to solve (4.16) and (4.17) simultaneously, which requires solving a quintic equation. However, the Abel-Ruffini theorem [71–74] states that no algebraic solutions exist to general polynomial equations of fifth or higher degrees with arbitrary co-efficients. Thus, $v$ can be obtained using numerical root-finding methods like Regula-Falsi, Newton-Raphson, or Laguerre's, etc.

We obtain the achievable rate with the knowledge at transmitter with water-filling,

$$C_{\mathsf{WF}} = 2\int_{-\frac{W}{2}}^{-f_a} \log_2\left(1 + \frac{\left(v - \alpha_3^2 P^3\left(\frac{3}{4}B^2 - f^2\right)^2 - N_0\right)}{\alpha_3^2 P^3\left(\frac{3}{4}B^2 - f^2\right)^2 + N_0}\right) df \tag{4.18}$$

Solving this integral, assuming $P_{\mathsf{ACI}}(f) >> N_0$ ($\mathsf{ACI}$ significantly higher than nominal noise floor) and ignoring the complex terms (which result only in the non-applicable range of $f > B$), we obtain the achievable rate for a uniform input spectrum with the transmitter accounting for third order distortions with water-filling power allocation as

$$\begin{aligned} C_{\mathsf{WF}} &= 2\int_{-\frac{W}{2}}^{-f_a} \log_2\left(1+\frac{\left(v-\alpha_3^2P^3\left(\frac{3}{4}B^2-f^2\right)^2-N_0\right)}{\alpha_3^2P^3\left(\frac{3}{4}B^2-f^2\right)^2+N_0}\right)df \\ &= 2\int_{-\frac{W}{2}}^{-f_a} \log_2\left(\frac{v}{\alpha_3^2P^3\left(\frac{3}{4}B^2-f^2\right)^2+N_0}\right)df \end{aligned} \tag{4.19}$$

Solving this integral assuming $P_{\mathsf{ACI}}(f) >> N_0 \Rightarrow \alpha_3^2P^3\left(\frac{3}{4}B^2-f^2\right)^2 >> N_0$ we have,

$$C_{\mathsf{WF}} = 2\int_{-\frac{W}{2}}^{-f_a} \log_2(v)df - 2\int_{-\frac{W}{2}}^{-f_a} \log_2\left(\alpha_3^2P^3\left(\frac{3}{4}B^2-f^2\right)^2\right)df \tag{4.20}$$

We can simplify this as,

$$\begin{aligned} C_{\mathsf{WF}} = 2\int_{-\frac{W}{2}}^{-f_a} \log_2(v)df - 2\int_{-\frac{W}{2}}^{-f_a} \log_2\left(\alpha_3^2P^3\right) - \\ 4\int_{-\frac{W}{2}}^{-f_a} \log_2\left(\frac{\sqrt{3}}{2}B+f\right) - 4\int_{-\frac{W}{2}}^{-f_a} \log_2\left(\frac{\sqrt{3}}{2}B-f\right) \end{aligned} \tag{4.21}$$

All the integrals above are in standard form. Solving them and simplifying, we obtain

$$\begin{aligned} C_{\mathsf{WF}} = 2\left(\frac{W}{2}-2f_a\right)\log_2\left(\frac{v}{\alpha_3^2P^3}\right) - 4\left(f_a-\frac{W}{2}\right) + \sqrt{3}B\log_2\left(\frac{\frac{\sqrt{3}}{2}B-\frac{W}{2}}{\frac{\sqrt{3}}{2}B-f_a}\right) + \\ 2f_a\log_2\left(\frac{3}{4}B^2-f_a^2\right) - W\log_2\left(\frac{3}{4}B^2-\frac{W^2}{4}\right) \end{aligned} \tag{4.22}$$

**Discrete Domain**

For the case of a discrete channelized spectrum, the level $v$ of the water-filling technique is computed using $\sum_{n=\kappa_1}^{\kappa_2}\left(v-\left(P_{\mathsf{ACI}}[n]+N_0\right)\right)^+ = P_{\mathsf{max}}$. The water-filling algorithm [66, 67] is employed to evaluate $v$ and the achievable rate is then computed as,

$$C_{\mathsf{WF|dis}} = \sum_{n=\kappa_1}^{\kappa_2} \log_2\left(1+\frac{\left(v-\alpha_3^2P^3\left(3N(1-N)-2n(n+1)+6nN\right)^2-N_0\right)^+}{\alpha_3^2P^3\left(3N(1-N)-2n(n+1)+6nN\right)^2+N_0}\right) \tag{4.23}$$

## 4.3 Receiver Performance Metrics

Practical deployment and operations of shared spectrum systems demand that the receivers be immune to a 'certain amount' of 'harmful' interference. The FCC, OFCOM, and other regulatory agencies have repeatedly emphasized this fact through their consultations and proceedings [30,33]. However, metrics to quantify the 'quality' of receivers need to be carefully evolved, given the extent of diverse requirements and operating characteristics of different technologies. The metrics should capture the interplay between the receiver characteristics and the input spectrum relative to the operational bandwidth of the desired signal. Using the analysis presented in the preceding sections, we outline a generalized framework to measure receiver performance and this can be extended for the development of standards and band specific metrics for receiver performance.

In this section, we propose a methodology to quantify the impact of receiver nonlinearity on its performance. Comparative quantification of receivers belonging to diverse RAT requires technology and spectrum agnostic test conditions. We use the information theoretic limits of a non-ideal receiver to quantify its performance with respect to an ideal receiver. We propose that the uniform input spectrum be used as a reference input since (a) it offers analytical tractability, (b) it is easily reproducible experimentally, (c) it provides for an unbiased input from a spectrum-centric perspective, and (d) it gives a performance measure as a function of in-band to out-of-band received power. In the discrete domain, a uniform input spectrum amounts to exciting the receiver with an equally spaced multi-tone input spanning its pre-selector bandwidth to measure its impact on desired channels. The framework developed in the initial sections and the achievable rate analysis of the preceding sections of this chapter can now be directly applied for quantifying a receiver's performance. Using this methodology, we now define receiver performance metrics to quantify the impact of nonlinearity and adjacent channel signals.

**Definition 2.** *We define the Receiver Performance Metric,* $\sigma(f) = \frac{C_{\mathsf{NonidealRx}}(f)}{C_{\mathsf{IdealRx}}(f)}$ *as the ratio of the achievable rate by a given receiver to the maximum rate achievable by the link. We also define Fractional Rate Loss, as* $\varepsilon(f) = 1 - \sigma(f) = \frac{C_{\mathsf{IdealRx}}(f) - C_{\mathsf{NonidealRx}}(f)}{C_{\mathsf{IdealRx}}(f)}$.

We note that the objective of a given receiver may not be to optimize for these information theoretic metrics and the practical operating radio environment may vary significantly between various bands of operation (and may not resemble uniform input spectrum). However, as stated before, this analysis is meant to be used as an initial reference point in quantifying receivers and is expected to pave the way in initiating the research necessary for bridging the gap between

theoretical metrics developed from hypothetical reference points and practical performance metrics required for operational deployment of technology.

## 4.4 Numerical Simulations and Experimental Results

### 4.4.1 Adjacent Channel Interference for Example Practical Measurement

In order to demonstrate the practical utility and importance of the proposed representation in Chapter 3, and to illustrate the interplay between nonlinearity and pre-selector filter, we present results from a practical measurement example. Measured spectrum traces were collected from the Microsoft Spectrum Observatory in the range between $500$ MHz and $700$ MHz. This spectrum has several active TV stations operating and the FCC is soon planning a reverse auction to open this spectrum for commercial broadband with sharing.

For computation of the third order distortion, the spectrum was channelized with a bandwidth $\mathcal{W} = 1$ MHz and the pre-selector bandwidth was assumed to span the entire range of frequencies. The noise floor was computed to be less than $-100$ dBm for the $1$ MHz channel and $\mathsf{IIP}_3 = -5$ dBm was assumed. The third order distortion on this spectrum trace was computed using the representation presented in this chapter and is as shown in Fig. 4.1a. While searching for white spaces for opportunistic wireless operations, the raw spectrum measurement will yield insufficient information. For example, the channels between $660$ MHz and $670$ MHz appear to be unoccupied, but for the receiver parameters considered in this computation, as evident from the figure, the third order distortion produces strong interference.

Further, we vary the pre-selector bandwidth, while keeping $\mathcal{W} = 1$ MHz, and evaluate the average interference power arising due to receiver nonlinearity for a $10$ MHz channel between $660$ MHz and $670$ MHz. Note that each value of filter bandwidth gives a different $\beta$. The results are presented in Fig. 4.1b. As expected, with decreasing nonlinearity, the interference power decreases and better filter selectivity ensures better co-existence. As seen, the interplay between pre-selector filter and receiver nonlinearity is an important consideration for receiver compatibility evaluation and adjacent channel co-existence analysis, which are imperative in next generation heterogeneous wireless systems.

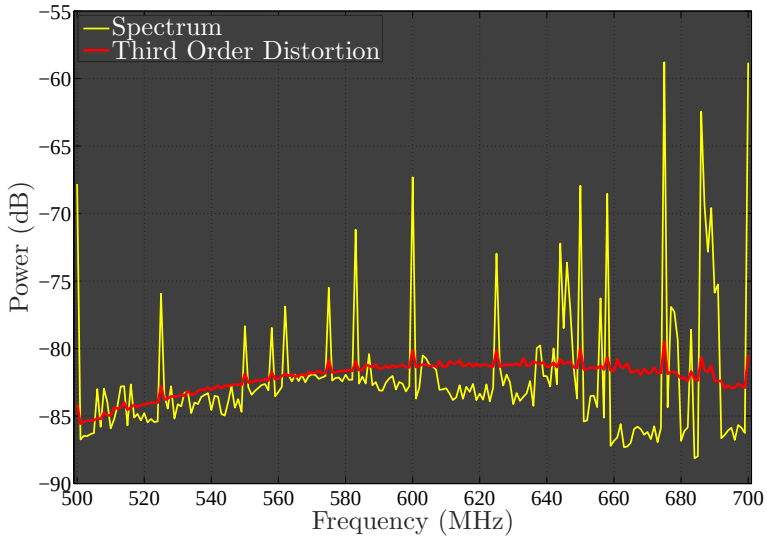


(a)

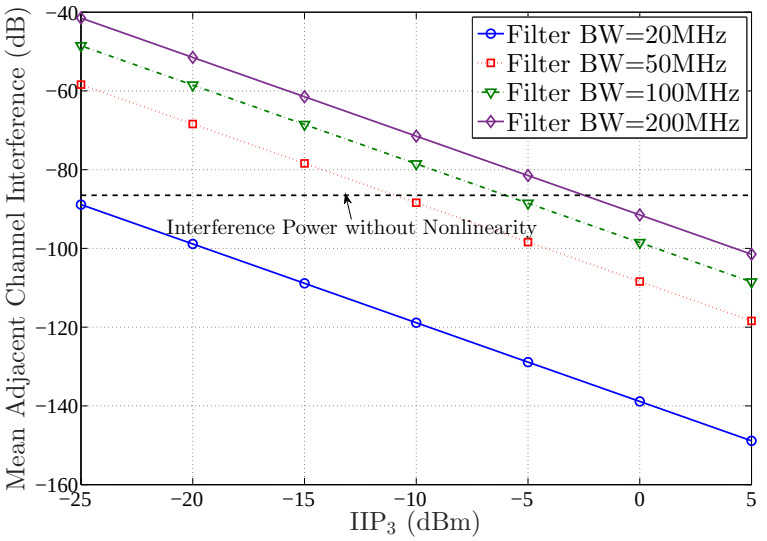


(b)

Figure 4.1: (a) Practical measured spectrum and computation of third order distortion levels (b) Variation of Mean Interference Power between 660 MHz-670 MHz due to Adjacent Channel Interference for different $\mathsf{IIP}_3$ and front-end filter Bandwidths for the measured spectrum.

### 4.4.2 Adjacent Channel Interference

In this section, we examine the behavior of the adjacent channel interference for the test input spectrum as described in Section 4.2.1. We carry out numerical evaluations for a pre-selector bandwidth, $B = 150$ MHz. Signal bandwidth $W$ is varied from $1$ MHz to $150$ MHz. We present results for various values of the receiver nonlinearity by varying $\mathsf{IIP_3}$. The behavior of $P_{\mathsf{ACI}}$ with $\beta = \frac{K}{N}$, the fraction of the channels used, is shown in Fig. 4.2. Note that the adjacent channel interference increases as the number of desired channels are increased because compressive distortion and cross modulation are proportional to the number of desired channels, which results in third order distortion noise.

### 4.4.3 Achievable Rates

In this section, we present the numerical evaluations of achievable rates analyzed in Section 4.2. Figure 4.3 shows the achievable rate of the non-ideal receiver for various values of nonlinearity with varying $\beta$ considering the total third order distortion. Due to compressive distortion, even when the signal bandwidth hypothetically occupies the entire pre-selector bandwidth ($\beta = 1$) we see the performance detriment. From a receiver-centric point of view, when $\beta = 1$, the receiver is not actively 'sharing' spectrum with other users, even if it is operating in a shared spectrum band. We note that the focus of this chapter is to develop a framework for adjacent channel co-existence analysis in dynamic spectrum sharing scenarios and not to address the generic issues relating receiver nonlinearity. Issues of gain compression due to compressive distortion when $\beta = 1$ are not unique to spectrum sharing systems, and it has been dealt in great detail in the literature. Thus, in Fig. 4.4 we present the results for achievable rate ignoring the effects of compressive distortion for the desired channels. As expected, as $\beta \to 1$, the achievable rate approaches the ideal case.

### 4.4.4 Receiver Performance Metrics

In this section, we discuss the receiver performance metrics presented in Definition 2. To gauge the detriment in performance, we present results in terms of fractional rate loss, compliment of the receiver performance metric. Figure 4.5 shows the fractional rate loss for different power levels of the input spectrum. As evident from the figures, nonlinearity can potentially cause very high rate loss. Such curves can be used as reference points to compare the adjacent channel co-existence abilities of receivers belonging to diverse technologies. As an example use case, consider the newly

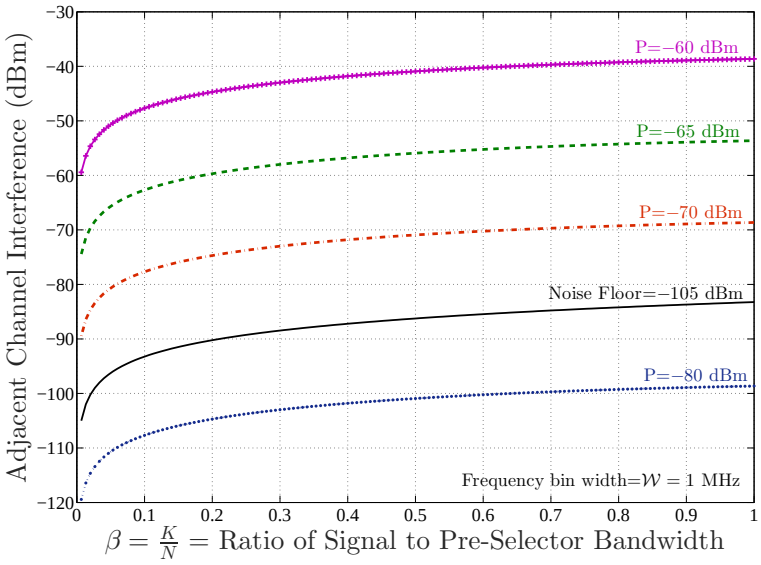


Figure 4.2: Variation of Adjacent Channel Interference, $P_{\mathsf{ACI}}$ with $\beta$, $\mathsf{IIP_3} = -15$ dBm.

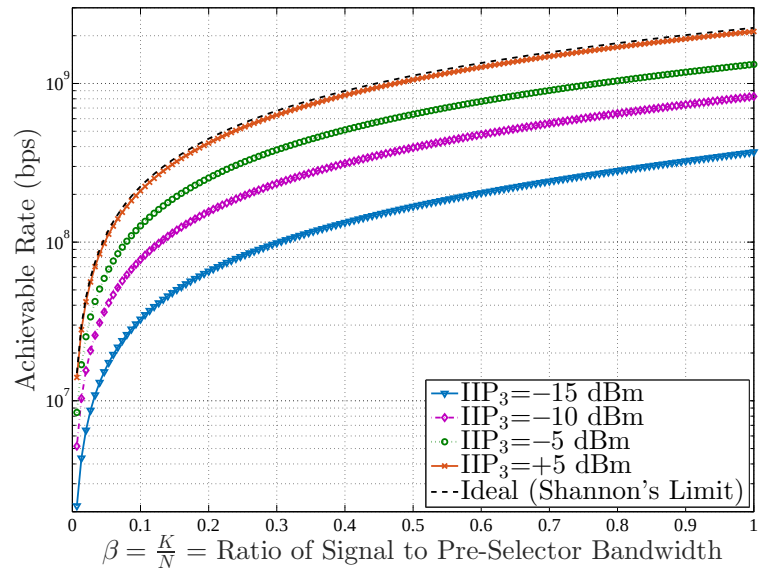


Figure 4.3: Variation of Achievable Rate with $\beta$, $P = -60$dBm.

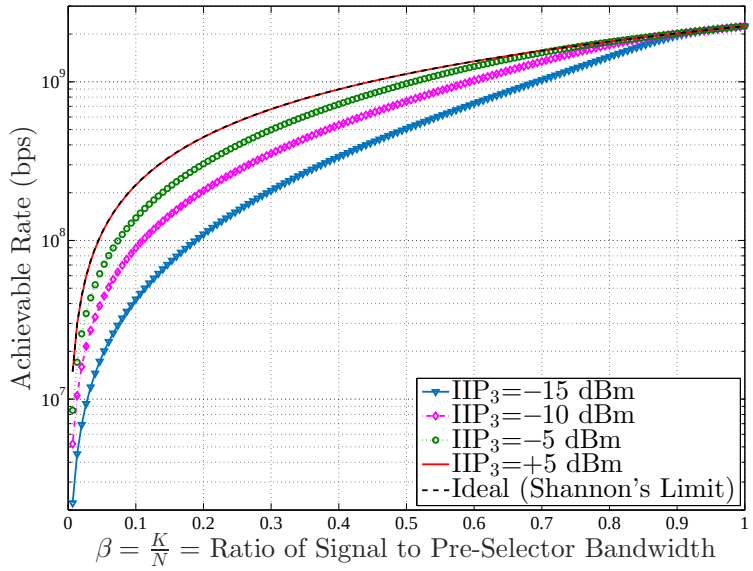


Figure 4.4: Variation of Achievable Rate with $\beta$, $P = -60$dBm, No Compressive Distortion.

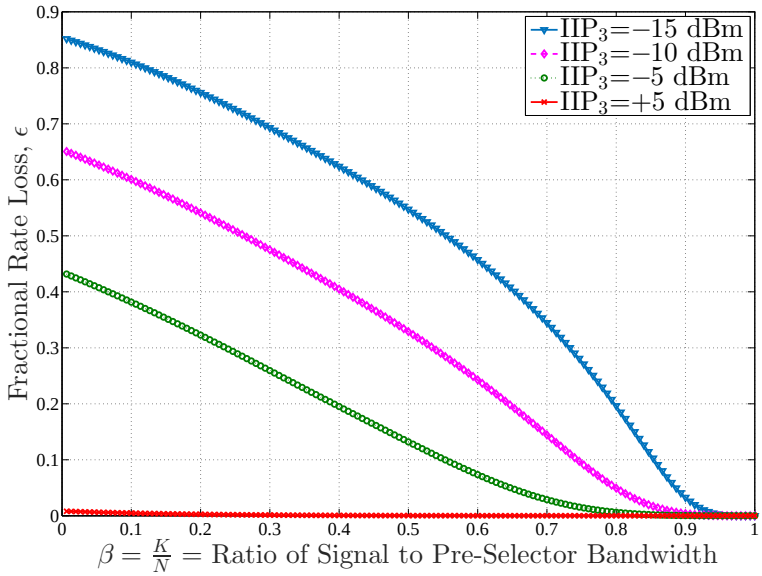


Figure 4.5: Variation of Fractional Rate Loss, $\varepsilon$ with $\beta$, $P = -60$dBm, No Compressive Distortion.

opened spectrum in the 3.5 GHz band for sharing. There are 15 channels in the band, and a given wireless service user will occupy one channel. Thus, for a receiver pre-selector spanning the entire band, $\beta = 0.067$, but for a receiver with pre-selector spanning 2 channels (20 MHz), $\beta = 0.5$. From the Fig. 4.5, it is evident that for low values of $\beta < 0.1$, the fractional rate loss even for an $\mathsf{IIP}_3$ of $-5$dBm is around $40\%$, which is very high. Comparing this with a receiver whose $\beta = 0.5$, the loss for $\mathsf{IIP}_3$ of $-5$dBm is around $12\%$ and the loss for $\mathsf{IIP}_3$ of $-10$dBm is around $32\%$. This gives a framework for comparing adjacent channel co-existence performance of disparate receivers using reference input spectrum. In addition, although the simulations have not been performed for a specific system or band, such studies offer empirical bounds on the performance limits that can be expected.

### 4.4.5 Bit Error Rate

Bit Error Rate (BER) is another useful metric to gauge the performance of a given communication link. In this section we present the results of bit error rate performance of a receiver with nonlinearity for different values of $\mathsf{IIP}_3$ for a 16-QAM modulation with RSC(11,15) coding in AWGN channel. The adjacent channel interference resulting from nonlinear distortion was computed as per Proposition 4 and the resulting SINR was used to evaluate BER. Figure 4.7 shows the curves for various values of receiver nonlinearity, for $\beta = \frac{1}{15}$, with $-60$ dBm received power in each adjacent channel. At low in-band $E_b/N_0$, nonlinearity has a minimal effect since noise power will either be of the same order as the distortion power or higher. However, as $E_b/N_0$ increases, nonlinear distortion dominates and effectively degrades the overall $E_b/N_0$ resulting in performance loss.

### 4.4.6 Theoretical Receiver Performance Metric and Practical Throughput

We have carried out throughput measurements in the presence of adjacent channel interfering signals causing third order distortions using USRP X310. The measurements are carried out for 3 different front-end gains and nonlinearity ($\mathsf{IIP}_3$). We want to make it clear that, while throughput may be linked to the achievable rate analysis and may follow a similar trend, a direct comparison between theoretical rate analysis and practical throughput is not meaningful. Rate is computed using raw SINR, but depending on the modulation and coding, for instance, a relatively small detriment in SINR may not be significant to cause any detriment in throughput, especially at high SINR values. With this caveat that the measurement results cannot be directly compared to the

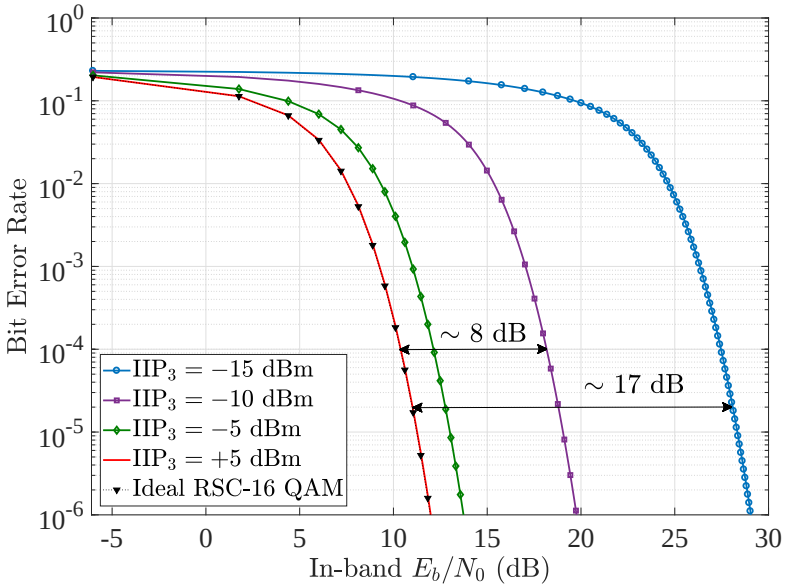


Figure 4.6: Bit Error Rate for RSC Coded 16-QAM system for different receiver nonlinearities

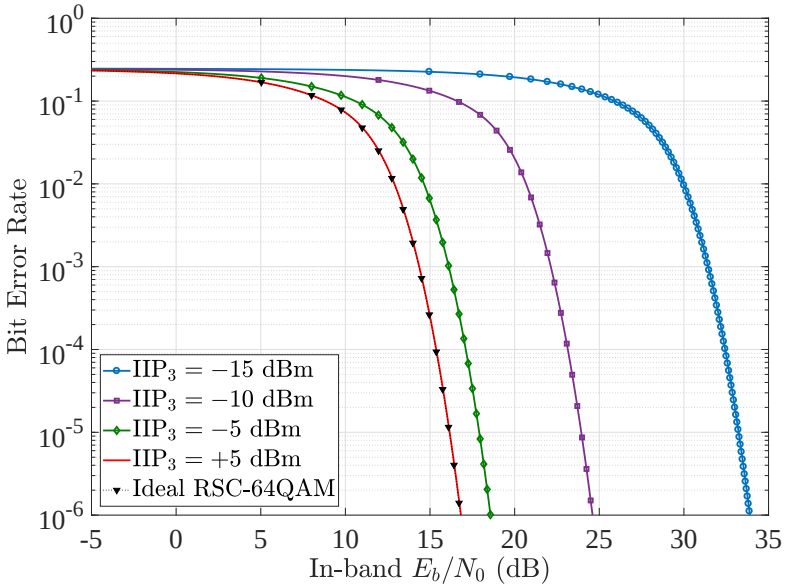


Figure 4.7: Bit Error Rate for RSC Coded 64-QAM system for different receiver nonlinearities

measured throughput, we present the results of the throughput measurements in the chapter. This adds credibility to the theoretical analysis, which aims at quantifying and comparing disparate receivers based on their front-end parameters. This provides the required experimental support for the work in this chapter.

The experimental setup is as shown in Fig. 4.8. The interfering signals are $50$ kHz FM signals, and the desired signal is a $1$ MHz wide OFDM signal with $16$-QAM modulation and $4/5$ rate convolutional coding. The frequency bin width, $\mathcal{W} = 1$ MHz, with $\beta = \frac{1}{5}$. The center frequency of the desired signal was $1544$ MHz, with interferers at $1542$ MHz, $1543$ MHz, $1545$ MHz, and $1546$ MHz. The results are presented in Table II. The theoretical receiver performance metric, $\sigma$ is computed using Definition 2. The theoretical rate for nonlinear receiver, $C_{\mathsf{NonIdeal}}$ is computed using (4.22), using signal power $P$ and measured receiver $\mathsf{IIP_3}$ and noise floor. $C_{\mathsf{Ideal}}$ was computed as the Shannon's limit. This is directly related to the achievable raw bit rate. Thus, two cases which may yield almost the same measured throughput loss, may have different receiver performance metrics. This is because the decrease in raw $\mathsf{SINR}$ may not be sufficient to cause any dent in the throughput for a given modulation and coding, but the calculation of raw bit rate gets significantly affected for the same change in $\mathsf{SINR}$. However, the trend precisely maps to the actual receiver performance. Maximum distortion for the OFDM signal was produced in the center of the channel, with the channel edges facing the least distortions. We note that results for this OFDM signal may vary if the frequency of the interferers is varied, so that different parts of the OFDM signal face maximum interference. Such an elaborate study is however beyond the scope of this chapter, and a topic of future research.

### 4.4.7 Random RF Environment and Worst Case Performance

Consider a realistic scenario, in which a given radio has to operate and co-exist in an unknown and random multi-RAT RF environment. In most practical scenarios, while instantaneous receiver signal power will vary randomly, certain characteristics of the RF environment, such as statistical maximum received power in adjacent channels, expected received power in desired channel, among others, can be ascertained with the knowledge of network topology. In such a scenario, the given radio's capability for adjacent channel co-existence needs to be evaluated a priori. Given the radio receiver nonlinearity, noise floor, and pre-selector filter bandwidth, in this section, we use the representations developed and the achievable rate analysis presented to carry out feasibility of co-existence for an example use case.

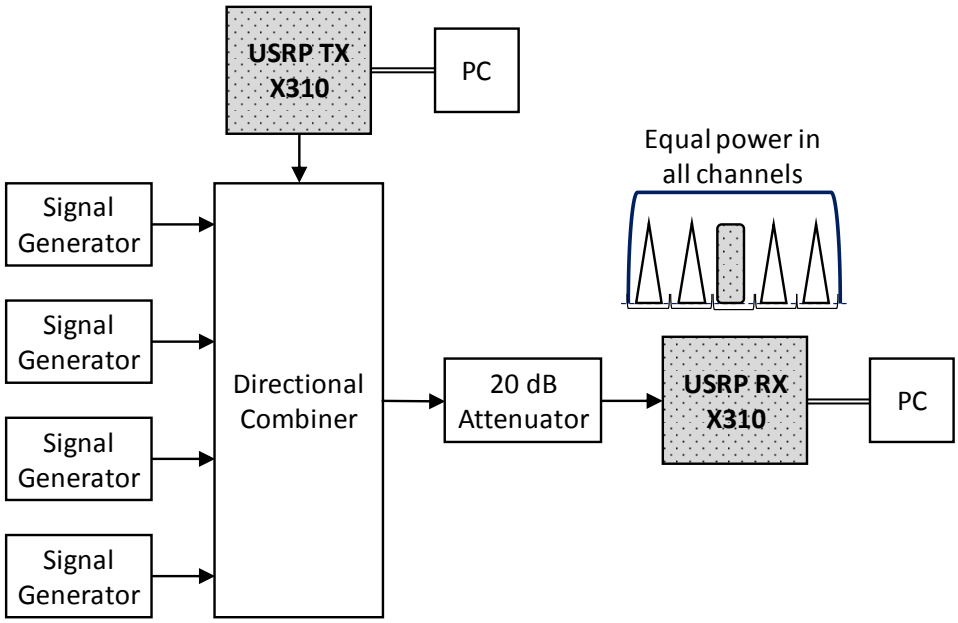


Figure 4.8: Schematic Diagram of Experimental Setup for Throughput Measurement.

Table II: Results of Throughput Measurement

| Receive RF Gain (dB) | Measured IIP3 (dBm) | Signal Power (dBm) | 1 MHz Noise Floor (dBm) | Throughput without Interferers (kbps) | Throughput with Interferers (kbps) | % Loss in Throughput | Theoretical Rx Performance Metric, $\sigma$ |
|---|---|---|---|---|---|---|---|
| 0 | 7.5 | –22.85 | –94.84 | 442.934 | 437.223 | 0.01 | 0.7 |
| | | –32.45 | | 446.778 | 443.912 | 0.00 | 0.9880 |
| | | –42.84 | | 450.223 | 451.224 | -- | 1 |
| 20 | 3.2 | –22.84 | –92.16 | 445.213 | 0.337 | 99.92 | 0.0448 |
| | | –32.43 | | 462.563 | 56.064 | 87.87 | 0.2647 |
| | | –42.47 | | 442.080 | 428.070 | 0.03 | 0.5891 |
| 30 | –4.2 | –22.81 | –89.91 | 440.342 | 0.272 | 99.94 | 0.0002 |
| | | –32.85 | | 440.648 | 5.556 | 98.73 | 0.0025 |
| | | –42.42 | | 440.490 | 25.465 | 94.21 | 0.0916 |

Let $P_{\mathsf{min}}$ and $P_{\mathsf{max}}$ denote the range of values over which the received power varies with a uniform random distribution. Assume that the radio spans $N$ channels, and that the received power in each of these $N$ channels is independent and identically distributed. To quantify the performance loss, we use Proposition 4 to evaluate the nonlinear distortion power, and then evaluate the resulting capacity detriment through extensive network simulations. In addition, an upper bound on the performance loss can be obtained by evaluating the nonlinear distortions assuming maximum received power, $P_{\mathsf{max}}$ in each adjacent channel. This provides worst case performance of the receiver for a random RF environment.

Figure 4.9 shows a Monte-Carlo simulation result for a random radio environment along with an empirical upper bound on fractional rate loss. To obtain each point, received power across all frequencies of the pre-selector was assumed to be i.i.d with a uniform random distribution ranging from $P_{min}$ and $P_{max}$. Thus each realization results in a unique $P_{\mathsf{ACI}}$ at the desired channel which is evaluated using the representations of the preceding sections and the maximum adjacent channel interference in each realization was obtained using the maximum power across all frequency bins for that realization. Each point on the curve represents the results averaged over 10,000 realizations. This experiment was repeated for different variance of received power across frequencies. In particular, $P_{max}$ was varied from $-50$ dBm to $20$ dBm in steps of $2$ dB and $P_{min}$ was fixed at $-60$ dBm. Thus, the x-axis of the figure represents the variation of $P_{max} - P_{min}$ from $10$ dB to $80$ dB. The average fractional loss is shown along with its upper bound for a receiver with $\mathsf{IIP_3} = -5$ dBm and $\beta = 0.1$.

## 4.5 Conclusions

Analysis on adjacent channel interference showed that the maximum number of third order distortion products is produced at the center of the pre-selector filter and the relevant simulations showed the extent to which the apparent noise-floor increases due to nonlinearity. Analysis and evaluation of achievable rates for a reference input spectrum revealed the utility of such analysis for comparative quantification of receiver performance and the detriment caused due to adjacent channel interference. The work presented in this chapter will offer a comprehensive generalized framework for adjacent channel co-existence analysis and comparative quantification of receiver performance which will aid in the development of band and standard specific metrics and spectrum management schemes. Future work includes an analysis of information theoretic upper bounds for achievable rates accounting for nonlinear RF front-ends. Achievable rate analysis

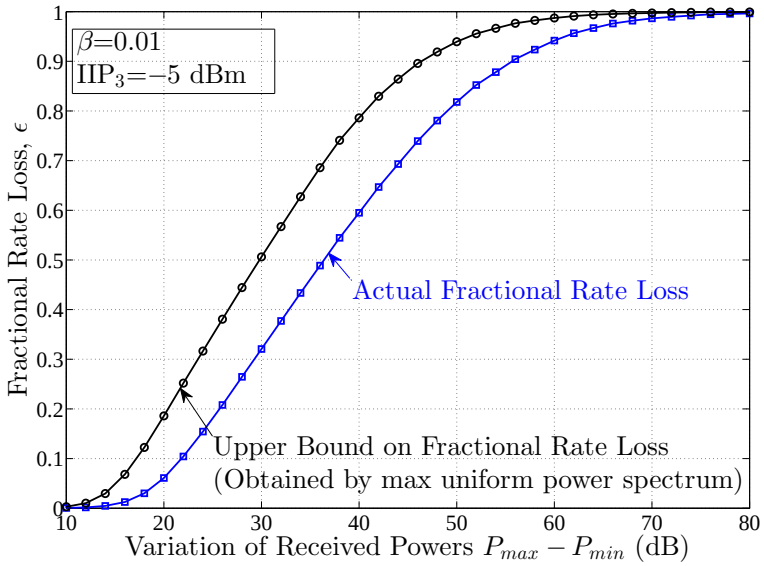


Figure 4.9: Average variation of Fractional Rate Loss in a random radio environment and empirical upper bound

beyond treating interference as noise in these scenarios could provide valuable insights on network design. In addition, carrying out a similar analysis on the detriments caused due to receiver nonlinearity on a comprehensive set of communication metrics such as latency, rigorous analysis of bit error rate, link reliability, etc., will provide insightful details for robust operational design of next generation wireless systems.

# Chapter 5

# Receiver Nonlinearity Aware Dynamic Resource Allocation: Two User Case

## 5.1 Introduction

In this chapter, we demonstrate the benefits of receiver nonlinearity aware network resource management through a simple two-user case by developing a numerical optimization framework. We consider the nonlinear distortion faced by receivers due to adjacent channel signals and propose a framework to carry out resource allocation inclusive of receiver distortions for opportunistic access. We show through simulations that such an allocation can considerably increase data rates and spectrum efficiency. In addition, distortion aware allocation ensures that all receivers, irrespective of their nonlinearity and performance, ensure (as feasible) the minimum Quality of Service (QoS) while maximizing for network throughput. Thus, in a heterogeneous environment, all receivers including legacy systems can be accommodated by distortion aware allocations. The goal of this chapter is to provide insights into developing network level frameworks inclusive of receiver nonlinearity and impairments, and the potential improvements receiver nonliearity awareness brings to spectrum efficiency.

### 5.1.1 Main Contributions

The main contributions of this chapter are:

1. Development of a novel framework to consider receiver nonlinear distortions for resource

allocation;

2. Examine the behavior of the framework with varying nonlinearity of users; and
3. Demonstrate the benefits of receiver nonlinearity aware resource allocation

Section 5.2 covers development of the system model for distortion aware resource allocation for a two user case. Section 5.3 deals with the optimization problem formulation for the developed system model. In Section 5.4 the simulation results of the numerical optimization carried out for the formulated problem are presented.

## 5.2 System Model

In this chapter, we propose that dynamic resource allocations be carried out with knowledge of receiver nonlinearity and show that such an allocation will lead to increased data rate and efficiency. In this section, we describe the system model to formulate the optimization problem required to incorporate the receiver nonlinearity into resource allocations.

We consider a simple case of two users in the same band, of total bandwidth $BW$, as shown in Fig. 5.1. Without loss of any generality, we normalize the bandwidth for ease of analysis and set $BW = 1$. We simplify the problem assuming that both users have the same pre-selector bandwidth $B_p$, and receiver non-linearity specification $\mathsf{IIP}_3$. We note that for the radios to operate in the entire band, the pre-selector bandwidth, $B_p = 1$. In this chapter, since we address the problem of overlapping pre-selectors of receivers in the adjacent channel, we constrain the pre-selector bandwidth to span more than half of the entire band. This is in accordance with practical designs as discussed in previous chapters. We assume that both users are co-located (extension to different geo-locations is straight forward), meaning the power incident on both the RF front-ends is identical. Under such a scenario, the spectrum manager has to dynamically allocate frequency and power resources for both users.

Let $f_{L_1}$ and $f_{H_1}$; and $f_{L_2}$ and $f_{H_2}$ denote the range of signaling bandwidths of signals 1 and 2 respectively. Thus, $f_{H_1} - f_{L_1}$ and $f_{H_2} - f_{L_2}$ are the bandwidths of operation for the two users as shown in Fig. 5.1. We further simplify the problem by fixing $f_{L_1} = 0$ and $f_{H_2} = 1$ for this two user problem. If $P_1$ and $P_2$ denote the received power levels for the two users, the resource allocation scheme (or spectrum manager) should optimize over four parameters viz., $f_{H_1}$, $f_{L_2}$,

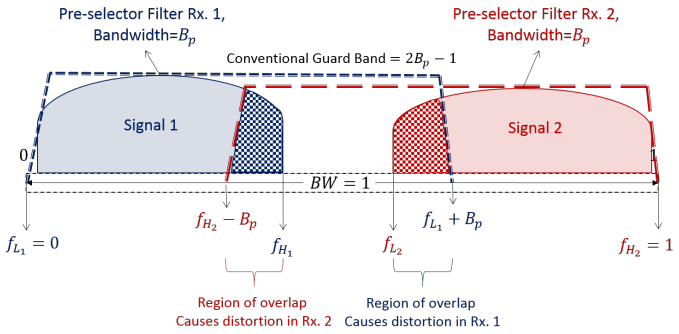


Figure 5.1: System Model

$P_1$, and $P_2$. Note that in this chapter we directly deal with the received power levels and not the transmit power levels since interference is principally dictated only by received powers. With the help of a database for transmitter and receiver locations and knowing the propagation models, the spectrum manager can easily compute the required transmit power levels for the respective users.

## 5.3 Problem Formulation

The SINR for the two receivers, taking into account the adjacent channel interactions, is given by the following equations.

$$\mathsf{SINR}_1 = \frac{P_1}{P_{ADJ_1} + N_0 + P_{CC}} \tag{5.1}$$

$$\mathsf{SINR}_2 = \frac{P_2}{P_{ADJ_2} + N_0 + P_{CC}} \tag{5.2}$$

where $\mathsf{SINR_k}$ is the Signal-to-Interference-Noise-Ratio for user $k$, $P_{ADJ_k}$ is the adjacent channel interference caused due to nonlinear distortion of the RF front-end for user $k$, $N_0$ is the AWGN noise, and $P_{CC}$ is the average co-channel interference power.

Receiver 1 faces adjacent channel interference from the energy of receiver 2, which falls in the bandwidth of pre-selector filter 1. Thus, the adjacent channel interference power for receiver 1 can be approximated as,

$$\begin{aligned} P_{ADJ_1} &= \frac{1}{\mathsf{IIP_3}^2} \int_{\omega_1 = f_{L_1}}^{f_{H_1}} \int_{\omega_2 = f_{L_2}}^{f_{L_1}+B_p} P_1^2(\omega_1) P_2(\omega_2)\, d\omega_1\, d\omega_2 \\ &= \frac{1}{\mathsf{IIP_3}^2} \left( \frac{f_{L_1} + B_p - f_{L_2}}{f_{H_2} - f_{L_2}} \right) P_1^2 P_2 \end{aligned} \tag{5.3}$$

$$\mathsf{SINR_1} = \frac{P_1(f_{H_2} - f_{L_2})\mathsf{IIP_3}^2}{(f_{L_1} + B_p - f_{L_2})P_1^2P_2 + (N_0(f_{H_1} - f_{L_1}) + P_{CC})(f_{H_2} - f_{L_2})\mathsf{IIP_3}^2} \tag{5.6}$$

$$\mathsf{SINR_2} = \frac{P_2(f_{H_1} - f_{L_1})\mathsf{IIP_3}^2}{(f_{H_1} + B_p - f_{H_2})P_1P_2^2 + (N_0(f_{H_2} - f_{L_2}) + P_{CC})(f_{H_1} - f_{L_1})\mathsf{IIP_3}^2} \tag{5.7}$$

$$\begin{aligned}\mathcal{R} = (f_{H_1} - f_{L_1})\log_2\left(1 + \frac{P_1(f_{H_2} - f_{L_2})\mathsf{IIP_3}^2}{(f_{L_1} + B_p - f_{L_2})P_1^2P_2 + (N_0(f_{H_1} - f_{L_1}) + P_{CC})(f_{H_2} - f_{L_2})\mathsf{IIP_3}^2}\right) + \\ (f_{H_2} - f_{L_2})\log_2\left(1 + \frac{P_2(f_{H_1} - f_{L_1})\mathsf{IIP_3}^2}{(f_{H_1} + B_p - f_{H_2})P_1P_2^2 + (N_0(f_{H_2} - f_{L_2}) + P_{CC})(f_{H_1} - f_{L_1})\mathsf{IIP_3}^2}\right)\end{aligned} \tag{5.8}$$

Similarly, the power due to adjacent channel interference for receiver 2 can be approximated as,

$$\begin{aligned}P_{ADJ_2} &= \frac{1}{\mathsf{IIP_3}^2}\int_{\omega_1=f_{L_2}}^{f_{H_2}}\int_{\omega_2=f_{H_2}-B_p}^{f_{H_1}} P_1(\omega_1)P_1^2(\omega_2)\,d\omega_1\,d\omega_2 \\ &= \frac{1}{\mathsf{IIP_3}^2}\left(\frac{f_{H_1} + B_p - f_{H_2}}{f_{H_1} - f_{L_1}}\right)P_1P_2^2\end{aligned} \tag{5.4}$$

Note that to obtain the closed form expressions for adjacent channel signal powers, we assume uniform distribution of the total power across the bandwidth of the band limited signal.

Thus, the $\mathsf{SINR}$ for both the receivers can be written as given by (5.6) and (5.7) (shown in the next page). The sum data rate per unit bandwidth is given by,

$$\mathcal{R} = (f_{H_1} - f_{L_1})\log_2(1 + \mathsf{SINR_1}) + (f_{H_2} - f_{L_2})\log_2(1 + \mathsf{SINR_2}) \tag{5.5}$$

Therefore, the sum data rate for both users can be obtained as given by (5.8) (shown in the next page).

### 5.3.1 Lower Bound

The lower bound (best possible blind allocation without receiver nonlinearity awareness) on the data rate that could be achieved is when a sufficient guard band (of $2B_p - 1$) is allocated to ensure no overlap of signaling bandwidth with the adjacent channel pre-selector filter. Thus, $f_{H_1} = f_{H_2} - B_p$ and $f_{L_2} = f_{L_1} + B_p$. Thus for our problem,

$$\mathcal{R}_{lb} = (f_{H_2} - B_p - f_{L_1})\log_2(1 + \mathsf{SINR_1}) + (f_{H_2} - f_{L_1} - B_p)\log_2(1 + \mathsf{SINR_2}) \tag{5.9}$$

with maximum receive power, $P_{max}$.

### 5.3.2 Upper Bound

The highest data rate that could be achieved is when the receivers are ideal (completely linear) and adjacent channel interference is absent. By the symmetry of the problem, the optimal allocation for sum data rate in this case would be to ensure non-overlap of signaling bandwidths, $f_{H_1} = f_{L_2} = f \in (f_{L_1}, f_{H_2})$. Thus for our problem,

$$\mathcal{R}_{ub} = (f - f_{L_1}) \log_2(1 + \mathsf{SINR}_1) + (f_{H_2} - f) \log_2(1 + \mathsf{SINR}_2) \tag{5.10}$$

with a maximum receive power, $P_{max}$.

Thus, $R_{lb} \leq R \leq R_{ub}$ where $R$ is the achievable rate.

In this chapter, we carry out maximization of the sum data rate while assuring a minimum rate to each user. Sum data rate has been used as an objective to optimize network performance by several researchers before [75–77]. Also, several measures of fairness have been explored in [78–82]. In this chapter, we choose the minimum rate as a simple constraint to ensure some fairness for users with poor receivers. Let this minimum rate be denoted by $R_{min_1}$ and $R_{min_2}$, for users 1 and 2 respectively. Other constraints are the upper and lower bounds for various variables of optimization. The powers would have to be positive and would have a maximum upper limit. The allotted frequencies for both users need to fall within the range of the band. Formalizing these, we can arrive at the optimization problem. Thus, the optimization problem can be formulated as given by (5.11) and (5.12) (shown in the next page).

## 5.4 Simulation Results

In this section, we present the results obtained by carrying out the numerical optimization for the problem developed in the previous section. The simulation parameters are summarized in Table 5.1. In order to compare our results, we use lower and upper bounds achievable for this problem and compare them with the solution obtained by our optimization problem.

For the lower bound, in a normalized unit bandwidth case, the operable bandwidth is $0.3$ to each user. The sum data rate achievable in such a scenario is computed to be $R_{lb} = 5.98$ bps/Hz (with

$$\max_{P_1,P_1,f_{H_1},f_{L_2}} \mathcal{J} = (f_{H_1}-f_{L_1})\log_2\left(1+\frac{P_1(f_{H_2}-f_{L_2})\mathsf{IIP_3}^2}{(f_{L_1}+B_p-f_{L_2})P_1^2P_2+(N_0(f_{H_1}-f_{L_1})+P_{CC})(f_{H_2}-f_{L_2})\mathsf{IIP_3}^2}\right)+$$
$$(f_{H_2}-f_{L_2})\log_2\left(1+\frac{P_2(f_{H_1}-f_{L_1})\mathsf{IIP_3}^2}{(f_{H_1}+B_p-f_{H_2})P_1P_2^2+(N_0(f_{H_2}-f_{L_2})+P_{CC})(f_{H_1}-f_{L_1})\mathsf{IIP_3}^2}\right) \quad (5.11)$$

s.t.

$$(f_{H_1}-f_{L_1})\log_2\left(1+\frac{P_1(f_{H_2}-f_{L_2})\mathsf{IIP_3}^2}{(f_{L_1}+B_p-f_{L_2})P_1^2P_2+(N_0(f_{H_1}-f_{L_1})+P_{CC})(f_{H_2}-f_{L_2})\mathsf{IIP_3}^2}\right) \geq R_{min_1}$$
$$(f_{H_2}-f_{L_2})\log_2\left(1+\frac{P_2(f_{H_1}-f_{L_1})\mathsf{IIP_3}^2}{(f_{H_1}+B_p-f_{H_2})P_1P_2^2+(N_0(f_{H_2}-f_{L_2})+P_{CC})(f_{H_1}-f_{L_1})\mathsf{IIP_3}^2}\right) \geq R_{min_2}$$
$$0 \leq P_1 \leq P_{max}$$
$$0 \leq P_2 \leq P_{max}$$
$$f_{L_1} \leq f_{H_1} \leq f_{L_1}+B_p$$
$$f_{H_2}-B_p \leq f_{L_2} \leq f_{H_1} \quad (5.12)$$

Table 5.1: Simulation Parameters

| | | |
|---|---|---|
| Normalized Total Bandwidth | : | $BW = 1$ |
| Number of receivers | : | $K = 2$ |
| Pre-selector Bandwidth | : | $Bp = 0.7$ |
| Max received power for both users | : | $P_{max} = -30$ dBm |
| Noise Power (per Hz) | : | $N_0 = -165$ dBm |
| Co-Channel Interference Power | : | $P_{CC} = -60$ dBm |

each user getting $2.99$ bps/Hz) and is the lower bound.

For the upper bound, in a normalized unit bandwidth case, $0 \leq f \leq 1$ (e.g. 0.5). The sum data rate achievable in this scenario is computed to be $R_{ub} = 9.97$ bps/Hz and is the upper bound.

### 5.4.1 Sum Data Rate with Varying IIP3

In this section, we present the results obtained by varying the IIP3 of both receivers from $-30$ dBm to $0$ dBm in steps of $1$ dBm. The minimum rate constraint was set to $R_{min} = 0$ bps/Hz for each receiver. We assume identical receivers in this case. As seen in Fig. 5.2, receiver distortion aware allocation consistently gives better sum data rate than the lower bound and converges to the upper bound as the receivers get linear.

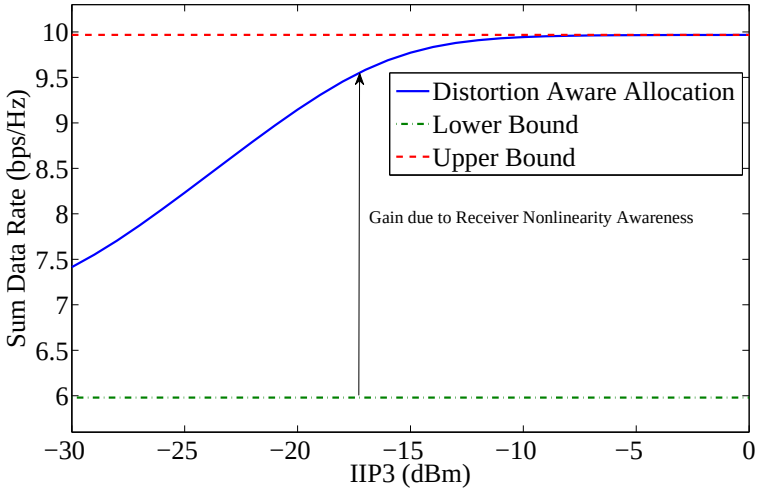


Figure 5.2: Variation of Sum Data Rate with IIP3 for $R_{min} = 0$ bps/Hz

### 5.4.2 Variation of Minimum Rate Constraint

We now present the total data rate achieved when the minimum rate constraint ($R_{min}$) for each receiver was set to $2, 3$, and $4$ bps/Hz respectively in Fig 5.3. As seen from the figure, to accommodate for a higher minimum rate for each receiver, the powers or the bandwidth will have to be reduced at the cost of total data rate. Thus as the minimum rate constraint for each receiver is increased, the total data rate obviously drops (since one receiver cannot be favored at the cost of the other). Moreover, with highly nonlinear receivers (IIP3 $< -21$ dBm), satisfying a minimum rate constraint of $4$ bps/Hz becomes infeasible. In each case, the sum data rate obtained is higher than the lower bound, but as the receivers approach linearity the sum data rate approaches the upper bound.

### 5.4.3 Rate, Power and Bandwidth per User

In this section, we present the individual data rates achieved for both users in Fig. 5.4, and the corresponding optimal power and bandwidth allocations obtained in Fig. 5.5. For brevity, we present these results only for the one case with minimum rate constraint of $R_{min} = 3$ bps/Hz. As IIP3 increases, the received power for each user increases since the distortion decreases and the capability to handle the nonlinearity increases. For bandwidth, one receiver is favored over the other so long as the minimum rate constraint is met, to maximize sum data rate. This ensures that one of the receivers faces less distortion than the other, thereby increasing the sum data rate. The

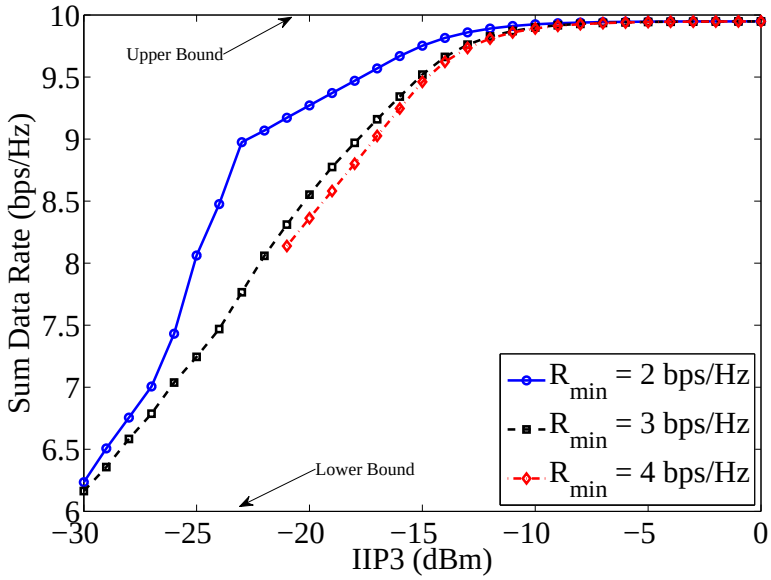


Figure 5.3: Sum Data Rates for different Minimum Rate Constraints

same pattern is seen in the individual data rates.

### 5.4.4 Different Receiver Nonlinearity

In this section, we fix the IIP3 of Receiver 2 to $-20$ dBm and vary the IIP3 of Receiver 1 from $-30$ dBm to $0$ dBm. Again, for brevity we present the results for the case with $R_{min} = 3$ bps/Hz. Clearly, for different values of IIP3, Receiver 1 illustrates cases with worse and better nonlinearity compared to Receiver 2. Figure 5.6 shows the sum data rate and data rates of individual users with varying nonlinearity of Receiver 1. As seen from the figure, as long as the distortion in Receiver 1 is higher than in Receiver 2, Receiver 2 is assigned a higher data rate ensuring the minimum rate constraint to both receivers. However, as the distortion in Receiver 1 becomes less than in Receiver 2, Receiver 1 is assigned a higher data rate ensuring the minimum rate constraint for Receiver 2. Also, since Receiver 2 always faces a high distortion, the sum rate does not approach the upper bound ($9.97$ bps/Hz) even if Receiver 1 becomes distortion free. The developed system model favors the receiver with less distortion to maximize the overall sum data rate of the network.

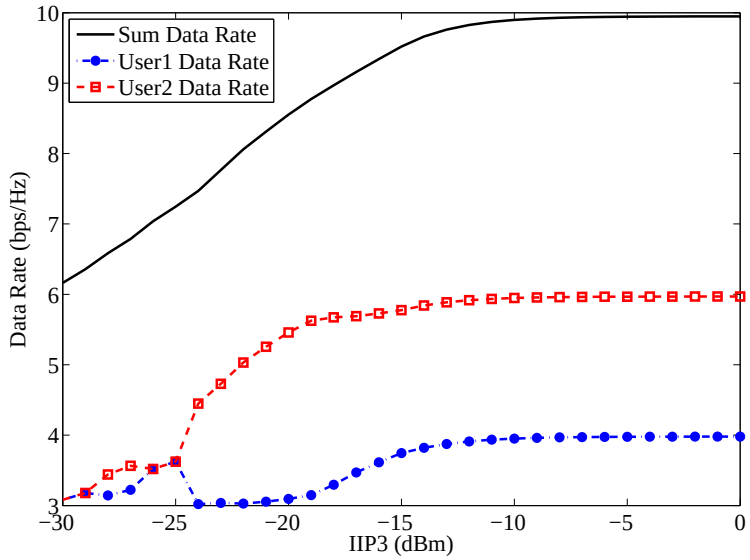


Figure 5.4: Individual data rates achieved for each user for $R_{min} = 3$ bps/Hz

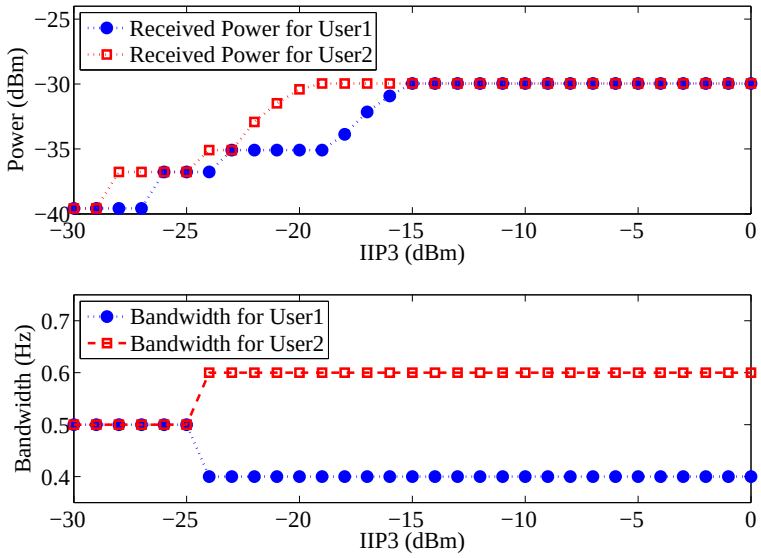


Figure 5.5: Optimal Power and Bandwidth allocations for $R_{min} = 3$ bps/Hz

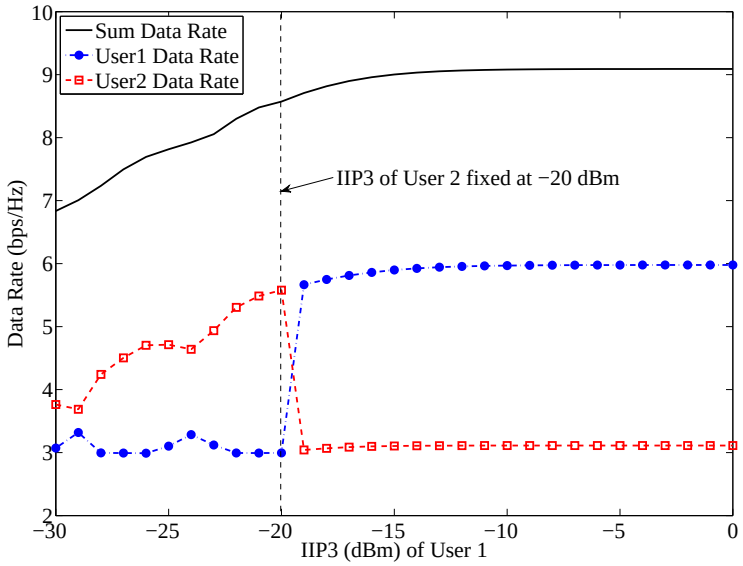


Figure 5.6: Data Rates for Different Receiver Nonlinearity, $R_{min} = 3$ bps/Hz

## 5.5 Conclusions

In this chapter, we proposed a novel framework for resource allocation considering the nonlinear distortions in receivers. Receiver nonlinearity aware dynamic spectrum allocations achieved higher data rates as compared to the conventional lower bound approach for receivers with high nonlinear distortions. As the distortions decrease, the sum data rate approaches the upper bound. Further, it was observed that poor receivers were suitably compensated for their nonlinearity by ensuring the required minimum rate, while still maximizing for the overall network data rate. Such an inclusive optimization will not only ensure the required QoS for all users but also maximize the spectrum efficiency by providing optimal solutions. Future work would include generalizing the problem for a multiuser case in a random radio environment, for different network topologies.

# Chapter 6

# Receiver-Centric Efficient Spectrum Access: Multi-RAT Network Co-existence with Receiver Nonlinearity

## 6.1 Introduction

As seen in the previous chapters, RF front-end nonlinearity significantly impairs receiver performance. Receivers are susceptible to harmful adjacent channel interference, especially in next generation networks with diverse radio access technologies, co-existing in spatio-temporal-spectral proximity. Vulnerabilities in receiver front-ends can have a severe detrimental effect on network performance and spectrum co-existence. Our preliminary study in Chapter 5 and [50, 51] revealed that spectral assignment accounting for receiver characteristics can potentially increase spectrum efficiency over receiver-agnostic access. Further, in [108] an initial study of a channel assignment technique accounting for receiver nonlinearity, was presented. In addition to the reports of regulatory and standardization bodies, this work is motivated by our initial findings, which showed promising gains in spectrum efficiency and network performance for receiver-centric frameworks. In this chapter, we propose a generalized receiver-centric framework that accounts for receiver front-end nonlinearity, pre-selector filter bandwidth, and transmitter out-of-band emission characteristics for networks with diverse RF layer characteristics.

### 6.1.1 Main Contributions

The main contributions of this chapter are:

1. We develop frameworks for spectral access and network optimization taking into account (a) receiver RF front-end nonlinearity, (b) receiver pre-selector filter characteristics, and (c) transmitter out-of-band emission characteristic masks;
2. We propose computationally efficient algorithms for optimization in the proposed framework;
3. We demonstrate through extensive network simulations that the proposed framework of receiver-centric spectrum access and network management yields significant gains in spectral efficiency and network performance over receiver-agnostic spectrum access and ensures co-existence in dense and diverse next generation wireless networks; and
4. In addition, we analyze the performance of the proposed algorithms against the optimal solution using extensive simulations and demonstrate that the proposed algorithms achieve order-optimal solutions for complex receiver-centric network optimization.

Even though receiver nonlinearity has been extensively studied, it has not been employed to design efficient spectrum access frameworks. To the best of our knowledge, this is the first attempt to develop a comprehensive network management framework inclusive of receiver nonlinearity and imperfections.

In Section 6.2, we develop a receiver-centric network optimization framework for the case of a single or co-located transmitter with multiple receivers with diverse characteristics, In Section 6.3, we develop a receiver-centric network optimization framework for the generalized case of multiple transmit-receive links with diverse radio technologies, In Section 6.4, we present a framework to incorporate the transmitter out-of-band emissions in receiver-centric network optimization, and in Section 6.5, we present the results of network simulations.

## 6.2 Framework for Single Transmitter, Multiple Receivers

In this section, we consider a network with $N$ receivers wirelessly connected to a single transmitter or gateway, over $N$ discrete adjacent channels. The $N$ receivers have disparate technologies and

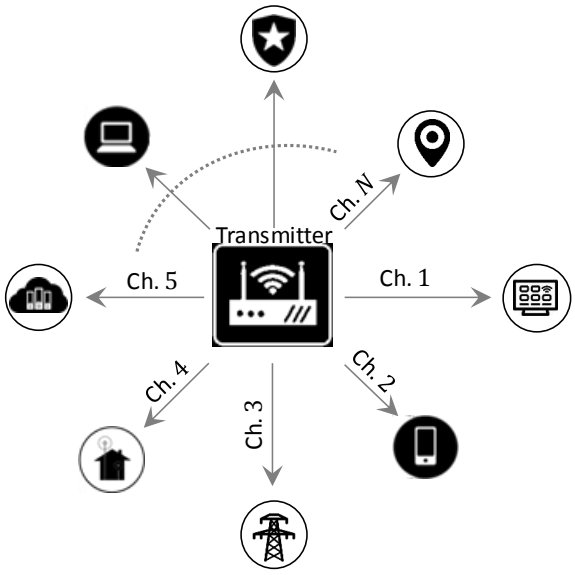


Figure 6.1: Illustration of heterogeneous nodes on different channels with diverse RF front-ends with a single transmitter

hence, have diverse RF front-end characteristics. We assume the receivers are distributed in a geographical area within the range of the transmitter, as shown in Fig. 6.1. Consider the downlink channel allocation problem.

We further assume that the transmitter is using an omnidirectional antenna, simultaneously transmitting on $N$ channels, each with a bandwidth $W$. Each of those $N$ downlink channels has a center frequency $f_\ell, \ell \in [1, N]$. Let each receiver be indexed by $n \in [1, N]$, use a unique channel, and have a unique front-end nonlinearity described by the overall third order intermodulation intercept point, IIP3.

An example use case of this is the IoT networks of the next generation wireless systems, with a transmitter gateway delivering disparate downlink information for myriad nodes of the network, serving different interests. Typically, each node comprises of an inexpensive receiver with a potentially different technology (WiFi, Bluetooth, Zigbee, etc.) and RF front-end. This can be conceptualized for indoor networks such as smart homes, or outdoor networks, where for example, the transmitter gateway can be based on a UAV based platform. Note that the framework presented here is generic and not technology specific. Thus, it can be adopted for any scenario in which multiple receivers are being served by a single transmitter on different channels.

### 6.2.1 Adjacent Channel Interference Formulation

In this section, we discuss the formulation for evaluating the adjacent channel interference. We initially formulate assuming that the pre-selector filter of each receiver in the network spans the entire band of operation, and later discuss the development to relax this assumption. Thus, each receiver receives $N$ signals, of which one is the desired signal, and the others are adjacent channel signals. The received power on each channel for receiver $n$ is denoted as $P_{R_n} = P_T d_n^{-\mu}$, where $P_T$ is the transmitted power per channel, $d_n$ is the distance of the receiver $n$ from the transmitter, and $\mu$ is the path loss exponent. For simplicity, we do not assume any frequency selective fading and hence, the received power is the same across all frequencies for a given receiver. The noise power in the bandwidth $W$ is denoted by $\eta$.

We now define an indicator function,

$$x_{n\ell} = 1_{\{\text{Channel } \ell \text{ is allocated to receiver } n, \text{ denoted as } \ell \rightarrow n\}}. \tag{6.1}$$

For a given channel $\ell$, the number of intermodulation products produced due to nonlinearity for the receiver $n$ is given by,

$$\kappa_\ell^n = \mid \Psi_{\ell,N} \mid + \mid \Upsilon_{\ell,N} \mid, \tag{6.2}$$

where $\mid \bullet \mid$ represents the cardinality of the set. In this case, since the pre-selector of all receivers spans the entire bandwidth, the number of interferers encountered by any receiver is only dependent on the channel $\ell$. The adjacent channel interference due to intermodulation distortion faced by receiver $n$ is given by,

$$P_{\mathsf{ACI}_n} = \alpha_{3_n}^2 P_{R_n}^3 \sum_{\ell=1}^{N} x_{n\ell} \kappa_\ell^n, \tag{6.3}$$

where $\alpha_3$ is the coefficient of the third order nonlinearity, which can be obtained from $\mathsf{IIP}_3$. As evident from (7.11), each receiver faces a different interference depending on its nonlinearity and channel assignment. The goal of a dynamic spectrum management and co-existence framework is to account for all these parameters, in addition to location of the nodes, and assign channels to each receiver to optimize for an objective. In this chapter, we consider network sum data rate (or, just sum rate) as the objective function and seek to allocate channels to maximize the sum rate.

### 6.2.2 Channel Assignment Framework

We now describe the channel assignment framework for sum rate maximization. Sum rate maximization is a widely used metric to quantify network performance [83–88]. Also, fairness of some measure (e.g. [89–91]) is important for networks. In this chapter, we ensure that the spectrum is equally divided among all users and optimize over channel allocations. This ensures spectrum for each user irrespective of the receiver parameters, while not complicating framework to analyze the main theme of the importance of receiver nonlinearity in spectrum access.

Treating the adjacent channel interference as additive noise, the data rate of receiver $n$ and the network-wide sum rate are given by,

$$R_n = W \ \log_2 \left( 1 + \frac{P_{R_n}}{\alpha_{3_n}^2 P_{R_n}^3 \sum_{\ell=1}^{N} x_{n\ell} \kappa_\ell^n + \eta} \right), \tag{6.4}$$

$$R = W \ \sum_{n=1}^{N} \log_2 \left( 1 + \frac{P_{R_n}}{\alpha_{3_n}^2 P_{R_n}^3 \sum_{\ell=1}^{N} x_{n\ell} \kappa_\ell^n + \eta} \right). \tag{6.5}$$

The sum rate maximization framework can now be formulated as,

$$\mathcal{J}_1 = \max_{x_{n\ell}} \ W \ \sum_{n=1}^{N} \log_2 \left( 1 + \frac{P_{R_n}}{\alpha_{3_n}^2 P_{R_n}^3 \sum_{\ell=1}^{N} x_{n\ell} \kappa_\ell^n + \eta} \right) \tag{6.6}$$

$$\text{s.t} \ \sum_{\ell=1}^{N} x_{n\ell} = 1; \quad \sum_{n=1}^{N} x_{n\ell} = 1. \tag{6.7}$$

This formulation is nonlinear and non-convex in the channel assignment variables and it is hard to obtain computationally efficient algorithms. Henceforth, this objective function is referred as the 'original problem 1'. We now approximate the original problem 1 and reduce the complexity of the objective function. Further, we utilize the approximate objective function and propose a computationally efficient algorithm for channel assignment. We have,

$$R = W \ \sum_{n=1}^{N} \log_2 \left( \alpha_{3_n}^2 P_{R_n}^3 \sum_{\ell=1}^{N} x_{n\ell} \kappa_\ell^n + \eta + P_{R_n} \right) - W \ \sum_{n=1}^{N} \log_2 \left( \alpha_{3_n}^2 P_{R_n}^3 \sum_{\ell=1}^{N} x_{n\ell} \kappa_\ell^n + \eta \right). \tag{6.8}$$

Lower-bounding the sum rate in (7.16), we get,

$$R \geq W \sum_{n=1}^{N} \log_2 \left(\eta + P_{R_n}\right) - W \sum_{n=1}^{N} \log_2 \left( \alpha_{3_n}^2 P_{R_n}^3 \sum_{\ell=1}^{N} x_{n\ell} \kappa_\ell^n + \eta \right). \tag{6.9}$$

Using Jenson's inequality, we have

$$\begin{aligned} \sum_{n=1}^{N} \log_2 \left( \alpha_{3_n}^2 P_{R_n}^3 \sum_{\ell=1}^{N} x_{n\ell} \kappa_\ell^n + \eta \right) &\leq \log_2 \left( \sum_{n=1}^{N} \alpha_{3_n}^2 P_{R_n}^3 \sum_{\ell=1}^{N} x_{n\ell} \kappa_\ell^n + \sum_{n=1}^{N} \eta \right), \\ &\leq \log_2 \left( \sum_{n=1}^{N} \sum_{\ell=1}^{N} \alpha_{3_n}^2 P_{R_n}^3 x_{n\ell} \kappa_\ell^n + N\eta \right). \end{aligned} \tag{6.10}$$

Using (7.18) in (7.17) we have,

$$R \geq W \sum_{n=1}^{N} \log_2 \left(\eta + P_{R_n}\right) - W \ \log_2 \left( \sum_{n=1}^{N} \sum_{\ell=1}^{N} \alpha_{3_n}^2 P_{R_n}^3 x_{n\ell} \kappa_\ell^n + N\eta \right). \tag{6.11}$$

We intend to carry out channel assignments such that the sum rate, $R$ is maximized. In order to maximize $R$, from (7.19) it is clear that $W \log_2 \left( \sum_{n=1}^{N} \sum_{\ell=1}^{N} \alpha_{3_n}^2 P_{R_n}^3 x_{n\ell} \kappa_\ell^n + N\eta \right)$ needs to be minimized, since the first term on R.H.S of (7.19) is a constant. Since $\log_2(\bullet)$ is a monotonically increasing concave function, minimizing the total adjacent channel interference, $P_{\mathsf{ACI}} = \sum_{n=1}^{N} \sum_{\ell=1}^{N} \alpha_{3_n}^2 P_{R_n}^3 x_{n\ell} \kappa_\ell^n$ will minimize the function, since $N\eta$ is a constant.

### 6.2.3 Problem Formulation

Let $\mathbf{k}_n = [\kappa_1^n \kappa_2^n \ldots \kappa_N^n]^T$ denote a vector, where $\kappa_\ell^n$ denotes the number of adjacent channel interfering signals encountered by receiver $n \in [1, N]$ when placed (assigned) in channel $\ell \in [1, N]$. We now define a matrix $\mathbf{K} = [\mathbf{k}_1 \ \mathbf{k}_2 \ \mathbf{k}_3 \ \ldots \ \mathbf{k}_n]$ whose $\ell^{\text{th}}$ row represents the number of adjacent channel signals entering each of the $N$ receivers when placed in the $\ell^{\text{th}}$ channel, as shown in (7.20).

$$\begin{array}{l} \\ 1^{\text{st}}\text{channel} \rightarrow \\ 2^{\text{nd}}\text{channel} \rightarrow \\ \\ N^{\text{th}}\text{channel} \rightarrow \end{array} \begin{array}{c} \begin{array}{cccc} 1^{\text{st}}\text{Rx.} & 2^{\text{nd}}\text{Rx.} & & N^{\text{th}}\text{Rx.} \end{array} \\ \begin{pmatrix} \alpha_{3_1}^2 \kappa_1^1 P_{R_1}^3 & \alpha_{3_2}^2 \kappa_1^2 P_{R_2}^3 & \dots & \alpha_{3_N}^2 \kappa_1^N P_{R_N}^3 \\ \alpha_{3_1}^2 \kappa_2^1 P_{R_1}^3 & \alpha_{3_2}^2 \kappa_2^2 P_{R_2}^3 & \dots & \alpha_{3_N}^2 \kappa_2^N P_{R_N}^3 \\ \vdots & \vdots & & \vdots \\ \alpha_{3_1}^2 \kappa_N^1 P_{R_1}^3 & \alpha_{3_2}^2 \kappa_N^2 P_{R_2}^3 & \dots & \alpha_{3_N}^2 \kappa_N^N P_{R_N}^3 \end{pmatrix} \end{array} = \mathbf{K}_{N \times N} \tag{6.12}$$

Let $\mathbf{X}$ denote a binary-integer channel assignment matrix with rows representing receivers and columns representing channels, such that $\sum_{\forall n} \mathbf{X}_{n,\ell} = 1$; $\sum_{\forall \ell} \mathbf{X}_{n,\ell} = 1$. These conditions impose that there exist only one non-zero element in each row and in each column of the assignment matrix $\mathbf{X}$. This ensures that each receiver is assigned a unique channel and vice versa.

The number of interfering signals for any receiver depends on the channel assigned and the pre-selector bandwidth. Thus the adjacent channel interference for the $n^{\text{th}}$ receiver is given by the $n^{\text{th}}$ element of $\text{diag}(\mathbf{XK})$. The total adjacent channel interference is given by,

$$P_{\mathsf{ACI}} = \text{tr}(\mathbf{XK}) \tag{6.13}$$

where $\text{tr}(\bullet)$ represents the trace of the matrix. Our goal now is to minimize the network wide adjacent channel interference given by (6.13). Thus, the modified optimization problem can be formulated as,

$$\mathcal{J}_2 = \min_{\mathbf{X}} \ \text{tr}(\mathbf{XK}) \tag{6.14}$$

$$\text{s.t.} \quad \sum_{\forall n} \mathbf{X}_{n,\ell} = 1 \ ; \sum_{\forall \ell} \mathbf{X}_{n,\ell} = 1. \tag{6.15}$$

Evidently, the numerical optimization to solve this problem has a complexity of the order of $\mathcal{O}(N!)$. In the next section, we propose a computationally efficient greedy algorithm to solve this problem.

### 6.2.4 Greedy Algorithm for Channel Assignment

We need to iteratively find an assignment matrix $\mathbf{X}$ such that $\text{tr}(\mathbf{XK})$ is minimized. In other words, we need to pick $N$ elements of matrix $\mathbf{K}$ whose sum is the least, with the constraint that each of those elements is from a unique row and column. The following greedy algorithm is developed as

a solution to the minimization problem.

**Algorithm 2** Greedy Algorithm for Receiver Nonlinearity Aware Channel Assignment

1: FORMULATE: $\mathbf{K}$.
2: INITIALIZE: $\mathbf{X} = \mathbf{0}_{N\times N}$.
   Define Sets $\mathscr{C}_\ell = \{1, 2, \ldots, N\}$; $\mathscr{C}_n = \{1, 2, \ldots, N\}$
3: **for** $1, 2, \ldots, N$ **do**
4: $\quad (\ell^*, n^*) = \arg\min_{(\ell,n)} [\mathbf{K}]; \;\; \forall \ell \in \mathscr{C}_\ell \; \forall n \in \mathscr{C}_n$
5: $\quad [\mathbf{A}]_{n^*,\ell^*} = 1$
6: $\quad \mathscr{C}_\ell = \mathscr{C}_\ell \setminus \{\ell^*\}; \mathscr{C}_n = \mathscr{C}_n \setminus \{n^*\}$
7: **end for**

The intuition for this algorithm is that, in each iteration, it picks the least element of the matrix $\mathbf{K}$ and assigns that receiver (column index, $n^*$) to the corresponding channel (row index, $\ell^*$). All elements of this row and column are permanently excluded in the future iterations. This process is repeated until all receivers are assigned a channel. Note that the rows and columns of channel assignment matrix $\mathbf{X}$ represent the receiver and channels; and vice versa for the adjacent channel interference matrix $\mathbf{K}$. Thus, it warrants a flip of indices in the algorithm.

**Remark:** The $q^{\text{th}}$ iteration of the algorithm (lines 3 to 7) involves finding the minimum among $(N - q + 1)^2$ elements. Note that there is a dimensionality reduction of the search space for finding the minimum element in $\mathbf{K}$ in each iteration of the algorithm. The average computations for serial sorting is $O\left((N - q + 1)^2\right)$ for the $q^{\text{th}}$ iteration. Thus for $N$ iterations, the computational complexity of the algorithm is $O\left(N^3\right)$, which is efficient compared to the exponential complexity of the original problem.

### 6.2.5 Pre-selector Spans a Factor of the Entire Band

In the preceding section, we made an assumption that the pre-selector filter of each receiver spanned the entire band of operation. In practice, different receivers have different pre-selector bandwidths. However, receivers do have to operate over the entire band. Consequently, receivers will have multiple pre-selector filters, each spanning an integer factor of the entire band as shown in Fig. 6.2.

Let $M_n$ be the number of pre-selector filters for receiver $n$. It is reasonable to assume that each pre-selector filter of receiver $n$ spans an equal number of channels, and is a factor of $N$. Thus, each pre-selector filter for receiver $n$ spans $\frac{N}{M_n}$ channels. This clearly changes the number of signals producing intermodulation products at any given channel $\ell$ for a receiver $n$.

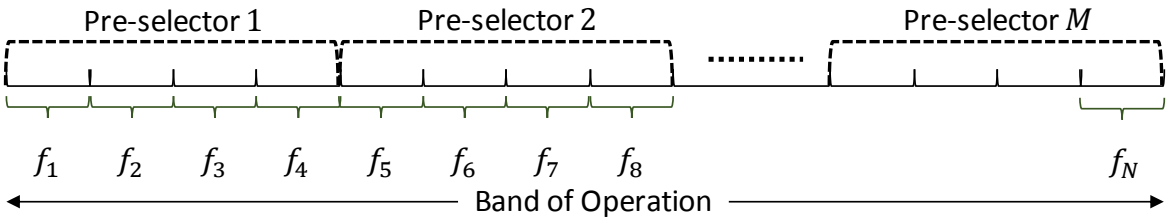


Figure 6.2: Illustration of a receiver with $M$ pre-selector filters spanning the band of operation of $N$ channels, where $\frac{N}{M}$ is a positive integer.

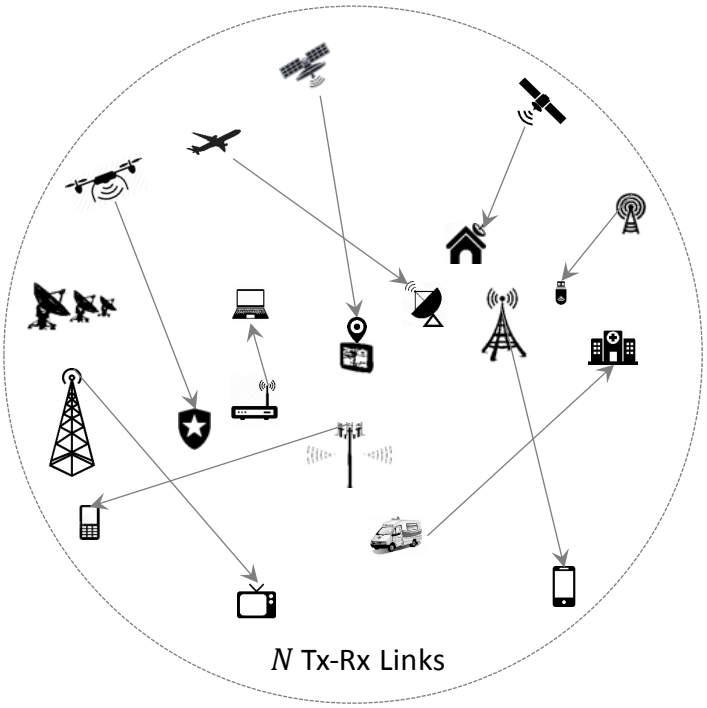


Figure 6.3: Illustration of heterogeneous nodes with diverse RF front-ends sharing spectrum in the wireless network.

Any given channel $\ell \in [1, N]$ maps to a frequency bin $\ell'_n \in [1, M_n]$ in the pre-selector of receiver $n$. The frequency bin to which a given channel is mapped can be obtained as,

$$\ell'_n = ((\ell - 1) \bmod M_n) + 1, \tag{6.16}$$

where $a \bmod b = a - b\lfloor \frac{a}{b} \rfloor$ is modulo operation. The number of intermodulation products at a given channel $\ell$ for a receiver $n$ with $M_n$ pre-selector filters is given by,

$$\kappa_\ell^n = \left|\Psi_{\ell'_n, M_n}\right| + \left|\Upsilon_{\ell'_n, M_n}\right|, \tag{6.17}$$

where $|\bullet|$ is the cardinality of the set. The computations, approximations, and framework for receiver nonlinearity aware channel allocation of the preceding sections can be now be used for receivers with different pre-selector filters with this modification to calculate the number of intermodulation products.

## 6.3 Generic Framework for Multiple Transmitter-Receiver Pairs

In this section, we consider a network of $N$ transmitters and $N$ receivers ($N$ Tx-Rx pairs) communicating over $N$ distinct adjacent channel links. As before, we assume the network is a multi-RAT system with disparate receiver front-ends. We assume the transmitters and receivers are distributed in a geographical area and the network topology is known to the centralized controller. We also assume that all the transmitters have omni-directional antennas. Each channel has the center frequency $f_\ell$, $\ell \in [1, N]$ and bandwidth $W$. Each receiver $n \in [1, N]$ has a unique front-end nonlinearity described by its third order intermodulation intercept point $\mathsf{IIP}_{3_n}$. We consider the channel allocation for the $N$ links with an objective to maximize the sum rate of the network.

### 6.3.1 Adjacent Channel Interference Formulation

In this section, we formulate the adjacent channel interference encountered by receiver $n \in [1, N]$. We initially assume that the pre-selector filters of all receivers span the entire band of operation with bandwidth $NW$ for simplicity, and later relax this assumption. Thus, each receiver receives

$N$ signals (one of which is desired), but the power of each of those signals is dependent on the distance of all the transmitters from the given receiver $n$.

We define an indicator function for channel allocation,

$$x_{n\ell} = 1_{\{\text{Channel } \ell \text{ is allocated to receiver } n, \text{ denoted as } \ell \to n\}}. \tag{6.18}$$

We define an indicator function to denote all the adjacent channel bins $\{j,k\} \in \Psi_{\ell,N}$ causing pair-wise intermodulation distortion for a given channel $\ell$ as,

$$y_{\ell}^{j,k} = 1_{\{\text{if } \{j,k\} \in \Psi_{\ell,N}\}}. \tag{6.19}$$

Now the adjacent channel interference due to pair-wise intermodulation at channel $\ell$, given that the received signal amplitude in channels $j,k$ is respectively given by $A_j, A_k$, can be written as,

$$\rho_{\ell}^{\mathsf{2tone}} = \alpha_3 \sum_{j=1}^{N} \sum_{k=1}^{N} y_{\ell}^{j,k} A_j^2 A_k. \tag{6.20}$$

We define an indicator function to denote all the adjacent channel bins $\{i,j,k\} \in \Upsilon_{\ell,N}$ causing triple intermodulation distortion for a given channel $\ell$ as,

$$z_{\ell}^{i,j,k} = 1_{\{\text{if } \{i,j,k\} \in \Upsilon_{\ell,N}\}}. \tag{6.21}$$

Now the adjacent channel interference due to triple intermodulation at channel $\ell$, given that received signal amplitude in channels $i,j,k$ are respectively given by $A_i, A_j, A_k$ can be written as,

$$\rho_{\ell}^{\mathsf{3tone}} = \alpha_3 \sum_{i=1}^{N} \sum_{j=1}^{N} \sum_{k=1}^{N} z_{\ell}^{i,j,k} A_i A_j A_k. \tag{6.22}$$

Let $d_{nj}$ denote the distance between receiver $n \in [1,N]$ and transmitter $j \in [1,N]$. The received power at receiver $n$ from transmitter $j$ is then given by $P_{R_{nj}} = P_{T_j} d_{nj}^{-\mu}$ where $P_{T_j}$ is the transmit power of transmitter $j$ and $\mu$ is the propagation loss exponent. The total nonlinear adjacent channel interference due to intermodulation distortion for a given link with receiver $n$ is,

$$\rho_n = \alpha_3 \sum_{\ell=1}^{N} x_{nl} \left( \sum_{j_1=1}^{N} \sum_{k_1=1}^{N} \sum_{u_1=1}^{N} \sum_{v_1=1}^{N} y_{\ell}^{j_1,k_1} \; x_{u_1 j_1} x_{v k_1} P_{T_{u_1}} \sqrt{P_{T_{v_1}}} \; d_{nu_1}^{-\mu/2} d_{nv_1}^{-\mu/2} \right.$$
$$\left. + \sum_{i_2=1}^{N} \sum_{j_2=1}^{N} \sum_{k_2=1}^{N} \sum_{t_2=1}^{N} \sum_{u_2=1}^{N} \sum_{v_2=1}^{N} z_{\ell}^{i_2,j_2,k_2} \; x_{t_2 i_2} x_{u_2 j_2} x_{v_2 k_2} \sqrt{P_{T_{t_2}} P_{T_{u_2}} P_{T_{v_2}}} \; d_{nt_2}^{-\mu/2} d_{nu_2}^{-\mu/2} d_{nv_2}^{-\mu/2} \right). \quad (6.23)$$

Evidently, equation (6.23) is a cumbersome formulation. We thus seek to re-formulate the adjacent channel interference due to nonlinear distortions using matrices to provide a simpler representation. For this, we first formulate a distance vector and a diagonal distance matrix for receiver $n$ with respect to the transmitters as,

$$\mathbf{d}_n = \begin{bmatrix} d_{n1}^{-\mu/2} \\ d_{n2}^{-\mu/2} \\ \vdots \\ d_{nj}^{-\mu/2} \end{bmatrix}; \quad \mathbf{D}_n = \begin{bmatrix} d_{n1}^{-\mu/2} & 0 & \cdots & 0 \\ 0 & d_{n2}^{-\mu/2} & \cdots & 0 \\ \vdots & & \ddots & \vdots \\ 0 & \cdots & 0 & d_{nj}^{-\mu/2} \end{bmatrix}. \quad (6.24)$$

We now define the 'amplitude' vector $\boldsymbol{A} = [\sqrt{P_{T_1}} \; \sqrt{P_{T_n}} \; \cdots \; \sqrt{P_{T_n}}]^T$ and the diagonal matrix $\mathbf{G} = \mathrm{diag}(P_{T_1} \; P_{T_2} \; \cdots \; P_{T_n})$ as described in Chapter 3. Now, $\mathbf{d}_n\mathbf{G}$ and $\mathbf{D}_n\mathbf{A}$ give the received amplitude values at receiver $n$ from all the transmitters. This can be used to compute the adjacent channel interference.

However, it is to be noted that channel assignment itself impacts the adjacent channel interference power since received power on each channel is different and nonlinear adjacent channel interference is dependent on relative spectral locations of interfering signals. Thus, evaluation of adjacent channel interference cannot be agnostic to channel allocation and has to be inclusive of it. We define the channel allocation permutation matrix $\mathbf{X}$ with rows representing the channels and columns representing the receivers. Also recall that the adjacent channel interference accounting for pair-wise and triple intermodulation distortion for receiver $n$ was formulated in Chapter 3 (propositions 1 and 2) as,

$$\rho_n = \alpha_{3_n} \left( [1 \; 1 \; \cdots \; 1] \left( \mathbf{L}_n^{\mathsf{A}} \; \mathbf{G} \; \mathbf{L}_n^{\mathsf{B}} \boldsymbol{A} \right) + 2 \sum_{\forall i \in \Upsilon_n^{\iota}} \boldsymbol{A}^T \mathbf{L}_{n,i}^{\mathsf{C}} \mathbf{G}^{1/2} \mathbf{L}_{n,i}^{\mathsf{D}} \boldsymbol{A} \right). \quad (6.25)$$

We need to modify this formulation to include the true received powers accounting for network topology and channel allocations. Note that the above equation was formulated to provides extreme flexibility to include the channel allocation information by manipulating the amplitude vector $\boldsymbol{A}$

and diagonal matrix $\mathbf{G}$ by pre- and post-multiplying with the channel allocation matrix $\mathbf{X}$.

Thus, we formulate the total amplitude of adjacent channel interference encountered by receiver $n$ accounting for intermodulation products, network topology and channel allocation as,

$$\rho_n = \alpha_{3_n} \Bigg( [1\ 1\ \cdots\ 1] \left( \mathbf{L}_n^{\mathsf{A}} \underline{\mathbf{X}\ \mathbf{d}_n^T\ \mathbf{G}\ \mathbf{X}^T}\ \mathbf{L}_n^{\mathsf{B}} \underline{\mathbf{X}\ \mathbf{D}_n\ \boldsymbol{A}} \right) + 2 \sum_{\forall i \in \Upsilon_n^{\iota}} \underline{\boldsymbol{A}^T\ \mathbf{D}_n^T\ \mathbf{X}^T}\ \mathbf{L}_{n,i}^{\mathsf{C}}\ \underline{\mathbf{X}\ \mathbf{d}_n^T \mathbf{G}^{1/2}\ \mathbf{X}^T}\ \mathbf{L}_{n,i}^{\mathsf{D}}\ \underline{\mathbf{X}\ \mathbf{D}_n\ \boldsymbol{A}} \Bigg), \quad (6.26)$$

where the manipulations due to pre- and post-multiplications are underlined for ease in reading.

### 6.3.2 Framework for Channel Assignment

For ease of representation, we denote the binary set of channel assignment indicator variables by $\mathcal{X} = \{x_{n\ell};\ \forall n, \ell \in [1, N]\}$, and $\mid \mathcal{X} \mid = N^2$. The intermodulation distortion power for receiver $n$ is given by $P_{\mathsf{ACI}_n}(\mathcal{X}) = \mid \rho_n \mid^2$. If $\eta$ is AWGN, the rate for receiver $n$ and the network-wide sum rate is given by,

$$R_n = W \log_2 \left( 1 + \frac{P_{T_n} d_{nn}^{-\mu}}{P_{\mathsf{ACI}_n}(\mathcal{X}) + \eta} \right), \quad (6.27)$$

$$R = W \sum_{n=1}^{N} \log_2 \left( 1 + \frac{P_{T_n} d_{nn}^{-\mu}}{P_{\mathsf{ACI}_n}(\mathcal{X}) + \eta} \right). \quad (6.28)$$

The sum rate maximization problem can now be formulated as,

$$\mathcal{J}_3 = \max_{\mathcal{X}} \sum_{n=1}^{N} \log_2 \left( 1 + \frac{P_{T_n} d_{nn}^{-\mu}}{P_{\mathsf{ACI}_n}(\mathcal{X}) + \eta} \right) \quad (6.29)$$

$$\text{s.t} \sum_{\ell=1}^{N} x_{n\ell} = 1; \sum_{n=1}^{N} x_{n\ell} = 1. \quad (6.30)$$

This is a non-convex, nonlinear, complex, mixed binary integer optimization problem and has an inconvenient form. Thus, we use the matrix representation to refine this formulation. The adjacent channel interference power for receiver $n$ as a function of the channel assignment matrix $\mathbf{X}$, is

denoted by $P_{\mathsf{ACI}_n}(\mathbf{X}) =\mid \rho_n \mid^2$. The Signal-to-Noise-plus-Interference-Ratio for receiver $n$ is,

$$\mathsf{SINR}_n = \frac{P_{T_n} d_{nn}^{-\mu}}{P_{\mathsf{ACI}_n}(\mathbf{X})}. \tag{6.31}$$

The maximization problem can now be written in terms of the permutation matrix as,

$$\mathcal{J}_3 = W \max_{\mathbf{X}} \sum_{n=1}^{N} \log_2 \left(1 + \frac{P_{T_n} d_{nn}^{-\mu}}{P_{\mathsf{ACI}_n}(\mathbf{X}) + \eta}\right) \tag{6.32}$$

$$\text{s.t} \sum_{\ell=1}^{N} \mathbf{X}_{n\ell} = 1; \quad \sum_{n=1}^{N} \mathbf{X}_{n\ell} = 1. \tag{6.33}$$

The complexity of this nonlinear binary-integer assignment problem is $\mathcal{O}(N!)$. We can lower bound the objective function and use similar arguments as presented in Section 6.2.2 to transform the sum rate maximization problem into sum interference minimization, $\min \sum_{n=1}^{N} \mid \rho_n \mid^2$, where $\rho_n$ is given by (6.26). However, this will not give any advantage unlike with the case with co-located transmitters to design fast algorithms owing to the complexity of the underlying phenomena. Thus, we develop a fast heuristic algorithm for this optimization problem and analyze the results. Research on possible ways to develop optimal algorithms for this problem is beyond the scope of this chapter and dissertation.

### 6.3.3 Heuristic Algorithm: Simulated Annealing

In the preceding subsection, we developed the framework for receiver nonlinearity aware network sum rate maximization. As was evident, the maximization problem is highly complex. In this section, we employ a heuristic technique and develop a fast algorithm based on Simulated Annealing (SA) and demonstrate that there exist such meta-heuristic approaches to solve the proposed framework and obtain an approximation of the global optimum.

SA is a meta-heuristic probabilistic technique to approximate the global optimum solution of a given objective. Its utility is pronounced, especially when the problem is exceedingly complex with the exponentially scaling search space. It was first proposed by [92] and [93] gives a comprehensive review. It has been previously applied to channel allocation in [94–96].

The channel assignment problem at hand is essentially a combinatorial optimization problem of finding the best permutation out of the $N!$ possible assignments. We define the state

**Algorithm 3** SA based Receiver Nonlinearity Aware Channel Assignment

INITIALIZATIONS

FORMULATE: Network topology matrices $\boldsymbol{A},\ \mathbf{G},\ \mathbf{d}_n,\ \mathbf{D}_n$

INITIAL STATE: Random Assignment, $\mathcal{S} = \{s_1\ s_2\ \cdots\ s_N\}$

FORMULATE: Channel Assignment Permutation Matrix, $\mathbf{X}(\mathcal{S})$

COMPUTE: $\rho_n,\ \forall n \in [1, N]$ using equation (6.26) and $P_{\mathsf{ACI}_n}(\mathbf{X}) = |\rho_n|^2$

EVALUATE: $R = W \sum_{n=1}^{N} \log_2 \left(1 + \frac{P_{T_n} d_{nn}^{-\mu}}{P_{\mathsf{ACI}_n}(\mathbf{X}) + \eta}\right)$

INITIALIZE: Initial Temperature, $T$
Cutoff Temperature, $T_{\mathsf{min}}$
Update Constant, $\lambda \in (0, 1)$

ITERATIONS

**while** $T > T_{\mathsf{min}}$ **do**
  Generate two random integers $i \in [1, N], j \in [1, N] : i \neq j$
  Update to neighboring state by swapping the channel assignment of receivers $i, j$ in $\mathcal{S}$: $\mathcal{S}_{\mathsf{new}} = \mathcal{S}\left(\mathtt{swap}(s_i, s_j)\right)$
  Formulate new Channel Assignment Permutation Matrix, $\mathbf{X}(\mathcal{S}_{\mathsf{new}})$
  Compute $\rho_n,\ \forall n \in [1, N]$ using equation (6.26) and $P_{\mathsf{ACI}_n}(\mathbf{X}) = |\rho_n|^2$
  Evaluate $R_{\mathsf{new}} = W \sum_{n=1}^{N} \log_2 \left(1 + \frac{P_{T_n} d_{nn}^{-\mu}}{P_{\mathsf{ACI}_n}(\mathbf{X}) + \eta}\right)$
  Compute $\delta_e = R_{\mathsf{new}} - R$; and $p_{\delta_e} = \exp\left(\frac{\delta_e}{T}\right)$
  **if** $\delta_e < 0$ **then**
    $R = R_{\mathsf{new}}$; and $\mathcal{S} = \mathcal{S}_{\mathsf{new}}$
  **else**
    Generate a random number $\zeta \sim \text{Unif}(0, 1)$
    **if** $\zeta \leq p_{\delta_e}$ **then**
      $R = R_{\mathsf{new}}$; and $\mathcal{S} = \mathcal{S}_{\mathsf{new}}$
    **end if**
  **end if**
  Update $T = \lambda T$
**end while**

$\mathcal{S} = \{s_1\ s_2\ \cdots\ s_N\}$ to represent the channels allocated to users $\{1, 2, \cdots, N\}$ respectively. Clearly, $s_i \in [1, N]$ are unique. The idea behind simulated annealing is to start with a random state and check the value of the objective function at a neighboring state. If the neighboring objective is greater, update to the neighboring state, else update with a certain probability. Updating to the neighboring state with a certain probability even when it yields a lower objective is to ensure that the solution does not get stuck in local minimum. However, with increasing iterations the probability of updating to the neighboring state yielding lower objective is decreased, thus ensuring convergence. This process of gradual decrease in the probability which leads to convergence was inspired by the controlled cooling of materials to reduce lattice defects in metallurgy and hence the name SA.

The SA based channel assignment is described in Algorithm 7. The initialization includes formulating the several network topology matrices, initializing a random channel assignment state $\mathcal{S}$, formulating the channel assignment permutation matrix $\mathbf{X}$, computing adjacent channel interference power $P_{\mathsf{ACI}}$ and the sum rate. Further, the initial temperature $T$, cutoff temperature $T_{\mathsf{min}}$ and the update constant are set. Through the iterations, to update to a neighboring state, two unique random integers in the range $[1, N]$ are chosen. The channel assignment of those two receivers is swapped, thus creating a new assignment state. The network sum rate of this new assignment and the difference, $\delta_e$, between the current and new network sum rate are computed. If the new rate is higher ($\delta_e > 0$), then the new assignment is retained. If the new rate is lower, the new assignment is retained with a probability of $p_{\delta_e} = \exp\left(\frac{\delta_e}{T}\right)$. This is implemented by generating a uniform random number between $0$ and $1$ and comparing it with $p_{\delta_e}$.

### 6.3.4 Pre-selector Spans a Factor of the Entire Band

In the preceding discussions, we assumed that a single pre-selector filter spans the entire band of operation for all receivers. However, this assumption may not hold as receivers may have multiple pre-selectors spanning the band of operation to minimize the adjacent channel signals entering the front-end as shown in Fig. 6.2.

As detailed in Section 6.2.5, we assume receiver $n$ has $M_n$ pre-selector filters, each spanning $\frac{N}{M_n}$ channels. A given channel $\ell \in [1, N]$ for a receiver $n$ maps to a frequency $\ell'_n = ((\ell - 1) \mod M_n) + 1$ as before. However, to compute the adjacent channel interference, we need to evolve different steps. This is because the received amplitude on each channel for a given network is different and dependent on the channel allocation itself due to the nature of network topology.

For a given channel $\ell$ the pre-selector filter for a receiver $n$ spans the channels $[\ell - \ell'_n, \ell - \ell'_n + M_n]$. We now define a filter matrix for each channel for a given receiver $n$ as,

$$\mathbf{F}_{n,\ell} = \underbrace{\left[ \underbrace{\mathbf{0}}_{M_n \times (\ell - \ell'_n)} \middle| \underbrace{\mathbf{I}}_{M_n \times M_n} \middle| \underbrace{\mathbf{0}}_{M_n \times (N + \ell'_n - \ell - M_n)} \right]}_{M_n \times N}, \tag{6.34}$$

where $\mathbf{0}$ is a zero matrix and $\mathbf{I}$ is an identity matrix. Thus, $\mathbf{F}_{n,\ell}$ is the characteristic of a given receiver. Along with that, the matrices $\mathbf{L}_n^{\mathsf{A}}, \mathbf{L}_n^{\mathsf{B}}, \mathbf{L}_{n,i}^{\mathsf{C}}, \mathbf{L}_{n,i}^{\mathsf{D}}$ are now defined for the pre-selector filter width $M_n$. To use the formulation in (6.26), we need the radio-environment matrices. For a given channel assignment matrix $\mathbf{X}$ with channel $\ell$ assigned to receiver $n$, and the network topology matrix $\mathbf{D}_n$, we formulate,

$$\boldsymbol{A}'_{n,\ell} = \mathbf{F}_{n,\ell}\, \mathbf{X}\, \mathbf{D}_n \boldsymbol{A};\ \mathbf{G}'_n = \mathrm{diag}\left(\boldsymbol{A}'_n\right) = \mathbf{F}_{n,\ell}\, \mathbf{X}\, \mathbf{d}_n^T \mathbf{G}\, \mathbf{X}^T\, \mathbf{F}_{n,\ell}^T. \tag{6.35}$$

The adjacent channel interference due to intermodulation distortion is now calculated as,

$$\rho_n = \alpha_{3_n} \left( [1\ 1\ \cdots\ 1] \left( \mathbf{L}_n^{\mathsf{A}}\, \mathbf{G}'_n\, \mathbf{L}_n^{\mathsf{B}}\, \boldsymbol{A}'_n \right) + 2 \sum_{\forall i \in \Upsilon_n^{\iota}} \boldsymbol{A}'^T_n\, \mathbf{L}_{n,i}^{\mathsf{C}}\, \mathbf{G}'^{1/2}_n\, \mathbf{L}_{n,i}^{\mathsf{D}}\, \boldsymbol{A}'_n \right). \tag{6.36}$$

Thus, to evaluate the adjacent channel interference $\rho_n$ on step 11 of Algorithm 3, we follow the steps shown in Algorithm 4. The rest of the algorithm remains the same as for channel assignment.

**Algorithm 4** Steps to compute $\rho_n$ when pre-selector spans a factor N

1: Note the channel assigned to receiver $n$ as, $\ell = i : s_i = n, s_i \in \mathcal{S}$
2: Compute $\ell'_n = ((\ell - 1) \mod M_n) + 1$
3: Compute $\boldsymbol{A}'_{n,\ell} = \mathbf{F}_{n,\ell}\, \mathbf{X}\, \mathbf{D}_n \boldsymbol{A}$
4: Formulate $\mathbf{G}'_n = \mathrm{diag}\left(\boldsymbol{A}'_n\right)$
5: Compute $\rho_n$ using equation (6.36)

## 6.4 Modeling Transmitter Masks and OOBE

In the discussion thus far, we ignored the adjacent channel interference due to the Out-Of-Band-Emission (OOBE) of transmitters. However, transmitter leakage into adjacent bands is an important aspect that needs to be modeled for next generation wireless network

design. Assume the link $n \in [1, N]$ is assigned channel $c \in [1, N]$. Let $\epsilon^n_{\ell c}$ denote the fraction of the power emitted by the transmitter on link $n$ on channel $\ell$ when assigned channel $c$, as illustrated in Fig. 6.4. For $c = \ell$, this represents the in-band power and hence, $\epsilon^n_{cc} = \epsilon^n,\ \forall c \in [1, N]$ where $\epsilon^n$ is the fraction of in-band power emitted. Let $\mathbf{E}_n$ represent the emission matrix for transmitter $n$ whose columns $c \in [1, N]$ represent its transmit mask when assigned to that channel,

$$\mathbf{E}_n = \begin{bmatrix} \epsilon^n_{11} & \epsilon^n_{12} & \dots & \epsilon^n_{1N} \\ \epsilon^n_{21} & \epsilon^n_{22} & \dots & \epsilon^n_{2N} \\ \vdots & \vdots & \ddots & \vdots \\ \epsilon^n_{N1} & \epsilon^n_{N2} & \dots & \epsilon^n_{22} \end{bmatrix}. \tag{6.37}$$

If $\boldsymbol{P} = [P_1 P_2 \cdots P_N]^T$ represents the vector of transmit powers of the $n$ transmitters, and $\mathbf{X}$ is the channel assignment permutation matrix, the 'transmit power profile' of the network denoted by the vector $\boldsymbol{P}^{\mathsf{Tx}}$,

$$\boldsymbol{P}^{\mathsf{Tx}} = \sum_{n=1}^{N} \mathbf{E}_n \, \mathbf{X} \, \mathbf{L}_n^{\mathsf{Tx}} \, \mathbf{X} \, \boldsymbol{P}, \tag{6.38}$$

where the rows represent the $N$ channels can be formulated as, $\mathbf{L}_n^{\mathsf{Tx}} = \mathbf{e}_n \mathbf{e}_n^T$, $\mathbf{e}_n$ is the unit basis vector in $\Re^N$. This formulation gives the total contribution of each transmitter on a given channel. The transmit amplitude vector is given by,

$$\boldsymbol{A}^{\mathsf{Tx}} = \left[\boldsymbol{P}^{\mathsf{Tx}}\right]^{1/2}. \tag{6.39}$$

Using this transmit amplitude vector $\boldsymbol{A}^{\mathsf{Tx}}$, the adjacent channel interference for receiver $n$ can be computed using the formulation,

$$\rho_n = \alpha_{3_n} \Bigg( [1\ 1\ \cdots\ 1] \left( \mathbf{L}^{\mathsf{A}} \, \mathbf{d}_n^T \, \mathbf{G}_n^{\mathsf{Tx}} \, \mathbf{L}_n^{\mathsf{B}} \, \mathbf{D}_n \boldsymbol{A}^{\mathsf{Tx}} \right) + 2 \sum_{\forall i \in \Upsilon^{\iota}_n} \left[\boldsymbol{A}^{\mathsf{Tx}}\right]^T \mathbf{D}_n^T \, \mathbf{L}^{\mathsf{C}}_{n,i} \, \mathbf{d}_n^T \left[\mathbf{G}^{\mathsf{Tx}}\right]^{1/2} \mathbf{L}^{\mathsf{D}}_{n,i} \, \mathbf{D}_n \boldsymbol{A}^{\mathsf{Tx}} \Bigg). \tag{6.40}$$

The adjacent channel interference power is computed as $P_{\mathsf{ACI}_n} = |\rho_n|^2$. If the pre-selector filter for the given receiver $n$ spans a factor of the entire operational bandwidth, the adjacent channel interference can be computed using Algorithm 4, by replacing step 3, as $\boldsymbol{A}'_{n,\ell} = \mathbf{F}_{n,\ell} \, \mathbf{D}_n \boldsymbol{A}^{\mathsf{Tx}}$.

In addition, there is co-channel interference caused by overlapping OOBE from adjacent channel

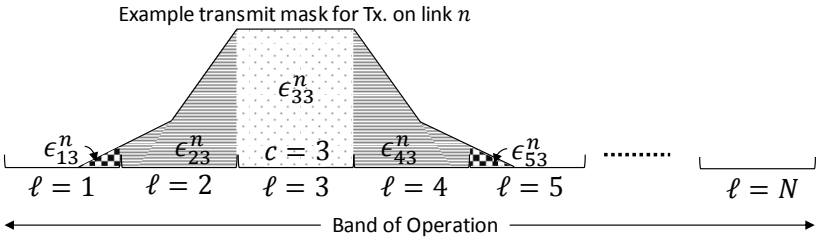


Figure 6.4: Example of transmit mask with Out Of Band Emissions (OOBE) where desired channel is $\ell = 3$. It ideally should restrict all transmit power to that channel.

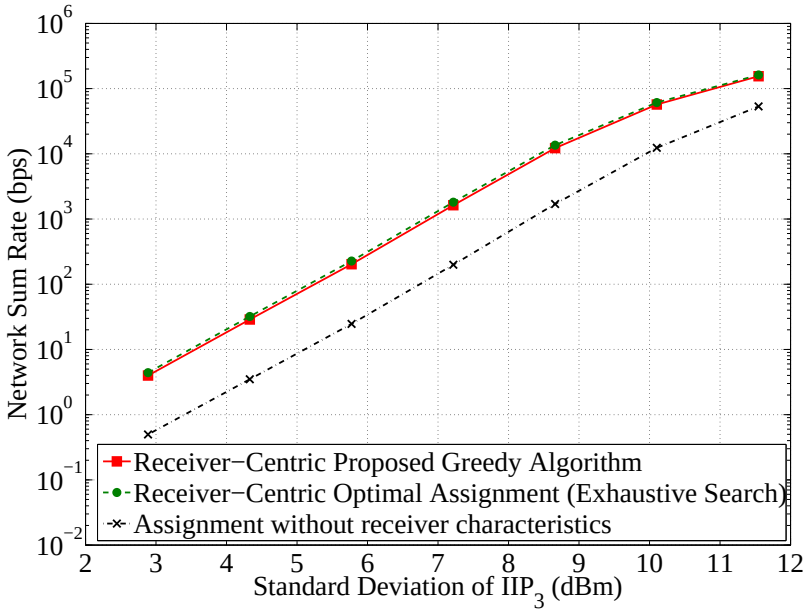


Figure 6.5: Variation of Network Sum Rate with $\mathsf{IIP}_3$ diversity. Proposed Greedy Algorithm is close to true optimal solution.

transmitters. For a given receiver $n$, this can be computed as,

$$P_{\mathsf{OOBE}_n} = \mathbf{e}_n \left( \mathbf{X}^T \boldsymbol{P}^{\mathsf{Tx}} - \boldsymbol{P} \right). \tag{6.41}$$

The total interference, $P_{\mathsf{INT}_n}$ due to ACI and OOBE for receiver $n$ is then given by $P_{\mathsf{INT}_n} = P_{\mathsf{ACI}_n} + P_{\mathsf{OOBE}_n}$. Channel Assignment can then be optimized using Algorithm 7 using $P_{\mathsf{INT}_n}$ (in place of $P_{\mathsf{ACI}_n}$) to compute the sum rate.

## 6.5 Simulation Results

### 6.5.1 Case 1: Single Transmitter, Multiple Receivers

In this section, we present the simulation of the case with a single (or co-located) transmitter gateway downlink with multiple receivers described in Section 6.2. The simulations are performed assuming the receivers to be uniformly distributed inside a circle of radius $50$ m with the transmitter located at the centre of the circle. The receivers form a Poisson Point Process [97–101]. The transmit power is equal for all channels and is set to $30$ dBm. We initially perform simulations over small networks to verify the results of the proposed greedy algorithm with the optimal solution, which is obtained by an exhaustive surface search. Following this, we demonstrate the benefits of receiver-centric channel allocation for scalability of diverse-RAT networks.

#### Varying $\mathsf{IIP}_3$ Diversity

In this section, we consider a network of $N = 8$ nodes on downlink over $8$ distinct channels with each channel spanning $W = 1$ MHz. The pre-selector is assumed to span the entire operating bandwidth of $B = 8$ MHz. The $\mathsf{IIP}_3$ of all the devices are uniformly distributed in the range $\mathsf{IIP}_3 \sim \text{Unif}\left(\mathsf{IIP}_{3_{\mathsf{min}}}, \mathsf{IIP}_{3_{\mathsf{max}}}\right)$. In order to vary the diversity of devices, we fix $\mathsf{IIP}_{3_{\mathsf{min}}} = -30$ dBm and vary $\mathsf{IIP}_{3_{\mathsf{max}}}$ from $-20$ dBm to $+10$ dBm in steps of $5$ dB. For each $\mathsf{IIP}_3$ range, Monte-Carlo simulations are carried out and the results are averaged over $10,000$ network realizations and network sum rate is plotted as a function of the $\mathsf{IIP}_3$ standard deviation as shown in Fig. 6.5. The transmit power for each user is was selected as $P_T = 30$ dBm. We compare the optimal assignment for the sum rate maximization obtained through exhaustive surface search to the greedy algorithm proposed in this chapter. A randomized channel assignment without receiver characteristics is used as baseline for comparison [108]. Without the knowledge of receiver characteristics, there

is no way to compare the difference between assignments since all users are operating on distinct channels. Hence, a randomized assignment is chosen as the baseline [108]. Firstly, receiver-centric channel assignment significantly increases the network sum rate − an order of magnitude improvement is seen. Secondly, the assignment of the proposed greedy algorithm is very close to the optimal solution when averaged over large network realizations.

**Impact on Scalability**

An important consideration while studying heterogeneous and diverse RAT systems is to assess the scalability of co-existence in such operations. The density of connected devices is expected to exponentially increase in next generation wireless networks. Thus, it is important to study the impact of receiver-centric awareness in such dense networks with diverse devices. We consider a total bandwidth, $B = 10$ MHz with nodes uniformly distributed in a circular area with radius $50$ m. The density of nodes is varied from $0.001$ nodes per m$^2$ ($\sim$ just 1 node) to $0.05$ nodes per m$^2$ ($\sim$ 400 nodes). Each node is allocated a channel spanning $W = \frac{B}{N}$ Hz, where $N$ is the number of nodes in the network. Simulations with the proposed greedy channel assignment algorithm are carried out for channel assignment for $10,000$ network realizations and the results are presented. For each realization, $\mathsf{IIP}_3$ is uniformly distributed between $-30$ dBm and $+10$ dBm for the nodes, and the pre-selector is assumed to span the entire $10$ MHz for all nodes. As the node density increases, the number of adjacent channel interferers increases causing a drop in the network sum rate. This is where receiver-centric channel assignment can potentially yield very high spectral efficiency gains. Figure 6.6 shows that a gain of several orders of magnitude is obtained due to to receiver-centric channel assignment with increasing node density.

We next carry out simulations with the same setup, except for the pre-selector filter span. We relax the assumption that the span of pre-selector filter all nodes is equal to entire bandwidth. Instead, the pre-selector filter for each node is a uniform random factor of $N$ (the total number of channels) in each network realization. This is in addition to the random $\mathsf{IIP}_3$ of each receiver. The results are as shown in Fig. 6.7. Naturally, when the pre-selector filter spans less than the entire band of possible channels, the amount of adjacent channel interfering signals that impact the desired channel is less. Thus, we see a better overall network sum rate, irrespective of receiver-centric assignment compared to Fig. 6.6. However, the spectral efficiency with receiver-centric allocations that takes into account the vulnerabilities of all receiver nodes in the network is orders of magnitude better than receiver agnostic allocations. The absence of 'smoothness' in the curves

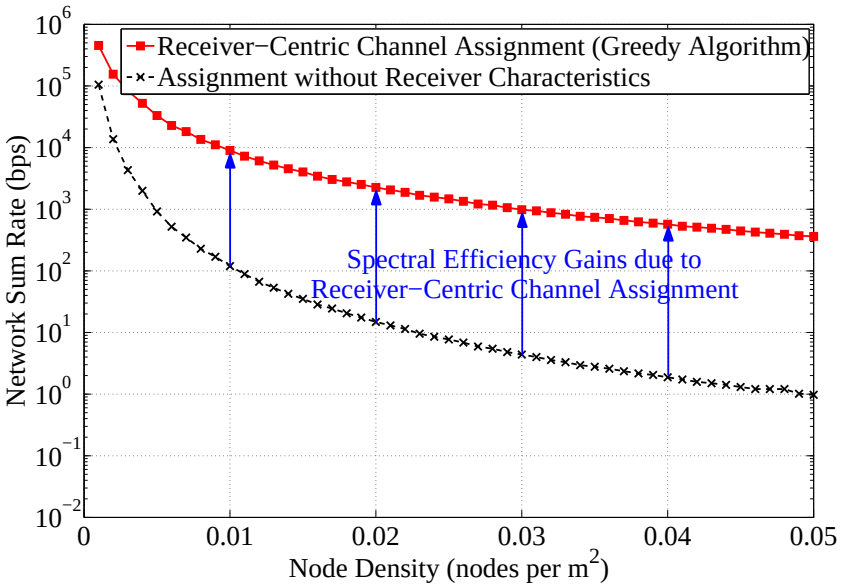


Figure 6.6: Network Sum Rate with Increasing Node Density, pre-selector spans entire bandwidth: Receiver-Centric assignment is spectrally efficient with high gains for network scalability

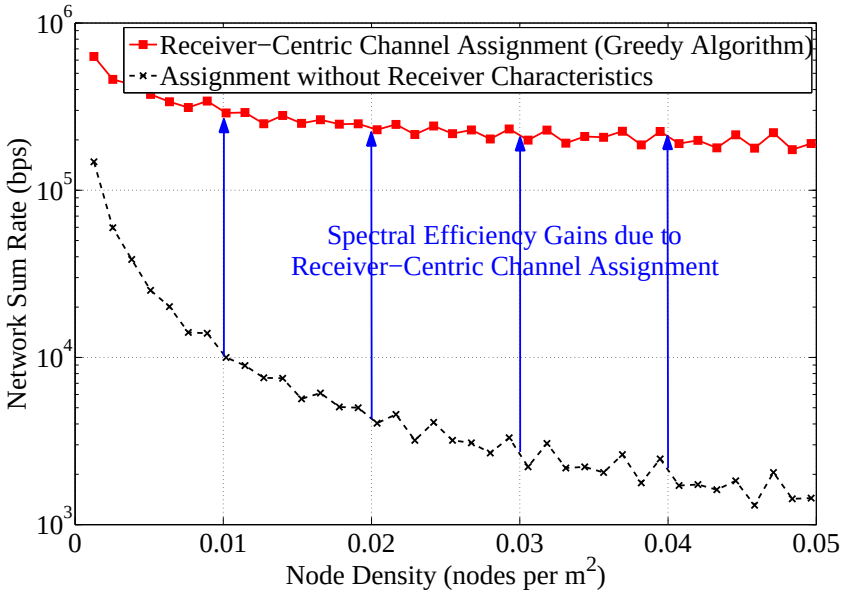


Figure 6.7: Network Sum Rate with Increasing Node Density, pre-selector spans a factor of bandwidth: High spectrum efficiency for Receiver-Centric assignment aids in network scalability

despite $10,000$ network realizations is due to the fact that network sum rate depends on the number of choices available for pre-selector filter bandwidths, which numerically vary significantly for different numbers ranging from $N \approx 1$ to $N \approx 400$ (e.g. prime numbers do not have any divisors, while even numbers generally have large number of divisors).

### 6.5.2 Multiple Transmitter-Receiver Pairs

In this section, we present the simulation results for the general setting of $N$ Tx-Rx pairs communicating over $N$ adjacent channels over a geographic area as described in Section 6.3. The simulations are performed assuming the transmitters and receivers are distributed inside a circle of radius $500$ m, uniformly at random. Thus, all the nodes in the network form a Poisson Point Process [97–101]. The transmit power for a given transmitter is randomly chosen between $10$ dBm and $80$ dBm.

#### Varying $\mathsf{IIP}_3$ Diversity

In this section, we consider a network of $N = 8$ Tx-Rx pairs over $8$ distinct channels with each channel spanning $W = 1$ MHz. The pre-selector is assumed to span the entire operating bandwidth of $B = 8$ MHz. The $\mathsf{IIP}_3$ of all the devices are uniformly distributed in the range $\mathsf{IIP}_3 \sim \text{Unif}\left(\mathsf{IIP}_{3_{\text{min}}}, \mathsf{IIP}_{3_{\text{max}}}\right)$. In order to vary the diversity of devices, we fix $\mathsf{IIP}_{3_{\text{min}}} = -30$ dBm and vary $\mathsf{IIP}_{3_{\text{max}}}$ from $-20$ dBm to $+10$ dBm in steps of $5$ dB. As the $\mathsf{IIP}_3$ variance increases, diversity of receiver performance also increases. For each range, Monte-Carlo simulations are carried out, and the results are averaged over $10,000$ network realizations. Network sum rate is plotted as a function of the $\mathsf{IIP}_3$ standard deviation as shown in Fig. 6.8. We compare the optimal the sum rate maximization obtained through exhaustive search, to the sum rate from randomized channel assignment without receiver characteristics (baseline for comparison [108]) and demonstrate the impact of utilizing receiver characteristics in channel assignments. As evident from the simulations, receiver-centric channel assignment significantly increases the network sum rate, by orders of magnitude. As the diversity of devices increases, an increase in network sum rate is anticipated, owing to an increase in receivers with 'good' characteristics. However, receiver-centric assignment significantly increases the network sum rate in comparison, primarily because 'receiver characteristic awareness' can protect vulnerable receivers from interference, while boosting the rate to 'good' receivers.

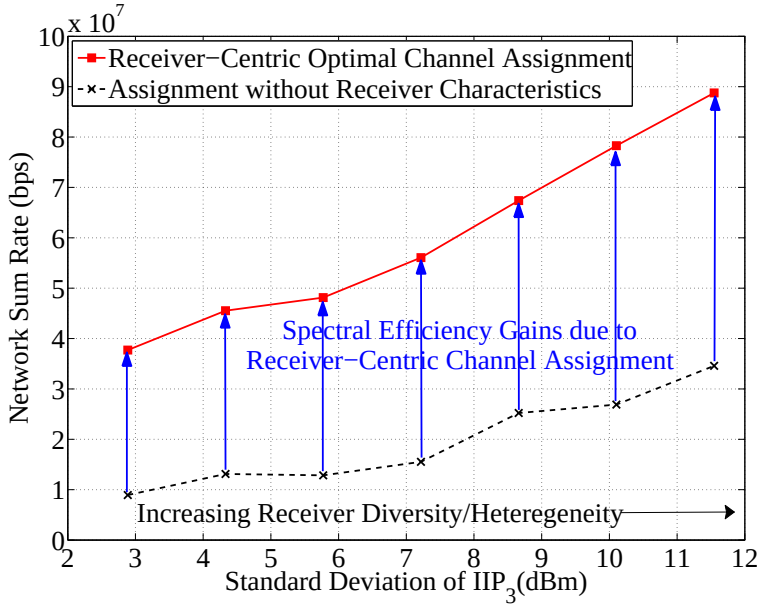


Figure 6.8: Network Sum Rate with increasing $\mathsf{IIP}_3$ diversity:
High spectrum efficiency gains for more diverse-RAT networks

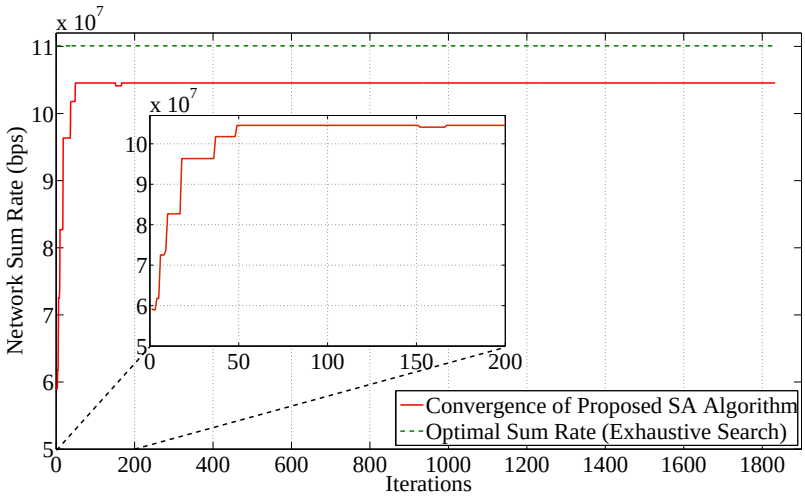


Figure 6.9: Sample convergence of proposed Simulated Annealing (SA) algorithm for $N = 8$: Order Optimal solution obtained

**Simulated Annealing Algorithm**

In this section, we present the results of the proposed heuristic algorithm based on Simulated Annealing (SA) for the channel assignment problem. We consider a network of $N = 8$, Tx-Rx pairs over $8$ distinct channels with each channel spanning $W = 1$ MHz. The pre-selector is assumed to span the entire operating bandwidth of $B = 8$ MHz. The $\mathsf{IIP}_3$ of all the devices are uniformly distributed in the range $\mathsf{IIP}_3 \sim \text{Unif}\,(\mathsf{IIP}_{3_{\mathsf{min}}}, \mathsf{IIP}_{3_{\mathsf{max}}})$. We plot the convergence of the simulated annealing algorithm, and compare its performance against the optimal obtained through exhaustive search. The convergence for a sample network realization is shown in Fig. 6.9. The average rate of convergence was found to be about $122$ iterations with a standard deviation of about $30$ (rounding off to nearest decimal) over $10,000$ network realizations. Monte-Carlo simulations indicated an order-optimal solution, with the mean performance after $150$ iterations over $10,000$ network realizations found to be $93.41\%$ of the optimal value. The worst case performance was found to be $83.12\%$ of the optimal value. Fig. 6.10 shows the sample convergence for a network with $N = 100$ nodes.

**Impact of Scalability**

In this section, we present a final result of network simulations and examine the gains of the receiver-centric framework with increasing node density with varying $\mathsf{IIP}_3$ characteristics. We consider a total bandwidth, $B = 20$ MHz. The density of nodes is varied from $0.001$ nodes per m$^2$ to $0.05$ nodes per m$^2$. Each node is allocated a channel, spanning $W = \frac{B}{N}$ Hz, where $N$ is the number of nodes in the network for a given density. Simulations with the proposed SA based assignment algorithm are carried out for $10,000$ network realizations for each node density and the results are presented. For each realization, $\mathsf{IIP}_3$ is uniformly distributed between $-30$ dBm and $+10$ dBm for each node, and the pre-selector is assumed to span an integer factor of the entire bandwidth of $20$ MHz, selected uniformly at random for each node. As the node density increases, the number of adjacent channel interferers increases causing a drop in the network sum rate. With receiver-centric assignments, co-existence of diverse nodes can be ensured with relatively high spectrum efficiency at high node density. Fig. 6.11 shows that gains of several orders of magnitude are obtained due to receiver-centric channel assignment at higher node densities. These results show the substantial spectrum efficiency gains possible by receiver-centric spectrum access proposed in this chapter and presents a strong case for potential improvements in next generation wireless networks.

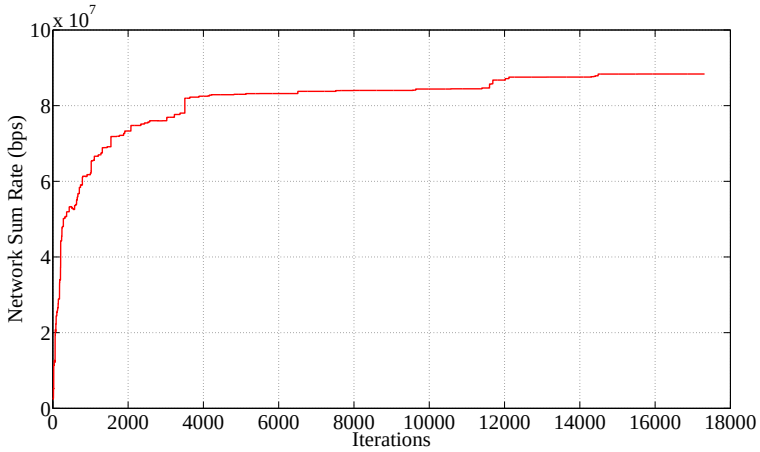


Figure 6.10: Sample convergence of proposed Simulated Annealing (SA) algorithm for $N = 100$: $\sim 17,000$ iterations to converge

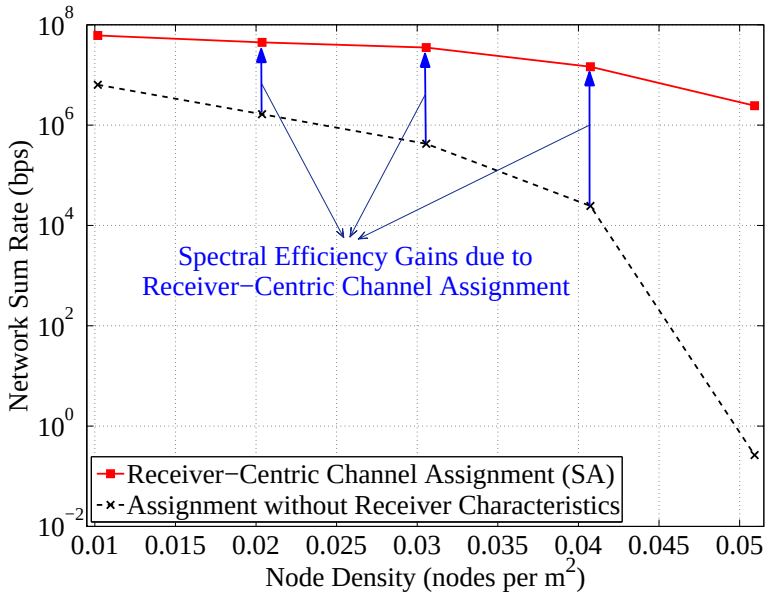


Figure 6.11: Network Sum Rate with Increasing Node Density: Receiver-Centric assignment gives high spectrum efficiency gains, enabling scalability and node densification

## 6.6 Conclusions

In this chapter, we demonstrated that receiver-centric spectrum access and network optimization will substantially increase spectrum efficiency in next generation diverse-RAT dense wireless networks. Spectrum efficiency gains of several orders of magnitude were observed through extensive network simulations for dense and diverse wireless networks with channel assignment frameworks accounting for receiver front-end nonlinearity compared to receiver agnostic assignment. We proposed computationally efficient network optimization frameworks and algorithms to account for receiver front-end nonlinearities and transmitter out-of-band emission masks. This approach yields high network performance gains and promotes harmonious co-existence of dense wireless networks. The impact of adjacent channel interference on diverse and heterogeneous networks is demonstrated in this chapter. Next generation spectrum access and network optimization frameworks should account for RF front-end nonlinearity and imperfections.

This work has the potential to pave the way for new research frontiers in receiver-centric frameworks and algorithms for efficient spectrum access and network management. Computationally efficient algorithms with analytical performance guarantees need to be developed for the proposed receiver-centric frameworks. Development of downlink power control algorithms with channel allocation can further increase network performance. The assumption of fixed channel bandwidths for all users can be relaxed and computational algorithms to obtain bounded approximations for demand based resource allocations is a promising area of future research.

# Chapter 7

# Receiver Impairment Aware Efficient Spectrum Access

## 7.1 Introduction

In this chapter, we propose a comprehensive framework to account for the receiver imperfections arising due to imperfect image frequency rejection, phase noise, and ADC aliasing for informed channel allocations to maximize network sum rate. We describe the receiver architecture considered and devise an effective methodology to account for the impact of these parameters on the communication link. We use this methodology to develop a network optimization framework to maximize network sum data rate (or sum rate) while accounting for receiver impairments. We assume an automated centralized spectrum manager (e.g. Spectrum Access System of $3.5$ GHz CBRS) controlling the spectral access of all nodes in the network.

Throughout the discussion in this chapter, we assume a Direct Conversion Receiver (DCR) architecture [41] as shown in Fig 7.1 [55], which is increasingly common in next generation wireless systems [41–45]. The front-end Band Pass Filter (BPF) typically spans the entire range of RF frequencies the receiver is designed to operate over. Thus, the desired signal bandwidth is typically a small fraction of the front-end BPF. Moreover, since this is an RF filter, it generally exhibits poor selectivity. Consequently, unwanted signals from adjacent bands enter the receiver front-end. This is especially true when receivers are designed to operate in a wide range of frequencies. The unwanted signals that enter the receiver front-end can produce interference at the desired frequency/channel due to receiver impairments.

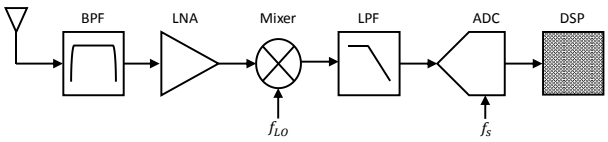


Figure 7.1: An example direct conversion receiver architecture

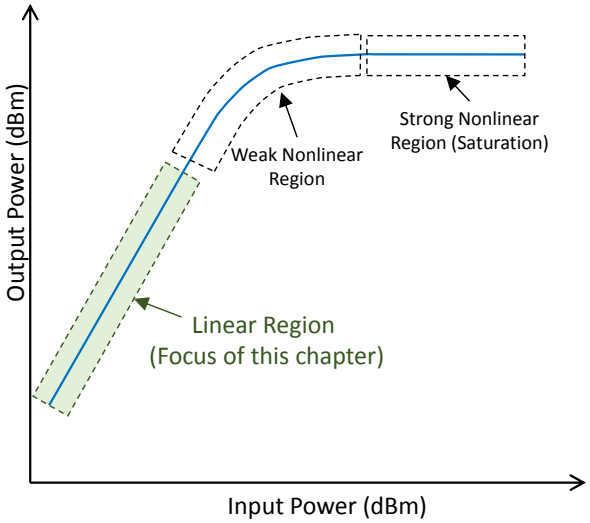


Figure 7.2: Transfer characteristics of a typical receiver

The receiver transfer characteristics can be divided into 3 regions as shown in Fig. 7.2: Linear, Weak Nonlinear, and Strong Nonlinear. Previously, we have considered the impact of nonlinear third order distortions on receiver operations for carrying out informed channel/resource allocations to improve spectral efficiency [49, 108]. Third order distortions mainly occur when the receiver is operating in the nonlinear regions. However, multiple components of the receiver chain produce unwanted distortions even in the linear operating regions. Accounting for adjacent channel interference due to receiver impairments in the linear operating regions for resource allocations is missing in the existing literature. In this chapter, we focus on the receiver impairments occurring in the linear operating regions and formulate a framework for receiver-characteristics-aware resource allocation.

We consider three major receiver impairments that lead to adjacent channel interference viz., imperfect image frequency rejection, frequency selectivity of baseband filter response, and imperfect sampling leading to ADC aliasing. Due to these effects, components of signals from adjacent channels appear in the desired channel at the output of the RF front-end. This spectral

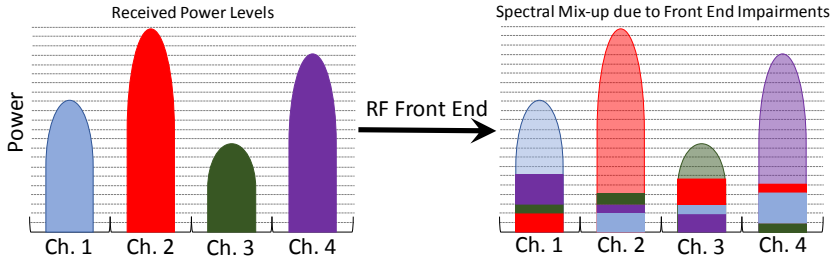


Figure 7.3: Illustration of spectral redistribution in a receiver due to front-end impairments

re-distribution (or spectral mix-up) due to front-end impairments is illustrated in Fig. 7.3, where signals of different channels are color-coded.

The importance of receiver-characteristics-aware resource allocation is schematically illustrated in Fig. 7.4 for a simple case of 4 users in 4 channels. The top-left figure illustrates the magnitude of adjacent channel interference occurring due to receiver-agnostic resource allocations through color-coded depiction. The corresponding example for the throughput achieved for each of those users as against the required demand is illustrated in the bottom-left figure. The impact on interference power accounting for receiver characteristics in resource allocations is shown in the top-right figure. Corresponding throughput achieved by the users is depicted in the bottom-right figure. Thus, resource allocations accounting for receiver impairments in addition to channel conditions and other network parameters can potentially improve overall network efficiency.

### 7.1.1 Main Contributions:

The main contributions of this chapter are:

1. We develop a receiver impairment aware network optimization framework to account for (a) imperfect image frequency rejection, (b) phase noise, and (c) ADC aliasing;

2. We approximate the complex non-convex objective function to a tractable form and develop an optimal, a greedy, and a heuristic algorithm to solve the approximate objective function for different network topologies;

3. We demonstrate through network simulations that the proposed receiver impairment aware framework for spectrum access yields higher spectrum efficiency gains for diverse RAT

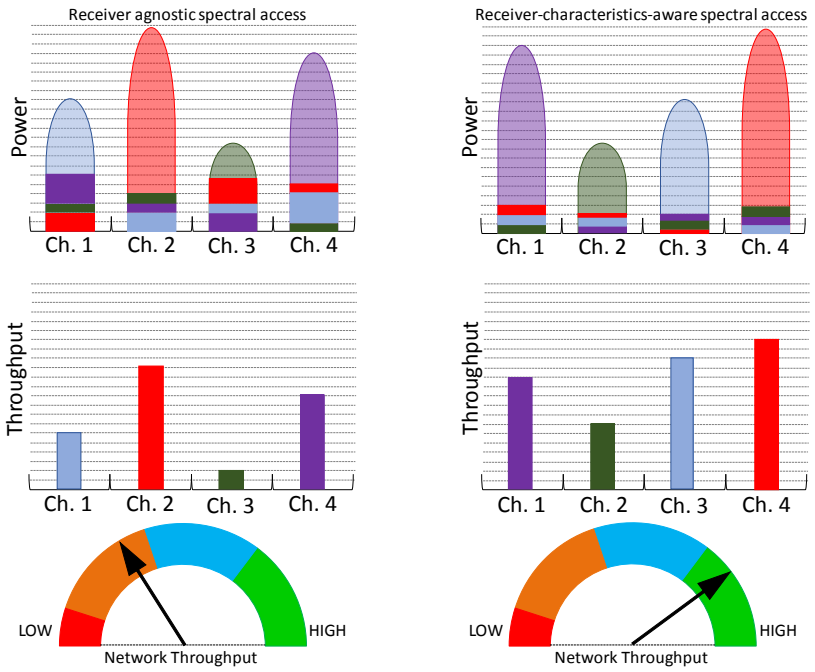


Figure 7.4: Illustratiion on the importance of receiver-characteristics-aware resource allocation

networks in; and

4. We examine the performance of the proposed algorithms against optimal solutions and demonstrate through simulations that the proposed algorithms achieve close-to-optimal solutions over several randomized network realizations.

In Section 7.2, we discuss the representation of various receiver impairments. In Section 7.3, we (a) develop a receiver impairment aware network optimization framework for a network with single/co-located transmitter serving multiple receivers, e.g. IoT Gateway, UAS platform, etc.; (b) approximate the complex non-convex objective function to a tractable form; and (c) develop an optimal and a greedy algorithm to solve the approximate objective function. In Section 7.4, we (a) develop a generalized receiver impairment aware optimization framework for a network multiple transmit-receive pairs; and (b) develop a computationally efficient heuristic algorithm to solve the complex non-convex objective function. In Section 7.5, we (a) examine the performance of the framework and algorithms; and (b) demonstrate the network efficiency gains obtained due to receiver-impairment aware spectrum access through extensive network simulations.

## 7.2 Impact of Receiver Impairments

In this section, we describe the quantitative formulation of the impact of the three receiver impairments using the models developed in [52, 55, 102] as the basis. We describe the framework specific to our use case of interest and direct the readers keen on elaborate analysis to those references.

Consider a receiver front-end band pass filter spanning $N$ channels (indexed by $n \in [1, N]$) of equal bandwidth, $W$. Let $P_R[n]$ denote the power received in the channel $n$. Throughout the discussion in this chapter, we assume the receiver is operating in the linear region.

### 7.2.1 Mixer – Image Frequency Rejection

We assume the local oscillator frequency to be the center of the front-end band pass filter. Imperfect mixing results in the image frequency signal component appearing at the desired channel $\ell$. Using the developments in [102], we re-formulate the mixer output at the desired channel $\ell \in [1, N]$ specific to our use case as,

$$P_{\mathsf{mix}}[n] = P_R[n] + \beta[N - n + 1]\ P_R[N - n + 1] \tag{7.1}$$

where $P_{\mathsf{mix}}[n]$ is the mixer output at channel $n$, and $\beta[n]$ denotes the image frequency rejection ratio of the receiver for channel $n$. This can now be easily represented in the matrix form [102], as shown in Table 7.1 for $N = 4$. Note that in practice, only one of the 4 output channels will be a desired channel.

### 7.2.2 Phase Noise

Local oscillator phase noise results in signals from adjacent channels leaking into the desired channel. The channels immediately adjacent to the desired channel cause maximum interference, and the phase noise eventually falls below the thermal noise as the spectral separation between desired and interfering channels increases [41]. Thus, in this chapter, we ignore the impact of channels other than the ones in the immediate vicinity. If $\nu[n]$ is the fraction of the power in

channel $n$ that leaks to adjacent channels, phase noise can be represented as,

$$P_{\mathsf{PN}}[n] = P_{\mathsf{mix}}[n] + \nu[n \oplus_N 1]P_{\mathsf{mix}}[n \oplus_N 1] + \nu[n \ominus_N 1]P_{\mathsf{mix}}[n \ominus_N 1] \tag{7.2}$$

where $\oplus_N$ and $\ominus_N$ are modular addition and subtraction over the set $[1, N]$.

### 7.2.3 ADC Aliasing

The input signal to the ADC spans $N$ channels with a bandwidth $NW$. However, receivers are limited by the maximum bandwidth they can process as specified by the ADC sampling. In general, if there are $Q < N$ channels (indexed by $q \in [1, Q]$) of width $W$ in the first Nyquist zone of the ADC, there will be aliasing. This means that the receiver can support at most $Q$ channels. If $Q = N$, then no aliasing takes place.

Thus, only $Q$ of the original $N$ channels remain at the ADC output with the signals from the remaining $N - Q$ channels aliasing into one of the $Q$ output channels. With the assumptions of this chapter, the set of channels remaining at the output of the ADC is given by,

$$\Psi_{Q,N} = \left\{ \frac{N-Q}{2} + 1, \frac{N-Q}{2} + 2, \ldots, \frac{N+Q}{2} \right\} \tag{7.3}$$

In general, the mapping between $n$ and $m$ is given by

$$n = \left( \frac{N-Q}{2} \right) + q;\ m \in [1, Q] \tag{7.4}$$

In practical receivers, an anti-aliasing channel selection filter before the ADC filters out the unwanted frequencies and selects the desired channel $n$. The key difference between the RF/baseband filter and anti-aliasing filter is that the passband of the RF/baseband filter spans $N$ channels, whereas the anti-aliasing channel selection filter caters to the ADC sampling rate and spans only $Q$ channels. The output of this filter for channel $n$ can be written as,

$$P_{\mathsf{AAF}}[n] = |G[n]|^2 \, P_{\mathsf{PN}}[n] \tag{7.5}$$

where $P_{\mathsf{AAF}}[n]$ is the anti-aliasing filter output at channel $n$, and $G[n]$ is the linear gain of the filter for channel $n$.

We can now re-formulate the analysis in [102] to obtain the ADC output for channel $q \in [1, Q]$

within the first Nyquist zone which can be written as,

$$P_{\mathsf{ADC}}[q] = \sum_{k=-\lceil \frac{N}{Q} \rceil + 1}^{\lceil \frac{N}{Q} \rceil - 1} P_{\mathsf{AAF}} \left[ \left( \frac{N-Q}{2} \right) + q - kQ \right] \tag{7.6}$$

This can be represented using matrices as shown in Table 7.1 for $N = 4$ and $Q = 2$.

### 7.2.4 Entire Receiver Chain

The output power of the channel $m$ in the first Nyquist zone post sampling for the receiver chain can be written as,

$$P_{\mathsf{ADC}}[m] = \sum_{k=-\lceil \frac{N}{Q} \rceil + 1}^{\lceil \frac{N}{Q} \rceil - 1} |G[i-kQ]|^2 \cdot$$
$$(P_{\mathsf{mix}}[i-kQ] + \nu[(i-kQ) \oplus_N 1] P_{\mathsf{mix}}[(i-kQ) \oplus_N 1] + \nu[(i-kQ) \ominus_N 1] P_{\mathsf{mix}}[(i-kQ) \ominus_N 1]) \tag{7.7}$$

where $i = \left(\frac{N-Q}{2}\right) + m$, and $P_{\mathsf{mix}}$ is given by (7.1). The matrix representation for the entire receiver front-end can be written as,

$$\boldsymbol{P}_{\mathsf{ADC}} = \mathbf{A}\boldsymbol{P} \tag{7.8}$$

where $\mathbf{A} = \mathbf{A}_{\mathsf{ADC}}\ \mathbf{A}_{\mathsf{AAF}}\ \mathbf{A}_{\mathsf{PN}}\ \mathbf{A}_{\mathsf{mix}}$, and $\boldsymbol{P} = [P_R[1]\ P_R[2]\ \cdots\ P_R[N]]^T$. Notationally, the received power on channel $m$ post sampling can be written in a simplified manner as,

$$P_{\mathsf{ADC}}[q] = \sum_{\ell=1}^{N} a_{\ell q} P_{R_\ell} \tag{7.9}$$

where $a_{\ell m}$ is the corresponding entry of the matrix $\mathbf{A}$, the coefficient representing all front-end impairments. For the remainder of this chapter, for simplicity and without loss of generality, we assume that the image frequency rejection and phase noise are frequency independent.

Table 7.1: Example Matrix Representation [102] of Receiver Impairments for $N = 4,\ Q = 2$

| | |
|---|---|
| Mixer | $\boldsymbol{P}_{\mathsf{mix}} = \underbrace{\begin{bmatrix} 1 & 0 & 0 & \beta[4] \\ 0 & 1 & \beta[3] & 0 \\ 0 & \beta[2] & 1 & 0 \\ \beta[1] & 0 & 0 & 1 \end{bmatrix}}_{\mathbf{A}_{\mathsf{mix}}} \begin{bmatrix} P_R[1] \\ P_R[2] \\ P_R[3] \\ P_R[4] \end{bmatrix}$ |
| Phase Noise | $\boldsymbol{P}_{\mathsf{PN}} = \underbrace{\begin{bmatrix} 1 & \nu[2] & 0 & \nu[4] \\ \nu[1] & 1 & \nu[3] & 0 \\ 0 & \nu[2] & 1 & \nu[4] \\ \nu[1] & 0 & \nu[3] & 1 \end{bmatrix}}_{\mathbf{A}_{\mathsf{PN}}} \begin{bmatrix} P_{\mathsf{mix}}[1] \\ P_{\mathsf{mix}}[2] \\ P_{\mathsf{mix}}[3] \\ P_{\mathsf{mix}}[4] \end{bmatrix}$ |
| ADC | $\boldsymbol{P}_{\mathsf{ADC}} = \underbrace{\begin{bmatrix} 1 & 0 & 1 & 0 \\ 0 & 1 & 0 & 1 \end{bmatrix}}_{\mathbf{A}_{\mathsf{ADC}}} \underbrace{\begin{bmatrix} \lvert G[1]\rvert^2 & 0 & 0 & 0 \\ 0 & \lvert G[2]\rvert^2 & 0 & 0 \\ 0 & 0 & \lvert G[3]\rvert^2 & 0 \\ 0 & 0 & 0 & \lvert G[4]\rvert^2 \end{bmatrix}}_{\mathbf{A}_{\mathsf{AAF}}} \begin{bmatrix} P_{\mathsf{PN}}[1] \\ P_{\mathsf{PN}}[2] \\ P_{\mathsf{PN}}[3] \\ P_{\mathsf{PN}}[4] \end{bmatrix}$ |

## 7.3 Case 1: Co-Located Transmitters with Multiple Receivers

Consider a network with $N$ receivers and a single transmitter or co-located multi-transmitter gateway, over $N$ discrete adjacent channels, each with a bandwidth $W$. The $N$ receivers have different front-end technologies and, hence, have diverse RF front-end characteristics. We assume the receivers are distributed in a geographical area within the range of the transmitter as shown in Fig. 7.5.

Further, we assume that the transmitter is using an omnidirectional antenna simultaneously accessing all $N$ channels. The $N$ downlink channels are centered around $f_\ell, \ell \in [1, N]$ respectively. Let each receiver be indexed by $n \in [1, N]$. Each receiver $n$ is using a unique channel, and has a unique characteristic, described by the parameters $\beta_n$, $\nu_n$, $G_n$, and $Q_n$.

An example use case would be the IoT networks of the next generation wireless systems, with a transmitter gateway delivering disparate downlink information for myriad nodes of the network, providing different services. Typically, each node comprises of an inexpensive receiver with a potentially different technology (WiFi, Bluetooth, Zigbee, etc.) and RF front-end. This can be conceptualized for indoor networks such as smart homes, or outdoor networks, where for example, the transmitter gateway can be based on a UAV platform. Note that the framework presented here

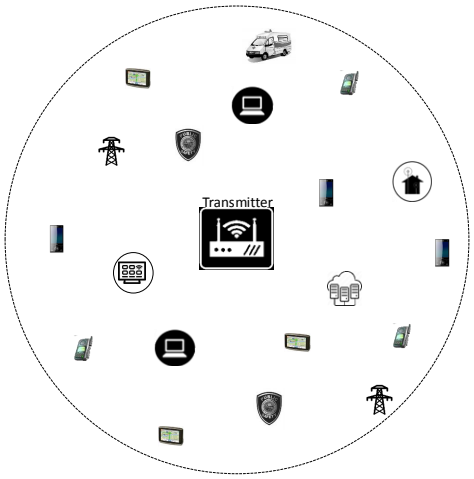


Figure 7.5: Illustration of heterogeneous nodes with diverse RF front-ends with a single/co-located transmitter.

is generic and not technology specific. Thus, it can be adopted for any scenario in which multiple receivers are being served by a single transmitter on different channels.

### 7.3.1 Adjacent Channel Interference Formulation

We discuss the methodology for evaluating the adjacent channel interference due to receiver impairments in this section. From the previous discussions we know that each receiver receives $N$ signals, of which one is the desired signal, and others are adjacent channel signals. The received power on each channel for receiver $n$ is denoted as $P_{R_n} = P_T d_n^{-\mu}$, where $P_T$ is the transmitted power per channel, $d_n$ is the distance of the receiver $n$ from the transmitter, and $\mu$ is the path loss exponent. For simplicity, we do not assume any frequency selective fading and, hence, the received power is the same across all frequencies for a given receiver. The noise power in the bandwidth $W$ is denoted by $\eta$.

We now define an indicator function,

$$x_{n\ell} = 1_{\{\text{Channel } \ell \text{ is allocated to receiver } n, \text{ denoted as } \ell \rightarrow n\}}. \tag{7.10}$$

For a given channel $\ell \in [1, N]$, the coefficient of adjacent channel interference from channel $i \in [1, N]$ for the receiver $n \in [1, N]$ is denoted by $a_{i\ell}^n$. In this case, since the received power on each channel is the same, the number of interferers encountered by any receiver is only dependent

on the channel $\ell$. The adjacent channel interference faced by receiver $n$ is then given by,

$$P_{\mathsf{ACI}_n} = P_{R_n} \sum_{\forall \ell} \sum_{\forall i \neq \ell} x_{n\ell}\, a^n_{i\ell}. \tag{7.11}$$

As evident from (7.11), each receiver faces a different interference depending on its impairments, and channel assignment. The goal of the spectrum access framework is to account for all these parameters in addition to the location of nodes, and assign channels to each receiver to optimize for an objective. We consider sum rate as the objective function and seek to allocate channels to maximize the network wide sum rate.

### 7.3.2 Objective Function

We now describe the channel assignment framework for sum rate maximization. Treating the adjacent channel interference as additive noise, the data rate of receiver $n$ and the network-wide sum rate are given by,

$$R_n = W\ \log_2\left(1 + \frac{P_{R_n} \sum_{\forall \ell} x_{n\ell} a_{\ell\ell}}{P_{R_n} \sum_{\forall \ell} \sum_{\forall i \neq \ell} x_{n\ell}\, a^n_{i\ell} + \eta}\right), \tag{7.12}$$

$$R = W \sum_{\forall n} \log_2\left(1 + \frac{P_{R_n} \sum_{\forall \ell} x_{n\ell} a_{\ell\ell}}{P_{R_n} \sum_{\forall \ell} \sum_{\forall i \neq \ell} x_{n\ell}\, a^n_{i\ell} + \eta}\right). \tag{7.13}$$

The sum rate maximization framework can now be formulated as,

$$\mathcal{J}_1 = \max_{x_{n\ell}}\ W \sum_{\forall n} \log_2\left(1 + \frac{P_{R_n} \sum_{\forall \ell} x_{n\ell} a_{\ell\ell}}{P_{R_n} \sum_{\forall \ell} \sum_{\forall i \neq \ell} x_{n\ell}\, a^n_{i\ell} + \eta}\right) \tag{7.14}$$

$$\text{s.t} \sum_{\forall \ell} x_{n\ell} = 1; \quad \sum_{\forall n} x_{n\ell} = 1. \tag{7.15}$$

This formulation is nonlinear and non-convex in the channel assignment variables and it is hard to obtain computationally efficient algorithms. Hence, we approximate this 'original' objective function to reduce the complexity and obtain a tractable form. We then use the approximated objective function and propose a computationally efficient algorithm for channel assignment. We have,

$$R = W \sum_{\forall n} \log_2 \left( P_{R_n} \sum_{\forall \ell} \sum_{\forall i \neq \ell} x_{n\ell}\, a_{i\ell}^n + \eta + P_{R_n} \sum_{\forall \ell} x_{n\ell} a_{\ell\ell} \right) - W \sum_{n=1}^{N} \log_2 \left( P_{R_n} \sum_{\forall \ell} \sum_{\forall i \neq \ell} x_{n\ell}\, a_{i\ell}^n + \eta \right). \quad (7.16)$$

Lower-bounding the sum rate in (7.16), we get,

$$R \geq W \sum_{\forall n}^{N} \log_2 \left( \eta + P_{R_n} \sum_{\forall \ell} x_{n\ell} a_{\ell\ell} \right) - W \sum_{\forall n} \log_2 \left( P_{R_n} \sum_{\forall \ell} \sum_{\forall i \neq \ell} x_{n\ell}\, a_{i\ell}^n + \eta \right). \quad (7.17)$$

Using Jenson's inequality, we have

$$\begin{aligned} \sum_{\forall n} \log_2 \left( P_{R_n} \sum_{\forall \ell} \sum_{\forall i \neq \ell} x_{n\ell}\, a_{i\ell}^n + \eta \right) &\leq \log_2 \left( \sum_{\forall n} \sum_{\forall \ell} \sum_{\forall i \neq \ell} P_{R_n} x_{n\ell}\, a_{i\ell}^n + \sum_{\forall n} \eta \right), \\ &\leq \log_2 \left( \sum_{\forall n} \sum_{\forall \ell} \sum_{\forall i \neq \ell} P_{R_n} x_{n\ell}\, a_{i\ell}^n + N\eta \right). \end{aligned} \quad (7.18)$$

Using (7.18) in (7.17) we have,

$$R \geq W \sum_{\forall n} \log_2 \left( \eta + P_{R_n} \sum_{\forall \ell} x_{n\ell} a_{\ell\ell} \right) - W \log_2 \left( \sum_{\forall n} \sum_{\forall \ell} \sum_{\forall i \neq \ell} P_{R_n} x_{n\ell}\, a_{i\ell}^n + N\eta \right). \quad (7.19)$$

The original objective function was formulated to maximize the sum rate, $R$. Based on the bounds for $R$ from (7.19), it is clear that $W \log_2 \left( \sum_{\forall n} \sum_{\forall \ell} \sum_{\forall i \neq \ell} P_{R_n} x_{n\ell}\, a_{i\ell}^n + N\eta \right)$ needs to be minimized to maximize $R$, since the first term on R.H.S of (7.19) is a constant. Since $\log_2(\bullet)$ is a monotonically increasing concave function, minimizing the sum adjacent channel interference, $P_{\mathsf{ACI}} = \sum_{\forall n} \sum_{\forall \ell} \sum_{\forall i \neq \ell} P_{R_n} x_{n\ell}\, a_{i\ell}^n$ will minimize the entire function, since $N\eta$ is a constant.

### 7.3.3 Problem Formulation

Let $P_{\mathsf{ACI}_{n\ell}}$ denote the adjacent channel interference faced by receiver $n \in [1, N]$ when placed in channel $\ell \in [1, N]$. We now define a matrix $\mathbf{K}$ whose $\ell^{\text{th}}$ row represents the adjacent channel interference faced by each of the $N$ receivers when placed in the $\ell^{\text{th}}$ channel, as shown in (7.20).

$$\begin{array}{l} \\ 1^{\text{st}}\text{channel} \rightarrow \\ 2^{\text{nd}}\text{channel} \rightarrow \\ \\ N^{\text{th}}\text{channel} \rightarrow \end{array} \begin{array}{c} \begin{array}{cccc} 1^{\text{st}}\text{Rx.} & 2^{\text{nd}}\text{Rx.} & & N^{\text{th}}\text{Rx.} \end{array} \\ \begin{pmatrix} P_{R_1}\sum_{\forall i\neq 1} a_{i1}^1 & P_{R_2}\sum_{\forall i\neq 1} a_{i1}^2 & \dots & P_{R_N}\sum_{\forall i\neq 1} a_{i1}^N \\ P_{R_1}\sum_{\forall i\neq 2} a_{i2}^1 & P_{R_2}\sum_{\forall i\neq 2} a_{i2}^2 & \dots & P_{R_N}\sum_{\forall i\neq 2} a_{i2}^N \\ \vdots & \vdots & & \vdots \\ P_{R_1}\sum_{\forall i\neq N} a_{iN}^1 & P_{R_2}\sum_{\forall i\neq N} a_{iN}^N & \dots & P_{R_N}\sum_{\forall i\neq N} a_{iN}^N \end{pmatrix} \end{array} = \mathbf{K}_{N\times N} \quad (7.20)$$

We denote the channel assignment binary-integer permutation matrix $\mathbf{X}$, with rows representing receivers and columns representing channels, such that $\sum_{\forall n} \mathbf{X}_{n,\ell} = 1$; $\sum_{\forall \ell} \mathbf{X}_{n,\ell} = 1$. These conditions impose that there exist only one non-zero element in each row and in each column of the assignment matrix $\mathbf{X}$. This ensures that each receiver is assigned a unique channel and vice versa.

The number of interfering signals for any receiver depends on the channel assigned. Thus the adjacent channel interference for the $n^{\text{th}}$ receiver is given by the $n^{\text{th}}$ element of $\text{diag}(\mathbf{XK})$. The total adjacent channel interference is given by,

$$P_{\mathsf{ACI}} = \text{tr}(\mathbf{XK}) \quad (7.21)$$

where $\text{tr}(\bullet)$ represents the trace of the matrix. Our goal now is to minimize the network wide adjacent channel interference given by (7.21). Thus, the modified optimization problem can be formulated as,

$$\mathcal{J}_2 = \min_{\mathbf{X}} \ \text{tr}(\mathbf{XK}) \quad (7.22)$$

$$\text{s.t.} \quad \sum_{\forall n} \mathbf{X}_{n,\ell} = 1 \, ; \sum_{\forall \ell} \mathbf{X}_{n,\ell} = 1. \quad (7.23)$$

We have now converted a complex non-convex problem to a binary-integer assignment problem. The computational complexity of exhaustive search for this optimization problem is $\mathcal{O}(N!)$, which is exponential. Thus, we identify two computationally efficient algorithms to solve this problem.

### 7.3.4 Algorithms for Channel Assignment

#### Munkres Algorithm

We need to pick $N$ elements of matrix $\mathbf{K}$ whose sum is the least, with the constraint that each of those elements is from a unique row and column. This binary-integer assignment problem has an optimal solution in the Hungarian algorithm [103, 104] and solves in $\mathcal{O}(N^3)$ using the Munkres method [105]. Let $\mathbf{k}_\ell^{\mathsf{r}}$ represent the $\ell^{\text{th}}$ row vector and $\mathbf{k}_n^{\mathsf{c}}$ represent the $n^{\text{th}}$ column vector of the matrix $\mathbf{K}$. This algorithm finds the optimal assignment through iterative row and column operations of the cost matrix, by identifying the least interference that a given receiver *has* to suffer in each pass. Munkres algorithm adapted for this problem is presented in Algorithm 5, and details of original algorithm can be found in [105].

**Algorithm 5** Munkres Algorithm for Receiver Impairments Aware Channel Assignment

1: FORMULATE: $\mathbf{K}$. Assign $\mathbf{K}' = \mathbf{K}$. $\mathbf{X} = \mathbf{0}_{N\times N}$.
2: ROW REDUCTION: $\forall \ell, n \in [1, N], [\mathbf{K}']_{\ell,n} = [\mathbf{K}]_{\ell,n} - \arg\min_n \mathbf{k}_\ell^{\mathsf{r}}$
3: COLUMN REDUCTION: $\forall \ell, n \in [1, N], [\mathbf{K}']_{\ell,n} = [\mathbf{K}]_{\ell,n} - \arg\min_\ell \mathbf{k}_n^{\mathsf{c}}$
4: Find a minimal set $\mathcal{S}$ of lines, to cover all zeros in $\mathbf{K}'$.
5: **if** $\mid \mathcal{S} \mid = N$ **then**
6: Identify the set of independent zeros in $\mathbf{K}'$,
7: Formulate a set $\mathcal{A} = (\ell, n)$ representing the corresponding rows-column pair
8: Optimal Assignment Found: $[\mathbf{X}]_{n,\ell} = 1, \forall (\ell, n) \in \mathcal{A}$
9: **else**
10: Find $k = \arg\min_{\ell,n} \mathbf{K}'$ such that $k$ is not covered by any line in $\mathcal{S}$
11: Formulate $\mathbf{K}''_{\ell,n} = \mathbf{K}_{\ell,n} - k, \forall (\ell, n)$ not covered by any line in $\mathcal{S}$
12: $\mathbf{K}''_{\ell,n} = \mathbf{K}_{\ell,n} + k, \forall (\ell, n)$ covered by 2 lines in $\mathcal{S}$
13: $\mathbf{K}''_{\ell,n} = \mathbf{K}_{\ell,n}$, for all other elements
14: Go to STEP 2
15: **end if**

#### Greedy Algorithm

In this algorithm, we iteratively find an assignment matrix $\mathbf{X}$ such that $\mathrm{tr}(\mathbf{XK})$ is minimized. The greedy algorithm is developed as a solution to the minimization problem, as described in Algorithm 6. The intuition for this algorithm is that in each iteration, it picks the least element of the matrix $\mathbf{K}$ and assigns that receiver (column index, $n^*$) to the corresponding channel (row index, $\ell^*$). All elements of this row and column are permanently excluded in the future iterations. This

process is repeated until all receivers are assigned a channel. Note that the rows and columns of channel assignment matrix $\mathbf{X}$ represents the receivers and channels; and vice versa for the adjacent channel interference matrix, $\mathbf{K}$. Thus, it warrants a flip of indices in the algorithm.

**Algorithm 6** Greedy Algorithm for Receiver Impairments Aware Channel Assignment

1: FORMULATE: $\mathbf{K}$.
2: INITIALIZE: $\mathbf{X} = \mathbf{0}_{N\times N}$.
   Define Sets $\mathscr{C}_\ell = \{1, 2, \ldots, N\}$; $\mathscr{C}_n = \{1, 2, \ldots, N\}$
3: **for** $1, 2, \ldots, N$ **do**
4: $\quad (\ell^*, n^*) = \arg\min_{(\ell,n)} [\mathbf{K}]; \;\; \forall \ell \in \mathscr{C}_\ell \; \forall n \in \mathscr{C}_n$
5: $\quad [\mathbf{A}]_{n^*,\ell^*} = 1$
6: $\quad \mathscr{C}_\ell = \mathscr{C}_\ell \setminus \{\ell^*\}; \mathscr{C}_n = \mathscr{C}_n \setminus \{n^*\}$
7: **end for**

**Remark:** The $q^{\text{th}}$ iteration of the algorithm (lines 3 to 7) involves finding the minimum among $(N - q + 1)^2$ elements. Note that there is a dimensionality reduction of the search space for finding the minimum element in $\mathbf{K}$ in each iteration of the algorithm. The average computations for serial sorting is $O\left((N - q + 1)^2\right)$ for the $q^{\text{th}}$ iteration. Thus for $N$ iterations, the computational complexity of the algorithm is $O\left(N^3\right)$, which is efficient compared to the exponential complexity of the original problem.

## 7.4 Generalization for Multiple Transmitter-Receiver Pairs

We consider a network of $N$ transmitters and $N$ receivers ($N$ Tx-Rx pairs) communicating over $N$ distinct adjacent channels as shown in Fig. 7.6. The network consists of multi-RAT operations with diverse receiver front-ends. Assume that the transmitters and receivers are distributed in a geographical area and the network topology is known to a centralized spectrum manager. Also assume that all the transmitters use omni-directional antennas. Each channel has the center frequency $f_\ell$, $\ell \in [1, N]$, and bandwidth $W$. We now consider the channel allocation for the $N$ links with an objective to maximize the sum rate of the network.

### 7.4.1 Adjacent Channel Interference Formulation

We formulate the adjacent channel interference faced by each receiver $n \in [1, N]$, which receives $N$ signals (one of which is desired), but the power of each of those signals is a function of the

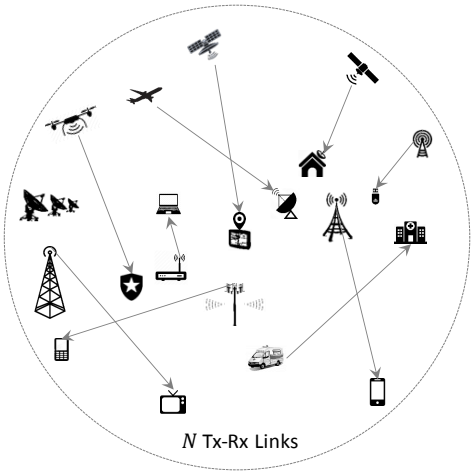


Figure 7.6: Illustration of heterogeneous nodes with diverse RF front-ends sharing spectrum in the wireless network

distance of all the transmitters from the given receiver $n$. As before, the indicator function for channel allocation is defined as, $x_{n\ell} = 1_{\{\text{Channel } \ell \text{ is allocated to receiver } n, \text{ denoted as } \ell \to n\}}$.

Let $d_{nj}$ denote the distance between receiver $n \in [1, N]$ and transmitter $j \in [1, N]$. The received power at receiver $n$ from transmitter $j$ is then given by $P_{R_{nj}} = P_{T_j} d_{nj}^{-\mu}$ where $P_{T_j}$ is the transmit power of transmitter $j$ and $\mu$ is the propagation loss exponent. The adjacent channel interference faced by receiver $n$ is then given by,

$$P_{\mathsf{ACI}_n} = \sum_{\forall \ell} \sum_{\forall i \neq \ell} \sum_{\forall j \neq n} x_{n\ell} x_{ji} a_{i\ell}^{n} P_{T_j} d_{nj}^{-\mu} \tag{7.24}$$

We now define the diagonal distance matrix for receiver $n$ in relation to all the transmitters in the network as,

$$\mathbf{D}_n = \begin{bmatrix} d_{n1}^{-\mu/2} & 0 & \cdots & 0 \\ 0 & d_{n2}^{-\mu/2} & \cdots & 0 \\ \vdots & & \ddots & \vdots \\ 0 & \cdots & 0 & d_{nj}^{-\mu/2} \end{bmatrix}. \tag{7.25}$$

Evaluating adjacent channel interference in this generalized case depends on the channel assignment, which dictates the received power on different channels of the given receiver. From equation (7.8), we have $P_{\mathsf{ACI}_n} = \mathbf{A}_n \boldsymbol{P}_{R_n}$, where $\mathbf{A}_n$ is the front-end matrix for receiver $n$ and $\boldsymbol{P}_{R_n}$ is the received power vector at receiver $n$. However, evaluating adjacent channel power cannot be agnostic to channel allocations. In addition, mapping the channels post-digitization into the

$Q_n \leq N$ channels of the first Nyquist zone for the receiver $n$, makes it further complicated. Let channel $\ell \in [1, N]$ be mapped to the channel $q_n(\ell) \in [1, Q_n]$ of the first Nyquist zone for the receiver $n$, where $Q_n$ number of channels in the first Nyquist zone for the receiver $n$. The mapping between the two is given by,

$$q_n(\ell) = \begin{cases} \ell \mod \left(\frac{N+Q_n}{2}\right) & \text{if } \ell > \frac{N+Q_n}{2}, \\ \ell \mod \left(\frac{N-Q_n}{2}+1\right) & \text{if } \ell < \frac{N+Q_n}{2} \end{cases} \tag{7.26}$$

Thus, if $\boldsymbol{P}$ is the $N \times 1$ transmit power vector, we can compute the adjacent channel interference for receiver $n$ as,

$$P_{\mathsf{ACI}_n} = \sum_{\forall \ell} x_{n\ell}\, \mathbf{e}_{q_n(\ell)} \mathbf{A}_n \mathbf{X}\, \mathbf{D}_n \boldsymbol{P}_T \tag{7.27}$$

where $\mathbf{e}_{q_n(\ell)}$ is the unit basis vector in the $\mathbb{R}^{Q_n}$ space, and $\boldsymbol{P}_T$ is the $N \times 1$ transmit power vector.

### 7.4.2 Framework for Channel Assignment

For ease of representation, we denote the binary set of channel assignment indicator variables by $\mathcal{X} = \{x_{n\ell};\ \forall n, \ell \in [1, N]\}$, and $\mid \mathcal{X} \mid = N^2$. The adjacent channel interference power for receiver $n$, $P_{\mathsf{ACI}_n}(\mathcal{X})$ is given by equation (7.27). If $\eta$ is AWGN, the rate for receiver $n$ and network-wide sum rate is given by,

$$R_n = W \log_2 \left(1 + \frac{P_{T_n} d_{nn}^{-\mu}}{P_{\mathsf{ACI}_n}(\mathcal{X}) + \eta}\right), \tag{7.28}$$

$$R = W \sum_{n=1}^{N} \log_2 \left(1 + \frac{P_{T_n} d_{nn}^{-\mu}}{P_{\mathsf{ACI}_n}(\mathcal{X}) + \eta}\right). \tag{7.29}$$

The network sum-rate maximization problem can now be formulated as,

$$\mathcal{J}_3 = \max_{\mathcal{X}} \sum_{n=1}^{N} \log_2 \left(1 + \frac{P_{T_n} d_{nn}^{-\mu}}{P_{\mathsf{ACI}_n}(\mathcal{X}) + \eta}\right) \tag{7.30}$$

$$\text{s.t} \sum_{\ell=1}^{N} x_{n\ell} = 1; \sum_{n=1}^{N} x_{n\ell} = 1. \tag{7.31}$$

This is non-convex, nonlinear, mixed binary integer combinatorial optimization problem. This problem is akin to the traveling salesman problem, but with a major difference that the weight of

an edge of a graph is dependent on the entire path taken, and is unknown a priori. This poses a different set of constraints and makes it a challenging problem. We can lower bound the objective function and use similar arguments as presented in Section 7.3.2 to transform the sum-rate maximization problem into sum interference minimization, $\min \sum_{n=1}^{N} P_{\mathsf{ACI_n}}$. However, this will not give any advantage unlike with the case with co-located transmitters to design fast algorithms owing to the complexity of the underlying phenomena. Research on possible ways to develop optimal algorithms for this problem is beyond the scope of this chapter. Thus, we develop a fast heuristic algorithm for this optimization problem and analyze the results.

### 7.4.3 Heuristic Algorithm: Simulated Annealing

In this section, we employ a heuristic technique and develop a fast algorithm based on Simulated Annealing (SA). We demonstrate that there exists meta-heuristic approaches to solve the proposed framework and obtain an approximation of the global optimum.

SA is a meta-heuristic probabilistic technique to approximate the global optimum solution of a given objective. It is especially useful for problems with exceedingly complex objectives where the search space scales exponentially. SA was first proposed by [92], and [93] gives a comprehensive review. It has been previously applied to channel allocation in [94–96].

The channel assignment problem at hand is essentially a combinatorial optimization problem of finding the best permutation out of the $N!$ possible assignments. We define the state $\mathcal{S} = \{s_1\ s_2\ \cdots\ s_N\}$ to represent the channels allocated to users $\{1, 2, \cdots, N\}$ respectively. Clearly, $s_i \in [1, N]$ are unique. The idea behind SA is to start with a random state and check the value of the objective function at a neighboring state. If the neighboring objective is greater, update to the neighboring state; otherwise, update with a certain probability. Updating to the neighboring state with a certain probability even when it yields a lower objective is to ensure that the solution does not get stuck in a local minimum. However, with increasing iterations, the probability of updating to the neighboring state yielding lower objective is decreased, thus ensuring convergence. This process of gradual decrease in the probability, which leads to convergence was inspired by the controlled cooling of materials to reduce lattice defects in metallurgy and hence the name SA.

The SA based channel assignment is described in Algorithm 7. The initialization includes formulating several network topology matrices, initializing a random channel assignment state $\mathcal{S}$,

**Algorithm 7** SA based Receiver Nonlinearity Aware Channel Assignment

INITIALIZATIONS

FORMULATE: Network topology matrices $\mathbf{P}_T,\ \mathbf{D}_n$

INITIAL STATE: Random Assignment, $\mathcal{S} = \{s_1\ s_2\ \cdots\ s_N\}$

FORMULATE: Channel Assignment Permutation Matrix, $\mathbf{X}(\mathcal{S})$

COMPUTE: $P_{\mathsf{ACI}_n}(\mathcal{X}) = \sum_{\forall \ell} x_{n\ell}\ \mathbf{e}_{q_n(\ell)} \mathbf{A}_n \mathbf{X}(\mathcal{S})\ \mathbf{D}_n \boldsymbol{P}_T,\ \forall n \in [1, N]$

EVALUATE: $R = W \sum_{n=1}^{N} \log_2 \left(1 + \frac{P_{T_n} d_{nn}^{-\mu}}{P_{\mathsf{ACI}_n}(\mathcal{X}) + \eta}\right)$

INITIALIZE: Initial Temperature, $T$
Cutoff Temperature, $T_{\mathsf{min}}$
Update Constant, $\lambda \in (0, 1)$

ITERATIONS

**while** $T > T_{\mathsf{min}}$ **do**
  Generate two random integers $i \in [1, N], j \in [1, N] : i \neq j$
  Update to neighboring state by swapping the channel assignment of receivers $i, j$ in $\mathcal{S}$:
    $\mathcal{S}_{\mathsf{new}} = \mathcal{S}\left(\mathtt{swap}(s_i, s_j)\right)$
  Formulate new Channel Assignment Permutation Matrix, $\mathbf{X}(\mathcal{S}_{\mathsf{new}})$
  Compute new $P_{\mathsf{ACI}_n}(\mathcal{X}) = \sum_{\forall \ell} x_{n\ell}\ \mathbf{e}_{q_n(\ell)} \mathbf{A}_n \mathbf{X}(\mathcal{S}_{\mathsf{new}})\ \mathbf{D}_n \boldsymbol{P}_T,\ \forall n \in [1, N]$
  Evaluate $R_{\mathsf{new}} = W \sum_{n=1}^{N} \log_2 \left(1 + \frac{P_{T_n} d_{nn}^{-\mu}}{P_{\mathsf{ACI}_n}(\mathcal{X}) + \eta}\right)$
  Compute $\delta_e = R_{\mathsf{new}} - R$; and $p_{\delta_e} = \exp\left(\frac{\delta_e}{T}\right)$
  **if** $\delta_e < 0$ **then**
    $R = R_{\mathsf{new}}$; and $\mathcal{S} = \mathcal{S}_{\mathsf{new}}$
  **else**
    Generate a random number $\zeta \sim \text{Unif}(0, 1)$
    **if** $\zeta \leq p_{\delta_e}$ **then**
      $R = R_{\mathsf{new}}$; and $\mathcal{S} = \mathcal{S}_{\mathsf{new}}$
    **end if**
  **end if**
  Update $T = \lambda T$
**end while**

formulating the channel assignment permutation matrix $\mathbf{X}$, computing adjacent channel interference power $P_{\mathsf{ACI}}$ and the sum rate. Further, the initial temperature $T$, cutoff temperature $T_{\mathsf{min}}$ and the update constant are set. Through the iterations, two unique random integers in the range $[1, N]$ are chosen to update to a neighboring state. The channel assignment of those two receivers are swapped, thus creating a new assignment state. The network sum rate of this new assignment and the difference $\delta_e$ between the current and new network sum rate are computed. If the new rate is higher ($\delta_e > 0$), then the new assignment is retained. If the new rate is lower, the new assignment is retained with a probability of $p_{\delta_e} = \exp\left(\frac{\delta_e}{T}\right)$. This is implemented by generating a uniform random number between $0$ and $1$ and comparing it with $p_{\delta_e}$.

## 7.5 Simulation Results

In this section, we demonstrate the benefits of receiver impairments aware channel allocation with network simulation results. For this, we define a measure to capture the diversity of the receivers in the network. As previously discussed, the impairments considered in this chapter are imperfect image frequency rejection, phase noise, and imperfect anti-aliasing filter. For a given receiver, these values are chosen independently at random from a uniform distribution. In order to compute the extent of receiver diversity in a given network, the standard deviation of the joint distribution of these parameters is computed. Given the independence in the variance of these parameters, the logarithm of the standard distribution renders numerically convenience.

**Definition 3.** *The receiver diversity measure of a network is defined as the logarithm of the standard deviation of the joint distribution of the receiver impairment parameters. Thus,*

$$\mathsf{Diversity\ Measure} : \log \sigma = \frac{1}{2} \ln \left( \mathbb{E}[\beta^2]\mathbb{E}[\nu^2]\mathbb{E}[G^2] - (\mathbb{E}[\beta])^2 (\mathbb{E}[\nu])^2 (\mathbb{E}[G])^2 \right) \tag{7.32}$$

*where $\mathbb{E}(\cdot)$ denotes expectation.*

### 7.5.1 Single Transmitter, Multiple Receivers

In this section, we present the simulation of the case with single (or co-located) transmitter gateway downlink with multiple receivers described in Section 7.3. The simulations are performed assuming the receivers to be uniformly distributed inside a circle of radius $50$ m with

the transmitter located at the centre of the circle. The resulting node distribution will be a Poisson Point Process in the two-dimensional plane [97–101]. The transmit power is equal for all channels and is set to $30$ dBm. A total bandwidth of $B = 20$ MHz is considered.

**Increasing Receiver Impairment Diversity**

Monte-Carlo simulations are carried out and the results are averaged over $10,000$ network realizations and network sum rate is plotted as a function of the Diversity Measure, $\log \sigma$ as shown in Fig. 7.7. The impairment parameters, $\beta$, $\nu$, and $G$ for a given receiver are each chosen independently in the range of a fixed minimum of $-40$ dB while the maximum is varied from $-30$ dB to $0$ dB, for varying diversity. We compare three cases, (a) without accounting for receiver impairments (baseline), (b) proposed greedy algorithm, and (c) optimal Munkres algorithm. As seen in the figure, as diversity of receivers in the network increases, the gains obtained due to receiver impairments aware allocation significantly increases. This is expected because, with increasing diversity, receiver impairment awareness can enable allocations to cater to vulnerabilities of poor receivers. Also, with increasing diversity the overall network throughput reduces as, poor receivers limit the overall network performance irrespective of the allocations. The Munkres algorithm, which is optimal, performs better than the greedy algorithm. However, the greedy algorithm is much simpler to implement in terms of memory requirements.

**Increasing Node Density**

Scalability of networks is of prime importance for next generation multi-RAT systems. Increasing the number of connected devices per unit area is a key requirement of 5G systems. In this section we analyze the impact of receiver impairment aware spectrum access on network scalability. The density of nodes is varied from $0.01$ nodes per m$^2$ ($\sim$ 20 node) to $0.05$ nodes per m$^2$ ($\sim$ 400 nodes). Each node is allocated a channel spanning $W = \frac{B}{N}$ Hz, where $N$ is the number of nodes in the network. Simulations with the proposed framework with Munkres and the greedy algorithms are carried out for channel assignment for $10,000$ network realizations and the results are presented. The receiver impairment parameters $\beta$, $\nu$, and $G$ are each chosen independently in the range between $-40$ dB and $0$ dB. The simulation results are shown in Fig. 7.8. As the node density increases, access agnostic to receiver impairments has a greater possibility of higher adjacent channel interference, compared to access accounting for receiver impairments. From the figure, we observe that it is possible to maintain the overall network efficiency even with

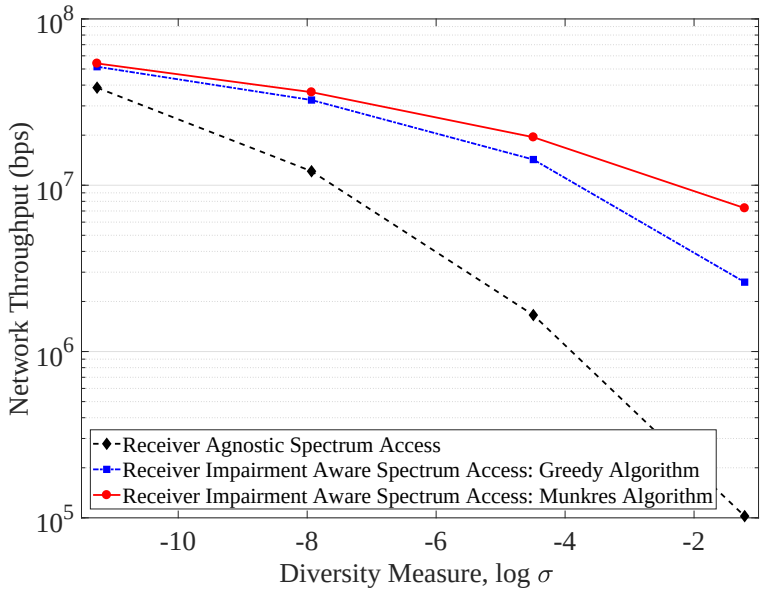


Figure 7.7: Comparison of network throughput with varying diversity of receiver impairments: Significant spectrum efficiency gains with receiver impairment aware spectrum access.

increasing node density with receiver impairment awareness, thereby providing higher spectrum efficiency gains with increasing node density.

### 7.5.2 Multiple Transmit-Receive Pairs

In this section, we present the network simulation results of multiple transmit-receive pairs, as discussed in Section 7.4. The SA algorithm is used to solve the complex optimization framework for this generalized case. The simulations are performed assuming the transmitters and receivers are uniformly distributed inside a circle of radius $500$ m. The transmit power for a given transmitter is randomly chosen between $0$ dBm and $100$ dBm. The overall network bandwidth considered was $B = 20$ MHz.

#### Convergence of SA algorithm

We analyze the convergence of the proposed SA for a small network and compare its performance with the optimal solution. We choose networks with a relatively small number of nodes ($N = 8$ and $N = 10$) as it is possible to obtain the optimal solutions in such cases through exhaustive surface search. We carry out Monte-Carlo simulations for $10,000$ realizations of networks for both

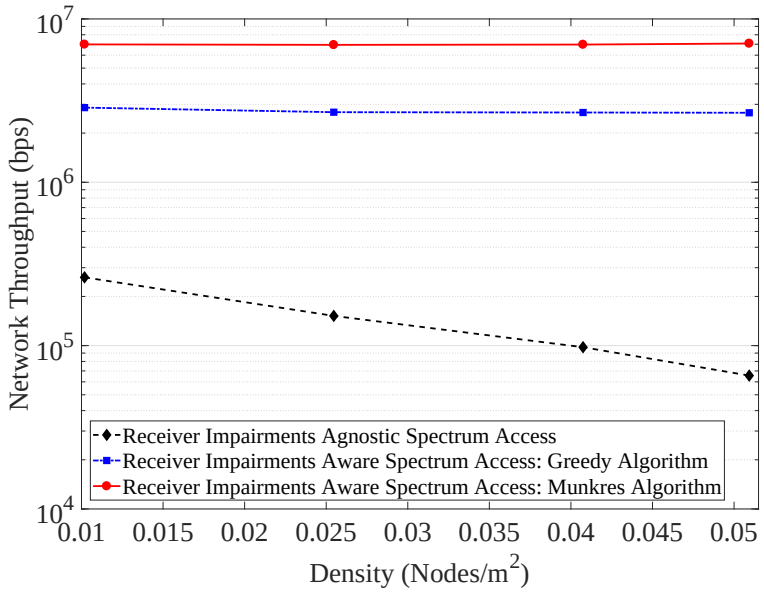


Figure 7.8: Comparison of network throughput with increasing node density of receiver impairments: Significant spectrum efficiency gains with receiver impairment aware spectrum access.

$N = 8$ and $N = 10$. With each case, the convergence of the algorithm in terms of number of iterations and its performance relative to the optimal was noted. Each node had a channel spanning $W = \frac{B}{N}$ Hz.

For the case with $N = 8$, SA took a maximum of $153$ iterations with a mean of $92$ iterations to converge. While SA converged to the optimal solution for many realizations, the average performance after $150$ iterations was found to be $97.03\%$ of the optimal value and the worst performance was $87.84\%$ of the optimal value.

For the case with $N = 10$, SA took a maximum of $702$ iterations with a mean of $504$ iterations to converge. Again, while SA converged to the optimal solution for many realizations, the average performance after $150$ iterations was found to be $98.32\%$ of the optimal value, and the worst performance was $88.41\%$ of the optimal value. A sample convergence plot of SA for a random network realization is shown in Fig. 7.9.

### Varying Receiver Impairment Diversity

We present the results of Monte-Carlo network simulations over $10,000$ realizations with uniformly random distribution of the network for different diversity measures, $\log \sigma$ of the

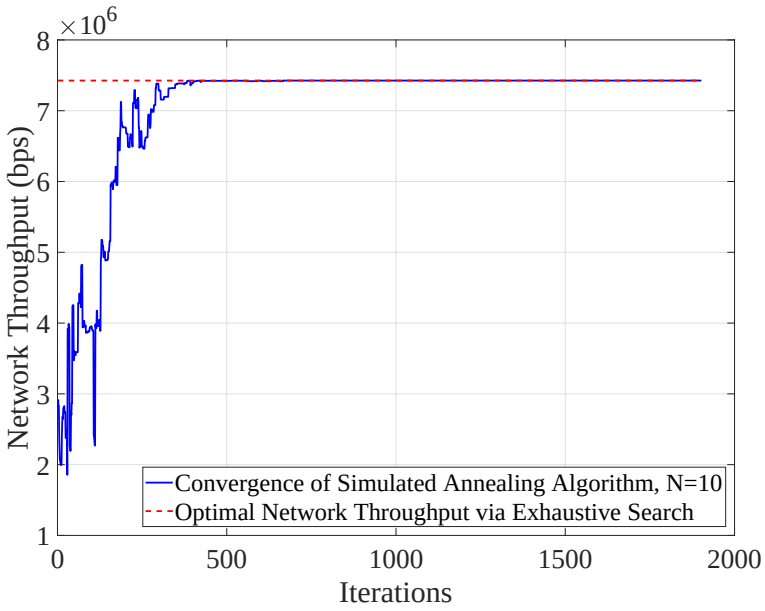


Figure 7.9: Convergence of the SA Algorithm for a network with $N = 10$ nodes for a random network realization.

receivers in the network. The number of nodes considered was $N = 40$ with each node having a channel of $W = \frac{B}{N}$ Hz. As before, the impairment parameters, $\beta$, $\nu$, and $G$ for a given receiver are each chosen independently in the range of a fixed minimum of $-40$ dB while the maximum is varied from $-30$ dB to $0$ dB, for varying diversity. We compare the SA algorithm with receiver agnostic allocation in Fig. 7.11. On the x-axis, the diversity measure is varied, and the left y-axis represents the average network throughput for different diversity measures of receiver impairments. As the receiver diversity increases, the network efficiency gains increase with receiver impairments aware spectrum access. The percentage gains relative to the receiver agnostic spectrum access is presented on the right y-axis of the figure, which shows a multi-fold increase in the gains with increasing receiver diversity in the network.

### Increasing Node Density

We present the performance of receiver-impairment aware spectrum access with the SA algorithm against receiver agnostic access as a function of increasing node density of the network. The density of nodes is varied from $0.01$ nodes per m$^2$ to $0.05$ nodes per m$^2$. Each node is allocated a channel, spanning $W = \frac{B}{N}$ Hz, where $N$ is the number of nodes in the network for a given density. Simulations with the proposed SA based assignment algorithm are carried out for $10,000$ network realizations for each node density and the results are presented. The receiver impairment

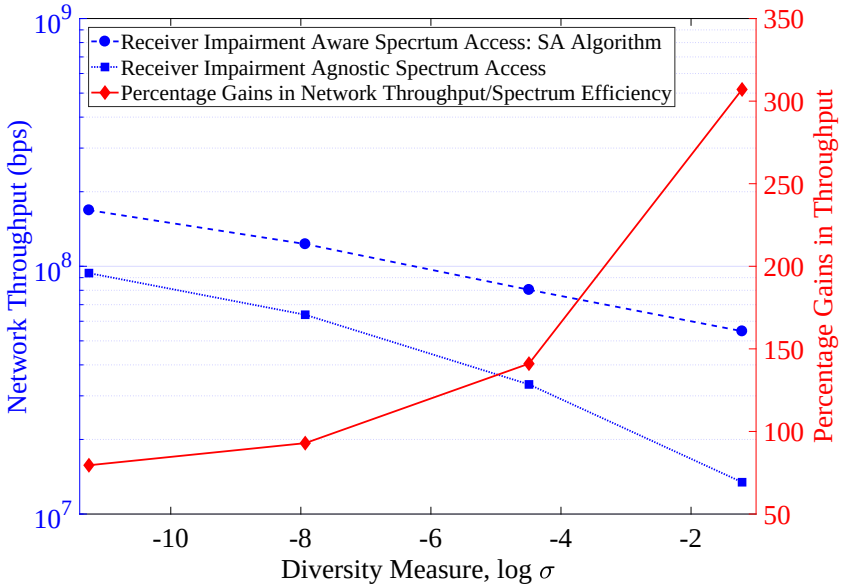


Figure 7.10: Comparison of network throughput with varying diversity of receiver impairments: Significant spectrum efficiency gains with receiver impairment aware spectrum access.

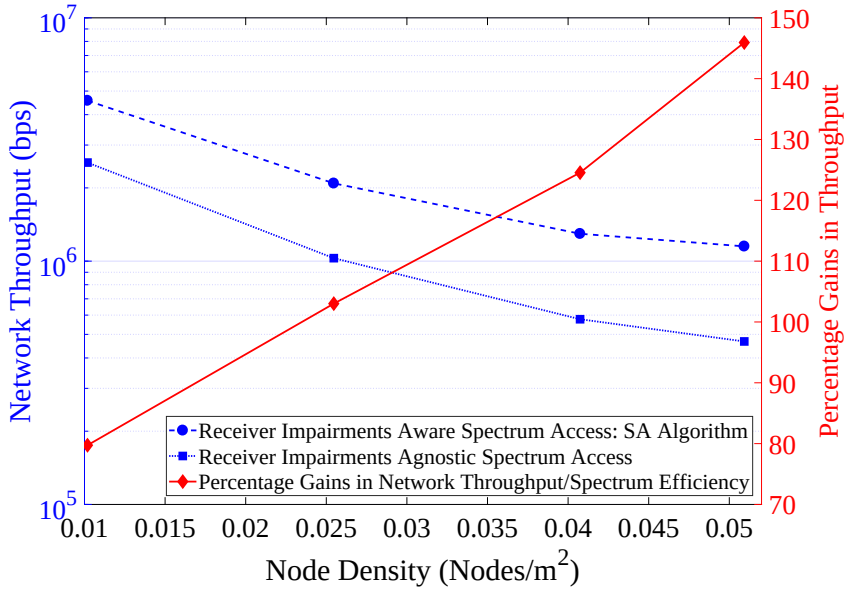


Figure 7.11: Comparison of network throughput with increasing node density of receiver impairments: Significant spectrum efficiency gains with receiver impairment aware spectrum access.

parameters $\beta$, $\nu$, and $G$ are each chosen independently in the range of $-40$ dB and $0$ dB. The simulation results are shown in Fig. 7.8. Comparison of Network Throughput with and without receiver impairment aware access is presented on the left Y-axis scale. The percentage gains in throughput relative to the receiver agnostic access is presented on the right Y-axis scale. As seen from the figure, even with most generalized networks with varying transmit powers and distances, receiver impairments aware spectrum access provides significant network efficiency gains with increasing node density.

## 7.6 Conclusions

In this chapter, we demonstrated the impact of receiver impairments aware spectrum access on spectrum efficiency gains and co-existence for next generation multi-RAT networks. For networks with single or co-located transmitter serving multiple receivers spread over a geographical area (e.g. IoT Gateway, UAV platform, etc.), the proposed framework with optimal algorithms yielded over an order of magnitude improvement in spectrum efficiency and network throughput. For generalized networks with multiple transmit-receivers pairs spread over a geographical area, the spectrum efficiency improved by several times with receiver impairment aware access. For all networks, higher gains were seen with receiver impairment aware access with increasing receiver diversity. Furthermore, receiver impairment aware access significantly improved the network efficiency gains with increasing node density and connected devices. Thus, receiver impairments aware spectrum access is of paramount importance for network efficiency and co-existence in next generation multi-RAT wireless networks.

Future work includes development of computationally efficient, optimal or performance tractable algorithms for receiver impairment aware access of networks with multiple transmit-receivers pairs spread over a geographical area. Frameworks and algorithms for network optimization with channel bonding and aggregation for multi-RAT networks accounting for receiver impairments is another important research direction.

# Chapter 8

# Scalability of Interference Networks with Receiver Nonlinearity

## 8.1 Introduction

In the preceding chapters, we primarily treated adjacent channel interference (ACI) as additive noise and outlined several ways of dealing with it. While spectrum access accounting for receiver vulnerabilities yield spectrum efficiency gains in terms of network wide raw data rate, it does not provide intuition on the limits of network operations. The more fundamental questions regarding the scalability of such networks through network level interference avoidance remain unanswered in the literature. The next generation wireless networks in heterogeneous and dynamic spectrum environments whose operations are constrained by the nonlinear interference emanating from signals on adjacent channels are in this chapter termed *Nonlinear Adjacent Channel Interference Networks (NACIN)*. ACI has been previously dealt in [109–113]. We emphasize that all existing works on adjacent channel interference management are under the linearity assumption and are not directly applicable to handle nonlinear interference arising from RF imperfections. In this chapter, we propose to develop novel schemes for nonlinear interference avoidance and analyze the scalability of such networks.

In Chapter 3, we proposed a framework to understand the interactions of signals on adjacent channels and their impact at a given desired channel. Using this framework we propose an practical achievable scheme for nonlinear adjacent channel interference avoidance to study and assess the scalability of such networks. The proposed scheme also gives valuable insights for channel assignments and wireless network design through nonlinear interference avoidance.

Further, we propose a scheme to evaluate the upper bound on scalability of such networks. This gives a unique insight into the operations of next generation heterogeneous networks with adjacent channel co-existence.

The analysis carried out in this chapter yields a systematic methodology for the protection of incumbent operations with highly sensitive receivers. The radio-astronomy receivers, Fixed Satellite System Earth Stations, GPS receivers, and many more operations require a high receiver sensitivity to capture weak desired signals. Thus, such incumbent operations have to be protected from the interference attributed to adjacent channel interference arising from intermodulation distortions. Ensuring complete interference protection for such incumbent operations is critical for the successful deployment of secondary systems for opportunistic access even on adjacent channels in the spatio-temporal vicinity of such primary systems. We use the analysis presented in this paper to develop practical achievable schemes to ensure the complete protection of channels occupied by sensitive incumbents from any nonlinear adjacent channel interference. The outcome of this demonstrates that there exist schemes to protect primary legacy systems from secondary interference due to nonlinear adjacent channel interference, without the need of any exclusion zone. For incumbents, such an assurance will potentially pave the way for an easier transition to open up more bands for opportunistic access and increase overall spectrum utilization. Further, we develop algorithmic scheme to evaluate the upper bound on scalability for interference networks with receiver nonlinearity. Given the complex nature of interference, it is extremely challenging to develop closed form solutions, owing to the intractability of the underlying phenomena. This remains an open problem.

### 8.1.1 Main Contributions

The main contributions of this paper are:

1. Introduce the concept of Nonlinear Adjacent Channel Interference Networks (NACIN) encountered in next generation heterogeneous and dynamic spectrum access networks in Section 8.2;

2. Analyze the interactions of signals in adjacent channels causing nonlinear interference at a given desired channel and extend this to baseband modulated symbols in Section 8.3;

3. Propose practical achievable schemes (lower bound) for interference avoidance in NACINs to assess the operational scalability of such networks in Sections 8.4 and 8.5;

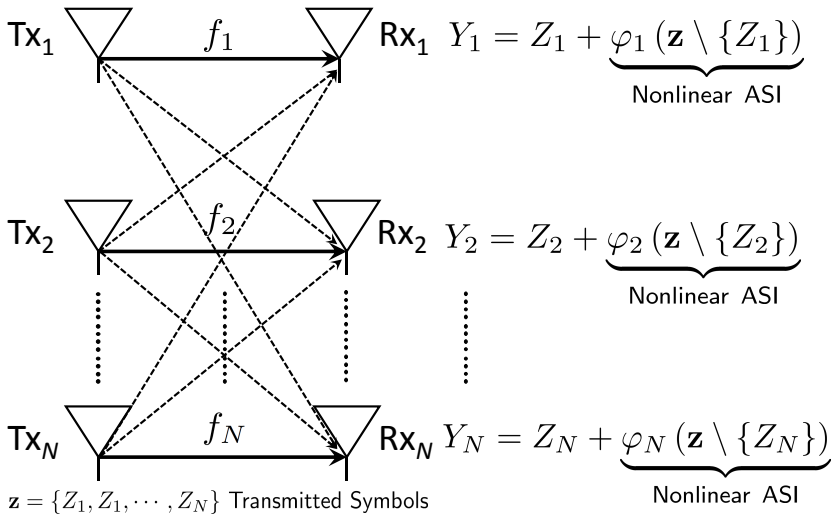


Figure 8.1: Nonlinear Adjacent Channel Interference Network (NACIN). Dashed lines represent interference

4. Propose practical achievable schemes for protection of sensitive incumbents from nonlinear interference due to intermodulation distortion arising due to secondary operations in adjacent channels in Section 8.6; and

5. Compute a theoretical upper bound on scalability of NACIN, and demonstrate that it yields a strong bound relative to the practical achievable scheme in sections 8.7 and 8.8.

## 8.2 Nonlinear Adjacent Channel Interference Network (NACIN)

Consider a network of $N$ transmitters and $N$ receivers with diverse Radio Access Technologies (RAT) communicating over $N$ equal and distinct band limited channels (or frequency bins) over a shared spectrum band. The receiver pre-selector filters span all the $N$ channels, and thus receive signals in channels adjacent to the desired signal. Due to the nonlinearity of the receiver front-ends, each receiver encounters interference due to the signals entering the RF chain in the adjacent channels. Unlike co-channel interference, this adjacent channel interference is nonlinear function of the signals, as shown in Fig. 8.1 and this network is called a *Nonlinear Adjacent Channel Interference Network (NACIN)*. Combating such nonlinear interference is challenging due to the following reasons: (1) Interfering signals are present on adjacent channels and hence

will require additional degrees of freedom in the receiver architecture, (2) The nonlinear structure of the interference increases the computational complexity, and (3) The multi-RAT is operating in a shared spectrum network of dissimilar signals and independent networks, as opposed to traditional homogeneous networks.

The fundamental network capacity of such a network is an open problem. Further, it also depends on the receiver model and characterization used in describing the nonlinear structure of the interference. As mentioned in the previous section, in this chapter, we assume the third order polynomial nonlinearity for receivers and proceed towards analyzing the limits of such a network. Since interference cancellation in such nonlinear networks is a hard problem, the practical achievable limits on network capacity is dictated by the number of interference-free symbols that can be recovered by 'avoiding' the interference.

## 8.3 Adjacent Symbol Interference

In this section, we analyze the structure of two-tone intermodulation interference emanating from adjacent frequency bins.

**Baseband Representation of Modulated Signal**

A digitally modulated signal $\tilde{Z}(t)$ at a carrier frequency $f_c$ can be represented as [114, 115],

$$\tilde{Z}(t) = A(t)\cos(2\pi f_c t + \Phi(t)), \tag{8.1}$$

where $A(t)$ represents the amplitude modulation and $\Phi(t)$ represents the phase modulation. Using certain trigonometric identities, the modulated signal can be written as,

$$\tilde{Z}(t) = U(t)\cos(2\pi f_c t) - jV(t)\sin(2\pi f_c t), \tag{8.2}$$

where $U(t)$ and $V(t)$ are the in-phase and quadrature components of the baseband signal of bandwidth $B << f_c$. The angular frequency, $\omega_c = 2\pi f_c$.

The signal $Z(t) = U(t) + jV(t)$ is called the complex envelope of $\tilde{Z}(t)$, which is a complex signal with bandwidth $B$. This representation, at a given time instant is the digital symbol transmitted, and is convenient for the analysis of digitally modulated signals.

### 8.3.1 Intermodulation Interference

Recall from Theorem 1 of Chapter 3 that, $\Psi_n$ is the set of all ordered pairs $(j,k); \forall j,k \in [1,N]; \forall j,k \neq n$ of adjacent channel frequency bins that produce intermodulation products at a given frequency bin $n \in [1,N]$, where,

$$\Psi_n = \Bigg\{ \left( n - 2\left\lfloor \frac{n-1}{2} \right\rfloor, n - \left\lfloor \frac{n-1}{2} \right\rfloor \right), \cdots, (n-2, n-1), (n+1, n+2), \cdots, \left( n + \left\lfloor \frac{N-n}{2} \right\rfloor, n + 2\left\lfloor \frac{N-n}{2} \right\rfloor \right) \Bigg\}. \quad (8.3)$$

Consider three frequencies, equally spaced and adjacent to each other in the same band, at $\omega_1, \omega_2,$ and $\omega_3$ with $\omega_1 < \omega_2 < \omega_3$. Since they are equally spaced, $\mid \omega_1 - \omega_2 \mid = \mid \omega_2 - \omega_3 \mid$, $2\omega_2 - \omega_3 = \omega_1$, and $2\omega_2 - \omega_1 = \omega_3$ hold true. Without loss of generality, we assume $\omega_1$ as the desired frequency and the other two are adjacent channel interfering signals. We examine the interference resulting due to the intermodulation products of $\omega_2$ and $\omega_3$ on the frequency $\omega_1$ using the complex IQ signal representations. We note that several works [41, 42] have deduced the interaction between signals of adjacent channels and the intermodulation product. We extend those works here to analyze the interaction of complex IQ baseband modulated symbols on adjacent channels and the resulting nonlinear interference. The two interferers are represented as,

$$\begin{aligned} \tilde{Z}_2 &= U_2 \cos(\omega_2) - jV_2 \sin(\omega_2) \\ \tilde{Z}_3 &= U_3 \cos(\omega_3) - jV_3 \sin(\omega_3) \end{aligned} \quad (8.4)$$

Note that the time index $t$ is omitted for convenience. The receiver model is given by, $Y = \alpha_1 Z + \alpha_2 Z^2 + \alpha_3 Z^3$ where $Z = Z_2 + Z_3$.

**Lemma 6.** *The received complex baseband symbol $Y_1$ at the frequency $\omega_1$ is given by,*

$$Y_1 = Z_1 + 3\alpha_3 \, Z_2^2 Z_3^*, \quad (8.5)$$

*where $Z_k = U_k + jV_k$, the complex baseband symbol (envelope) of the signal. Thus, generalizing for $N$ signals, the received symbol model is given by,*

$$Y_n = Z_n + 3\alpha_{3_n} \sum_{\forall (j,k) \in \Psi_n} Z_j^2 Z_k^*, \quad (8.6)$$

*where $\Psi_n$ is the set of all ordered pairs $(j,k); i,j \in [1,N]$ given by (8.3) of Theorem 1 and $\alpha_{3_n}$ is the third-order co-efficient of the receiver in frequency bin $n$.*

*Proof.* See Appendix 8.9. □

The term $\left(3\alpha_3 \sum_{\forall i,j \in \Psi} Z_i^2 Z_j^*\right)$ in (8.6) represents the interference emanating from the baseband complex modulated symbols of the adjacent channels and hence is termed *Adjacent Symbol Interference (ASI)*.

### 8.3.2 Cross Modulation Interference

We now briefly describe the ASI caused due to cross modulation of $Z_1$ over $Z_0$. Upon expanding the third order terms and specifically focusing on $Z_0 Z_1^2$, we find the cross modulation terms at $\omega_0$ as follows,

$$\begin{aligned} \mathsf{ASI_{CM}} &= \left(\frac{U_1^2+V_1^2}{2}\right) U_0 \cos(\omega_0) - j\left(\frac{U_1^2+V_1^2}{2}\right) V_0 \sin(\omega_0) \\ &= \left(\frac{U_1^2+V_1^2}{2}\right) (U_0 \cos(\omega_0) - jV_0 \sin(\omega_0)) \\ Z_{\mathsf{ASI_{CM}}} &= \frac{1}{2} \mid Z_1 \mid^2 Z_0. \end{aligned} \tag{8.7}$$

As evident, the cross modulation does not affect the phase of the desired signal. Instead it only modulates the desired signal in amplitude according to the variations in the interfering signal. Generalizing for $N$ signals, assuming unit gain for the receiver, we have the ASI due to cross modulation as,

$$Y_i = Z_i + \frac{3}{4}\,\alpha_3\, Z_i \sum_{k \neq i} \mid Z_k^2 \mid . \tag{8.8}$$

Since cross modulation principally is just a time-varying scaled version of the desired symbol itself, we can ignore its effects. Moreover cross modulation becomes significant only when the adjacent symbol power is orders of magnitude higher than the desired signal. In this case the receiver faces a phenomenon called 'blocking' or 'desensitization' and traditional interference cancellation algorithms will typically not work under this condition.

**Note:** For the remainder of this chapter, we focus on intermodulation distortion caused due to

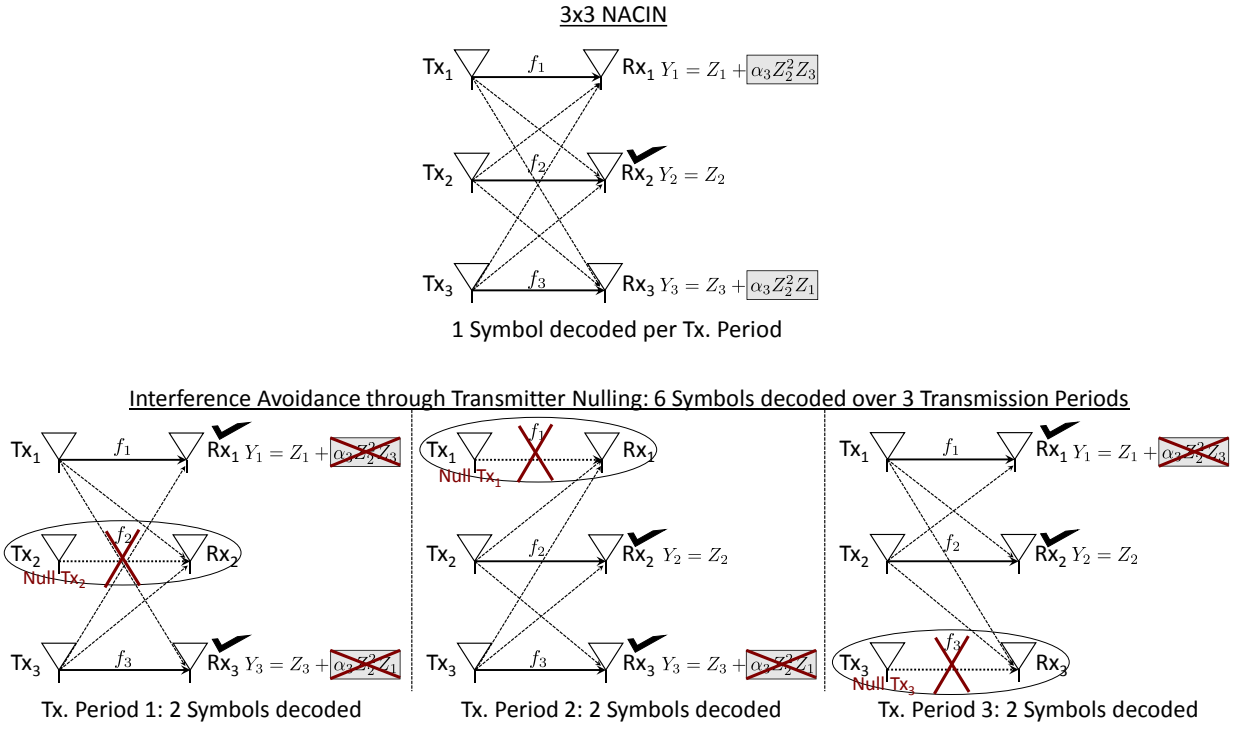


Figure 8.2: $3 \times 3$ NACIN and Interference Avoidance through Transmitter Nulling

pairwise interactions of signals on adjacent channels. Study on all other kinds of nonlinear distortions is left as a topic of future research.

## 8.4 Interference Avoidance in a $3 \times 3$ NACIN

Consider a $3 \times 3$ NACIN as shown in the left panel of Fig. 8.2. The nodes are transmitting simultaneously on three equal and band limited channels centered around $f_1$, $f_2$ and $f_3$. Due to RF front-end nonlinearity on the receivers, they encounter pairwise intermodulation interference from symbols on adjacent channels. As explained in the previous sections, the structure of this adjacent symbol interference is nonlinear, and specifically for a $3 \times 3$ network, the interfering terms for each receiver are as shown in the Left panel Fig. 8.2. Symbols $Z_2$ and $Z_3$ interact to cause interference at $\mathsf{Rx}_1$, and symbols $Z_1$ and $Z_2$ interact to cause interference at $\mathsf{Rx}_3$, the interactions between the symbols is different. Further, $\mathsf{Rx}_2$ does not face any pairwise intermodulation interference, and receives the interference-free desired symbol. Using the analysis presented in the previous section, we formalize these observations and proceed to outlay

a scheme to exploit the structure of interfering symbols for interference avoidance.

From Theorem 1 we see that for $N = 3$, the set of interfering frequency bins $\Psi_1 = \{(2,3)\};\ \Psi_2 = \phi; \Psi_3 = \{(1,2)\}$, where $\phi$ represents a null set. Accordingly, the Tx-Rx pair using the frequency bin (or channel) $n = 2$ does not face any ASI. In the ensuing discussion we assume that presence of any interfering term results in the loss of the desired symbol. As stated before, interference cancellation is a tough problem for NACINs operating in shared spectrum. While we acknowledge that in practice it depends on the power of the interference, for the purpose of evaluating network performance limits it is a valid assumption. Besides, the assumption represents the worst case scenario designing schemes for total interference protection for primary in shared spectrum. Note that we have described the channel allocation schemes that consider assignments incorporating front-end nonlinearity in the previous chapters. But they do not accurately specify limits on network scalability with nonlinear interference.

As seen from the top panel in Fig. 8.2, one symbol on $n = 2$ is successfully decoded per transmission period in a $3 \times 3$ NACIN. Consequently the three Tx-Rx pairs can be scheduled on $n = 2$ by rotation. The Degrees of Freedom, DoF for a network is defined as the maximum number of symbols successfully decoded by the network per transmit period. Thus, $\mathsf{DoF} = 1$ is achieved.

However, we exploit the structure of the third order nonlinear distortion and examine the interfering terms more closely. We see that the symbol $Z_2$ on $n = 2$ is a common interfering term for the other Tx-Rx pairs on both $n = 1$ and $n = 3$. Thus, nulling $\mathsf{Tx}_2$ will enable the successful decoding of two symbols per transmission period. An interesting phenomenon exhibited due to nonlinearity is that removing one interfering symbol avoids interference on two links. Consequently we see that nulling one transmitter per transmission period following a round-robin mechanism could be carried out and such a scheme yields two successfully decoded symbols per transmission on this $3 \times 3$ network, as shown in the bottom panel of Fig. 8.2. Thus, exploiting the interference structure, 6 symbols can be decoded in 3 transmission periods and $\mathsf{DoF} = 2$ is achievable for such a network.

## 8.5 Practical Achievable Scheme for Interference Avoidance in a $N \times N$ NACIN

In this section, we examine the $N \times N$ NACIN and develop an practical achievable scheme for interference avoidance through channel nulling.

### 8.5.1 Definitions and Notations

In this section, we introduce some definitions and notations [1]. We define an indexing function $x_n$, which denotes whether the frequency bin $n$ is active or nulled as,

$$x_n = \begin{cases} 1 & \text{if bin } n \text{ active} \\ 0 & \text{if bin } n \text{ nulled} \end{cases} \tag{8.9}$$

We denote the set of all ordered pairs causing ASI over the NACIN as the union of all $\Psi_n$ in (8.3) as,

$$\Upsilon = \bigcup_{\forall n \in [1,N]} \Psi_n \tag{8.10}$$

As long as $\Upsilon \neq \phi$ (null set), there exists ASI on at least one link in the NACIN.

We define an operation $\Xi(\bullet)$ on a set of ordered pairs, as the ordered multiset of the union of all singletons formed by the set of the ordered pairs on which it is operated upon. Essentially, if $G = \{(a_1, b_1), (a_2, b_2), \cdots, (a_N, b_N)\}$ is a set of ordered pairs, then $\Xi(G) = \{a_1, b_1, a_2, b_2, \cdots, a_N, b_N\}$.

Let $\Theta_n = \Xi(\Psi_n)$ denote the ordered set of all frequency bins (with repetition) causing ASI at bin $n$ as obtained from taking the union of all singletons formed from $\Psi_n$. Let $\lambda_k^n = \sum_{j=1}^{|\Theta_n|} \delta_{\Theta_n^j k}$, where $\Theta_n^j$ is the $j^{\text{th}}$ element of the ordered set $\Theta_n$ and $\delta_{\Theta_n^j k}$ is the Kronecker delta function, denote the number of occurrences of frequency bin $k \neq n$ in the set $\Theta_n$. Let $\mathbf{s} = [s_1, s_2, \cdots, s_N]^T$ be a $N \times 1$ vector whose $n^{\text{th}}$ row denotes the number of ASI terms contributed by the frequency bin $n$. It is obtained as, $s_n = \sum_k \lambda_k^n$ denote the number of ASI terms contributed by the $n^{\text{th}}$ active link.

[1] Note that we have reused some symbols from previous chapters for denoting different notations

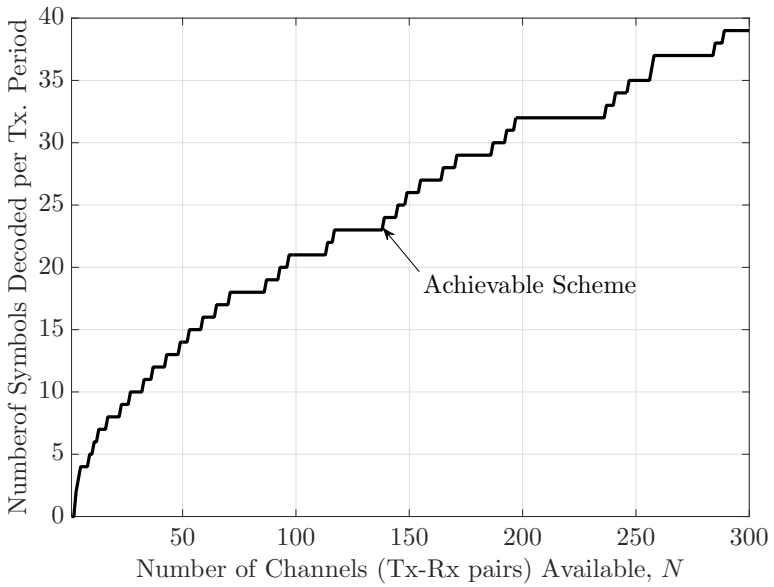


Figure 8.3: practical achievable scheme with Interference Avoidance for NACIN

### 8.5.2 Problem Formulation

Using the definitions and notations described, we now proceed toward a formal description of the problem. The objective is to maximize the number of active channels in the NACIN, while ensuring none of the Tx-Rx pairs on those active channels encounter ASI. In other words, the question asked is, what is the least number of channels that need to be nulled so that none of the active channels suffer any ASI? Thus, the problem is formulated as,

$$\mathcal{J} = \max \sum_{n=1}^{N} x_n \tag{8.11}$$

$$\text{s.t. } \Upsilon = \phi \tag{8.12}$$

This is a combinatorial problem of choosing $K \in [1, N]$ nodes to maximize a given metric, with an important added complexity where the cost of choosing a node can be ascertained only with the knowledge of all the $K$ nodes chosen. This represents a complicated version of knapsack and thus is NP hard.

**Algorithm 8** practical achievable scheme for NACIN

INITIALIZE: $\mathcal{T} = [1, N]$. Set of all active channel
INITIALIZE: $\Upsilon = \bigcup_{n \in \mathcal{T}} \Psi_n$.
INITIALIZE: $\Theta_n = \Xi(\Psi_n)\ \forall n \in \mathcal{T}$
INITIALIZE: $\lambda_k^n = \sum_{j=1}^{|\Theta_n|} \delta_{\Theta_n^j k};\ \forall k, n \in \mathcal{T}$
INITIALIZE: $\mathbf{s}$: $s_n = \sum_k \lambda_k^n, \forall k, n \in \mathcal{T}$
**do**
    $n^* = \arg\max_n[\mathbf{s}]\ \forall n \in \mathcal{T}$.
    $[\mathbf{s}]_{n^*} = 0$
    $\Psi_n = \Psi_n \setminus \{(j,k)\}$ $\begin{cases} \text{if } j = n^* \text{ or } k = n^*; \\ \forall (j,k) \in \Psi_n,\ \forall n \in \mathcal{T} \end{cases}$
    $\Upsilon = \Upsilon \setminus \Psi_{n^*}$
    $\mathcal{T} = \mathcal{T} \setminus n^*$
    $\Theta_n = \Xi(\Psi_n)\ \forall n \in \mathcal{T}$
    $\lambda_k^n = \sum_{j=1}^{|\Theta_n|} \delta_{\Theta_n^j k};\ \forall k, n \in \mathcal{T}$
    Update $\mathbf{s}$ : $s_n = \sum_k \lambda_k^n, \forall k, n \in \mathcal{T}$
**while** $\Upsilon \neq \phi$

### 8.5.3 Practical Achievable Scheme

In this section, we propose an practical achievable scheme for the formulated problem. The intuition behind this scheme is to sequentially null the channel which contributes to maximum ASI terms until the active channels are free from any ASI. The scheme is formalized in Algorithm 8.

The behavior of the practical achievable scheme versus the number of Tx-Rx pairs (channels) is as shown in Fig. 8.3. We note that this is a practical practical achievable scheme. The optimality of this scheme is discussed in Section 8.8. We also note that for this analysis we have considered interference to be binary. Practical systems can accept non-zero interference while maintaining a certain assured quality of service.

## 8.6 Protection of Incumbent with Sensitive Receivers

Next generation shared spectrum will include incumbents with highly sensitive receivers. Examples include radio-astronomy receivers, fixed satellite system earth stations, GPS receivers, etc. These receivers will not only have to be protected from co-channel interference, but also from adjacent channel interference. We use the notations and definitions introduced in the previous

section.

### 8.6.1 Problem Formulation

We present two variants of the problem. The primary objective in both is to ensure the complete protection of the incumbent with sensitive receiver. In the first variant we assume even the secondary receivers cannot accept any adjacent channel interference due to two-tone intermodulation and in the second we assume that the secondary receivers are immune to adjacent channel interference (and hence, primary user protection is the only objective).

Let there be $N$ channels and the incumbent be located at any arbitrary channel denoted by $\ell \in [1, N]$. The problem is to accommodate as many secondary operations as possible in bands adjacent to the incumbent such that it does not cause any interference to the incumbent.

**Case 1: With Secondary Protection**

In this case, in addition to the primary user, all the secondary access users also receive complete protection from adjacent symbol interference. The problem is formulated as,

$$\mathcal{J} = \max \sum_{n=1}^{N} x_n \tag{8.13}$$

$$\text{s.t. } \Psi_\ell = \phi;\ \Upsilon = \phi \tag{8.14}$$

**Case 2: No Secondary Protection**

In this case, only the primary user receives complete protection from adjacent symbol interference, and the secondary users are assumed to be able to operate with interference. The problem is formulated as,

$$\mathcal{J} = \max \sum_{n=1}^{N} x_n \tag{8.15}$$

$$\text{s.t. } \Psi_\ell = \phi \tag{8.16}$$

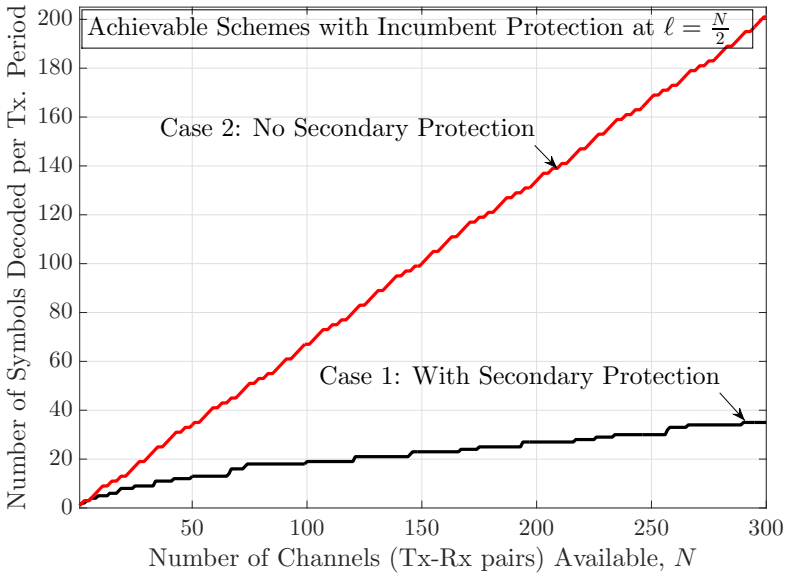


Figure 8.4: Practical achievable schemes with Incumbent Protection for NACIN

### 8.6.2 Practical Achievable Schemes for Incumbent Protection

In this section we propose two practical achievable schemes for incumbent protection for the two cases presented in the previous section. Channels which produce the maximum interference at bin $n = \ell$ are sequentially nulled until $\Psi_\ell = \phi$ and $\Upsilon = \phi$ for Case 1 as detailed in Algorithm 9. For Case 2, we are only concerned about the incumbent protection, and hence the channels are nulled only to satisfy the condition $\Psi_\ell = \phi$ as detailed in Algorithm 10.

The behavior of the practical achievable schemes is shown in Fig. 8.4. The implication of this analysis is that even extremely sensitive incumbent receivers can be protected from interference emanating from intermodulation distortion due to receiver nonlinearity. Thus, theoretically, secondary operations in channels adjacent to sensitive incumbents is possible even without geographical exclusion zones if the network is engineered to satisfy the constraints of interference protection. This instills the much needed confidence for incumbent operations with sensitive receivers to open the spectrum for sharing in next generation wireless networks, thus improving the overall spectrum utilization.

**Algorithm 9** Incumbent Protection with Secondary Protection

INITIALIZE: $\mathcal{T} = [1, N]$. Set of all active channels
INITIALIZE: $\Upsilon = \bigcup_{n \in \mathcal{T}} \Psi_n$.
INITIALIZE: $\Theta_n = \Xi(\Psi_n)\ \forall n \in \mathcal{T}$
INITIALIZE: $\lambda_k^n = \sum_{j=1}^{|\Theta_n|} \delta_{\Theta_n^j k};\ \forall k, n \in \mathcal{T}$
INITIALIZE: $\mathbf{s}$: $s_n = \sum_k \lambda_k^n, \forall k, n \in \mathcal{T}$
**do**
    **while** $\Psi_\ell \neq \phi$ **do**
    $k^* = \arg\max_k \lambda_k^\ell$
    $[\mathbf{s}]_{k^*} = 0$
    $\Psi_\ell = \Psi_\ell \setminus \{(j,k)\} \begin{cases} \text{if } j = k^* \text{ or } k = k^*; \\ \forall (j,k) \in \Psi_\ell \end{cases}$
    $\Upsilon = \Upsilon \setminus \Psi_{k^*}$
    $\mathcal{T} = \mathcal{T} \setminus k^*$
    $\Theta_n = \Xi(\Psi_n)\ \forall n \in \mathcal{T}$
    $\lambda_k^n = \sum_{j=1}^{|\Theta_n|} \delta_{\Theta_n^j k};\ \forall k, n \in \mathcal{T}$
    Update $\mathbf{s}$ : $s_n = \sum_k \lambda_k^n, \forall k, n \in \mathcal{T}$
    **end while**
    $n^* = \arg\max_n [\mathbf{s}]\ \forall n \in \mathcal{T}$.
    $[\mathbf{s}]_{n^*} = 0$
    $\Psi_n = \Psi_n \setminus \{(j,k)\} \begin{cases} \text{if } j = n^* \text{ or } k = n^*; \\ \forall (j,k) \in \Psi_n,\ \forall n \in \mathcal{T} \end{cases}$
    $\Upsilon = \Upsilon \setminus \Psi_{n^*}$
    $\mathcal{T} = \mathcal{T} \setminus n^*$
    $\Theta_n = \Xi(\Psi_n)\ \forall n \in \mathcal{T}$
    $\lambda_k^n = \sum_{j=1}^{|\Theta_n|} \delta_{\Theta_n^j k};\ \forall k, n \in \mathcal{T}$
    Update $\mathbf{s}$ : $s_n = \sum_k \lambda_k^n, \forall k, n \in \mathcal{T}$
**while** $\Upsilon \neq \phi$

**Algorithm 10** Incumbent Protection with No Secondary Protection

INITIALIZE: $\mathcal{T} = [1, N]$. Set of all active channels
INITIALIZE: $\Theta_\ell = \Xi(\Psi_\ell)$
INITIALIZE: $\lambda_k^\ell = \sum_{j=1}^{|\Theta_\ell|} \delta_{\Theta_\ell^j k};\ \forall k \mathcal{T}$
**do**
  $k^* = \arg\max_k \lambda_k^\ell$
  $[\mathbf{s}]_{k^*} = 0$
  $\Psi_\ell = \Psi_\ell \setminus \{(j,k)\} \begin{cases} \text{if } j = k^* \text{ or } k = k^*; \\ \forall (j,k) \in \Psi_\ell \end{cases}$
  $\mathcal{T} = \mathcal{T} \setminus k^*$
  $\Theta_\ell = \Xi(\Psi_\ell)$
  $\lambda_k^\ell = \sum_{j=1}^{|\Theta_\ell|} \delta_{\Theta_\ell^j k};\ \forall k \in \mathcal{T}$
**while** $\Psi_\ell \neq \phi$

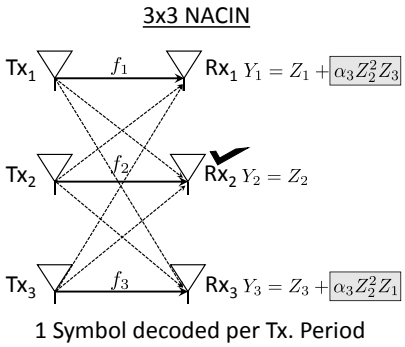


Figure 8.5: $3 \times 3$ NACIN

## 8.7 Upper Bound Scalability for $3 \times 3$ NACIN

Consider the $3 \times 3$ NACIN as shown in Fig. 8.5. In this section, we derive the information theoretic upper bound for this network. Let $W_1, W_2, W_3$ be the message drawn from the index set $\aleph_n$ for $n \in [1, 3]$ that result in the transmitted signals $Z_1^L, Z_2^L, Z_3^L$ respectively over $L$ channel access intervals. This is received by the receivers as $Y_1^L, Y_2^L, Y_3^L$, where the random sequence $Y_n^L \sim p(y_n^L \mid z_n^L)$. The receiver then applies some decoding rule to map the received sequence $Y_n^L$ to one of the indices in $\aleph_n$. The rate of each of the receivers is denoted by $R_1, R_2$ and $R_3$ respectively.

If $H(\cdot)$ denotes entropy, the network information rate for this is given by,

$$L(R_1 + R_2 + R_3) = H(W_1, W_2, W_3) \tag{8.17}$$

Table 8.1: Information received by different users per time slot

| Slots ↓ | $H(Y_1^L)$ | $H(Y_2^L)$ | $H(W_3 \mid Z_1^L, Z_2^L, (Z_2^2 Z_3)^L)$ |
|---|---|---|---|
| $L_1$ | ✓ | – | – |
| $L_2$ | – | ✓ | – |
| $L_3$ | – | – | ✓ |
| $L_{12}$ | ✓ | ✓ | – |
| $L_{13}$ | ✓ | – | ✓ |
| $L_{23}$ | ✓ | ✓ | – |
| $L_{123}$ | ✓ | ✓ | – |

Using the channel coding theorem and Fano's inequality, this can be simplified as follows,

$$
\begin{aligned}
L(R_1+R_2+R_3) =& H(W_1,W_2,W_3) && (8.18)\\
=& I(W_1,W_2,W_3;Y_1^L,Y_2^L) + H(W_1,W_2,W_3 \mid Y_1^L,Y_2^L) && (8.19)\\
\leq& \begin{array}{r} H(Y_1^L,Y_2^L) + H(W_1 \mid Y_1^L,Y_2^L) + H(W_2 \mid W_1,Y_1^L,Y_2^L) \\ +H(W_3 \mid W_1,W_2,Y_1^L,Y_2^L) \end{array} && (8.20)\\
\leq& H(Y_1^L,Y_2^L) + H(W_3 \mid W_1,W_2,Y_1^L,Y_2^L) && (8.21)\\
\leq& H(Y_1^L) + H(Y_2^L) + H(W_3 \mid W_1,W_2,Y_1^L,Y_2^L) && (8.22)\\
\leq& H(Y_1^L) + H(Y_2^L) + H(W_3 \mid Z_1^L,Z_2^L,(Z_2^2Z_3)^L) && (8.23)
\end{aligned}
$$

The above inequality in (8.23) is a very unique form where a multiplicative term has to be canceled to obtain the correct mapping. It is to be noted that for the multiplicative interference term to be received at $Y_1$, both transmitters 2 and 3 should be active. In the given $L$ slots, we need to carefully pick those slots where this scenario takes place. Thus, we divide the channel access into various slots. For a $3 \times 3$ network, the possible scenarios of channel access are for a given time slot: (a) only one of the three transmitters transmits, (b) any combination of 2 transmitters transmit, or (c) all three transmitters transmit. These combinations are enumerated in Table 8.1. $L_1$ is a time slot where only transmitter 1 is 'on', $L_{12}$ is a time slot where transmitters 1 and 2 are 'on', and so on. Over $L$ transmissions,

$$L = L_1 + L_2 + L_3 + L_{12} + L_{13} + L_{23} + L_{123} \tag{8.24}$$

The checkmarks (✓) in the table indicate that new information is obtained by that receiver for that time slot. For example, only receiver $n$ receives $Z_n$ in the time slot $L_n$. In the time slots $L_{12}$

receivers 1 and 2 receive $Z_1$ and $Z_2$ respectively. Although receiver 3 receives the intermodulation term $Z_2^2 Z_1^*$, the network does not receive any new information, as it is a repetition of information (Also note that the argument for receiver 3 assumes that $Z_1^L, Z_2^L$ are already given). Likewise for $L_{13}$, but no intermodulation products are received for this slot in any case.

However, the interesting slot is $L_{23}$. Receiver 2 receives $Z_2$, and hence new information is added to the network. Receiver 1 receives $Z_2^2 Z_3^*$, and this is also new information for the network which can be used further, as $Z_3$ is not yet known. Suppose that a genie delivers $Z_2$ and $Z_2^2 Z_3^*$ (as the argument inside the entropy function for receiver 3 says), it could decode $Z_3$ by zero-forcing, but this will not add any new information to the network as this can be obtained from information at receivers 1 and 2 itself. Thus, for this time slot, no new information is added by receiver 3 as reflected in the table. A similar explanation follows for the time slot $L_{123}$. This method of obtaining outer bounds is commonly called a genie-aided technique [117–125].

From this discussion, we have,

$$H(Y_1^L) = \Big(L - (L_2 + L_3)\Big) \log_2(P) \tag{8.25}$$

$$H(Y_2^L) = \Big(L - (L_1 + L_3 + L_{13})\Big) \log_2(P) \tag{8.26}$$

$$H(W_3 \mid Z_1^L, Z_2^L, (Z_2^2 Z_3)^L) = \Big(L - (L_1 + L_2 + L_{12} + L_{23} + L_{123})\Big) \log_2(P) \tag{8.27}$$

We now have,

$$H(Y_1^L) + H(Y_2^L) + H(W_3 \mid Z_1^L, Z_2^L, (Z_2^2 Z_3)^L) = \Big(2L - (L_1 + L_2)\Big) \log_2(P) \tag{8.28}$$

$$\leq 2L \log_2(P) \tag{8.29}$$

Substituting this in (8.23), we have

$$R_1 + R_2 + R_3 \leq 2 \log_2(P) \tag{8.30}$$

Thus, per channel use, a $3 \times 3$ NACIN can successfully decode a maximum of 2 symbols. This was what was achieved by the practical achievable scheme discussed in the previous sections as well. Thus, for a $3 \times 3$ NACIN, the network information capacity is 2 symbols per channel use.

## 8.8 Upper Bound for $N \times N$ NACIN

In this section, we discuss the upper bound for the scalability of NACIN. Consider $N$ transmitters and $N$ receivers. Let $\mathcal{T} = \{\tau_1, \tau_2, \cdots, \tau_{|\mathcal{T}|}\}$ represent the set of all slots. The cardinality of the set is given by, $| \mathcal{T} | = \sum_{n=0}^{N} \binom{N}{n}$ ,where $\binom{N}{n}$ denotes $N$-choose-$n$. Further, $\mathsf{info}(\tau_k)$, represents the number of mutually independent information symbols received in the slot $\tau_k$.

We seek to follow the genie-aided procedure described in Table 8.1 of evaluating the number of mutually independent symbols ($\mathsf{info}(\tau_k)$) that the network can obtain in each slot. However, the structure of the nonlinearity and intermodulation products renders the problem for obtaining a closed form for a generic case intractable. Thus, we propose an algorithmic scheme to determine $\mathsf{info}(\tau_k),\ \forall \tau_k \in \mathcal{T}$ by sequentially polling all the slots. This poses another challenge, where the number of slots, $| \mathcal{T} |$, increases exponentially. Nevertheless, we describe the algorithmic scheme that can be used to evaluate the upper bounds for a relatively low number of nodes depending on the computational infrastructure.

In Algorithm 11 we sequentially poll each transmission slot in $\mathcal{T}$. For each slot, $\zeta$ represents the set of independent data symbols and $\chi$ represents the set of independent interference symbols that the network can obtain. In each slot, $\tau_k$ the relevant interfering symbols are collected in the set $\Gamma_n^k$ for all nodes $n \in [1, N]$. Then, if $n \notin \zeta$, then this data symbol is added to the set, and $\mathsf{info}(\tau_k)$ is incremented. Similarly, all pairs of interfering symbols in $\Gamma_n^k(\ell)$ not in the set $\chi$ are added to $\chi$ and $\mathsf{info}(\tau_k)$ is updated when new information is added to the network. Then, all independent data symbols that can be obtained through algebraic manipulations of all terms in $\zeta$ and $\phi$ are decoded and the respective sets are updated. The process is repeated for all slots.

Fig. 8.6 gives the plot for the upper bound from $N = 3$ to $N = 16$ against the practical achievable scheme proposed in this chapter. The upper bound closely matches with the practical achievable scheme for the number of nodes considered. For $N = 3, 4, 5, 6, 7, 8, 9, 11, 12, 13, 14$ the practical achievable scheme and upper bound are the same, and thus the number of symbols decoded per transmit period is optimal. The maximum gap for the number of nodes considered here is 1. However, we note that the proposed practical achievable scheme is a greedy algorithm, and greedy schemes may diverge from the optimal for large $N$.

**Algorithm 11** Steps to Compute Upper Bound for NACIN

FORMULATE: $\Psi_n = \{\psi_1, \psi_2, \cdots \psi_{\kappa_n}\}, \forall n \in [1, N]$;
FORMULATE: $\mathcal{T} = \{\tau_1, \tau_2, \cdots \tau_{|\mathcal{T}|}\}$
INITIALIZE: $\mathsf{info}(\tau_k) = 0, \forall k \in [1, \mid \mathcal{T} \mid]$
**for** $k = 1, 2, \cdots \mid \mathcal{T} \mid$ **do**
    INITIALIZE: $\xi = \phi$; $\chi = \phi$ where $\phi$ is null set
    **for** $n = 1, 2, \cdots, N$ **do**
        $\Gamma_n^k = \psi_i : \{\psi_i\} \subset \{\tau_k\}, \forall \{\psi_i\} \in \Psi_n$
        **if** $n \notin \xi \wedge n \subset \tau_k$ **then**
            $\xi = \xi \cup \{n\}$
            $\mathsf{info}(\tau_k) = \mathsf{info}(\tau_k) + 1$
        **end if**
        **for** $\ell = 1, 2, \cdots, \mid \Gamma_n^k \mid$ **do**
            **if** $\{\Gamma_n^k(\ell)\} \notin \chi$ **then**
                $\chi = \chi \cup \{\Gamma_n^k(\ell)\}$
                **if** $\{n\} \not\subset \tau_k$ **then**
                $\mathsf{info}(\tau_k) = \mathsf{info}(\tau_k) + 1$
                **end if**
                **if** $\{\xi\}_i \subset \{\chi\}_j; \forall i \in [1, \mid \xi \mid], \forall j \in [1, \mid \chi \mid]$ **then**
                $\xi = \xi \cup \Big(\{\chi\}_j \setminus \{\xi\}_i\Big)$
                $\chi = \chi \setminus \{\chi\}_j$
                **end if**
            **end if**
        **end for**
    **end for**
    $\upsilon_k = N - \mathsf{info}(\tau_k)$
**end for**
Upper Bound: $R \leq N - \arg\min_k \upsilon_k$

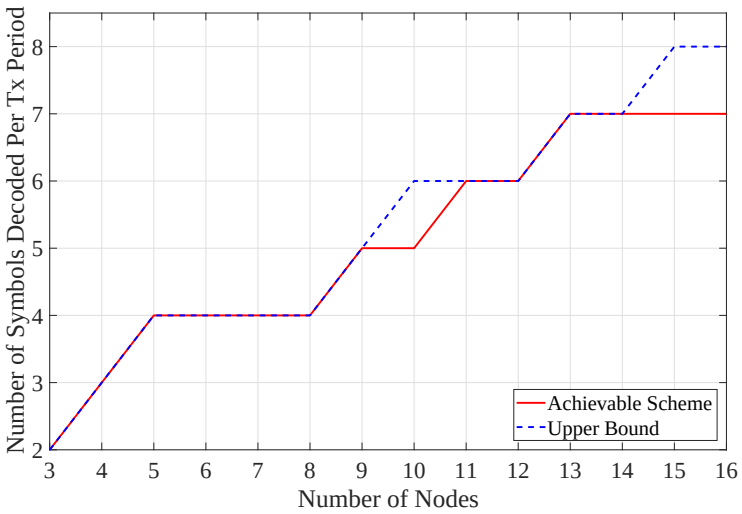


Figure 8.6: Upper Bound for $N \times N$ NACIN

## 8.9 Conclusions

This chapter introduces the Nonlinear Adjacent Channel Interference Networks (NACIN) encountered due to two-tone intermodulation distortions arising due to receiver nonlinearity in next generation heterogeneous and shared spectrum networks. Practical achievable schemes for interference avoidance to analyze the limits of such networks were proposed, and schemes to protect incumbent operations from interference were detailed. The operational scalability of the network devoid of nonlinear adjacent channel interference across the active channels assuming a third order polynomial approximation for the receivers was found to be a sub-linear function of the number of channels available for the proposed practical achievable scheme. Further, it was shown that secondary operations in adjacent channels ensuring complete protection from nonlinear adjacent channel interference for incumbent operations with sensitive receivers was possible without the need for exclusion zones. Interference avoidance schemes to enable such operations were proposed. With a nuance that allows secondary users to accept adjacent channel interference, it was shown that the scalability of the network with complete incumbent protection was an almost linear function of the number of available channels for the proposed practical achievable schemes. Further, we also proposed an algorithmic scheme to evaluate the upper bound on scalability of NACINs. We demonstrated through evaluations that the proposed upper bound scheme yields a strong bound relative to the practical achievable scheme. This also means that the proposed practical achievable scheme operates close to the network capacity, at least for

small values of $N$. The analysis in this chapter and the proposed schemes provide an assessment for the scalability of NACINs and also yield a systematic approach for interference avoidance in next generation heterogeneous and Multi-RAT network design.

Topics for future research include obtaining upper bounds through schemes that are computationally efficient, exploiting techniques from nonlinear algebra [126, 127] to develop nonlinear interference cancellation in NACIN, and extending the results in this chapter for multiple antenna systems.

# Appendix: Proof of Lemma 6

*Proof.* The receiver model is given by, $Y = \alpha_1 Z + \alpha_2 Z^2 + \alpha_3 Z^3$ where $Z = Z_2 + Z_3$. Consider the third order term,

$$Z^3 = (Z_2 + Z_3)^3 = Z_2^3 + Z_3^3 + 3Z_2^2 Z_3 + 3Z_2 Z_3^2 \tag{8.31}$$

We first consider the term $Z_2^3$ as follows,

$$\begin{aligned} Z_2^3 =& U_2^3 \cos^3(\omega_1) - jV_2^3 \sin(\omega_1) - 3jU_2^2 V_2 \cos^2(\omega_1)\sin(\omega_1) - 3U_2 V_2^2 \cos(\omega_1)\sin^2(\omega_1) \\ =& \frac{3U_2^3}{4}\cos(\omega_1) + \frac{U_2^3}{4}\cos(3\omega_1) - j\frac{3V_2^3}{4}\cos(\omega_1) + \frac{V_2^3}{4}\cos(3\omega_1) \\ & - j\frac{3}{2}U_2^2 V_2 \sin(3\omega_1) - \frac{3}{2}U_2 V_2^2 \cos(3\omega_1) \end{aligned} \tag{8.32}$$

As seen, it has terms only at frequency $3\omega_1$. Similarly, the expansion of $Z_3^3$ will have terms only at $3\omega_2$. Thus, we shall not pursue them further.

We now consider the term $Z_2^2 Z_3$.

$$\begin{aligned} Z_2^2 =& U_2^2 \cos^2(\omega_1) + V_2^2 \sin^2(\omega_1) - 2jU_2 V_2 \cos(\omega_1)\sin(\omega_1) \\ =& \frac{U_2^2 + V_2^2}{2} + \frac{U_2^2}{2}\cos(2\omega_1) - \frac{V_2^2}{2}\cos(2\omega_1) - jU_2 V_2 \sin(2\omega_1) \end{aligned} \tag{8.33}$$

$$
\begin{aligned}
Z_2^2 Z_3 &= \left[\frac{U_2^2+V_2^2}{2} + \frac{U_2^2}{2}\cos(2\omega_1) - \frac{V_2^2}{2}\cos(2\omega_1) - jU_2V_2\sin(2\omega_1)\right](U_3\cos(\omega_2) - jV_3\sin(\omega_2)) \\
Z_2^2 Z_3 &= \left(\frac{U_2^2+V_2^2}{2}\right)U_3\cos(\omega_2) + \left(\frac{U_2^2-V_2^2}{4}\right)U_3[\cos(2\omega_1-\omega_2)+\cos(2\omega_1+\omega_2)] \\
&\quad - j\frac{U_2U_3V_2}{2}[\sin(2\omega_1+\omega_2)+\sin(2\omega_1-\omega_2)] - j\left(\frac{U_2^2+V_2^2}{2}\right)V_3\sin(\omega_2) \\
&\quad + j\left(\frac{U_2^2-V_2^2}{4}\right)V_3[\sin(2\omega_1+\omega_2)-\sin(2\omega_1-\omega_2)] \\
&\quad - \frac{U_2V_2V_3}{2}[\cos(2\omega_1-\omega_2)-\cos(2\omega_1+\omega_2)]
\end{aligned}
\tag{8.34}
$$

The frequency component causing interference in the desired channel, $\omega_0$, is $2\omega_1 - \omega_2$. Thus, isolating only the frequency components causing interference, we obtain the adjacent symbol interfering terms as,

$$
\mathsf{ASI} = \left(\frac{U_2^2-V_2^2}{4}\right)U_3\cos(\omega_0) - j\frac{U_2U_3V_2}{2}\sin(\omega_0) - j\left(\frac{U_2^2-V_2^2}{4}\right)V_3\sin(\omega_0) - \frac{U_2V_2V_3}{2}\cos(\omega_0)
\tag{8.35}
$$

Re-arranging the ASI in the format of the standard digitally modulated signal to obtain the in-phase and the quadrature components we have,

$$
\mathsf{ASI} = \left[\left(\frac{U_2^2-V_2^2}{4}\right)U_3 - \frac{U_2V_2V_3}{2}\right]\cos(\omega_0) - j\left[\left(\frac{U_2^2-V_2^2}{4}\right)V_3 + \frac{U_2U_3V_2}{2}\right]\sin(\omega_0) \tag{8.36}
$$

Thus, the complex envelope (the digital symbol) causing Adjacent Symbol Interference is given by,

$$
Z_{\mathsf{ASI}} = U_{\mathsf{ASI}} + jV_{\mathsf{ASI}} \tag{8.37}
$$

where

$$
U_{\mathsf{ASI}} = \left[\left(\frac{U_2^2-V_2^2}{4}\right)U_3 - \frac{U_2V_2V_3}{2}\right];\;\; V_{\mathsf{ASI}} = \left[\left(\frac{U_2^2-V_2^2}{4}\right)V_3 + \frac{U_2U_3V_2}{2}\right] \tag{8.38}
$$

Similarly, the term $Z_2^2$ will create ASI components at the frequency $(2\omega_2 - \omega_1)$. Expanding the terms will give the exact relation. However, we now deduce a simpler method to arrive at the ASI, using just the complex envelope digitally modulated symbols based on the analysis carried out thus far.

We now represent $Z_{\mathsf{ASI}}$ in terms of the complex envelope symbols $Z_2 = U_2 + jV_2$ and $Z_3 = U_3 + jV_3$. Consider $Z_2^2 Z_3^*$,

$$\begin{aligned} Z_2^2 Z_3^* =& (U_2 + jV_2)^2 (U_3 + jV_3) \\ =& \left[(U_2^2 - V_2^2)U_3 - 2U_2 V_2 V_3\right] - j\left[(U_2^2 - V_2^2)V_3 + 2U_2 U_3 V_2\right] \\ =& 4U_{\mathsf{ASI}} + 4jV_{\mathsf{ASI}} \\ Z_2^2 Z_3^* =& 4Z_{\mathsf{ASI}}. \end{aligned} \tag{8.39}$$

Assuming unit gain for the receiver and ignoring the scaling factors, the received complex symbol $Y_1$ at the frequency $\omega_0$ is given by,

$$Y_1 = Z_1 + 3\alpha_3 \, Z_2^2 Z_3^*, \tag{8.40}$$

where $Z_1 = U_1 + jV_1$. □

# Chapter 9

# Conclusions

This dissertation is centered around the seminal idea of accounting for receiver characteristics and vulnerabilities for enhancing access to radio spectrum. We have introduced the basic foundations for capturing, quantifying, and managing the impact of receiver front-end nonlinearity on efficient spectrum access and co-existence in next generation heterogeneous and diverse wireless networks. We began this dissertation seeking to address four questions. We conclude the dissertation by summarizing the findings for those questions.

**How does receiver nonlinearity impact performance?**

We proposed a comprehensive mathematical workbench, which can be used to precisely understand and evaluate how receiver nonlinearity impacts performance. A tractable representation was developed to capture the spectrum re-distribution resulting from front-end nonlinearity to specify intermodulation, cross modulation, and compressive distortion resulting from receiver nonlinearity. This contribution develops a systematic framework, which re-imagines the third order nonlinearity to create a compact and convenient model, which acts as a technology enabler for multi-RAT co-existence, efficient spectrum access, and nonlinear adjacent channel interference cancellation, among other things. We have validated the accuracy of the proposed theoretical representation with experimental measurements.

**How much does receiver nonlinearity affect performance?**

Using the methodology developed to understand how nonlinearity impacts performance, we developed a framework to quantify receiver performance with information theoretic metrics. We analyze bounds on achievable rate of nonlinear receivers for a tractable test input spectrum and obtain closed form expressions exploiting the properties and characteristics of the nonlinear model. We use the rate analysis to propose metrics to quantify receiver performance with nonlinearity, compare disparate receivers' operation for a given radio environment, and evaluate the feasibility (or performance detriment) of a given receiver to operate in a specific radio environment. We capture the interplay between the front-end nonlinearity and the pre-selector RF filter bandwidth, and develop receiver performance metrics based on fractional rate loss relative to the capacity of the link. Extensive numerical evaluations illustrated that receiver nonlinearity can potentially reduce spectrum efficiency by orders of magnitude for 'poor' (high nonlinearity and/or low front-end filter selectivity) receivers. We also carried out experimental measurements and outlined guidelines to benchmark the proposed theoretical receiver performance metrics.

**How can receiver nonlinearity be managed?**

We proposed novel network optimization frameworks inclusive of receiver characteristics and vulnerabilities for efficient spectrum access and co-existence. Specifically, the frameworks can account for receiver pre-selector bandwidth, nonlinearity, imperfect image frequency rejection, phase noise, ADC aliasing, and leakage due to transmit masks for channel allocations. We further proposed computationally efficient algorithms to solve the network optimization and to obtain receiver characteristics aware channel allocations. The framework provides flexibility to cater to different network topologies and constraints. Through extensive network simulations, we demonstrated that the proposed framework accounting for receiver characteristics can potentially increase the spectrum efficiency by orders of magnitude, relative to receiver agnostic spectrum access. This contribution provides a foundation for next generation spectrum management systems to adopt receiver characteristic aware frameworks to enhance spectrum efficiency, scalability, and potentially avoid gridlocks in access and co-existence.

**How scalable are these networks for dense deployment?**

We analyzed the fundamental scaling laws for interference networks with receiver nonlinearity employing network level interference avoidance techniques. Network scalability for proposed practical achievable schemes for interference avoidance with zero threshold to interference was found to be sub-linear. However, in a dynamic spectrum access context, with complete protection only to the primary user, the scalability of the proposed practical achievable scheme improved considerably. The upper bounds developed closely matched with the practical achievable scheme as verified with numerical evaluations. The analysis provides valuable insights for next generation network design for dense deployment. Moreover, the schemes provide guarantees on harmful interference avoidance, instilling the necessary confidence for legacy spectrum to be opened up for opportunistic access.

**Broader Impact, Future Work, and Discussions**

The work in this dissertation provides the necessary foundations to influence the way we understand, design, and optimize the next generation wireless networks with heterogeneous and diverse receiver technologies. Besides the primary goal of substantially enhancing spectrum efficiency and co-existence of wireless networks, this research will help to reduce spectrum conflicts arising between different wireless networks that have in the past required arduous legal and regulatory intervention to resolve. This research will facilitate the development of metrics for assessing receiver performance and specifying the quality of receivers produced by consumer electronics. Creating rigorous benchmarks on performance for practical receivers is an important area of future work. This can potentially initiate the development of related standards and policy language.

Frameworks for accounting receiver characteristics for network optimization provide a rich set of new problems in algorithm development. For instance, developing computationally efficient algorithms with performance guarantees for the combinatorial channel allocation problem, which resembles the traveling salesman problem, but with a nuance that the weight of the graph edge itself depends on the overall path taken, is a problem for future research. In this dissertation, we primarily addressed centralized spectrum management frameworks. Development of algorithms for distributed network optimization accounting for receiver characteristics is another promising area of future research. For example, exploring game theoretic frameworks in this context may provide tractable formulations and solutions.

In addressing the scalability of interference networks with receiver nonlinearity, we provided a computationally intensive algorithmic scheme to evaluate the upper bound. Developing either closed form solutions or computationally efficient schemes for analyzing the scalability of upper bounds is a challenging problem. Extension of the proposed practical achievable scheme with multi-antenna receivers and development of nonlinear adjacent channel interference cancellation schemes is another challenging yet promising area of future research.

Development of wireless test beds with configurable front-end nonlinearity for validation of concepts and practical implementation of algorithms related to receiver-centric spectrum access is an area ripe for impactful future work.

# Bibliography


[1] *Cisco Visual Networking Index: Global Mobile Data Traffic Forecast Update, 20162021*, White Paper. Available: http://www.cisco.com/c/en/us/solutions/collateral/service-provider/visual-networking-index-vni/mobile-white-paper-c11-520862.pdf

[2] P. S. Ryan, "Treating the Wireless Spectrum as a Natural Resource," *Environmental Law Reporter*, vol. 35, no. 9, Sept. 2005, pp. 10,620-10,629.

[3] President's Council of Advisors on Science and Technology (PCAST) report, Realizing the Full Potential of Government-Held Spectrum to Spur Economic Growth, July 2012. Available: `http://www.whitehouse.gov/sites/default/files/microsites/ostp/pcast_spectrum_report_final_july_20_2012.pdf`

[4] M. Lopez-Benitez, and F. Casadevall, "An Overview of Spectrum Occupancy Models for Cognitive Radio Networks," *in NETWORKING 2011 Workshops*, ed. V. Casares-Giner, P. Manzoni, and A. Pont, pp. 32-41, Springer Berlin Heidelberg 2011.

[5] C. Ghosh, S. Roy, M. B. Rao, and D. P. Agarwal, "Spectrum Occupancy Validation and Modeling Using Real-time Measurements," *Proc. ACM Workshop on Cognitive Radio Networks*, pp. 25-30, 2010.

[6] C. Ghosh, S. Pagadarai, D. P. Agarwal, and A. M. Wyglinski, "A Framework for Statistical Wireless Spectrum Occupancy," *IEEE Transactions on Wireless Communications*, vol. 9, no. 1, January 2010.

[7] T. Harrold, R. Cepeda, and M. Beach, "Long-term measurements of spectrum occupancy characteristics," *2011 IEEE Symposium on New Frontiers in Dynamic Spectrum Access Networks (DySPAN)*, pp. 83-89, May 2011.

[8] Y. Sixing, Z. Qian, Z. Erqing, Y. Liang, L. Shufang, "Statistical Modeling for Spectrum Usage Characterizing Wireless Fading Channels and Mobile Service Dynamics," *IEEE Transactions on Vehicular Technology*, vol.62, no.8, pp.3800,3812, Oct. 2013.

[9] R.I.C. Chiang, G. B. Rowe, and K. W. Sowerby, "A quantitative analysis of spectral occupancy measurements for cognitive radio," *Proc. IEEE 65th Vehicular Tech. Conf. (VTC 2007 Spring)*, pp. 30163020, April 2007.

[10] M. Lopez-Benitez, and F. Casadevall, "Discrete-time spectrum occupancy model based on Markov Chain and duty cycle models," *2011 IEEE Symposium on New Frontiers in Dynamic Spectrum Access Networks (DySPAN)*, pp.90-99, 3-6 May 2011.

[11] S. M. Dudley, et al., "Practical Issues for Spectrum Management With Cognitive Radios," *Proceedings of the IEEE*, vol. 102, no. 3, pp. 242-264, 2014.

[12] J. M. Chapin and W. H. Lehr, "The Path to Market Success for Dynamic Spectrum Access Technology," *IEEE Communications Magazine*, May 2007, pp. 96-103.

[13] J. H. Reed, J. T. Bernhard, and J. M. Park, "Spectrum Access Technologies: The Past, the Present, and the Future," *Proceedings of the IEEE*, vol.100, no. Special Centennial Issue, pp.1676-1684, May 2012 (invited paper).

[14] T. M. Taher, R. B. Bacchus, K. J. Zdunek, and D.A. Roberson, "Long-term Spectral Occupancy Findings in Chicago," *Proc. IEEE DySPAN 2011*, pp. 100-107.

[15] T. M. Taher, R. B. Bacchus, K. J. Zdunek, and D.A. Roberson,, "Spectrum Utilization Study in Support of Dynamic Spectrum Access for Public Safety," *Proc. IEEE DySPAN 2010*.

[16] K. Patil, R. Prasad, and K. Skouby, "A Survey of Worldwide Spectrum Occupancy Measurement Campaigns for Cognitive Radio," 2011 International Conference on Devices and Communications (ICDeCom), pp.1-5, 2011.

[17] A. Martian, C. Vladeanu, I. Marcu, and I. Marghescu, "Evaluation of Spectrum Occupancy in an Urban Environment in a Cognitive Radio Context," *International Journal on Advances in Telecommunications*, vol. 3, no. 3& 4, pp. 172-181, 2010.

[18] J. M. Peha, "Sharing Spectrum Through Spectrum Policy Reform and Cognitive Radio," Proceedings of the IEEE, vol. 97, no. 4, April 2009, pp. 708-719.

[19] J. A. Stine, "Spectrum Consumption Models," in *Cognitive Radio Technology,* 2nd ed., B. A. Fette, Ed. Burlington, MA: Academy Publishers (Imprint of Elsevier), 2009, pp. 645-666.

[20] Commerce Spectrum Management Advisory Committee, *Interim Report of Interference and Dynamic Spectrum Access Sub Committee*, May 2010. Available: `http://www.ntia.doc.gov/files/ntia/meetings/csmac_may19_idsa_final.pdf`

[21] FCC News Release, "FCC Makes 150 MHz of Contiguous Spectrum Available for Mobile Broadband and Other Uses Through Innovative Sharing Policies," April 17, 2015. Available: `https://apps.fcc.gov/edocs_public/attachmatch/DOC-333083A1.pdf`

[22] FCC Report and Order and Second Notice of Proposed Rule Making, *Amendment of the Commissions Rules with Regard to Commercial Operations in the 3550-3650 MHz Band*, FCC 15-47, GN Docket No. 12-354, April 21, 2015.

[23] FCC Report and Order, *Amendment of the Commissions Rules with Regard to Commercial Operations in the 1695-1710 MHz, 1755-1780 MHz, and 2155-2180 MHz Bands*, FCC14-31, GN Docket No. 13-185, March 2014.

[24] FCC Spectrum Policy Task Force report, Report of the Spectrum Efficiency Working Group, November 2002. Available: `http://transition.fcc.gov/sptf/files/SEWGFinalReport_1.pdf`

[25] J. T. Dixon, "UHF-TV Taboos: The FCC Electromagnetic Compatibility Plan for UHF Television," *IEEE Transactions on Electromagnetic Compatibility*, vol. 6, no. 1, 1964, pp. 2932.

[26] M. J. Marcus, "Regulatory Approaches and Controlling Cochannel and Nearby Frequency Interference," *IEEE Wireless Communications*, April 2017, pp. 4-5.

[27] David Schiendler, "GPS-Interference Controversy Comes to a Boil," *IEEE Spectrum*, February 2012.

[28] T. S. Rappaport, et al., *Millimeter Wave Wireless Communication*, Prentice Hall, 2014; Chapter 7.

[29] S. Rangan, T. S. Rappaport, and E. Erkip, "Millimeter-Wave Cellular Wireless Networks: Potentials and Challenges," *Proc. of the IEEE*, Vol. 102, No. 3, March 2014.

[30] FCC Technological Advisory Council, "Interference Limits Policy: The use of harm claim thresholds to improve the interference tolerance of wireless systems," White Paper Version 1.0, February 2013.

[31] European Communications Office (ECO) Report 02, "The Impact of Receiver Parameters on Spectrum Management Regulations: A Pilot Study," June 2010.

[32] European Communications Committee (ECC) Report 127, "The Impact of Receiver Standards on Spectrum Management," October 2008.

[33] L. Davies and P. Winter, *Study of Current and Future Receiver Performance*, Final Report of OFCOM, January 2010.

[34] Presidential Memorandum, "Expanding America's Leadership in Wireless Innovation," June 14, 2013.

[35] Report to Congressional Committees, *Spectrum Management: Further Consideration of Options to Improve Receiver Performance Needed*, GAO-13-265, US Government Accountability Office, February 2013.

[36] J. A. Stine, "Model Based Spectrum Management, Part 1: Modeling and Computational Manual," MITRE Corporation, McLean, VA, Technical Report, 110131, 2011. Available: `http://www.mitre.org/work/tech_papers/2011/11_2071/11_2071.pdf`.

[37] J. A. Stine, "Model-Based Spectrum Management," Proc. *IEEE DySPAN 2011*, pp. 628-631.

[38] M. J. Marcus, "Harmful Interference and Its Role in Spectrum Policy," *Proceedings of the IEEE*, vol. 102, no. 3, pp. 265-269.

[39] Recommendation ITU-R SM.1134, "Intermodulation Interference Calculations in the Land-Mobile Service," Available: `https://www.itu.int/dms_pubrec/itu-r/rec/sm/R-REC-SM.1134-0-199510-S!!PDF-E.pdf`

[40] Preston Marshall, *Quantitative Analysis of Cognitive Radio and Network Performance*, Artech House, June 2010.

[41] B. Razavi, *RF Microelectronics*, 2nd Ed., Prentice Hall, 2012.

[42] K. McClaning, *Wireless Receiver Design for Digital Communications*, Scitech Publishers, North Carolina, 2012.

[43] R. Frevert, et al., *Modeling and Simulation for RF System Design*, Springer 2005.

[44] U. L. Rhode, J. Whitaker, and T. T. N. Bucher, *Communications Receivers*, McGraw Hill, 1997

[45] L. Smaini, *RF Analog Impairments Modeling for Communication Systems Simulation: Application to OFDM-based Transceivers*, 1st edition, Wiley, October 2012.

[46] A. V. Padaki, and J. H. Reed, "Impact of Intermodulation Distortion on Spectrum Preclusion for DSA: A New Figure of Merit," *Proc. IEEE DySPAN*, McLean, VA, 2014.

[47] C. W. Liu, and M. Damgaard, "IP2 and IP3 Nonlinearity Specifications for 3G/WCDMA Receivers," *High Frequency Electronics*, pp.16-25, June 2009.

[48] Vinay M. M, R. Paily and A. Mahanta, "Gain, NF and IIP3 Budgeting of LTE Receiver Front End," *2013 26th International Conference on VLSI Design and 2013 12th International Conference on Embedded Systems*, Pune, 2013, pp. 191-196.

[49] A. V. Padaki, R. Tandon, and J. H. Reed, "Receiver Non-Linearity Aware Resource Allocation for Dynamic Spectrum Access Systems," *Proc. IEEE MILCOM*, 2014, Baltimore, MD,

[50] A. V. Padaki, V. Marojevic, and J. H. Reed, "Role of Receiver Performance Data in Efficient Spectrum Utilization," *Proc. IEEE DySPAN*, 2014, McLean, VA.

[51] Aditya V. Padaki, Vuk Marojevic and Jeffrey H. Reed, "On the Importance of Inclusion of Receiver Performance Data in SAS to Improve Spectrum Efficiency," FCC Proceeding 12-354, SAS Workshop, January 2014.

[52] E. Y. Imana, "Cognitive RF Front-end Control," *Ph.D. Dissertation*, Dept. of ECE, Virginia Tech, 2014.

[53] M. Grimm, M. Allen, J. Marttila, M. Valkama and R. Thoma, "Joint Mitigation of Nonlinear RF and Baseband Distortions in Wideband Direct-Conversion Receivers," *IEEE Transactions on Microwave Theory and Techniques*, vol. 62, no. 1, pp. 166-182, Jan. 2014.

[54] J. Marttila, M. Allen, M. Kosunen, K. Stadius, J. Ryynanen and M. Valkama, "Reference Receiver Enhanced Digital Linearization of Wideband Direct-Conversion Receivers," *IEEE Transactions on Microwave Theory and Techniques*, vol. 65, no. 2, pp. 607-620, Feb. 2017.

[55] E. Y. Imana, T. Yang, and J. H. Reed, " Relaxing pre-selector filter selectivity requirements using cognitive RF front-end control," *Analog Integrated Circuits and Signal Processing*, vol. 78, no. 3, pp. 705-716, March 2014.

[56] M. Leffel, "Intermodulation distortion in a multi-signal environment," *RF Design*, pp. 78-84, June 1995.

[57] J. C. Pedro and N. B. de Carvalho, "On the Use of Multitone Techniques for Assessing RF Components' Intermodulation Distortion," *IEEE Transactions on Microwave Theory and Techniques*, vo. 47, no. 12, pp.2393–2402, Dec. 1999.

[58] N. B. de Carvalho and J. C. Pedro, "A Comprehensive Explanation of Distortion Sideband Asymmetries," *IEEE Transactions on Microwave Theory and Techniques*, vo. 50, no. 9, pp.2090–2101, Sep. 2002.

[59] J. C. Pedro and N. B. de Carvalho, *Intermodulation Distortion in Microwave and Wireless Circuits*, Artech House Pub., April 2003.

[60] D. H. Mahrof, E. A. M. Klumperink, J. C. Haartsen and B. Nauta, "On the Effect of Spectral Location of Interferers on Linearity Requirements for Wideband Cognitive Radio Receivers," *2010 IEEE Symposium on New Frontiers in Dynamic Spectrum*, Singapore, 2010, pp. 1-9.

[61] E. Rebeiz, A. Shahed Hagh Ghadam, M. Valkama, and D. Cabric, "Spectrum Sensing Under RF Non-Linearities: Performance Analysis and DSP-Enhanced Receivers," *IEEE Transactions on Signal Processing*, vol. 63, no. 8, pp. 1950-1964, April 2015.

[62] A. Gokceoglu, S. Dikmese, M. Valkama, and M. Renfors, "Energy Detection under IQ Imbalance with Single- and Multi-Channel Direct-Conversion Receiver: Analysis and Mitigation," in IEEE Journal on Selected Areas in Communications, vol. 32, no. 3, pp. 411-424, March 2014.

[63] G. H. Golub and C. F. Van Loan, *Matrix Computations*, Johns Hopkins University Press, $3^{th}$ edition, 1996.

[64] R. M. Gray, "Toeplitz and Circulant Matrices: A Review", *Foundations and Trends in Communications and Information Theory*, Now Publishers, vol. 2, no. 3, pp 155-239. Also available: `http://ee.stanford.edu/~gray/toeplitz.pdf`

[65] D. H. Mahrof, *Distortion Mitigation in Cognitive Radio Receivers,*, Ph.D. Dissertation, University of Twente, 2015.

[66] T. M. Cover and J. A. Thomas, *Elements of Information Theory*, John Wiley & Sons, 2006.

[67] R. G. Gallager, *Information Theory and Reliable Communication*, Wiley & Sons, 1968.

[68] S. Ihara, "On the capacity of channels with additive non-gaussian noise," *Information and Control*, vol. 37, no. 1, April 1978, pp. 34-39.

[69] I. W. McKeague, "On the capacity of channels with Gaussian and non-Gaussian noise," *Information and Control*, vol.51, no. 2, November 1981, pp. 153-173.

[70] J. Binia, "On the capacity of certain additive non-Gaussian channels," *IEEE Transactions on Information Theory*, vol. 25, no. 4, pp. 448-452, July 1979.

[71] M. I. Rosen, "Niels Hendrik Abel and Equations of the Fifth Degree," *American Mathematical Monthly*, vol. 102, no. 6, pp. 495-505, 1995.

[72] J. P. Tignol, "Ruffini and Abel on general equations," *Galois' Theory of algebraic equations (2nd ed.)*, World Sci., 2016.

[73] W. S. Burnside and A. W. Panton, *The Theory Of Equations Vol I*, Nabu Press, September, 2011.

[74] R. G. Ayoub, "Paolo Ruffini's Contributions to the Quintic," *Archive for History of Exact Sciences*, vol. 23, no. 3, 1980, pp. 253277.

[75] C. W. Tan, M. Chiang, and R. Srikant, "Fast Algorithms and Performance Bounds for Sum Rate Maximization in Wireless Networks," *IEEE/ACM Transactions on Networking*, Vol. 21, No. 3, June 2013.

[76] C. W. Tan, M. Chiang, and R. Srikant, "Maximizing Sum Rate and Minimizing MSE on Multiuser Downlink: Optimality, Fast Algorithms and Equivalence via Max-min SIR," *Proc. IEEE International Symposium in Information Theory*, 2009, pp. 2669-2673.

[77] P. C. Weeraddana, M. Codreanu, M. Latva-aho, A. Ephremides and C. Fischione, "Weighted Sum-Rate Maximization in Wireless Networks: A Review," *Foundations and Trends in Networking*, NOW Publishers, vol. 6, no. 1-2, 2012.

[78] T. Nandagopal, T. E. Kim, X. Gao, and V. Bharghavan, "Achieving MAC layer fairness in wireless packet networks," *Proc. 6th Annual International ACM Conference on Mobile Computing and Networking*, 2000.

[79] H. J. Kushner and P. A. Whiting, "Convergence of proportional-fair sharing algorithms under general conditions," *IEEE Transactions on Wireless Communications*, vol. 3, no. 4, pp. 1250-1259, July 2004.

[80] R. Kwan, C. Leung, and J. Zhang, "Proportional Fair Multiuser Scheduling in LTE," *IEEE Signal Processing Letters* vol.16, no.6, pp. 461-464, June 2009

[81] J. David, et al. "QoS and fairness constrained convex optimization of resource allocation for wireless cellular and ad hoc networks," *IEEE INFOCOM 2002*.

[82] R. Elliott, "A measure of fairness of service for scheduling algorithms in multiuser systems," *IEEE Canadian Conference on Electrical and Computer Engineering*, 2002.

[83] R. Srikant and Y. Lei, "Communication Networks: An Optimization, Control, and Stochastic Networks Perspective," *Cambridge University Press*, 2013.

[84] M. Chiang, C. W. Tan, D. P. Palomar, D. ONeill, and D. Julian, "Power Control By Geometric Programming," *IEEE Trans. on Wireless Communications*, vol. 6, no. 7, July 2007.

[85] C. W. Tan, S. Friedland, and S. H. Low, "Spectrum management in multiuser cognitive wireless networks: Optimality and algorithm," *IEEE J. Sel. Areas Commun.*, vol. 29, no. 2, pp. 421430, Feb. 2011.

[86] X. Lin, N. B. Shroff, and R. Srikant, "A tutorial on cross-layer optimization in wireless networks," *IEEE J. Sel. Areas Commun.*, vol. 24, no. 8, pp. 14521463, Aug. 2006.

[87] C. W. Tan, M. Chiang, and R. Srikant, "Maximizing sum rate and minimizing MSE on multiuser downlink: Optimality, fast algorithms and equivalence via max-min SINR," *IEEE Transactions on Signal Processing*, vol. 59, no. 12, pp. 61276143, Dec. 2011.

[88] A. Gjendemsj, D. Gesbert, G. E. Oien, and S. G. Kiani, "Binary Power Control for Sum Rate Maximization over Multiple Interfering Links," *IEEE Transactions on Wireless Communications*, vol.7, no.8, pp.3164-3173, August 2008.

[89] D. Nace and M. Pioro, "Max-Min Fairness and its Applications to Routing, Load-Balancing and Network Design: a tutorial," *IEEE Communications Surveys & Tutorials*, vol.10, no.4, pp. 5-17, Fourth Quarter 2008.

[90] B. Radunovic and J.Y. Le Boudec, "A Unified Framework for Max-Min and Min-Max Fairness with Applications," *IEEE/ACM Transactions on Networking*, vol.15, no.5, pp.1073-1083, Oct. 2007

[91] D. J. Leith, C. Qizhi, and V. G. Subramanian, "Max-Min Fairness in 802.11 Mesh Networks,"*IEEE/ACM Transactions on Networking*, vol.20, no.3, pp. 756-769, June 2012.

[92] S. Kirkpatrick, C. D. Gelatt, and M. P. Vecchi, "Optimization by Simulated Annealing," vol. 220, no. 4598, pp. 671-680, 1983.

[93] D. Bertsimas and J. Tsitsiklis, "Simulated Annealing," *Statistical Science*, vol. 8, no. 1, pp. 10-15, 1993.

[94] M. Duque-Anton, D. Kunz, and B. Ruber, "Channel assignment for cellular radio using simulated annealing," *IEEE Transactions on Vehicular Technology*, vol. 42, no. 1, pp. 14-21, 1993.

[95] M. Yu, X. Ma, and M. Zhou, "Radio Channel Allocations With Global Optimality and Bounded Computational Scale," *IEEE Transactions on Vehicular Technology*, vol. 63, no. 9, pp. 4670-4680, 2014.

[96] S. Dadallage, C. Yi, and J. Cai, "Joint Beamforming, Power, and Channel Allocation in Multiuser and Multichannel Underlay MISO Cognitive Radio Networks," in IEEE Transactions on Vehicular Technology, vol. 65, no. 5, pp. 3349-3359, May 2016.

[97] M. Haenggi and R. Ganti, *Interference in Large Wireless Networks*, in *Foundations and Trends in Networking*, NOW Publishers, 2008, vol. 3, no. 2, pp. 127248

[98] H. ElSawy, E. Hossain, and M. Haenggi, "Stochastic Geometry for Modeling, Analysis, and Design of Multi-Tier and Cognitive Cellular Wireless Networks: A Survey," *IEEE Communications Surveys and Tutorials*, vol. 15, no. 3, pp. 996-1019, Third Quarter, 2013.

[99] M. Haenggi, et al., "Stochastic Geometry and Random Graphs for the Analysis and Design of Wireless Networks," *IEEE Journal on Selected Areas of Communications*, September 2009.

[100] J. Andrews, R. Ganti, M. Haenggi, N. Jindal, and S. Weber, " Primer on Spatial Modeling and Analysis in Wireless Networks," *IEEE Communications Magazine*, pp. 156-163, November 2010.

[101] M. Haenggi, *Stochastic Geometry for Wireless Networks*, Cambridge University Press, November 2012.

[102] E. Imana, T. Yang, and J. Reed, "Suppressing the Effects of Aliasing and IQ Imbalance on Multi-band Spectrum Sensing," *IEEE Transactions on Vehicular Technology*, May 2016.

[103] H. W. Kuhn, "The Hungarian Method for the assignment problem," *Naval Research Logistics Quarterly*, no. 2, pp.83-97, 1955.

[104] H. W. Kuhn, "Variants of the Hungarian method for assignment problems," *Naval Research Logistics Quarterly*, no. 3, pp. 253-258, 1956.

[105] J. Munkres, "Algorithms for the Assignment and Transportation Problems," *Journal of the Society for Industrial and Applied Mathematics*, vol. 5, no.1, pp. 32-38, March 1957.

[106] FCC Public Notice, *3.5 GHz Licensing Framework*, FCC 13-144, GN Docket No. 12-354, November 01, 2013.

[107] C. W. Liu and M. Damgaard, "IP2 and IP3 Nonlinearity Specifications for 3G/WCDMA Receivers," *High Frequency Electronics* in High Frequency Design, pp. 16-26, June 2009.

[108] A. V. Padaki, R. Tandon, and J. H. Reed, "Efficient Spectrum Sharing with RF Diversity: Adapting to Nonlinearity of Front Ends," *accepted, IEEE Globecom 2015*.

[109] D. Gidony and I. Kalet, "Adjacent Channel Interference Cancellation for MSK-Type Signals Using Antenna Diversity in Rayleigh Fading Environment," IEEE Transactions on Communications, vol. 52, no. 2, February 2004.

[110] A. B. M. Bostamam, *Adjacent Channel Interference Mitigation Schemes for Software Defined Radio Receiver*, Ph.D. Dissertation, School of Integrated Design Engineering, Keio University, Japan, July 2008.

[111] E. Sakai, H. Nishimura , M. Inamori, and Y. Sanada, "Adjacent Channel Interference Cancellation Using Orthogonal Precoding for Fractional Sampling OFDM Receiver," *Wireless Personal Communication*, vol. 72, pp. 211-225, Springer 2013.

[112] T. Renk, C. Kloeck, C. Koerner, and K. Jondral, "Increasing Spectral Efficiency by Managing Adjacent Channel Interference," *First ACM International Workshop on Technology and Policy for Accessing Spectrum*, August 5, 2006.

[113] N. Kovalevska, *Simulation of Adjacent Channel Interference Cancellation*, Master's Thesis, Dept. of Physics, University of Oslo, Dec. 2008.

[114] J. G. Proakis and M. Salehi, *Digital Communications*, 5th Ed., McGraw-Hill, 2007.

[115] A. Goldsmith, *Wireless Communications*, Cambridge University Press, 2005.

[116] A. V. Padaki, R. Tandon, and J. H. Reed, "On Scalability and Achievable Schemes for Nonlinear Adjacent Channel Interference Networks," *2017 IEEE International Conference on Communications*, Paris, France May 2017.

[117] G. Kramer, "Outer bounds on the capacity region of gaussian interference channels," *IEEE Transactions on Information Theory*, vol. 50, no. 3, pp.581-586, March 2004.

[118] R. H. Etkin, D. N. C. Tse, and H. Wang, "Gaussian Interference Channel Capacity to Within One Bit," *IEEE Transactions on Information Theory*, vol. 54, no. 12, pp. 5534-5562, Dec. 2008.

[119] V. S. Annapureddy and V. V. Veeravalli, "Gaussian Interference Networks: Sum Capacity in the Low-Interference Regime and New Outer Bounds on the Capacity Region," *IEEE Transactions on Information Theory*, vol. 55, no. 7, pp. 3032–3050, July 2009.

[120] S. Diggavi, M. Mitzenmacher, and H. D. Pfister, "Capacity Upper Bounds for the Deletion Channel," *2007 IEEE International Symposium on Information Theory*, Nice, 2007, pp. 1716-1720.

[121] X. Shang, G. Kramer, and B. Chen, "A new outer bound and the noisy-interference sum-rate capacity for the Gaussian interference channels," *IEEE Transactions on Information Theory*, vol. 55, no. 2, pp. 689-699, Feb. 2009.

[122] R. H. Etkin, "New sum-rate upper bound for the two-user Gaussian interference channel," *2009 IEEE International Symposium on Information Theory*, Seoul, Korea, June 2009.

[123] J. Nam, "On the High-SNR Capacity of the Gaussian Interference Channel and New Capacity Bounds," in IEEE Transactions on Information Theory, vol. 63, no. 8, pp. 5266-5285, Aug. 2017.

[124] A. S. Motahari and A. K. Khandani, "Capacity bounds for the Gaussian interference channel," *IEEE Transactions on Information Theory*, vol. 55, no. 2, pp. 620-643, Feb. 2009.

[125] A. Chaaban and A. Sezgin, "An extended Etkin-type outer bound on the capacity of the Gaussian interference channel," *IEEE Asilomar Conference on Signals, Systems, and Computers*, 2011, pp. 1860-1864.

[126] V. Dolotin and A. Morozov, *Introduction to Non-linear Algebra*, World Scientific Publishing Company, 2007

[127] A. Morozov and M. Serbin, "Non-Linear Algebra and Bogolubov's Recursion," *Theoretical and Mathematical Physics*, 2007, hep-th/0703258